UNIVERSITAT POLITÈCNICA DE CATALUNYA
BARCELONA TECH

Departament d'Eginyeria Civil i Ambiental
Laboratori d'Enginyeria Marítima

Programa de Doctorat en Ciències del Mar

Probabilistic characterization of single and concurrent metocean variables of Mexican coasts with seasonal variability using extreme value theory, with application to reliability of coastal structures

THESIS BY COMPENDIUM OF PUBLICATIONS

PhD Thesis presented by

Felícitas Calderón Vega

For the degree of DOCTOR

DIRECTED BY:

Dr. César Mosso Aranda

Dr. Adrián David García Soto

Barcelona, Febrero, 2020

DEDICATORIA

A Arlene Damara, Aldair Daniel y Adrián David.

Mis hijos, mi motor de vida.

Y *a David*

Mi amado esposo

To Arlene Damara, Aldair Daniel and Adrián David

My kids, the energy of my life.

And to David

Mi beloved husband

CONTENTS

Abstract

This thesis encompasses a set of different subjects related to metocean variables but studied from different perspectives. The metocean variables are mainly significant wave heights and wind velocities and, to a lesser extent, wave periods. The extreme value theory is used to probabilistically characterized the metocean variables by means of the generalized extreme value distribution (GEV). The effect of seasonality is included by considering monthly maxima and using harmonic and subharmonic functions (i.e., time dependency in the GEV model is incorporated). Although Mexican information was not available to this study, the studies are considered applicable to Mexican coasts in the Gulf of Mexico and the Pacific, since available public information from U.S. buoys located in the Atlantic and Pacific oceans relatively close to the Mexican coasts is employed. For the Pacific region, the GEV model accounting for seasonality is applied to data from a buoy (this is reported in an article in the appendix and summarized as a book chapter in the compendium of publications) and comparisons are carried out versus analogous results for buoys in the Gulf of Mexico obtained in a previous study (included also in the appendix). In other part of the thesis (another book chapter in the compendium), but also for the buoy in the Pacific Ocean, a study is carried out to assess the impact of including or excluding an atypical wave height in the seasonality and in future projections (i.e., wave heights associated with given return periods), since an atypically large significant wave heigh was observed for the considered buoy. One more study (an article in the compendium) introduces the wind velocity as a Metocean variable to be characterized with the time-dependent GEV model from data of a buoy in the Gulf of Mexico. This wind velocity is not for monthly maxima, but for the recorded wind velocity which simultaneously occurred with the maximum significant wave heights, thus it is also referred to as companion wind in this work. It is pointed out that the level of resolution is within that corresponding to the National Oceanic and Atmospheric Administration (NOAA) from US, where the significant wave height and wind speeds are denoted as WVHT and WSPD, respectively. The wind velocity is averaged over an eight-minute period recorded at 3.6 m above sea level and the significant wave height (the average of the highest one-third of all of the wave heights) over a 20-minute period. For the scope of this study, these metocean variables are used as directly given in the NOAA data. It is acknowledged that there may be a slight time lag between the occurrence of one measurement and the other (since the averaging sampling periods

differ) but the difference is not considered significant for practical purposes; besides, we are limited to the resolution of the available data. Nevertheless, the uncertainty and impact of these different sampling periods in the projections are recommended as future research subjects. This allowed to propose a simplified approach to determined concurrent significant wave heights and associated wind velocities for given return periods, while accounting for seasonality and quantitatively establishing the uncertainty in the correlated metocean variables in question. This proposal can be potentially used for design and engineering purposes, if the metocean are considered as hazards which imposed demands on coastal (and structural) engineering systems. Additionally, the effect of varying the considered time window for the extreme projections is explored. In a final study (also an article in the compendium), an introduction to the reliability of coastal (and also structural) engineering systems is presented; a breakwater is used as case-study. The coastal structure is subjected to the action of wave heights with different wave periods, for which the joint Longuet-Higgins distribution is used, and the overtopping probability of failure is computed by using classical and revisited reliability approaches. Future studies could combine the characterization of metocean variables as time-dependent GEV models and the used reliability approaches to further investigate the reliability of coastal and offshore systems.

Resumen

Esta tesis abarca diferentes temas relacionados con variables meteoceanográficas (metocean) pero estudiadas desde diversas perspectivas. Estas variables son principalmente el oleaje significativo y la velocidad de viento, y en menor medida el período de oleaje. Se emplea la teoría de valores extremos para caracterizar probabilísticamente las variables meteoceanográficas mediante el uso de la distribución de extremos generalizada (GEV, por sus siglas en inglés), incluyendo el efecto de la estacionalidad al considerar valores máximos mensuales, así como funciones armónicas y subarmónicas, lo que significa que el modelo GEV es función del tiempo. Aunque no se contó con información mexicana para el presente trabajo, se considera que lo desarrollado aquí puede aplicarse a las costas mexicanas, ya que se usaron datos de boyas estadounidenses situadas en los océanos Atlántico y Pacífico y relativamente cercanas a costas mexicanas. Para la región del Pacífico se aplica el modelo GEV a una boya (esto se describe en un artículo en el apéndice y resumido como capítulo de libro en el compendio de publicaciones) y los resultados se comparan con resultados análogos de un estudio previo, pero para boyas localizadas en el Golfo de México (dicho estudio también está contenido en el apéndice). En otra parte de la tesis, pero también para la boya del Pacífico (otro capítulo de libro en el compendio), mediante un estudio se estima el impacto de incluir o excluir un dato atípico de la altura de oleaje en la estacionalidad y proyecciones a futuro (i.e., las alturas de oleaje asociadas a periodos de retorno dados), ya que se observó una ola atípicamente alta para la boya considerada. Un estudio más (un artículo del compendio) incorpora a las velocidades de viento como variable mete-oceanográfica para también caracterizarla como un modelo GEV que depende del tiempo, con datos de una boya situada en el Golfo de México. Estas velocidades de viento no corresponden a las máximas reportadas en cada mes, sino a aquellas que ocurrieron simultáneamente con las máximas alturas significativas generadas por oleaje, por lo tanto, en este trabajo también se le denota como viento acompañante (companion wind). Cabe resaltar que el nivel de resolución empleado es el correspondiente al de la Administración Nacional Oceánica y Atmosférica (NOAA por sus siglas en inglés), donde la altura de ola significativa y las velocidades de viento se denotan como WVHT y WSPD, respectivamente. La velocidad de viento se promedia para un periodo de 8 minutos y se registra a 3.6 m sobre el nivel del mar y la altura de ola significativa (el promedio del tercio superior de todas las alturas de ola) para un periodo de 20 minutos. Para los alcances de

este estudio, estas variables meteoceanográficas se toman directamente como están reportadas en los datos de la NOAA. Se reconoce que puede haber un ligero desfase de tiempo entre las mediciones de una variable y la otra (ya que los tiempos de muestreo para el promedio son distintos) pero no se considera que esta diferencia sea significativa para fines prácticos; además, estamos limitados a la resolución de los datos disponibles. No obstante, la incertidumbre y el impacto de estos diferentes periodos de muestreo en las proyecciones son consideradas como materias de investigación para futuros proyectos. Esto conllevó a proponer un método simplificado para determinar alturas de oleaje significativo concurrentes con los vientos asociados a la misma boya y tiempo y para un periodo de retorno dado, y al mismo tiempo incorporando efectos de estacionalidad y estableciendo de manera cuantitativa la incertidumbre para las variables correlacionadas mencionadas. Esta propuesta es potencialmente útil para propósitos de diseño e ingenieriles, si las variables meteoceanográficas se consideran como peligros que imponen demandas a sistemas de ingeniería costeros (y estructurales). Adicionalmente, se explora el efecto de utilizar diferentes ventanas de tiempo en las proyecciones de valores extremos. En un estudio final (también un artículo del compendio) se presenta una introducción a la confiabilidad de sistemas de ingeniería costera (y también estructural), usando un rompeolas como caso de estudio. La estructura costera se somete a la acción de oleaje con diferentes periodos, mediante el uso de la distribución de Longuet-Higgins, y se calculan las probabilidades de falla por rebase aplicando métodos de confiabilidad clásicos, y otros métodos consultados en retrospectiva y reconsiderados prospectivamente. Estudios futuros podrían combinar el uso de modelos GEV como función del tiempo para caracterizar variables meteoceanográficas con el uso de métodos de confiabilidad, para investigar más a fondo la confiabilidad de sistemas costeros y costa afuera.

Acknowledgments

The financial support from the Erasmus Mundus Coastal and Marine Engineering and Management (CoMEM) programme is gratefully acknowledged. I thank Laboratori d'Enginyeria Marítima, Universitat Politècnica de Catalunya and Universidad de Guanajuato. I am also very thankful to Sonja Marie Ekrann Hammer and Ø. Arntsen for their assistance through the Erasmus Mundus CoMEM programme procedure. I am gratefully to my supervisors César Mösso and David García for their patience and guidance. I am thankful to the externals revisors Rafael Ramirez Mendoza and Andrés Rodriguez for their time and valuables suggestions to improve this work. Thanks go to Rosa María Olea, Genoveva Comas and the administrative staff of UPC for their help. I also thank my family, friends and everyone who directly or indirectly help me to achieve this goal.

I. THESIS BODY

1. Introduction

Metocean variables as the wave height, wave period, the wind velocity which occurs simultaneously with the previous variables, among others, should be probabilistically characterized if they are to be used for the design and operation of coastal and marine infrastructure and for other engineering applications. The seasonal variation of extreme values for such metocean variables also affects the planning, design, construction, operation and maintenance of shore and offshore structures such as breakwaters, ports, oil facilities, etc. Moreover, values of metocean variables should be oft associated with return periods usually employed in codified design for practical applications. Furthermore, these seasonal wave heights and wind velocities act together, as adding demands, over maritime and structural systems which capacities must withstand the effects imposed by these uncertain metocean variables.

Other aspects as the possible influence of atypical large values in the estimation of extreme values, differences dependent on the considered region and even on the considered site (for example at two different oceans as the Pacific and the Atlantic, or two different locations within the same ocean), and the consideration of different time windows in the extreme value projections for given return periods can also be of interest to the researchers and designers.

Therefore, an adequate probabilistic characterization of the metocean variables, not only as single demands but also as concurrent demands, is important for research and practical purposes. For instance, the demands represented as probability distributions could be used, together with the capacity of coastal structures ad systems (which can be deterministic or probabilistic), to compute the probability of failure of such structures and systems. This is important for codified design.

1.1 Motivation

In general, metocean variables are related to phenomena relevant to researchers of several fields. Specifically, wind together with waves are metocean variables capable of substantially impact ports, maritime structures and offshore facilities, among other systems. The influen ce of these metocean variables is of great interest to researchers, engineers and decision makers, because they influence the planning, design, building, operation, maintenance and even decommission of important projects. This is the case for ultimate limit states but also for serviceability limit states. The former are important to prevent major failures of the above referred systems and the latter to keep the systems functional. These limit states are usually included in standards and guidelines, where also design criteria and acceptable safety and functionality limits are established.

Since the metocean variables can be considered as random demands imposed to systems which capacities must withstand such demands, for prescribed acceptable levels contained in codes and regulations, it is desirable to characterize such variables probabilistically. Also, operability and maintenance, among other issues, could depend on the seasonality of metocean variables. Moreover, these variables often do not act as single demands, but they act simultaneously on offshore facilities, coastal structures and other engineering systems, that are designed for extreme values associated to return periods. Consequently, it is of interest to inspect the correlation of variables as wave height and wind velocity associated with a prescribed return period. Extreme value theory is a key tool to investigate metocean variables associated with given return periods, and classic probabilistic techniques as regression and residual analysis can be also very useful tools. Among the probability distributions contained within the extreme value theory, the generalized extreme value distribution (GEV) is a powerful alternative since it encompasses the three well-known extreme value distributions in a single mathematical expression. Other aspects that could also be of interest for research and engineering purposes include, but are not limited to, the influence of the atypical values and considered time windows in extreme value projections, as well as regional and site to site differences in extrapolation of extreme values useful for design. The previous issues encourage the probabilistic characterization of metocean variables as, both, single

and concurrent acting random phenomena considering seasonality and using extreme value theory. Furthermore, this characterization could be used to compute the probability of failure of costal systems by using reliability theory.

1.2 Objectives

The objectives of the present study are to probabilistically characterize individual metocean variables (significant wave height and wind velocity) by using a GEV model and considering seasonality, also to develop a simple approach for determining concurrent metocean variables with seasonal variation (significant wave height and wind velocity) associated with given return periods by combining GEV models and classical regression and to inspect the influence of atypical values, considered time windows and a selected site in the projections of extreme values. Other objective is to introduce the use of reliability theory to compute the probability of failure of coastal structures.

1.3 Outline

This thesis is structured in two parts. First, the Thesis body, which summarises the thesis work. Second, the Compendium of papers, which provides the details of the study.

The background information is given in Section 2. Sub-section 2.1 describes the probability methods developed and employed, and Sub-section 2.2 outlines the lineal regression, correlation and residual analysis. In Sub-section 2.3 reliability theory is briefly summarized, and the overall discussion and general conclusions are given the section 4.

The compendium of papers is composed by two papers (Paper A and Paper B) and two book chapters (Book chapter 1 and Book chapter 2). The two papers are already published in international peer-reviewed journals. Other two papers are not part of the main body of the Thesis (Paper C and Paper D), but they are included in an appendix since they provide support to the work. All of them are listed below and enclosed after the Thesis Body.

Paper A. Correlation of Concurrent Extreme Metocean Hazards Considering Seasonality. Applied Sciences. Appl. Sci. 2020, 10, 4794; doi:10.3390/app10144794.

[Felícitas Calderón-Vega, Adrián-David García-Soto and César Mösso]

Paper B. Revisiting Two Simulation-Based Reliability Approaches for Coastal and Structural Engineering Applications. Applied Sciences. Appl. Sci. 2020, 10, 8176; doi:10.3390/app10228176
[Adrián-David García-Soto, Felícitas Calderón-Vega, César Mösso, Jesús-Gerardo Valdés-Vázquez and Alejandro Hernández-Martínez]

Book Chapter 1. Emerging Issues in Science and Technology Vol. 1. Chapter 11, Influence of an Atypical Value in the Extreme Wave Analysis Using Non-Stationary GEV Models. Print ISBN: 978-93-89562-66-8, eBook ISBN: 978-93-89562-67-5. DOI: 10.9734/bpi/eist/v1
[F. Calderón-Vega, C. Mösso and A. D. García-Soto]

Book Chapter 2. New Ideas Concerning Science and Technology. Describing the Summary of Single Site Extreme Wave Analysis in the Pacific Ocean Comparing Stationary and Non-Stationary GEV Models DOI: https://doi.org/10.9734/bpi/nicst/v4/2310E [F. Calderón-Vega, C. Mösso, A. D. García-Soto and E. Delgadillo-Ruiz]

Paper C. Single Site Extreme Wave Analysis in the Pacific Ocean Comparing Stationary and Non-stationary GEV Models. Curr ent Journal of Applied Science and Technology. 32(6): 1-12, 2019; Article no. CJAST.47420 [F. Calderón-Vega, C. Mösso, A. D. García-Soto and E. Delgadillo-Ruiz]

Paper D. Analysis of extreme waves with seasonal variation in the Gulf of Mexico using a time-dependent GEV model. Ocean Engineering. Ocean Engineering 73 (2013) 68–82 [F.Calderón-Vega, A.O.Vázquez-Hernández, A.D.García-Soto]

2. Background

In this section, the used methodologies in this work are briefly described as background. First, the development of extreme value theory and associated probability distributions are briefly mentioned (GEV model). These subjects are based on the articles included in the appendix. Then, the classic techniques of linear regression, correlation and residual analysis are presented. Finally, the reliability theory is described based on information in the literature. These approaches are the basis to achieve the objectives stated above.

2.1 Characterization of Metocean Variables with Time-Dependent GEV Models

2.1.1 Extreme Value Theory

Extreme value theory can be employed to project values of a random variable to return periods of interest. These projected values are useful for engineering applications to designing structures subjected to the effects of environmental phenomena for a life cycle, e.g., a port which must withstand the effect of the extreme expected environmental effects during its lifetime. This means that the design is conditioned by the maximum expected effects (e.g., wave height) likely to occur in the lifetime of the port (or other system of interest).

From the analysis of extreme value data, the extreme value theory is derived. This subject encompasses a set of tools and techniques to model and quantify the stochastic behaviour, in terms of magnitude and frequency, of the extreme events.

If asymptotic theory is postulated, the maximum values can be represented with the generalized extreme value distributions first presented by Fisher and Tippet, and further developed by Gumbel (Chakrabarti, 2001). It is reported that several issues can affect the assessment of the extreme values when a probability model is used, as the amount of available data recordings, selection and exclusion of information, among other aspects (e.g., Prpic-Oršić, 2007, Martucci, 2010).

Several models have been proposed to characterize metocean behavior, including models which accounts for site conditions (e.g., Isaacson and Mackenzie, 1981; Muir and ElShaarawi, 1986; Prevosto and al., 2000; Stansell, 2005; Tayfun and Fedele

2007; Jensen, et al., 2011; Mazas and Hamm, 2011; Muraleedharan, et al., 2012; Solari and Losada, 2012; Soares and Carvalho, 2012). Not so many studies include the seasonality; some early studies as that by Mietus (1998) considered the seasonal variation applied to the wind speed in the Baltic Sea; also Jönsson et al. (2002) indicated the large seasonal variation in a metocean variable (wave height) for the Baltic Sea. It is reported that non-stationary models for wave variables lead to smaller bias and variance as those from stationary models. It was also proven that estimates from discrete seasonal models tend to be highly biased. Räämet and Soomere (2010) estimated the seasonal variation in wave climate in the Baltic Sea using a high-resolution version of a wave model.

2.1.2 Extreme Time-Dependent GEV Distribution

The GEV distribution for maximum values in a block of time is used to modeling the seasonality of significant wave heights (e.g. Leadbetter et al., 1983). The GEV has the ability of covering the three families of well-known extreme value CDFs (the so-called Gumbel, Weibull and Frechet probability distributions) as (Coles, 2001)

$$G(x) = exp\left\{-\left[1+\xi\left(\frac{x-\mu}{\psi}\right)\right]_{+}^{-1/\xi}\right\} \rightarrow \xi \neq 0 \quad (1)$$

$$G(x) = exp\left\{-exp\left[-\left(\frac{x-\mu}{\psi}\right)\right]\right\} \rightarrow \xi = 0$$

The corresponding PDF is expressed as

$$g(x) = \frac{1}{\psi}\left[1+\xi\left(\frac{x-\mu}{\psi}\right)\right]_{+}^{-\left(1+1/\xi\right)} exp\left\{-\left[1+\xi\left(\frac{x-\mu}{\psi}\right)\right]_{+}^{-1/\xi}\right\} \rightarrow \xi \neq 0 \quad (2)$$

$$g(x) = \frac{1}{\psi} exp\left(-\frac{x-\mu}{\psi}\right) exp\left\{-exp\left[-\left(\frac{x-\mu}{\psi}\right)\right]\right\} \rightarrow \xi = 0$$

where [a]+ denotes max (a, 0), - ∞ <μ <∞ denotes the location parameter, ψ> 0 denotes the scale parameter and ξ denotes the shape parameter; the shape parameter defines which of the three well-known PDFs is represented. If ξ ≠ 0, it corresponds to the Fréchet PDF when ξ> 0 and corresponds to the Weibull PDF when ξ <0; when ξ → 0 the Gumbel PDF is more suitable for the considered data.

The Fisher-Tippet theorem defines a distinct behavior for every type of distribution in the tail region. The tail of the Weibull distribution is bounded, whereas it is heavy or light, if the Frechet or Gumbel distributions are considered, respectively. A feature of the Gumbel distribution is the exponential decay of the tail. In contrast, the decay as a function of a power is characteristic of the Fréchet distribution. Only one of the three well-known extreme value distributions is adopted to approximate the behavior of the random variable.

In subsequent chapters, a time-dependent GEV model considering seasonal behavior is described. It assumes that monthly maximum values, z_i, observed at times t_i, are independent. Adoption of monthly maxima captures important features of the upper tail of the distribution (Katz et al., 2002).

The parameters assessment is affected by the reduced data when a time window below one year is used; this should be kept in mind, because some seasons may not have recorded data in the used series; a minimum of data per month should preferably be stipulated, for instance rejecting the maximum monthly events with less than 60% of recorded values (Mendez et al., 2007).

2.1.3 Inclusion of Seasonality

Cyclical changes along a given year define the seasonality of a random variable. The variation within a year for extreme wave heights has been modeled by using extreme value theory (Morton et al. ,1997; Carter and Challenor, 1981). Patterns of wave intensity and the probability distribution associated with different wave heights, accounting for seasonality, has also been adequately reproduced (Räämet and Soomere, 2010). Seasonal weather patterns are commonly associated with a recurrent yearly behaviour that can be represented by sinusoidal expressions. In general terms, this can be considered as a winter-summer variation, including other systematic weather patterns linked to climatic phenomena (e.g., hurricanes and cold

fronts). By observing such patterns, to represent the seasonal variability as a superposition of harmonic functions seems reasonable.

Among the several possibilities to represent this non-stationary behaviour in the GEV models, harmonic functions can be adopted, and their parameters determined by regression. In the studies included in this thesis the following expressions are used (Mendez et al., 2008; Menéndez et al., 2009)

$$\theta = \begin{cases} \mu(t) = \beta_0 + \beta_1\, cos(2\pi t) + \beta_2\, sin(2\pi t) + \beta_3\, cos(4\pi t) + \beta_4\, sin(4\pi t) \\ \psi(t) = \alpha_0 + \alpha_1\, cos(2\pi t) + \alpha_2\, sin(2\pi t) + \alpha_3\, cos(4\pi t) + \alpha_4\, sin(4\pi t) \\ \xi(t) = \gamma_0 + \gamma_1\, cos(2\pi t) + \gamma_2\, sin(2\pi t) + \gamma_3\, cos(4\pi t) + \gamma_4\, sin(4\pi t) \end{cases} \quad (3)$$

Where t is in years and $\psi(t > 0)$; θ includes the location, scale and shape ($\mu(t)$, $\psi(t)$ and $\xi(t)$) parameters, respectively; β_0, α_0 and γ_0 denote mathematical expectation; the amplitudes of the harmonics are represented by β_i, α_i and γ_i (i=1 or i=2) and those of the subharmonics by β_i, α_i andγ_i (i=3 or i=4).

2.1.4 Fitting technique

Among the available approaches to determine coefficients of the model by regression, and to fit the data to known probability distributions, the maximum likelihood method is a powerful alternative. This approach is used for several of the studies contained in the Thesis, since it leads to an adequate fitting, less bias and, in general, more efficient estimators for long return periods and not very large data sets, as stated by Lettenmaier and Burges (1982). The so-called maximum likelihood method estimates parameters of a L function, so that the probability of observing the sample set {x_1,...x_n} is maximum. The following expression can be used to represent L (Benjamin and Cornell, 1970)

$$L(\theta; x_1, x_2, \ldots, x_n) = f(x_1, \ldots x_n; \theta) = \prod_{i=1}^{n} f(x_i; \theta) \quad (4)$$

where $L(\theta; x_1, x_2, \ldots, x_n)$ defines the joint density function associated with all initial extreme values and is known as the likelihood function, which initial extreme values are selected from a given distribution family. The maximum compatibility between the sample of maxima X_1,...X_n, and density function $f(x_1, \ldots x_n; \theta)$ is searched;

θ denotes the parameter vector for the probability distribution function. Usual assumptions include that the samples are independent and identically distributed. Instead of *L*, its natural logarithm is often considered, and it is known as the log-likelihood function, *l*, given below

$$l(\theta; x_1, x_2, \ldots, x_n) = \sum_{i=1}^{n} log\,[f(x_1, \ldots x_n; \theta)] \tag{5}$$

By minimizing the previous equation, maximum likelihood estimators, $\hat{\theta}$, are deemed as the parameter values with the maximum likelihood, for which the following set of equations must be solved (for j=1,...,r):

$$\sum_{i=1}^{n} \frac{\partial}{\partial \theta_j} log[f(x_1, \ldots x_n; \theta)] = 0 \tag{6}$$

If this is applied to the GEV distribution, the log-likelihood function yields

$$l\left(X_{MAX}; \mu, \psi, \xi\right) = -N \log \psi - \left(\frac{1}{\xi} + 1\right) . \sum_{i=1}^{N} \log\left(1 + \xi \frac{x_i - \mu}{\psi}\right) - \sum_{i=1}^{N}\left(1 + \xi \frac{x_i - \mu}{\psi}\right)^{-1/\xi} \tag{7}$$

where the *N* observations of maximum monthly values are defined as $x_1,\ldots,x_N$.

2.1.5 Assessment of the Uncertainty

The Fisher method is used to incorporate the uncertainty in the models. For such a purpose, the maximum value of the log-likelihood function is obtained for certain parameter estimators$\left(\hat{\theta}\right)$ and used, so that the more likely compatibility between the observed set of extreme data and the theoretical model is reached. Therefore, *l(x;θ)* is a measure of the adequacy of the sample when the population parameters have a given value θ=$\hat{\theta}$.

If *l(x;θ)* undergoes significant variations when θ changes, it can be considered that the data sample and *θ* are strongly related, which can be quantitatively determined with $\partial l / \partial \theta$ evaluated at $\hat{\theta}$. The variance evaluated in $\hat{\theta}$ is required to assess *h* with respect to each unknown parameter.

By assessing the variance, the hessian matrix of the negative value of $l(x;\theta)$, evaluated at $\hat{\theta}$, can then be determined and it is frequently referred to as the observed information matrix, I_0 given by

$$I_0 = \begin{bmatrix} -\frac{\partial^2 l(\hat{\theta})}{\partial \theta_1{}^2} & \cdots & \cdots & -\frac{\partial^2 l(\hat{\theta})}{\partial \theta_1 \partial \theta_p} \\ \vdots & \ddots & -\frac{\partial^2 l(\hat{\theta})}{\partial \theta_i \partial \theta_j} & \vdots \\ \vdots & -\frac{\partial^2 l(\hat{\theta})}{\partial \theta_j \partial \theta_i} & \ddots & \vdots \\ -\frac{\partial^2 l(\hat{\theta})}{\partial \theta_p \partial \theta_1} & \cdots & \cdots & -\frac{\partial^2 l(\hat{\theta})}{\partial \theta_p{}^2} \end{bmatrix} = \quad (8)$$

where p denotes the number of estimated parameters for the probability distribution considered. The observed information matrix is equivalent to the Fisher information matrix (asymptotically, and not with the estimators but with the real parameter values). It can be shown that $\hat{\theta}$ is normally distributed. The I_0 matrix is used to obtain the standard deviations of $\hat{\theta}_1 \ldots, \hat{\theta}_p$, the so-called standard errors of the obtained punctual estimators,

$$se(\theta_i) = \sqrt{J_{i,j}} \quad (9)$$

This is possible by recognizing that for the inverse of this matrix, $J = I_0^{-1}$, the square roots of the diagonal elements correspond to the standard deviations. In other words, the I_0 matrix represents the surface curvature of the approximated log-likelihood function.

To compute confidence intervals for the estimators, the normality property of the maximum likelihood estimators at level (1-α) leads to

$$ci(\theta_i) = \theta_i \pm z_{\alpha/2} se(\theta_i) \quad (10)$$

where $z_{\alpha/2}$ is the quantil (1- α /2) of the standard normal distribution function. Alternatively, other techniques like Bootstrap methods are reported by Chavez-Demoulin and Davidson (2005) to quantify uncertainties. For this thesis, the previous methodology (Coles, 2001) is employed.

2.1.6 Selection of the Model

The optimal model to represent the non-stationary behavior of the studied metocean variables is pursued by a parameterization with two sinusoidal harmonics (Pμ=2, Pψ=2 y Pξ=2). Simple models like the Gumbel homogeneous distribution given by $\theta^1 = (\beta_0 \alpha_0)$, or complex models given by $\theta^b = (\beta_0, \beta_1, \beta_2, \beta_3, \beta_4, \alpha_0, \alpha_1, \alpha_2, \alpha_3, \alpha_4, \gamma_0, \gamma_1, \gamma_2, \gamma_3, \gamma_4,)$, can be chosen. In several of the articles contained in the compendium and the appendix, the genetic algorithms nomenclature (Goldberg, 1989) is followed. A binary codification is considered. This leads to code the model as a binary chromosome c=[$g_1 g_2 . g_3 g_4 . g_5 . g_6 g_7$] where g_i denotes binary genes representing the factors of interest. Each gene can have only a couple of outcomes, i.e., g_i=1 when the ith factor is turned on, or g_i=0 when it is not. The gene g1(β_1, β_2) is use to model the annual cycle for the location parameter, whereas g2(β_3, β_4) to model the semi-annual cycle for the location parameter; likewise g3$(\alpha_1, \alpha_2)$is used to model the annual cycle for the scale parameter, whereas g4(α_3, α_4) to model the semi-annual cycle for the scale parameter; finally, g5 is a gene used to model a constant o zero shape parameter (γ_0), whereas g6(γ_1, γ_2) to model the scale parameter (Goldberg, 1989)

A search selective methodology known as Stepwise, which in turn combines a couple of techniques denoted as Forward Selection and Backward Elimination, is performed as a mean to encounter the most suitable model. Every time that a gene is turned on in the Forward Selection, the Backward Elimination checks whether the gene must be kept or not. This leads to code the model as a 7-gene chromosome c=[g1,g2,g3,g4,g5,g6,g7] , where every gene will have zero or unity values (Menéndez et al., 2007).

The Akaike Information Criteria (AIC) (Akaike, 1973), given by

$$AIC = -2l(\hat{\theta}) + 2p \qquad (11)$$

where p is the number of parameters and $l(\hat{\theta})$ is the maximum of the log-likelihood computed from each model, is used as criterion to discriminate between competing models, and it also represents a compromise between goodness-of-fit and simplicity.

2.1.7 Verification of the Model

The adequacy of the model to represent the metocean variables, is verified by means of quantile-quantile plots (QQ) and probability plots. Note also that, since for extreme value distributions special interest is focused on the tail of the distribution, a very convenient standardization for the extreme metocean variables can be achieved transforming the empirical model distribution into a Gumbel distribution, so that a quantitative description of the goodness-of-fit is represented. This variable change is denoted as W and is given by

$$W(t) = \frac{1}{\hat{\xi}(t)} log\left[1 + \hat{\xi}(t)\left(\frac{x - \hat{\mu}(t)}{\hat{\psi}(t)}\right)\right] \quad (12)$$

where the maximum monthly *N* observations $\{x_1,\ldots,x_n\}$ happen at times $\{t_1,\ldots,t_n\}$.

When the metocean variable of interest is adequately modeled, the resulting statistics correspond to a standardized Gumbel variable. The W(t) statistics given as a function of time, are a measure of the stationarity in the metocean variable. The probability of the Gumbel distribution for the W(t) statistic is computed using

$$Pr\{W \leq x\} = exp(-e^{-x}) \quad (13)$$

The probability values for the extreme data samples,$\{\tilde{F}(x_{(i)})\}$, and the evaluated probabilities by using the W(t) statistic, are compared in the probability plots.

The QQ plots are determined by sorting the sample values and the quantiles computed with the assumed theoretical distribution are plotted as well. This leads to model quantiles given by W(i)=W(x(i), t(i)), and the associated logarithmic transformation must be applied to the direct sample data, so that they can be scaled to Gumbel by means of

$$\left\{-log\left(-log\left(\tilde{F}(x_{(i)})\right)\right), W_{(i)}\right\} \quad (14)$$

2.1.8 Return Periods

Return period values for the metocean variables are given by

$$X_q(t,\theta) = X_q(\mu(t),\psi(t),\xi(t)) = \begin{cases} \mu(t) - \dfrac{\psi(t)}{\xi(t)}\left\{1 - \left[-\log(1-q)\right]^{-\xi(t)}\right\} & if \quad \xi(t) \neq 0 \\ \mu(t) - \psi(t)\log\left[-\log(1-q)\right] & if \quad \xi(t) = 0 \end{cases} \tag{15}$$

where q is the exceedance probability defined from G t(x)=1-q (the time-dependent GEV distribution function equated to 1-q), and the estimated quantil Xq(t,θ), is the time dependent value of the metocean variable for the return period R=1/q.

The following chapter presents the classic probability techniques of linear regression, correlation and analysis of residuals, which are used in one of the papers in the compendium. The concepts are based on what is reported in the literature (Benjamin and Cornell, 1970; Jordaan, 2004; Kottegoda and Rosso, 2008).

2.2 Lineal Regression, Correlation and Residuals

The linear regression can be used to study the linear relationship of two metocean variables, as it was carried out for significant wave heights and wind velocities in one of the papers in the compendium (see Figure 1 extracted from Paper A). In Figure 1 it is shown that a linear relationship can represent scatter data about a mean regression line, by considering wind velocities (V_w; y variable) and significant wave heights (H_s; x variable). If H_s is considered as the independent variable, and V_w the dependent one, it can be considered that V_w is conditioned on a given value of H_s.

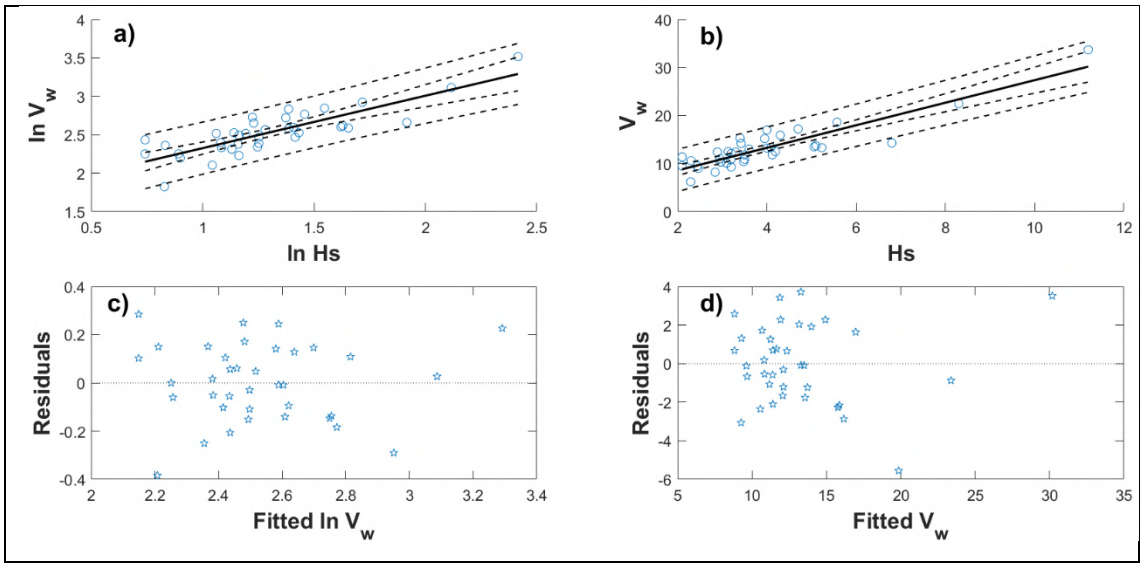

Figure 1. Regression analysis of wind velocities and significant wave heights by using (a) nonlinear and (b) linear models (after Paper A). Residuals in (c) correspond to regression in (a) and residuals in (d) correspond to regression in (b) (after Paper A in the compendium).

If we go back to the common use of x and y as the independent and dependent variables, respectively, and a normal distribution about a straight line with constant variance for all the x values is assumed, a given y value, y_i defined as

$$y_i = a + bx_i + e_i \tag{16}$$

will deviate from the line by the amount e_i which is sampled from a normal distribution function with variance σ^2.

The regression line can be estimated using the least squares method. If A and B are *denoted as* random variables, it is possible to obtain two estimators for a and b, denoted as â and $\hat{b}$, respectively. It is then desired to minimize the errors (in fact, the sums of the squares of the errors), equal to $\sum_{i=1}^{n} e_1^2$; in other words, the following minimization is pursued

$$Min\left(\sum_{i=1}^{n}[y_i - (a + bx_i)]^2\right) \tag{18}$$

which can be solved by differentiation, looking for the parameters of interest a and b, which leads to the simultaneous equations

$$\sum_{i=1}^{n} -2(y_i - a - bx_i) = 0 \tag{19}$$

$$\sum_{i=1}^{n}[-2y_i(y_i - a - bx_i)] = 0 \tag{20}$$

which yield the desired estimators $\hat{a}$ and $\hat{b}$ when solving

$$n\hat{a} + \hat{b}\sum_{i=1}^{n} x_i = \sum_{i=1}^{n} y_i \tag{21}$$

and

$$\hat{a}\sum_{i=1}^{n} x_i + \hat{b}\sum_{i=1}^{n} x_i^2 = \sum_{i=1}^{n} x_i y_i \tag{22}$$

By eliminating $\hat{a}$ and solving for $\hat{b}$

$$\hat{b} = \frac{n\sum_{i=1}^{n} x_i y_i - \left(\sum_{i=1}^{n} x_i\right)\sum_{i=1}^{n} y_i}{n\sum_{i=1}^{n} x_i^2 - \left(\sum_{i=1}^{n} x_i\right)^2} \quad (23)$$

Equation 21 can then be stated as

$$n\hat{a} + bn\bar{x} = n\bar{y}, \qquad or \quad \bar{y} = \hat{a} + \hat{b}\bar{x} \quad (24)$$

where

$$\hat{a} = \bar{y} - \hat{b}\bar{x} \quad (25)$$

Note that sometimes the variables x and y are not related by a linear relationship, but if other kind of (non-linear) relationship holds, and it can be transformed into a linearized space, the method described above still can be used. This is the case of Figure 1b, where Vw and Hs were linearized by taking natural logarithms before the regression line was computed.

In Figure 1a and 1b the uncertainty in the model parameters is represented by intervals for mean and future values (inner and outer dashed lines, respectively). The obtaining of these intervals is not described in detail here, but they can be obtained by using the t-distribution. Alternatively, the intervals for mean and future values can be closely approximated with simplified equations proposed in Paper A of the compendium.

It is also noted that if it is of interest, the correlation (correlation coefficient) can also be determined with the quantities computed during the regression, but not described here. Moreover, the analysis of residuals can be used as a tool to verify if the assumptions made to perform the regression are met. Neither this is described in detail herein, but Figure 1c and 1d show an example of the residual analyses for the cases in Figure 1a and 1b, respectively (Paper A of the compendium).

In the next chapter the basic concepts of the reliability theory are introduced, since they are used in one of the articles in the compendium to compute the probability of failure of coastal structures.

2.3 Basic Concepts or Reliability Theory

The concepts in this chapter are the basis of reliability theory and the background used to develop Paper B in the compendium. They were originally developed to compute the probability of failure (or its complement, the reliability) of structures and structural systems, but they have been extended to other fields. In this thesis the reliability of coastal systems is introduced in Paper B using these basic concepts and other techniques reported in the literature. Some reliability approaches are found in the specialized literature (as the ones cited in Paper B in the compendium) and the basic concepts reported below are based on Hong (2008) and other references (e.g., Madsen et al., 1986), and in turn in the references contained in those works.

2.3.1 Reliability Analysis

A general formulation for the reliability of a system element can be established by considering the limit state function Z expressed as

$$Z=g(X)=R-L \tag{26}$$

where, broadly speaking, R and L can be considered as the capacity and demand of the element, respectively. If $f_R(r)$ and $f_L(l)$ represent the probability density function (PDF) of the independent random variables R and L , then $F_R(r)$ and $F_L(l)$ correspond to their cumulative distribution functions (CDF). Besides, $F_Z(z)$ is considered as the PDF of Z. Therefore, the probability of failure P_f can be expressed as

$$P_f = P(R - L < 0) = P(Z < 0) \tag{27}$$

If the probability of failure is represented by an integral the following equation is given

$$P_f = P(Z < 0) = \iint_{z=r=l<0} f_R(r) f_L(l) dr dl \tag{28}$$

It can be shown that the previous equation can be simplified as the following single integral

$$P_f = P(Z < 0) = \int_{-\infty}^{\infty} f_R(x)(1 - F_L(x))dx \tag{29}$$

or alternatively as

$$P_f = \int_{-\infty}^{\infty} F_R(x) f_L(x) dx \tag{30}$$

This can be represented in a simple and schematical way as shown in Figure 2 below.

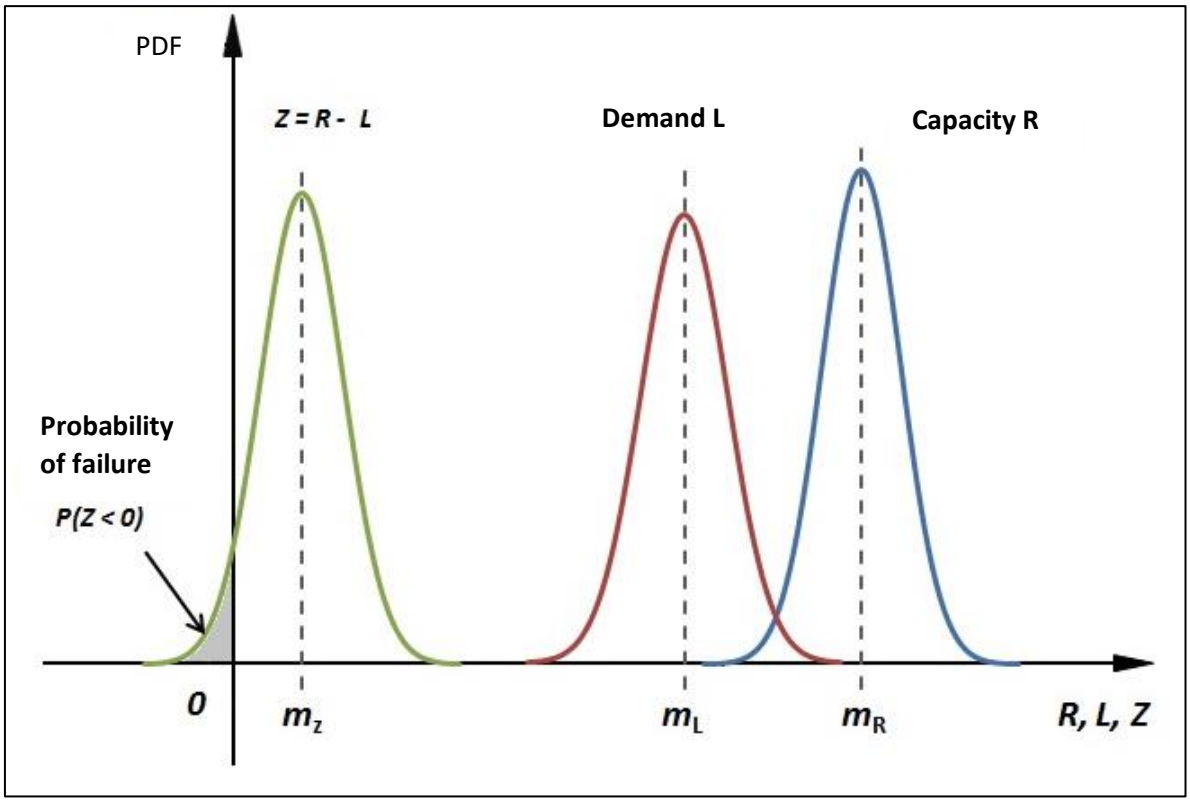

Figure 2. Schematic representation of the PDFs of capacity, demand, Z and the probability of failure

Unfortunately, closed form analytical expressions to compute the probability of failure are only available for a few special cases.

The reliability of an engineering system, P_R is related to its probability of failure through the following relation

$$P_R = P(R - L > 0) = P(Z > 0) = 1 - P(Z < 0) = 1 - P_f \tag{31}$$

In realistic engineering systems, which are usually more complex, more than two random variables are involved in the reliability analysis. If the performance of a system depends on several random variables expressed in a vector format as X, and the joint probability density function of the vector variables is $f_x(X)$, then Z can denote the limit state function (LSF), which represents the performance of the system, which can correspond to the following states: z=g(x)>0 for safety, z=g(x)=0 right on the limit state surface and z=g(x)<0 for failure. Likewise, the probability of failure involving several random variables can be stated as

$$P_f = P(Z > 0) \; = \; P(g(X) < 0 = \int_{z=g(x)<0} f_x(x)dx = \int_{\cap \mathrm{f}} f_x(x)dx \tag{32}$$

except that in this case the integration symbol should be understood as a multidimensional integration. In practical applications this integral does not have a close-form analytical solution. Alternatives, from numerical integration and simulation methods, to more recent approaches (e.g., see references in Paper B of the compendium), can be used, although they may be computationally intensive and time-consuming. In the following, classical solutions are presented since they are the basis of more complex and current methodologies.

2.3.2 Cornell Reliability Index

If for the LSF, Z, defined in Equation (26), both variables are uncorrelated and normally distributed , the so-called Cornell reliability index, β_c is obtained as

$$\beta_c = \frac{m_R - m_L}{\sqrt{\sigma_R^2 + \sigma_L^2}} \tag{33}$$

where m_R, σ_R, m_L and σ_L are the mean and standard deviation of the capacity and demand, respectively. The reliability index, β, and the probability of failure referred to above are related through the following expression

$$\beta = -\Phi^{-1}(p_f) \tag{34}$$

Where $\Phi^{-1}(\bullet)$ denotes the inverse of the standardized normal distribution function.

If the LSF is a linear function of the several random variables, sometimes referred to as a hyperplane, then

$$\mathrm{Z} = \mathrm{g(X)} = a_0 + \sum_{i=1}^{n} a_i X_i = a_0 + a^T X \tag{35}$$

Where a_0 and a_i are coefficients, and the Cornell reliability index can be extended to

$$\beta_c = \frac{a_0 + \sum_{1=1}^{n} a_i\, m_i}{\sqrt{\sum_{i=1}^{n}\sum_{j=1}^{n} a_i a_j C(X_i, X_j)}} = \frac{a_0 + a^T m_x}{\sqrt{a^T C_X a}} \tag{36}$$

where C_x denotes the covariance matrix.

If Z is not a linear function of X, the use of the first two probabilistic moments of Z do not suffice to carry out the reliability analysis. Therefore, a definition of the reliability index covering LSFs with nonlinear relationships is required.

2.3.3 First-Order Second-Moment Reliability Index

The LSF may not be unique. As an example, let R and L be positive defined random variables (e.g., lognormal variables). An alternative representation of Equation (26) is

$$Z = g(R, L) = \ ln(R/L) \tag{37}$$

Consequently, β is obtained as

$$\beta_{RE} = \frac{E(ln(R/L))}{\sqrt{Var(ln(R/L))}} \tag{38}$$

where E and Var stands for expectation and variance, respectively. This formulation was proposed by Rosenblueth and Esteva in 1972.

When Z is not a linear function of R and L, the problem can be solved by linearizing the LSF around the mean values of R and L. If Taylor series are used, such linearized Z, denoted as Z_{F0}, is represented by

$$Z \approx Z_{F0} = ln(m_R) - ln(m_L) + \frac{R - m_R}{m_R} - \frac{L - m_L}{m_L} \tag{39}$$

and β_{F0} can be computed with

$$\beta_{F0} = \frac{lnm_R - lnm_L}{\sqrt{v_R^2 + v_L^2}} \tag{40}$$

This reliability index is not unique, as explained by Ditlevsen (e.g., Madesen et al., 1986). If the linearization of the LFS is carried out around a point *x*, this leads to the linear limit state function Z_{F0} as

$$Z_{F0} = g(x) + \sum_{i=1}^{n} \frac{\partial g'(x)}{\partial x_i}(X_i - x_i) \tag{41}$$

And now β_{F0} is given by

$$\beta_{F0} = \frac{g(x) + \sum_{i=1}^{n} \frac{\partial g'(x)}{\partial x_i}(m_i - x_i)}{\sqrt{\sum_{i=1}^{n}\sum_{j=1}^{n} \frac{\partial g'(x)}{\partial x_i}\frac{\partial g'(x)}{\partial x_j} C(X_i, X_j)}} \tag{42}$$

Which is the so-called first-order second-moment reliability index. If the linearization is performed around the mean values, the reliability index is then referred to as a mean-value first-order second-moment (MVFOSM) reliability index. The Hasofer and Lind reliability index overcomes the problem of the dependency of β_{F0} on the linearization point.

2.3.4 The Hasofer and Lind Reliability Index

For the Hasofer and Lind reliability index the random variables are mapped into standard and uncorrelated *Y* variables with mean zero and the covariance matrix of Y being C_y=I. This transformation is represented by the following equation

$$\mathrm{Y} = \mathrm{A}(\mathrm{X} - \mathrm{E}(\mathrm{X})) \tag{43}$$

where A is linked to the covariance matrix of *X*, C_x, by the relation AC_XA^T=I

By considering the mapping from the standpoint of failure surfaces, the failure surface S_x in *x*-space is mapped into the corresponding failure surface S_y in *y*-space. The distance to the failure surface in y-space can be measured by

$$\beta(x) = [(x - E(X))^T C_X^{-1}(x - E(X))]^{1/2}, x \in S_x \quad (44)$$

from which the Hasofer and Lind reliability index is proposed as

$$\beta_{HL} = min\{(x - E(X))^T C_X^{-1}(x - E(X))\}^{1/2} \quad (45)$$

The point of the solution is denoted design point. The Hasofer and Lind reliability index β_{HL} has the advantage that it is invariant by using an equivalent LSF.

An iterative procedure to calculate the β_{HL} , by considering the standardized variables Y can be implemented by letting y_i be *i-th* iteration point. Then, the LSF is expanded at this point, as

$$g(y_{i+1}) = g(y_{i)} + \nabla g(y_i))^T (y_{i+1} - y_i) \quad (46)$$

where

$$\nabla g(y_i))^T = \left(\frac{\partial g(y)}{\partial y_1}, \frac{\partial g(y)}{\partial y_1}, \ldots, \frac{\partial g(y)}{\partial y_n}\right) \quad (47)$$

The point y_{i+1} leads to the shortest distance from the hyperplane to the origin and should meet the requirement

$$y_{i+1} = \lambda \quad (48)$$

It is pointed out that $\frac{(\nabla g(y_i))^T (y_i) - g(y_i)}{\sqrt{(\nabla g(y_i))^T \nabla g(y_i)}}$ is equivalent to the reliability index, if the expansion at point y_i is considered. If

$$\beta = \frac{g(y_i) - (\nabla g(y_i))^T (y_i)}{\sqrt{(\nabla g(y_i))^T \nabla g(y_i)}} \quad (49)$$

and

$$\alpha_i = -\frac{\nabla g(y_i)}{\sqrt{(\nabla g(y_i))^T \nabla g(y_i)}} \quad (50)$$

y_{i+1} can be reformulated as

$$y_{i+1} = \beta_i \alpha_i \quad or \quad y_{i+1} = ((\alpha_i)^T y_i)\alpha_i + \frac{g(y_i)}{\sqrt{(\nabla g(y_i))^T \nabla g(y_i)}} \alpha_i \quad (51)$$

The design point is the limit of the set $\{y_i\}$ calculated as per Equation (49).

2.3.5 First Order Reliability Method (FORM)

For practical engineering problems, the probability of failure is subjected to the issue of a distribution tail sensitive problem. In these cases, the first order reliability method (FORM) is adequate. It is similar to the Hasofer and Lind reliability approach, in the sense that the limit state function in the transformed space is approximated by a first-order approximation of the hyperplane. However, the transformation is based on the approximation to the actual PDF, so that the distribution tail sensitive problem can be considered.

Once again, we assume that the random variables, X, of the LSF are independent. If $f_{xi}(x_i)$ represents the PDF of X_i, and $\Phi(\bullet)$ and $\phi(\bullet)$ are the standard normal distribution and normal PDF respectively, a normal variate can be employed to approximate the actual random variable to look for a solution point, x_i, equivalent to the one searched for in the original problem. This is expressed as

$$\Phi\left(\frac{x_i-\mu_i}{s_i}\right)=F_{xi}(x_i) \tag{52}$$

and

$$\frac{1}{s_i}\Phi\left(\frac{x_i-\mu_i}{s_i}\right)=f_{xi}(x_i) \tag{53}$$

which solution yields

$$s_i=\phi\left(\Phi^{-1}(F_{xi}(x_i))\right)/f_{xi}(x_i) \tag{54}$$

and

$$\mu_i=x_i-s_i\Phi^{-1}(F_{xi}(x_i)) \tag{55}$$

If y_i is considered as the standardized variable defined by

$$y_{i=}\left(\frac{x_i-\mu_i}{s_i}\right) \tag{56}$$

The mean and the standard deviation of X_i in terms of the transformed random variable Y_i are

$$E(X_I)=E(\mu_i+s_iy_i)=\mu_i \tag{57}$$

and

$$\sigma_i = s_i \tag{58}$$

Sometimes referred to as the equivalent first two probabilistic moments in the transformed space. At the design point of interest, x_j, Taylor series can be used to approximate the LSF as

$$Z = g(x_j) + \sum_{i=1}^{n} \frac{\partial g'(x_j)}{\partial x_i}(X_i - (x_j)_i)$$

The mean value of Z, E(Z)is

$$\begin{aligned} E(Z) &= g(x_j) + \sum_{i=1}^{n} \frac{\partial g'(x_j)}{\partial x_i} E(X_i - (x_j)_i) \\ &= g(x_j) + \sum_{i=1}^{n} \frac{\partial g'(x_j)}{\partial x_i}(\mu_i - (x_j)_i) \end{aligned} \tag{59}$$

and its standard deviation is

$$\sigma_z = \sqrt{\sum_{i=1}^{n} \left(\frac{\partial g'(x_j)}{\partial x_i} s_i \right)^2} \tag{60}$$

Given that X_i are uncorrelated

$$x_{j+1} = \mu_j + \beta_j S_j \alpha_j \tag{61}$$

and the desired reliability index is

$$\beta_j = \frac{\left(g(x_j) + (\nabla \mathrm{g}(x_j))^T (\mu_j - x_j)\right)}{\sqrt{(\nabla \mathrm{g}(x_j))^T C_{xj} (\nabla \mathrm{g}(x_j))}} = \frac{E(Z)}{\sigma_z} \tag{62}$$

$$\begin{aligned} \alpha_j &= -\frac{S_j \nabla \mathrm{g}(x_j)}{\sqrt{(\nabla \mathrm{g}(x_j))^T C_{xj} (\nabla \mathrm{g}(x_j))}} \\ &= \frac{S_j \nabla \mathrm{g}(x_j)}{\sigma_z} \end{aligned} \tag{63}$$

where S_j is a matrix with standard deviations with non-zero elements only for $(S_j)_{ii} = s_j$.

Note that if the random variables are not uncorrelated (i.e., if they are dependent) the Jacobian, *J*, and its inverse is required to restated the random variables in the transformed space as a set of non-dependent random variables. This is mathematically represented, for a set of jointly distributed random variables xi (zi in the normalized space) and for the case of the inverse of the Jacobian (a lower-triangular matrix determined often numerically), as (Madsen et al., 1986)

$$J_{ij}^{-1} = \frac{\partial z_i}{\partial x_i} = \begin{cases} 0, & i < j \\ \dfrac{f_i(x_i|x_1, \dots, x_{i-1})}{\phi(z_i)} & \\ \dfrac{\dfrac{\partial F_i}{\partial x_i}(x_i|x_1, \dots, x_{i-1})}{\phi(z_i)}, & i > j \end{cases}, \quad i = j \tag{64}$$

where $\phi(z_i)$ is the PDF of a normal (standardized) random variable, and f_i and F_i denote the PDF and CDF for the variable i, respectively.

Even though the FORM is a powerful and versatile option, when non-derivable, highly non-linear and complex problems are to be faced, it may not be a feasible option to cope with such problems. In such cases the Monte Carlo simulation (MCS) may be more suitable. This approach in briefly described in the next section.

2.3.6 Monte Carlo Simulation

Monte Carlo simulation is a very powerful approach that can be used to assess the reliability of engineering systems. The method is relatively straightforward but computationally intensive. First, it is required to generate *n* sets values of the random variables for a given LSF. Then, the *n* sets of data are employed to evaluate the LSF *n* times. Finally, the probability of failure is simply computed as the ratio of the number of times that the LSF fell on the failure region over the whole set of simulations. If it is desired to express the reliability in terms of the reliability index, Equation (36) can be used.

To generate the random samples of the random variables, random numbers are required (based on a uniformly distributed random variable, *U*, between 0 and 1). This is achieved by denoting *R* as a random variable that is a function of *U* as given by

$$R = a + (b - a)U \tag{65}$$

It can be proved that the following relations hold

$$F_R(r) = F_U(u) \quad or \quad r = F_R^{-1}(F_U(u)) \tag{66}$$

and

$$f_R(r) = \frac{1}{b-a} f_U(u) \; = \frac{1}{b-a} \tag{67}$$

where $F_R^{-1}(\circ)$ is the inverse distribution function of R.

After some considerations, it can be stated that a value of random variable R, r_j, is obtained by equating its CDF to the CDF of U evaluated at u_i, or

$$r_i = a + (b - a)u_i \tag{68}$$

A schematic representation of the preceding procedure, known as inverse transformation method, for a random variable X and given PDF is shown in Figure 3,

and the mathematical expression is

$$x = F_R^{-1}(F_U(u)) \tag{69}$$

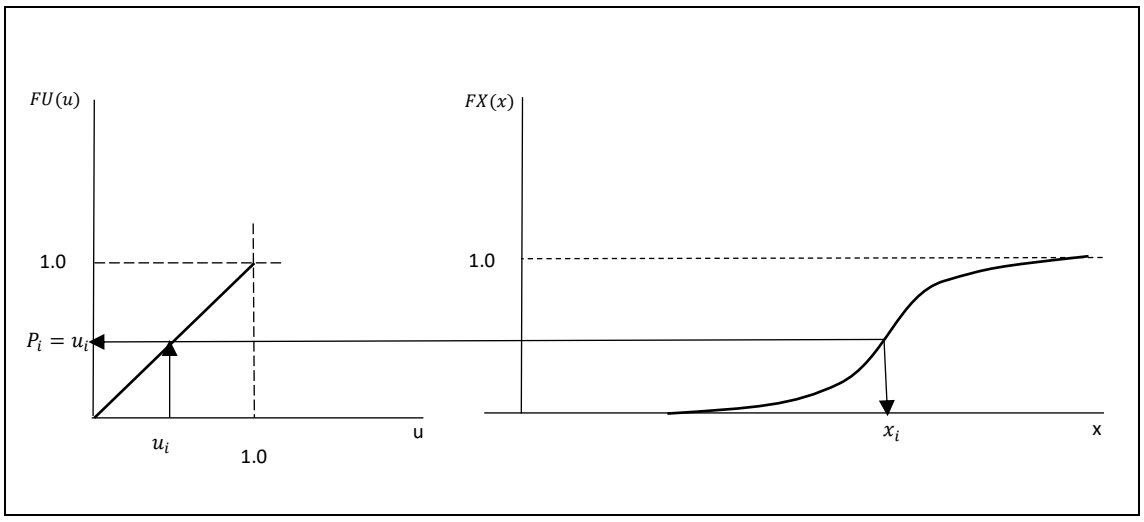

Figure 3. Inverse transformation method

When generating jointly distributed random numbers is of interest, the MCS can also be used, but some further aspects require to be addressed. This is briefly described here. When a set of x_i variables are not uncorrelated, its joint PDF can be expressed as

$$f_X(x) = f_{X1}(x_1) f_{X2}(x_2|x_1) \dots f_{Xn}(x_n|x_1, \dots, x_{n-1}) \tag{70}$$

and its CDF as

$$F_X(x) = F_{X1}(x_1) F_{X2}(x_2|x_1) \dots F_{Xn}(x_n|x_1, \dots, x_{n-1}) \tag{71}$$

Furthermore, if a set of values U generated from n independent standard uniformly distributed random variables is considered, the corresponding set of dependent random variables can be obtained with

$$\begin{cases} x_1 = F_{x_1}^{-1}(u_1) \\ \quad x_2 = F_{x_2}^{-1}(u_2|x_1) \\ \qquad \vdots \\ \quad x_n = F_{x_n}^{-1}(u_n|x_1, \dots, x_{n-1}) \end{cases} \tag{72}$$

where F-1(•) denotes the inverse of the cumulative distribution. The obtaining of this inverse of the CDF can prove to be challenging for non-common PDFs, for instance for the Longuet-Higgins distribution employed in Paper B of the compendium, where a numerical procedure is warranted.

Other techniques like importance sampling and surrogate models can be used to improve the efficiency of simulation methods. In this thesis, instead of these currently used approaches, other not so common techniques are revisited. The reader is referred to Paper B of the compendium for details.

3. Overall Discussion and General Conclusions

3.1 Conclusions

In this work metocean variables are probabilistically characterized as both, single and concurrent, random variables using extreme value theory. A variation of the so-called generalized extreme value (GEV) distribution to account for seasonal effects is used and applied to data from buoys located relatively close to Mexican coasts. The reliability of coastal systems is introduced by using methods that are common in structural engineering applications.

First an introduction is presented, followed by some theoretical background and finally the compendium of publications is included. The overall discussion and conclusions in this section are also based on the studies in the compendium and the appendix.

The specific description of the time-dependent GEV model and results by applying it to significant wave heights from buoys in the Gulf of Mexico, also used for comparison versus a buoy in the Pacific and other metocean variable (wind velocity) and other issues, includes that seasonality is introduced by using the harmonic functions to represent the annual and semiannual cycles of the extreme wave heights and that the scale, location and shape parameters in the GEV model vary from month to month. It is proved that the wave heights are seasonal, with the largest peaks in two seasons, the hurricanes and the cold fronts seasons. Seasonal significant wave heights can be projected to values associated with given return periods using the GEV model. In studies contained within this work, it is shown the ability of the time-dependent GEV model to capture the seasonal effects by comparing it against the limitations of its stationary counterpart.

The stationary and non-stationary GEV models are also applied to significant wave heights from a buoy in the Pacific and compared with the above-mentioned results for the Gulf of Mexico. The comparison of the stationary and non-stationary GEV models shows that the latter leads to a better representation of this meteocean variable, and it also leads to larger projected return period values than the former for winter season, as in the case for the Gulf of Mexico. Therefore, it is concluded that seasonality effects are also present in the Pacific Ocean, but they differ quantitatively from those in the Gulf of Mexico.

The results for significant wave height in the Pacific are also used to study the impact of including or excluding an atypically large significant wave height (due to an extraordinary hurricane). It was found that the stationary model is adequately modeled by a Frechet distribution (which can be inferred from the parameters of the GEV), and that excluding the atypical significant wave height impacts substantially in the average value and projected return period values. However, the other model parameters are somewhat unaffected in the stationary model. In contrast, by using the non-stationary GEV model, it is concluded that excluding or

including the atypical significant wave height may not affect the overall qualitative trend of the values associated with given return periods, but it does affect substantially from a quantitative standpoint. Nevertheless, excluding the atypical value may lead to a better fitting.

The used of the non-stationary GEV model is then extended to other metocean variable (wind velocity), together with the use of the classical regression technique described in the background, to investigate the correlation of maximum significant wave heights and companion wind velocities (i.e., the wind which was recorded simultaneously with the wave heights in a given buoy at the Gulf of Mexico). The time-dependent GEV models of the metocean variables are used to assess the adequacy of a proposed method to predict the wind velocity as a function of significant wave height, for a given return period. Besides, it is also explored how the time window selected to estimate return period values of metocean variables can affect the predicted return levels for some seasons. It is found that the selected time window (e.g., the first 20 years of recorded data, the whole set of data or the last 20 years of recorded data) does have an impact on projected extreme values. Nevertheless, this aspect is preliminary and it should not be categorically concluded that this is attributed to the climate change, but the time window selection for the fitting will have certainly an impact for design and engineering purposes (since the projected values change importantly). A main conclusion of this study is that correlation of significant weight height and companion wind velocity can be adequately represented by linear or power equations for given seasons (with different parameters but using the same mathematical expression), which are amenable to designers. It is also concluded that the uncertainty in the predicted associated wind velocities as a function of significant wave height is adequately evaluated by using the root mean squared error from the regression analysis. Simplified equations to very closely obtain the 95% confidence intervals of future values are proposed, which besides are also adequate to envelope the uncertainty estimated from the GEV models, for certain return period values by using an adequate value of a parameter. The proposed method is a straightforward, but effective, approach to obtain correlated metocean hazards for selected return periods. These hazards can be translated into demands imposed to a system, so that

the response can be computed for design purposes, with the additional advantage that the uncertainty is also defined.

As a final stage of this work, reliability methods developed in the 1990s are revisited and improved, using as case studies coastal and structural engineering applications. The methods are based on Monte Carlo simulations (MCS). It is mathematically defined how accurate the reliability index and other parameters are, when the number of required MCS are reduced. One method fits normality polynomials to the MCS to obtain the so-called reliability index (a measure of the probability of failure of the system), and the other method approximates the linearized limit state surface (by also using MCS) at the design point using multi-linear regression. It is concluded that a power law is adequate to represent the mean and standard deviation of the error for the probability of failure (expressed with the reliability index) as a function of the number of simulations. It allows to select a precision level, whereas reducing the number of required simulations The normality polynomial approach has also the advantage that a reliability index is always computed, regardless the number of simulations (unlike the case of the MCS); although the deviation from the exact probability of failure is important for few simulations, an intermediate level of simulations (perhaps in the order of 10^3 to 10^5) leads to smaller errors than the MCS. The multi-linear regression approach is found to be very effective to compute accurately the reliability index, provided enough MCS are carried out, while also allowing to estimate adequately the sensitivity factors and design points (from the first order reliability method, FORM, standpoint), which are normally not determined when MCS are performed. Additionally, if the tolerance in the multi-linear regression method is increased, the MCS can be reduced. It general, it is shown that the reliability methods revisited, and the additional information developed for guidance, can be successfully applied for coastal engineering structures, as for the case of the breakwater studied.

As final remarks, the findings reported in this work can be very relevant for practical applications, for instance for coastal and offshore structures, for planning, design, maintenance and other engineering activities. The selection of adequate models as those reported herein (for instance to account for seasonality) is important, since it has implications from the standpoint of designing coastal structures, management

tasks, reliability and risk assessments, as well as sustainability related issues, among others. Extending the presented studies to more buoys and other regions is recommended in order to probabilistically characterized extreme metocean activity, so that the design and management of coasts and ports by including seasonality can be improved, but also by accounting for correlated phenomena. The impact of selecting different models, for example stationary, non-stationary, different correlation schemes among the metocean variables, other metocean variables, etc., is also recommended as future research, since this could be also useful for issues as the sustainability of coasts and coast infrastructure. The proposed methods and expressions are considered adequate for practical purposes and amenable to designers, while also incorporating the seasonality effects and uncertainties in a simple way. It is also believed that further studies combining the characterization of metocean variables as time-dependent GEV models and the use of reliability approaches is a promising field of research, with an important potential to cope with practical problems related to coast and port engineering for Mexico and for other regions of the world.

3.2 Future research

The contents within the compendium of studies reported in this work can be extended and studied in more detail in different directions. Therefore, further research is recommended for (but not limited to) the following subjects:

- Extreme value analysis considering not only seasonality effects but also other effects (sometimes referred to as covariates in the literature), e.g., directionality effects.
- Explore interpolation techniques to extend the study to sites where data is unavailable (e.g., where there are no buoys), and also other approaches to account for effects for sites near the coast, where other variables as the fetch, swell, etc., may play a key role.
- Comparisons of the results using buoys data versus results that could be obtained by means of simulation techniques, global ocean wave prediction models, or other available approaches.
- The study on concurrent metocean hazards can be also extended to other variables as wave period, sea level, temperature, etc., to more than two

variables (using multiple regression), to other sites and regions, and comparisons with other techniques as environmental contours, other probabilistic models, etc., could be included in future studies.

- The employment of reliability theory to compute the probability of failure of coastal structures can be further investigated using different probabilistic characterizations of the metocean variables (including those developed in this work), as well as the capacity of coastal and maritime systems considered as random variables and including the use of other reliability techniques. In fact, it could be investigated the reliability of other types of coastal and marine systems, not only from the ultimate limit states standpoint but also from the serviceability standpoint. The reliability dependent on seasonality or other covariates can also be a subject of future research.
- Since the topics investigated in this work can have a significant impact or relevance in issues like environment, climate change, sustainability, coast management, planning and mitigation strategies, among many others, all these aspects are potentially future exploitable subjects to investigate.

4. References

1. Akaike, H., 1973. Information Theory and an Extension of the Maximum Likelihood Principle. In: Petrov, B.N., Csaki, F. (Eds.), Proceedings of the Second International Symposium on Information Theory. Akademia Kiado, Budapest, p.p. 267-281.
2. Carter, D.J.T., Challenor, P.G., 1981. Estimating return values of environmental parameters. Quarterly Journal of the Royal Meteorological Society, 107, 259-266.
3. Cavaleri, L.; Barbariol, F.; Benetazzo, A.Wind–Wave Modeling: WhereWe Are, Where to Go. J. Mar. Sci. Eng. 2020, 8, 260
4. Chakrabarti, S.K., 2001. Hydrodynamics of Offshore Structures. Computational Mechanics Publication, WIT Press, Southampton.
5. Chavez-Demoulin, V., Davison, A.C., 2005. Generalized additive modeling of sample extremes. J. R. Stat. Soc., Ser. C, Appl. Stat., pp 54.
6. Coles, S.G., 2001. An Introduction to Statistical Modelling of Extreme Values. London: Springer, 208.
7. Goldberg, D.E., 1989. Genetic Algorithms in Search, Optimization, and Machine Learning. Addison-Wesley, Reading, Mass. 372 pp.
8. Hong, H.P. Risk Analysis and Decision Making in Engineering; Course Notes; Western University: London, ON, Canada, 2008; 194p.
9. Isaacson, M., Mackenzie, N.G., 1981. Long-term distributions of ocean waves: A review. J. Waterw. Port Coastal Ocean Div. Am. Soc. Eng. 107,93–109.
10. Jack Benjamin, C. a. Cornell-Probability, Statistics, And Decisions for Civil Engineers McGraw-Hill Companies (1960)
11. Jensen, J.J., Olsen, A.S., Mansour, A.E. 2011. Extreme wave and wind response predictions. Ocean Engineering, 38, 2244-2253
12. Jönsson, A., Broman, B., Rahm, L., 2002. Variations in the Baltic Sea wave fields. Ocean Engineering, 30, 107-126.
13. Jordaan, I. Decisions under Uncertainty: Probabilistic Analysis for Engineering Decisions, 1st ed.; Cambridge University Press: Cambridge, UK, 2005; pp. 1–672.
14. Katz, R.W., Parlange, M.B., Naveau, P., 2002. Statistics of Extreme in Hydrology. Adv. Water Resour., 25, 1287-1304.
15. Kottegoda, N.T.; Rosso, R. Applied Statistics for Civil and Environmental Engineers, 2nd ed.; Blackwell Publishing-Wiley: Oxford, UK, 2008; pp. 1–718.
16. Leadbetter MR, Lindgrem G, Rootzén H. Extremes and related properties of random sequences and series. Springer. Verlag, New York; 1983.
17. Lettenmaier, D.P., Burges, S.J., 1982. Gumbel's extreme value 1 distribution, a new look, J. Hydraulics Division – ASCE 108, 502-504.

18. Madsen, H.O.; Krenk, S.; Lind, N.C. Methods of Structural Safety; Prentice-Hall, Inc.: Englewood Cliffs, NJ, USA, 1986.
19. Martucci, G., Carniel, S., Chiggiato, J., Sclavo, M., Lionello, P., Galati, M.B., 2010. Statistical trend analysis and extreme distribution of significant wave height from 1958 to 1999 – an application to the Italian Seas. Ocean Sci., 6, 525–538.
20. Mazas, F., Hamm, L., 2011. Multi-distribution approach to POT methods for determining extreme wave heights. Coastal Engineering, 58, Issue 5, 385-394.
21. Mendez, F. J., Menéndez ,M.,Luceño, Losada, I. J. ,2007. Analyzing monthly extreme sea levels with a time-dependent GEV model .Journal of Atmospheric and Oceanic Technology 24,894–911.
22. Méndez, F.J., Menéndez, M. Luceño, A., Medina, R., Graham. N.E. 2008. Seasonality and duration in extreme value distributions of significant wave height. Ocean Engineering, 35, Issue 1, 131-138.
23. Menéndez, M., Graham N.E., Méndez F., Losada, I., 2007. Long-term Trends in Extreme Significant Wave Height in the Northeast Pacific Ocean - an Application of Extreme Value Theory. EGU General Assembly.
24. Menéndez, M., Méndez, F. J., Izaguirre, C., Luceño, A., Losada, I. J., 2009. The influence of seasonality on estimating return values of significant wave height. Costal Engineering, vol. 56, pp 211-219.
25. Mietus, M., 1998. The Climate of the Baltic Sea Basin. Marine meteorology and related oceanographic activities. Report No. 41, World Meteorological Organisation, Geneva, 64 pp.
26. Morton, I.D., Bowers, J., Mould, G., 1997. Estimating return period wave heights and wind speeds using a seasonal point process model. Coastal Eng., 31, 305-326.
27. Muir, J.R., ElShaarawi, A.H., 1986. On the calculation of extreme wave heights, a review. Ocean Engineering 13,93–118.
28. Muraleedharan, G., Lucas, C., Soares, C.G., et al. 2012. Modelling significant wave height distributions with quantile functions for estimation of extreme wave heights. Ocean Engineering, 54, 119-131.
29. Prevosto, M., Krogstad, H.E., Robin, A., 2000. Probability distributions for maximum wave and crest heights. Coastal Engineering 40, 329–360
30. Prpiĉ-Orsîc, J., Dejhalla, R., Turk, A., 2007. Design sea state assessment using genetic algoritm approach. Ocean Engineering 34, 148-156
31. Räämet, A., Soomere, T., 2010. The Wave Climate and Its Seasonal Variability in the Northeastern Baltic Sea. Estonian Journal of Earth Sciences.

32. Räämet, A., Soomere, T., 2010. The Wave Climate and Its Seasonal Variability in the Northeastern Baltic Sea. Estonian Journal of Earth Sciences.
33. Rosenblueth, E.; Esteva, L. Reliability basis for some Mexican codes. Am. Concr. Inst. Spec. Publ. 1972, 31, 1– 42.
34. Soares, C.G, Carvalho, A.N., 2012. Probability distributions of wave heights and periods in combined sea-states measured off the Spanish coast. Ocean Engineering, 52, 13-21.
35. Solari, S., Losada, M.A., 2012. Unified distribution models for met-ocean variables: Application to series of significant wave height. Coastal Engineering, 68, 67-77.
36. Stansell, P., 2005. Distributions of extreme wave, crest and trough heights measured in the North Sea. Ocean Engineering, 32, 1015-1036
37. Tayfun, M.A., Fedele, F., 2007. Wave-height distributions and nonlinear effects. Ocean Engineering, Volume 34, Issues 11–12, 1631–1649.

4.1 References Paper A

1. Castillo, E.; Hadi, A.S.; Balakrishnan, N.; Sarabia, J.M. Extreme value and related models with applications in engineering and science; Wiley, 2004; 4. 1-362.
2. Hong, H.P. Estimate of extreme wind and wave loading and safety level of offshore structures. Risk Analysis, Proceedings of a Symposium, 11-12 August, University of Michigan, Ann Arbor, Michigan, USA, 1994; 4. 107-117.
3. Nessim, M.A.; Hong, H.P.; Swail, V.R.; Henderson, C.A. Design criteria for offshore structures under combined wind and wave loading. Journal of Offshore Mechanics and Arctic Engineering 1995. 117(1), 4 1-11.
4. Stephens, S.A.; Bell, R.G.; Lawrence, J. Applying Principles of Uncertainty within Coastal Hazard Assessments to Better Support Coastal Adaptation. J. Mar. Sci. Eng. 2017, 5, 40.
5. Di Risio, M.; Bruschi, A.; Lisi, I.; Pesarino, V.; Pasquali, D. Comparative Analysis of Coastal Flooding Vulnerability and Hazard Assessment at National Scale. J. Mar. Sci. Eng. 2017, 5, 51.
6. Gallotti, G.; Ventura, G.; Armigliato, A.; Zaniboni, F.; Pagnoni, G.; Wang, L.; Passaro, S.; Sacchi, M.; Tinti, S. Stability analysis and tsunamigenic mass-failure scenarios in Palinuro volcano complex, Tyrrhenian Sea. Proceedings of a European Geosciences Union, EGU 2020, On-line acce11, 2020; https://doi.org/10.5194/egusphere-egu2020-8270.
7. Wang, T.; Yang, Z.; Wu, W.-C.; Grear, M. A Sensitivity Analysis of the Wind Forcing Effect on the Accuracy of Large-Wave Hindcasting. J. Mar. Sci. Eng. 2018, 6, 139.

8. Wang, Y.; Zhang, L.; Michailides, C.; Wan, L.; Shi, W. Hydrodynamic Response of a Combined Wind–Wave Marine Energy Structure. J. Mar. Sci. Eng. 2020, 8, 253.
9. Sierra, J.P.; White, A; Mösso, C; Mestres, M. Assessment of the intra-annual and inter-annual variability of the wave energy resource in the Bay of Biscay (France). Energy. 2017, 141, 853.
10. Sierra, J.P.; Martín, C.; Mösso, C; Mestres, M; Jebbad, R. Wave energy potential along the Atlantic coast of Morocco. Renewable Energy. 2016, 96, 20.
11. Sierra, J.P.; Mösso, C.; González-Marco, D. Wave energy resource assessment in Menorca (Spain). Renewable Energy. 2014, 71, 51.
12. Sierra, J.P.; Casas-Prat, M; Virgili, M; Mösso, C; Sánchez-Arcilla, A. Impacts on wave-driven harbour agitation due to climate change in Catalan ports. Natural Hazards and Earth System Sciences. 2015, 15(8), 1695.
13. Sierra, J.P; Genius, A; Lionello, P; Mestres, M; Mösso, C; Marzo, L. Modelling the impact of climate change on harbour operability: The Barcelona port case study. Ocean Engineering. 2017, 141, 64.
14. Lin-Ye, J.; García-León, M.; Gràcia, V.; Ortego, M.I.; Lionello, P.; Conte, D.; Pérez-Gómez, B.; Sánchez-Arcilla, A. Modeling of Future Extreme Storm Surges at the NW Mediterranean Coast (Spain). Water 2020, 12, 472.
15. Ludeno, G.; Serafino, F. Estimation of the Significant Wave Height from Marine Radar Images without External Reference. J. Mar. Sci. Eng. 2019, 7, 432.
16. Chen, S.-T.; Wang, Y.-W. Improving Coastal Ocean Wave Height Forecasting during Typhoons by using Local Meteorological and Neighboring Wave Data in Support Vector Regression Models. J. Mar. Sci. Eng. 2020, 8, 149.
17. Gao, H.; Shao, Z.; Wu, G.; Li, P. Study of Directional Declustering for Estimating Extreme Wave Heights in the Yellow Sea. J. Mar. Sci. Eng. 2020, 8, 236.
18. Katalinić, M.; Parunov, J. Uncertainties of Estimating Extreme Significant Wave Height for Engineering Applications Depending on the Approach and Fitting Technique—Adriatic Sea Case Study. J. Mar. Sci. Eng. 2020, 8, 259.
19. Cavaleri, L.; Barbariol, F.; Benetazzo, A. Wind–Wave Modeling: Where We Are, Where to Go. J. Mar. Sci. Eng. 2020, 8, 260.
20. Weisse, R.; Gaslikova, L.; Geyer, B.; Groll, N.; Meyer, E. Coastdat - Model data for science and industry. Kuste, Westholsteinische Verlagsanstalt Boyens und Co. 2014, Issue 81, 5.
21. Weisse, R.; Groll, N. A multi-decadal wind-wave hindcast for the North Sea 1949-2014: CoastDat2. Earth System Science Data. 2017, 9(2), 955.

22. Ross, E.; Astrup, O. C.; Bitner-Gregersen, E.; Bunn N.; Feld, G.; Gouldby, B.; Liu, Y.; Randell, D.; Vanem, E.; Jonathan, P. On environmental contours for marine and coastal design. Ocean Engineering. 2020, 195, 1.
23. Vanem, E. A simple approach to account for seasonality in the description of extreme ocean environments. Mar Syst Ocean Technol. 2018, 13, 63.
24. Randell, D.; Feld, G; Ewans, K.; Jonathan, P. Distributions of return values for the ocean wave characteristics in the South China Sea using directional-seasonal extreme value analysis. Environmetrics. 2015, 26, 442.
25. Randell, D.; Turnbull, K.; Ewans, K.; Jonathan, P. Bayesian inference for nonstationary marginal extremes. Environmetrics. 2016, 27, 439.
26. Ross, E.; Randell, D.; Ewans, K.; Feld, G.; Jonathan, P. Efficient estimation of return value distributions from non-stationary marginal extreme value models using Bayesian inference. Ocean Eng. 2017, 142, 315.
27. Anokhin, V.; Randell, D.; Ross, E.; Jonathan, P. Spatial and seasonal variability of metocean design criteria in the southern south China Sea from covariate extreme value analysis. Proceedings of the ASME 2019 38th International Conference on Ocean, Offshore and Artic Eng., OMAE, Glasgow, Scotland, UK. 2019, 1.
28. Bitner-Gregersen, E. M. Comparison of wind and wave climate in open sea and coastal waters. Ocean Eng. 2018, 170, 199.
29. National Data Buoy Center (NDBC), website www.ndbc.noaa.gov (last accessed on June 2020).
30. Calderón-Vega, F; Vázquez-Hernández, A.O.; García-Soto, A.D. Analysis of extreme waves with seasonal variation in the Gulf of Mexico using a time-dependent GEV model. Ocean Eng 2013, 73, 68-82. DOI: 10.1016/j.oceaneng.2013.08.007.
31. Coles, S.G. An Introduction to Statistical Modelling of Extreme Values, 1st ed.; Springer-Verlag: London, UK, 2001; 4. 1-208.
32. Calderón Vega, F. Caracterización del Régimen Extremal del Oleaje en el Golfo de México Considerando la Variación Estacional. 2019. Santander, España. Tesis de Máster Universitario de Ingeniería de Costas y Puertos. Universidad de Cantabria (in Spanish).
33. Bitner-Gregersen, Elzbieta M., and Gramstad, Odin. "Potential Changes in the Joint Probabilistic Description of the North Atlantic Wave Climate." Proceedings of the ASME 2018 37th International Conference on Ocean, Offshore and Arctic Engineering. Volume 11B: Honoring Symposium for Professor Carlos Guedes Soares on Marine Technology and Ocean Engineering. Madrid, Spain. June 17–22, 2018. V11BT12A056. ASME. https://doi.org/10.1115/OMAE2018-77592.

34. Hong, H.P.; Zimmerman, T.J.; Bach, L. Probabilistic basis of resistance factors for use in oriented strand board. Proceedings of the 1st Structural Specialty Conference, Canadian Society of Civil Engineering, Edmonton, Alberta, Canada. 1996, 1223-1235.
35. Jordaan, I. Decisions under Uncertainty: Probabilistic Analysis for Engineering Decisions, 1st ed.; Cambridge University Press: Cambridge, UK, 2005; pp. 1-672.
36. Kottegoda, N.T; Rosso, R. Applied Statistics for Civil and Environmental Engineers, 2nd ed.; Blackwell Publishing-Wiley: Oxford, UK, 2008; pp. 1-718.
37. Faber, M.H. Statistics and Probability Theory: in Pursuit of Engineering Decision Support, 2nd ed.; Springer: Dordrecht, Heidelberg, London, New York, 2012; pp. 1-190.

4.2 References Paper B

1. Sudret, B. Surrogate-assisted reliability-based design optimization: A survey and a unified modular framework. Struct. Multidiscip. Optim. 2109, 60, 2157.
2. Straub, D.; Schneider, N.; Bismut, E.; Kim, H. Reliability analysis of deteriorating structural systems. Struct. Saf. 2020, 82, 101877.
3. Leira, B.; Thöns, S.; Faber, M.H. Reliability assessment of a bridge structure subjected to chloride attack. Struct. Eng. Int. 2018, 28, 318–324.
4. Gong, C.; Zhou, W. Importance sampling-based system reliability analysis of corroding pipelines considering multiple failure modes. Reliab. Eng. Syst. Safe. 2018, 169, 199.
5. Huang, P.; Huang, H.-Z.; Huang, T. A Novel Algorithm for Structural Reliability Analysis Based on Finite Step Length and Armijo Line Search. Appl. Sci. 2019, 9, 2546.
6. Biagi, V.D.; Kiakojouri, F.; Chiaia, B.; Sheidaii, M.R. A Simplified Method for Assessing the Response of RC Frame Structures to Sudden Column Removal. Appl. Sci. 2020, 10, 3081.
7. Marchelli, M.; Biagi, V.D.; Peila, D. Reliability-Based Design of Protection Net Fences: Influence of Rockfall Uncertainties through a Statistical Analysis. Geosciences 2020, 10, 280.
8. Biagi, V.D.; Marchelli, M.; Peila, D. Reliability Analysis and Partial Safety Factors Approach for Rockfall Protection Structures. Eng. Struct. 2020, 213, 110553.
9. Naseri, M.; Barabady, J. An Expert-Based Model for Reliability Analysis of Arctic Oil and Gas Processing Facilities. ASME J. Offshore Mech. Arct. Eng. 2016, 138, 051602.
10. Losada, M.A. ROM 0.0, Puertos del Estado Level II and III Verification Methods. In General Procedure and Requirements in the Design of Harbor and Maritime

Structures, Part I, 1st ed; Puertos del Estado: Madrid, Spain, 2002; Volume 1, pp. 160–185.
11. Hong, H.P. Application of polynomial transformation to normality in structural reliability analysis. Can. J. Civ. Eng. 1998, 25, 241.
12. Hong, H.P.; Nessim, M. The development of a design point and sensitivity factors from simulation results. In Proceedings of the sixth international conference on applications of statistics and probability in civil engineering, CERRA-ICASP 6, Mexico City, Mexico, 17–21 June 1991; pp. 313–319.
13. Hong, H.P.; Lind, N. Approximate reliability analysis using normal polynomial and simulation results. Struct. Saf. 1996, 18, 329.
14. Lima-Castillo, I.F.; Gómez-Martínez, R.; Pozos-Estrada, A. Methodology to Develop Fragility Curves of Glass Façades under Wind-Induced Pressure. Int. J. Civ. Eng. 2019, 17, 347.
15. Hall, P. Inverting an Edgeworth expansion. Ann. Stat. 1983, 11, 569.
16. Kendall, M.; Stuart, A.; Ord, J.K. Kendall's Advance Theory of Statistics; Oxford University Press: New York, NY, USA, 1987; Volume I.
17. Madsen, H.O.; Krenk, S.; Lind, N.C. Methods of Structural Safety; Prentice-Hall, Inc.: Englewood Cliffs, NJ, USA, 1986.
18. Lind, N.C. Information Theory and maximum product spacings estimation. J. R. Stat. Soc. B 1994, 56, 341– 343.
19. Lind, N.C. Statistical method for concrete quality control. In Proceeding of the 2nd International Colloquia on Concrete in Developing Countries, Bombay, India, 3-8 January 1998; Volume 1, pp 21–26.
20. Longuet-Higgins, M.S. On the Joint Distribution of Wave Periods and Amplitudes in a Random Wave Field. Proc. R. Soc. Lond. 1983, 389, 241.
21. Rosenblueth, E.; Esteva, L. Reliability basis for some Mexican codes. Am. Concr. Inst. Spec. Publ. 1972, 31, 1– 42.
22. Hong, H.P. Risk Analysis and Decision Making in Engineering; Course Notes; Western University: London, ON, Canada, 2008; 194p.
23. García-Soto, A.D.; Hernández-Martínez, A.; Valdés-Vazquez, J.G. Reliability analysis of reinforced concrete beams subjected to bending using different methods and design codes. Struct. Eng. Int. 2017 27, 300–307.
24. American Concrete Institute (ACI). Building Code Requirements for Structural Concrete; ACI 318-14; American Concrete Institute (ACI): Farmington Hills, MI, USA, 2014.

25. Zhang, H.D.; Soares, C.G. Modified Joint Distribution of Wave Heights and Periods. China Ocean Eng. 2016, 30, 359.
26. Nowak, A.S.; Collins, K.R. Reliability of Structures, 1st ed.; Mc Graw-Hill: Boston, MA, USA, 2000; pp. 120–129.

4.3 References Paper C

1. Shao, Z.; Liang, B.; Li, H.; Lee, D. Study of sampling methods for assessment of extreme significant wave heights in the South China Sea. Ocean Eng 2018, 168, 173-184. DOI: 10.1016/j.oceaneng.2018.09.015.
2. Vanem, E. Non-stationary extreme value models to account for trends and shifts in the extreme wave climate due to climate change. Appl Ocean Res 2015, 52, 201-211. DOI: 10.1016/j.apor.2015.06.010.
3. Feld, G.; Randell, D.; Wu, Y.; Ewans, K.; Jonathan, P. Estimation of storm peak and intrastorm directional-seasonal design conditions in the North Sea. Journal of Offshore Mechanics and Arctic Engineering 2015. 137(2), 021102, DOI: 10.1115/1.4029639.
4. Shao, Z.; Liang, B.; Li, H.; Wu, G.; Wu, Z. Blended wind fields for wave modeling of tropical cyclones in the South China Sea and East China Sea. Appl Ocean Res 2018, 71, 20-33. DOI: 10.1016/j.apor.2017.11.012.
5. Kapelonis, Zacharias G.; Gavriliadis, Panagiotis N.; Athanassoulis, Gerassimos A.; Extreme value análisis of dynamical wave climate projections in the Mediterranean Sea. Procedia Computer Science. YSC 4Th International Young Scientists Conference on Computacional Science, 2015, 66, 210-219.
6. Chaplin, R.G. Abrasion resistant concrete floors. Advances in Concrete Slab Technology. Ed. R.K. Dhir and J.G.L. Munday. 1980, 164-72.
7. Chaplin, R.G. The influence of cement replacement materials. Fine Agregate and curing on the abrasion resistance of industrial concrete floor slabs. Cement and Concrete Association , Slough, UK. 1986, 32.
8. Bortkiewicz, L., von Variationsbreite und mittlerer Fehler, Sitzungsber. Berli. Math. Ges. 1922, 21, 3-11.
9. Dodd, E. L.; The greatest and the least variate under general laws of error. Tans.Amer.Math Soc. 1923, 25, 525-39.
10. Tippett, L.H.C.; on the extreme individuals and the range of samples taken from a normal population, Biometrika, 1925, 17,364_387 https://doi.org/10.1093/biomet/17.3-4.364.
11. Fréchet, M. Sur la loi de probabilité de l'écart maximum, Ann. Soc. Polon. Math. Cracovie. 1957, 6, 93-116.

12. Fisher, R.A. and Tippett, L.H.C. Limiting Forms of the Frequency Distribution of the Largest or Smallest Members of a Sample. Proceedings of the Cambridge Philosophical Society,1928, 24, 180-190.
13. De Finetti, B., Obry, S. L'optimum nella misura del riscatto, Atti del II Congresso Nazionale di Scienza delle Assicurazioni, 1932, Vol. 2, Bardi, Trieste, Rome. 99–123
14. Gumbel, E.J. Statistical theory of extreme values and some practical applications. Applied Mathematics 1954 Series. 33 (1st ed.) U.S. Department of Commerce, National Bureau of Standards.
15. Gumbel, E.J. Les valeurs extrêmes des distributions statistiques. Annales de l'Institut Henri Poincaré, 1935, 5, pp.115-158.
16. Mises, R. von. (1936) La distribution de la plus grande de n valeurs. Amer. Math. Soc Reproduced in Selected Papers of Richard von Mises, II 1954, pp. 271-294.
17. Rice, J. Mathematical Statistics and Data Analysis. 2nd ed. Duxbury.1994.
18. Gnedenko, B. Sur la distribution limite du terme maximum d'une série aléatoire. Springer-Verlag, 1943, pp. 195-225.
19. Gumbel, E. J. Statistics of Extremes, Columbia University Press. 1958.
20. Galambos, J. The Asymptotic Theory of Extreme Order Statistics, Robert E. Krieger. Malabar, Florida. 2nd ed. 1987.
21. Leadbetter, M. R., Lindgrem, G., Rootzén, H. Extremes and Related Properties of Random Sequences and Series. Springer. Verlag, New York. 1983.
22. Coles, S.G. An Introduction to Statistical Modelling of Extreme Values, 1st ed.; Springer-Verlag: London, UK, 2001; pp. 1-208.
23. Katz, R.W. Stochastic modeling of hurricane damage. J. of App. Meteor., 2002, 41, pp. 754-762.
24. Johathan, P.; Ewans, K. Statistical modelling of extreme ocean environments for marine design: A review. Ocean Eng 2013, 91-109 DOI: 10.1016/j.oceaneng.2013.01.004
25. Calderón-Vega, F; Vázquez-Hernández, A.O.; García-Soto, A.D. Analysis of extreme waves with seasonal variation in the Gulf of Mexico using a time-dependent GEV model. Ocean Eng 2013, 73, 68-82. DOI: 10.1016/j.oceaneng. 2013.08.007.
26. Sanchez-Arcilla A.; Sierra, J.P.; Gracia, V.; Garcia, M.; Jimenez, J.A.; Mösso, C.; Valdemoro, H. Coastal sustainability for uncertain futures: a Spanish Mediterranean case from the RISES-AM project. A: Intenational Association for Hydraulic Research Congress. E-proceedings of the 36th IAHR World Congres. L'Haia, 2015 pp. 1-8.

27. Sanchez-arcilla, A.; Sierra, J.P.; Mösso, C.; Gracia, V.; Garcia, M. Progress on climate change detection and projections over Spain since the findings of the IPCC AR5. International Symposium CLIMATE-ES 2015; pp. 146.
28. Castillo E., Hadi A.S., Balakrishnan N., Sarabia J.M. Extreme Value and Related Models with Applications in Engineering and Science. 2005. Wiley-Interscience. New Jersey.
29. Menéndez, M.; Méndez, F.J.; Izaguirre, C.; Luceño, A.; Losada, I.J. The influence of seasonality on estimating return values of significant wave height. Ocean Eng 2009 56, pp. 211-219. DOI: 10.1016/j.coastaleng.2008.07.004.
30. Panchang, V.; Kwon Jeong Ch.; Demirbilek, Z. Analyses of extreme wave heights in the Gulf of Mexico for offshore engineering applications. J Offshore Mech Arct 2013, 135(3), pp. 1-15.

4.4 References Paper D

1. Akaike, H., 1973. Information Theory and an Extension of the Maximum Likelihood Principle. In: Petrov, B.N., Csaki, F. (Eds.), Proceedings of the Second International Symposium on Information Theory. Akademia Kiado, Budapest, p.p. 267-281.
2. Carter, D.J.T., Challenor, P.G., 1981. Estimating return values of environmental parameters.
3. Quarterly Journal of the Royal Meteorological Society, 107, 259-266.
4. Chakrabarti, S.K., 2001. Hydrodynamics of Offshore Structures. Computational Mechanics Publication, WIT Press, Southampton.
5. Coles, S.G., 2001. An Introduction to Statistical Modelling of Extreme Values. London: Springer, 208.
6. Isaacson, M., Mackenzie, N.G., 1981. Long-term distributions of ocean waves: A review. J. Waterw. Port Coastal Ocean Div. Am. Soc. Eng. 107,93–109.
7. Jensen, J.J., Olsen, A.S., Mansour, A.E. 2011. Extreme wave and wind response predictions. Ocean Engineering, 38, 2244-2253
8. Jönsson, A., Broman, B., Rahm, L., 2002. Variations in the Baltic Sea wave fields. Ocean Engineering, 30, 107-126.
9. Katz, R.W., Parlange, M.B., and Naveau, P. 2002. Statistics of Extreme in Hydrology. Adv. Water Resour., 25, 1287-1304.
10. Leadbetter, M.R., Lindgrem, G., Rootzén, H., 1983. Extremes and Related Properties of Random Sequences and Series. Springer. Verlag, New York.
11. Lettenmaier, D. P. y Burges, S. J.(1982) Gumbel's extreme value 1 distribution, a new look, J. Hydraulics Division – ASCE 108, 502-504.

12. Mackay, E.B.L., Challenor, P.G., Bahaj, A.S. 2010. On the use of discrete seasonal and directional models for the estimation of extreme wave conditions. Ocean Engineering, 37, Issues 5–6, 425-442.
13. Martucci, G., Carniel, S., Chiggiato, J., Sclavo, M., Lionello, P., Galati, M.B., 2010. Statistical trend analysis and extreme distribution of significant wave height from 1958 to 1999 – an application to the Italian Seas. Ocean Sci., 6, 525–538.
14. Mazas, F., Hamm, L. 2011. Multi-distribution approach to POT methods for determining extreme wave heights. Coastal Engineering, 58, Issue 5, 385-394.
15. Méndez, F.J., Menéndez, M. Luceño, A., Medina, R., Graham. N.E. 2008. Seasonality and duration in extreme value distributions of significant wave height. Ocean Engineering, 35, Issue 1, 131-138.
16. Mendez F.J., Menéndez, M. Luceño and Losada, I.J. 2007. Analyzing monthly Extreme Sea Levels with a Time-Dependent GEV Model. Journal of Atmospheric and Oceanic Tecnology. 24, 894-911.
17. Menéndez, M., (2007) Metodología para el Análisis Estadístico No Estacionario de Valores Extremos de Variables Geofísicas. Ph.D Thesis (In Spanish). University of Cantabria.
18. Menéndez, M., Graham N.E., Méndez F., Losada, I., 2007. Long-term Trends in Extreme Significant Wave Height in the Northeast Pacific Ocean - an Application of Extreme Value Theory. EGU General Assembly.
19. Mietus, M., 1998. The Climate of the Baltic Sea Basin. Marine meteorology and related oceanographic activities. Report No. 41, World Meteorological Organisation, Geneva, 64 pp.
20. Morton, I.D., Bowers, J., Mould, G., 1997. Estimating return period wave heights and wind speeds using a seasonal point process model. Coastal Eng., 31, 305-326.
21. Muir, J.R., ElShaarawi, A.H., 1986. On the calculation of extreme wave heights, a review. Ocean Engineering 13,93–118.
22. Muraleedharan, G., Lucas, C., Soares, C.G., et al. 2012. Modelling significant wave height distributions with quantile functions for estimation of extreme wave heights. Ocean Engineering, 54, 119-131.
23. Panchang, V.G., Li, D., 2006. Large Waves in the Gulf of Mexico Caused by Hurricane Ivan. American Meteorological Society.
24. Prevosto, M., Krogstad, H.E., Robin, A. 2000. Probability distributions for maximum wave and crest heights. Coastal Engineering 40, 329–360
25. Prpiĉ-Orsîc, J., Dejhalla, R., Turk, A., 2007. Design sea state assessment using genetic algoritm approach. Ocean Engineering 34, 148-156.

26. Räämet, A., Soomere, T., 2010. The Wave Climate and Its Seasonal Variability in the Northeastern Baltic Sea. Estonian Journal of Earth Sciences.
27. Soares, C.G, Carvalho, A.N. 2012. Probability distributions of wave heights and periods in combined sea-states measured off the Spanish coast. Ocean Engineering, 52, 13-21.
28. Solari, S., Losada, M.A. 2012. Unified distribution models for met-ocean variables: Application to series of significant wave height . Coastal Engineering, 68, 67-77.
29. Stansell, P. 2005. Distributions of extreme wave, crest and trough heights measured in the North Sea. Ocean Engineering, 32, 1015-1036.
30. Tayfun, M.A., Fedele, F. 2007. Wave-height distributions and nonlinear effects. Ocean Engineering, Volume 34, Issues 11–12, 1631–1649.

4.5 References Book Chapter 1

1. Shao, Z.; Liang, B.; Li, H.; Lee, D. Study of sampling methods for assessment of extreme significant wave heights in the South China Sea. Ocean Eng 2018, 168, 173-184. DOI: 10.1016/j.oceaneng.2018.09.015.
2. Vanem, E. Non-stationary extreme value models to account for trends and shifts in the extreme wave climate due to climate change. Appl Ocean Res 2015, 52, 201-211. DOI: 10.1016/j.apor.2015.06.010.
3. Feld, G.; Randell, D.; Wu, Y.; Ewans, K.; Jonathan, P. Estimation of storm peak and intrastorm directional-seasonal design conditions in the North Sea. Journal of Offshore Mechanics and Arctic Engineering 2015. 137(2), 021102, DOI: 10.1115/1.4029639.
4. Shao, Z.; Liang, B.; Li, H.; Wu, G.; Wu, Z. Blended wind fields for wave modeling of tropical cyclones in the South China Sea and East China Sea. Appl Ocean Res 2018, 71, 20-33. DOI: 10.1016/j.apor.2017.11.012.
5. Kapelonis, Zacharias G.; Gavriliadis, Panagiotis N.; Athanassoulis, Gerassimos A.; Extreme value análisis of dynamical wave climate projections in the Mediterranean Sea. Procedia Computer Science. YSC 4Th International Young Scientists Conference on Computacional Science, 2015, 66, 210-219.
6. Chaplin, R.G. Abrasion resistant concrete floors. Advances in Concrete Slab Technology. Ed. R.K. Dhir and J.G.L. Munday. 1980, 164-72.
7. Chaplin, R.G. The influence of cement replacement materials. Fine Agregate and curing on the abrasion resistance of industrial concrete floor slabs. Cement and Concrete Association, Slough, UK. 1986, 32.

8. Bortkiewicz, L., von Variationsbreite und mittlerer Fehler, Sitzungsber. Berli. Math. Ges. 1922, 21, 3-11.
9. Dodd, E. L.; The greatest and the least variate under general laws of error. Tans.Amer.Math Soc. 1923, 25, 525-39.
10. Tippett, L.H.C.; on the extreme individuals and the range of samples taken from a normal population, Biometrika, 1925, 17,364_387 https://doi.org/10.1093/biomet/17.3-4.364
11. Fréchet, M. Sur la loi de probabilité de l'écart maximum, Ann. Soc. Polon. Math. Cracovie. 1957, 6, 93-116.
12. Fisher, R.A. and Tippett, L.H.C. Limiting Forms of the Frequency Distribution of the Largest or Smallest Members of a Sample. Proceedings of the Cambridge Philosophical Society,1928, 24, 180-190.
13. De Finetti, B., Obry, S. L'optimum nella misura del riscatto, Atti del II Congresso Nazionale di Scienza delle Assicurazioni, 1932, Vol. 2, Bardi, Trieste, Rome. 99–123
14. Gumbel, E.J. Statistical theory of extreme values and some practical applications. Applied Mathematics 1954 Series. 33 (1st ed.) U.S. Department of Commerce, National Bureau of Standards.
15. Gumbel, E.J. Les valeurs extrêmes des distributions statistiques. Annales de l'Institut Henri Poincaré, 1935, 5, pp.115-158.
16. Mises, R. von. (1936) La distribution de la plus grande de n valeurs. Amer. Math. Soc Reproduced in Selected Papers of Richard von Mises, II 1954, pp. 271-294.
17. Rice, J. Mathematical Statistics and Data Analysis. 2nd ed. Duxbury.1994.
18. Gnedenko, B. Sur la distribution limite du terme maximum d'une série aléatoire. Springer-Verlag, 1943, pp. 195-225.
19. Gumbel, E. J. Statistics of Extremes, Columbia University Press. 1958.
20. Galambos, J. The Asymptotic Theory of Extreme Order Statistics, Robert E. Krieger. Malabar, Florida. 2nd ed. 1987.
21. Leadbetter, M. R., Lindgrem, G., Rootzén, H. Extremes and Related Properties of Random Sequences and Series. Springer. Verlag, New York. 1983.
22. Coles, S.G. An Introduction to Statistical Modelling of Extreme Values, 1st ed.; Springer-Verlag: London, UK, 2001; pp. 1-208.
23. Katz, R.W. Stochastic modeling of hurricane damage. J. of App. Meteor., 2002, 41, pp. 754-762.
24. Johathan, P.; Ewans, K. Statistical modelling of extreme ocean environments for marine design: A review. Ocean Eng 2013, 91-109 DOI: 10.1016/j.oceaneng.2013.01.004

25. Calderón-Vega, F; Vázquez-Hernández, A.O.; García-Soto, A.D. Analysis of extreme waves with seasonal variation in the Gulf of Mexico using a time-dependent GEV model. Ocean Eng 2013, 73, 68-82. DOI: 10.1016/j.oceaneng. 2013.08.007.
26. Sanchez-Arcilla A.; Sierra, J.P.; Gracia, V.; Garcia, M.; Jimenez, J.A.; Mösso, C.; Valdemoro, H. Coastal sustainability for uncertain futures: a Spanish Mediterranean case from the RISES-AM project. A: Intenational Association for Hydraulic Research Congress. E-proceedings of the 36th IAHR World Congres. L'Haia, 2015 pp. 1-8.
27. Sanchez-arcilla, A.; Sierra, J.P.; Mösso, C.; Gracia, V.; Garcia, M. Progress on climate change detection and projections over Spain since the findings of the IPCC AR5. International Symposium CLIMATE-ES 2015; pp. 146.
28. Calderón-Vega, F., Mösso, C., García-Soto, A. D., & Delgadillo-Ruiz, E. (2019). Single Site Extreme Wave Analysis in the Pacific Ocean Comparing Stationary and Non-stationary GEV Models. Current Journal of Applied Science and Technology, 32(6), 1-12. https://doi.org/10.9734/cjast/2019/v32i630038.
29. Menéndez, M.; Méndez, F.J.; Izaguirre, C.; Luceño, A.; Losada, I.J. The influence of seasonality on estimating return values of significant wave height. Ocean Eng 2009 56, pp. 211-219. DOI: 10.1016/j.coastaleng.2008.07.004.
30. Castillo E., Hadi A.S., Balakrishnan N., Sarabia J.M. Extreme Value and Related Models with Applications in Engineering and Science. 2005. Wiley-Interscience. New Jersey.
31. Panchang, V.; Kwon Jeong Ch.; Demirbilek, Z. Analyses of extreme wave heights in the Gulf of Mexico for offshore engineering applications. J Offshore Mech Arct 2013, 135(3), pp. 1-15.

4.6 References Book Chapter 2

1. Shao Z, Liang B, Li H, Lee D. Study of sampling methods for assessment of extreme significant wave heights in the South China Sea. Ocean Eng. 2018;168:173-184. DOI: 10.1016/j.oceaneng.2018.09.015.
2. Coles SG. An introduction to statistical modelling of extreme values. 1st ed.; Springer-Verlag: London, UK. 2001;1-208.
3. Katz RW. Stochastic modeling of hurricane damage. J. of App. Meteor. 2002;41:754-762.
4. Johathan P, Ewans K. Statistical modelling of extreme ocean environments for marine design: A review. Ocean Eng. 2013;91-109 DOI: 10.1016/j.oceaneng.2013.01.004

5. Calderón-Vega F, Vázquez-Hernández AO, García-Soto AD. Analysis of extreme waves with seasonal variation in the Gulf of Mexico using a time-dependent GEV model. Ocean Eng. 2013;73:68-82. DOI: 10.1016/j.oceaneng. 2013.08.007.
6. Sanchez-Arcilla A, Sierra JP, Gracia V, Garcia M, Jimenez JA, Mösso C, Valdemoro H. Coastal sustainability for uncertain futures: A spanish mediterranean case from the RISES-AM project. A: Intenational Association for Hydraulic Research Congress. E-proceedings of the 36th IAHR World Congres. L'Haia. 2015;1-8.
7. Sanchez-arcilla A, Sierra JP, Mösso C, Gracia V, Garcia M. Progress on climate change detection and projections over Spain since the findings of the IPCC AR5. International Symposium CLIMATE-ES. 2015;146.
8. Castillo E, Hadi AS, Balakrishnan N, Sarabia JM. Extreme value and related models with applications in engineering and science. Wiley-Interscience. New Jersey; 2005.
9. Menéndez M, Méndez FJ, Izaguirre C, Luceño A, Losada IJ. The influence of seasonality on estimating return values of significant wave height. Ocean Eng. 2009;56:211-219. DOI: 10.1016/j.coastaleng.2008.07.004.
10. Panchang V, Kwon Jeong Ch, Demirbilek Z. Analyses of extreme wave heights in the Gulf of Mexico for offshore engineering applications. J Offshore Mech Arct 2013;135(3):1-15.
11. Peng Q, Jin S. Significant wave height estimation from space-borne cyclone-GNSS reflectometry. Remote Sensing. 2019;11(5):584.

II. COMPENDIUM OF PAPERS

Paper A

Correlation of Concurrent Extreme Metocean Hazards Considering Seasonality.

Felícitas Calderón-Vega, Adrián-David García-Soto and César Mösso

Applied Sciences. Appl. Sci. 2020, 10, 4794; doi:10.3390/app10144794.

applied sciences

MDPI

Article

Correlation of Concurrent Extreme Metocean Hazards Considering Seasonality

Felícitas Calderón-Vega [1,2], Adrián-David García-Soto [1,*] and César Mösso [2,3]

[1] Department of Civil Engineering, Universidad de Guanajuato, Juárez 77, Zona Centro, Guanajuato P.C. 36000, Mexico; felicitas.calderon@upc.edu

[2] Laboratori d'Enginyeria Marítima, Universitat Politècnica de Catalunya, Jordi Girona 1-3, Mòdul D1, Campus Nord, 08034 Barcelona, Spain; cesar.mosso@upc.edu

[3] Centre Internacional d'Investigació dels Recursos Costaners, Jordi Girona 1-3, Mòdul D1, Campus Nord, 08034 Barcelona, Spain

* Correspondence: adgarcia@ugto.mx; Tel.: +52-473-1020100-2235

Received: 17 June 2020; Accepted: 9 July 2020; Published: 13 July 2020

Abstract: Simultaneous occurrence of metocean variables can present a multihazard to maritime systems. However, simplified design approaches to assess simultaneous significant wave heights and wind velocities are lacking, especially if seasonality is considered. This is addressed in this study by using extreme significant wave heights and companion wind velocities recorded in the Gulf of Mexico. Time-dependent, generalized extreme value (GEV) models and classical regression are the basis to propose a simplified approach to estimate correlated extreme significant wave heights and wind velocities associated with given return periods, accounting for seasonality and including measures of uncertainty. It is found that the proposed approach is a new but simple method to adequately characterize the concurrent extreme metocean variables and their uncertainty. It is concluded that the method is an effective probabilistic design tool to determine simultaneous extreme significant wave heights and companion wind velocities for desired return periods and seasonality.

Keywords: metocean variables; seasonality effects; multihazard; time-dependent GEV model

1. Introduction

Maritime structures, such as offshore facilities, breakwaters and other systems, are subjected to the effect of metocean variables, including extreme waves and extreme winds. These metocean variables can be considered as hazards that impose demands to these systems. Metocean variables can be characterized with a probability density function (PDF) frequently adopted from extreme value theory [1]. Among the metocean variables, extreme waves and winds can impact offshore facilities [2]; correlation of these two variables is important for design because they can occur simultaneously [3].

Recent studies on extreme waves and winds include the assessment of significant wave heights in the South China Sea using hindcast data [4], wind models to simulate waves in the South China Sea and the East China Sea [5], the use of radar images to estimate significant wave height [6], wave height forecasting during extreme events [7], assessment of wave heights by using generalized Pareto and Gumbel distributions [8], uncertainty assessment in extreme significant wave height by using different techniques [9] and a review on available wind–wave models and their limitations [10]. Additionally, hindcast for wind–wave for several decades was calculated and compared with observed data for estimating wave climate change and

for risk analysis [11,12]. Regarding studies on generalized extreme value (GEV) distribution, they are used lately to model different variables. For instance, GEV distributions resulted in a very adequate model of precipitation and evapotranspiration in India [13], and are also implemented in software to model annual maximum precipitation [14]; some variants of the method that consider nonstationarity are also found in the literature applied to river water levels [15]. The use of GEV for modeling extreme typhoon heading directions [16], joint PDFs for wave height and period [17] and for modeling extreme wave heights in the Mediterranean and at Portuguese locations [18,19] are also reported in recent literature. This shows that GEV models are a tool used currently to effectively characterize metocean and other variables. Nevertheless, no single study in recent literature on GEV reports a proposal like the one contained in the present study.

Studies regarding correlation of metocean variables are also available in the literature. Contour maps and joint distribution of environmental variables are used for marine and coastal design. Current approaches are summarized in [20], where nonparametric methods, copula models, hierarchical conditional models and conditional extremes models are used to compute contour maps for joint occurrence of significant wave height and wave period. Some of the important highlights reported in [20] include: that joint probabilities are important for reliability analysis as stipulated in guidelines and standards, that simultaneous occurrence of extreme events at prescribed return periods is of interest, that the values associated with such return periods are not uniquely defined (except by independent or perfectly correlated cases), that the problem may need to be studied in a case-by-case basis, that different techniques may be more suitable than others depending on the problem to be addressed, among other issues.

Studies on correlated metocean variables accounting for seasonality are also found in the literature. For instance, Vanem [21] develops weekly contour maps for wave height and wave period using selected return periods. The season-specific variability of simultaneous metocean variables can be important for planning [21]. In [21], a proposal is based on normalizing the data using the mean and standard deviation to remove seasonality, which can be added back later; it is argued that the whole set of data (i.e., from all the seasons) can be taken advantage of, opposite to fitting the data into separate bins, which results in a decrease in the fitted data. Nevertheless, the use of separate bins to fit the data is also used as an alternative to account for seasonality of metocean variables [22–25].

In the literature review, the use of hindcast data, consideration of seasonality and the use of different PDFs are found. However, most studies are based on complex or time-consuming methodologies. Nonetheless, Bitner-Gregersen [26] reports a summary of simplified expressions of practical applicability contained in guidelines, which will be useful later in this study. The study of concurrent metocean variables at different locations is important, since specific features of metocean climate depend not only on the region but also on the specific location [26]. Simple techniques to assess simultaneous significant wave heights and companion wind velocities are lacking, especially to account for seasonality.

The main objective of this study is to develop a simple approach to correlate extreme significant wave height and companion wind velocity for given return periods and accounting for seasonality. Time-dependent GEV models and classical regression applied to data from a buoy located in the Gulf of Mexico are used as the basis of this study. The results can be useful for design projects on multihazards of maritime systems, since extreme waves and companion winds can translate into simultaneous demands imposed on these systems.

2. Significant Wave Height and Wind Velocity Data Used

The significant wave heights and wind velocities are obtained from a buoy in the Gulf of Mexico operated by the National Data Buoy Center (NDBC, www.ndbc.noaa.gov). It is in the Gulf of Mexico at 25.942° N 89.657° W, denoted as buoy 42,001 [27]; its data were used in a previous study [28]. It is selected to illustrate the proposed approach because of its location at open sea and because it has recorded

simultaneous information of metocean variables since 1975, but the method can be readily extended to other buoys at open sea in the Gulf of Mexico or anywhere else. For the scope of the present study, the maximum monthly significant wave heights, *Hs*, recorded at buoy 42,001 are used, together with the wind velocity, V_w, recorded and listed in [27] within the same time bin. It is pointed out that V_w is not necessarily the monthly maximum wind speed, but the one which occurred simultaneously with the monthly maximum significant wave height (level of resolution within [27]); thus it is also referred to as companion wind. The significant wave height and wind speeds used are those defined in [27], denoted as WVHT and WSPD [27], respectively. The wind velocity is averaged over an eight-minute period and is recorded at 3.6 m above sea level [27]. For the scope of this study, the data are used as directly given in [27]. Both metocean variables, *Hs* and V_w, are to be probabilistically characterized with a model that can represent seasonality effects, as described in the following sections.

3. Extreme Value Analysis Considering Seasonality

In this section the method to perform the extreme value analysis considering seasonality is briefly summarized, since details are described in a previous study [28]. In the next section, the model is to be first applied separately to the significant wave height and wind velocities.

The model employs the generalized extreme value (GEV) family of distributions [29]. Instead of characterizing a random variable with the Gumbel, Weibull or Frechet PDF or cumulative functions (CDF), a single mathematical expression can be used, since it can represent the three. This is the GEV model used here and given by:

$$G(x) = \exp\left\{-\left[1+\xi\left(\frac{x-\mu}{\psi}\right)\right]_+^{\frac{-1}{\xi}}\right\} \rightarrow \xi \neq 0$$
$$G(x) = \exp\left\{-\exp\left[-\left(\frac{x-\mu}{\psi}\right)\right]\right\} \rightarrow \xi = 0 \quad (1)$$

or given by:

$$g(x) = \frac{1}{\psi}\left[1+\xi\left(\frac{x-\mu}{\psi}\right)\right]_+^{-\left(1+\frac{1}{\xi}\right)} \exp\left\{-\left[1+\xi\left(\frac{x-\mu}{\psi}\right)\right]_+^{\frac{-1}{\xi}}\right\} si\xi \neq 0$$
$$g(x) = \frac{1}{\psi}\exp\left(-\frac{x-\mu}{\psi}\right)\exp\left[-\exp\left(-\frac{x-\mu}{\psi}\right)\right] si\xi = 0 \quad (2)$$

if the PDF is to be used. In Equations (1) and (2), [*a*]+ implies the max (*a*,0), $-\infty < \mu < \infty$ is the location parameter, $\psi > 0$ is the scale parameter and ξ the shape parameter; ξ leads to the Gumbel distribution when equal to zero, and to the Frechet and Weibull distributions when $\xi > 0$ and $\xi < 0$, respectively.

For the GEV models of *Hs* and V_w, the block maxima concept is used. The monthly maximum *Hs* values are considered as the samples for the extreme value analysis, while for the samples of V_w, they do not necessarily correspond to the maximum, but to the companion wind velocities recorded when *Hs* occurred. The seasonality is a cyclic behavior linked to climatic patterns, which behave in a sinusoidal way every year. The common stationary model for extreme value analysis is extended to include time dependency. It is assumed that monthly maxima and companion values are independent random variables. Furthermore, it is assumed that the maximum (or companion) monthly values Z_t of observed *Hs* and V_w in month *t* follows the GEV distribution referred to above, which location $\mu(t) > 0$, scale $\psi(t) > 0$ and shape ξ (t) parameters are a function of time.

The CDF of Z_i is given by:

$$F_t(z) = \begin{cases} \left\{\exp\left\{-\left[1+\xi(t)\left(\frac{z-\mu(t)}{\psi(t)}\right)\right]_+^{\frac{-1}{\xi(t)}}\right\}\right. \\ \left.\exp\left\{-\exp\left[-\left(\frac{z-\mu(t)}{\psi(t)}\right)\right]\right\}\right. \end{cases} \quad (3)$$

where $[a]_+ = \max[a,0]$.

The GEV parameters account for nonstationarity with the following expression:

$$\theta = \begin{cases} \mu(t) = \beta_0 + \beta_1\cos(2\pi t) + \beta_2 sin(2\pi t) + \beta_3\cos(4\pi t) + \beta_4 sin(4\pi t) \\ \psi(t) = \alpha_0 + \alpha_1\cos(2\pi t) + \alpha_2 sin(2\pi t) + \alpha_3\cos(4\pi t) + \alpha_4 sin(4\pi t) \\ \xi(t) = \gamma_0 + \gamma_1\cos(2\pi t) + \gamma_2 sin(2\pi t) + \gamma_3\cos(4\pi t) + \gamma_4 sin(4\pi t) \end{cases} \quad (4)$$

where mean values are denoted with β_0, α_0 and γ_0, harmonic amplitudes by β_i, α_i and γ_i (for i = 1, 2) and subharmonic amplitudes by β_i, α_i and γ_i (for i = 3, 4); t is given in years. The maximum likelihood estimators for the location μ, scale ψ and shape ξ parameters vary during the year; the regression coefficients and the probability distribution parameters are determined through the method of maximum likelihood (MML), in which the likelihood function for the GEV model is given by:

$$l(\theta|t_i x_i) = -\sum_{i=1}^{m}\left\{\log\psi(t_i + \left(1+\frac{1}{\xi(t_i)}\right)\log\left[1+\xi(t_i)\left(\frac{x_i-\mu(t_i)}{\psi(t_i)}\right)\right]_+ + \left[1+\xi(t_i)\left(\frac{x_i-\mu(t_i)}{\psi(t_i)}\right)\right]_+^{\frac{-1}{\xi(t_i)}}\right\} \quad (5)$$

As previously noted, the location $\mu(t) > 0$, scale ψ(t) > 0 and shape ξ (t) parameters are expressed in terms of harmonic functions, whose amplitudes are regression parameters to be mathematically estimated.

The selective search methodology known as stepwise approach is used to find the best model, which encompasses the forward selection and backward elimination methods, which are described elsewhere [30]. The uncertainty of the selected model is accounted for by standard errors and confidence intervals [30]. The present study proposes an approach to compute concurrent metocean variables (*Hs* and V_w) associated with given return periods, for which the individual values associated with each variable are required. The values associated with return periods for each variable considered separately can be obtained with the following equation:

$$X_q(t,\theta) = X_q(\mu(t),\psi(t),\xi(t)) = \begin{cases} \mu(t) - \frac{\psi(t)}{\xi(t)}\left\{1-[-\log(1-q)]^{-\xi(t)}\right\} & if \quad \xi(t) \neq 0 \\ \mu(t) - \psi(t)\log[-\log(1-q)] & if \quad \xi(t) = 0 \end{cases} \quad (6)$$

where q corresponds to the exceedance probability as defined by $G_t(x) = 1 - q$ and the estimated quantile, and $X_q(t,\theta)$ corresponds to the time-dependent value associated with the return period $T_{\text{-}yr} = 1/q$ for a metocean variable of interest.

The model described in this section is applied to *Hs* and V_w in the following sections; first, for each individual variable, and then subsequently, the approach to correlate both metocean variables is presented.

4. Correlating Extreme Metocean Variables

4.1. Nonstationary Models Considered Separately

The time-dependent GEV model described in the previous section is first applied separately to each of the metocean variables. The significant wave height *Hs* and wind velocity V_w described before are employed. Recall that while for the GEV analysis of *Hs* the monthly maxima from buoy 42,001 are used,

the V_w data do not necessarily correspond to the monthly maximum recorded values, but to the companion wind velocities that occurred simultaneously with the monthly maximum *Hs*.

Figure 1 shows the maximum *Hs* recorded monthly (depicted with dots) and the 30 yr return period values, T-$_{30}$, estimated with the GEV model (depicted with a solid line). As in a previous study [28], clear peaks approximately around the seasons of December–February and August–October, associated with cold fronts and hurricanes, respectively, are observed in Figure 1.

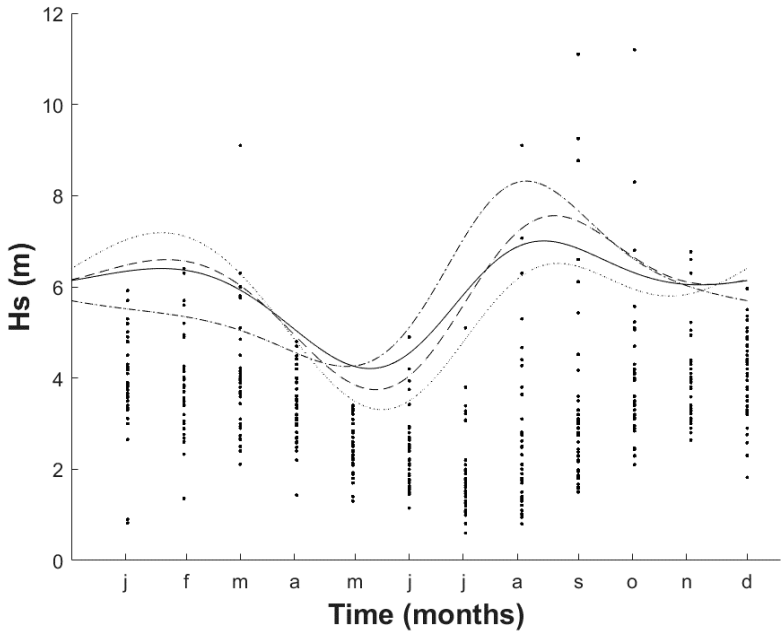

Figure 1. Monthly maximum and 30-yr return period values of *Hs* using different time ranges.

To inspect whether a difference using the updated information in the present study (i.e., with data up to 2019) and that from the previous study [28] (with data up to 2012) exists, the T-$_{30}$ values reported in [28] are also depicted in Figure 1 (dashed lines). It can be observed that inclusion of recent data points in the analysis does have an effect in the projected values, leading to a decrease in the peak *Hs* values for hurricane and cold front seasons—more noticeable for the former—and an increase at midyear months.

To further investigate the impact of selecting different time windows in the assessment of projected values associated with a given return period, two more lines are shown in Figure 1, which were computed using the oldest (dotted line) and the newest (dashed–dotted line) maximum 20 available recorded monthly data per year; selection of at least a 20 years range for the analysis is recommended to properly characterize metocean variables probabilistically [3]. There is a noticeable impact of using these different time windows to assess the *Hs* values for T-$_{30}$.

Determining if this could be attributed to climate change is feasible, since studies in the literature [31] report that higher or lower metocean variables could be attributed to climate change, which depends on region and location, although it is important to acknowledge uncertainty in claiming any categorical trend [31]. This potential variation in wave climate could importantly impact maritime structures [31]. Future studies are desirable to further investigate this topic; nevertheless, it can be concluded that selection of different time ranges does have an impact in the projected return values of *Hs* (and other metocean variables). Moreover, it is accepted that using more metocean data leads to more reliable extreme value analyses [2,3], but the use of less data and more recent data could lead to a higher projected return period value for some months. Consequently, future research and discussion on this issue is recommended.

Figure 2 is analog to Figure 1, except that V_w values are shown. Less accentuated peaks can be observed for hurricane and cold front seasons in Figure 2, perhaps because not the maximum, but the companion values are employed, even though the trends are similar, at least for the updated (solid line) and previously used [28] time ranges (dashed lines).

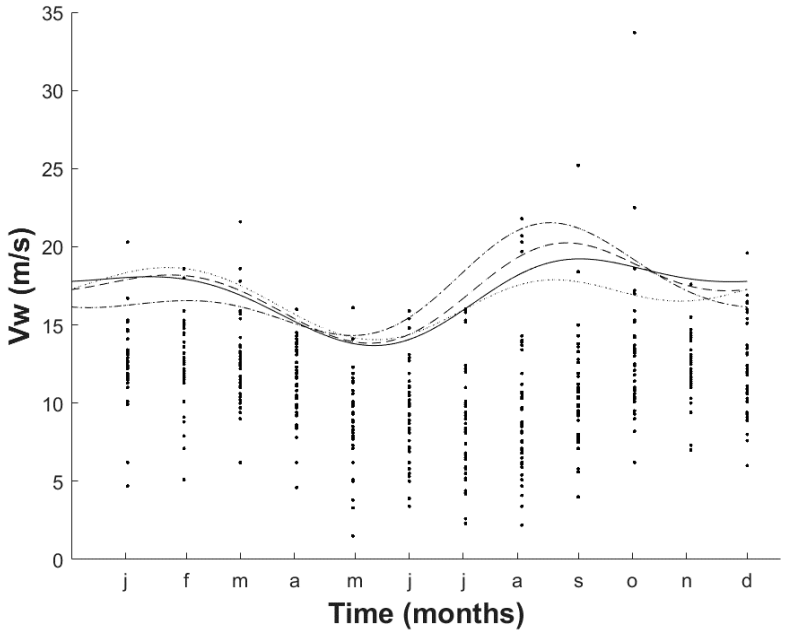

Figure 2. Monthly companion and 30-yr return period values of V_w using different time ranges.

For the scope of this study, only models corresponding to the solid lines in Figures 1 and 2 are used (i.e., the whole set of available data at buoy 42,001 is considered), although projected metocean variables for other return periods are also used. The values for other return periods, used later in this study, for each month are listed in Appendix A in Tables A1 and A2 for *Hs* and V_w, respectively. No details in this study are given about the parameters of the GEV models as were provided in previous studies (e.g., [28]), since attention is focused on proposing a simplified approach to correlate extreme *Hs* data and their companion V_w data associated with given $T_{\text{-}yr}$ values. This is developed in the following section.

4.2. Simplified Approach for Return Period Correlated Values

The proposal to estimate the simultaneous occurrence of extreme metocean variables is based on a modified version of the classical linear regression technique. This consists in including estimated values from the time-dependent GEV models in the previous section—together with the simultaneously observed monthly data for maximum *Hs* and companion V_w—in the regression analysis, to assess how adequate is the use of the return period value of the explanatory variable (in the regression analysis sense) to predict the return period value of the other variable and its uncertainty. This is to be carried out for each month of the year to estimate seasonal extreme (and companion) values associated with given return periods, so that they can be considered as a demand which is applied simultaneously to a maritime system (or other system). From this standpoint, significant wave heights and wind velocities can be considered as concurrent extreme metocean hazards accounting for seasonality, since they can be translated into load effects affecting a given maritime structure at the same time, at any desired season of the year. Moreover, such demands are usually related to given return periods for design purposes; consequently, it is convenient to establish them in terms of return periods. This is also the case for using contour maps in ocean engineering [20].

Before proceeding to introduce the proposal, the classical regression analysis using *Hs* as the explanatory variable and V_w as the variable to be predicted is described as follows by using the observed data only. Buoy 42,001 is used to illustrate the procedure, but this can be extended to any buoy with simultaneous recorded metocean data. *Hs* is selected as the explanatory variable because it was used in a previous study [28] to investigate maxima. As noted before, V_w is not necessarily the maximum, but the wind velocity observed simultaneously with the monthly maximum *Hs*. Naturally, it could be considered otherwise, e.g., maximum V_w and associated simultaneously recorded companion *Hs*, but also other pairs of concurrent values of *Hs* and V_w could be selected. This aspect is discussed later. From a designer perspective, it can be thought of as selecting an *Hs* value and using it to predict a V_w value that is expected to occur simultaneously; then, both can be used to estimate the imposed (adding) effects of both metocean variables acting over a system, which capacity is to be designed to withstand such demand. Since both metocean variables are random, this can be expressed in mathematical terms [32,33] as:

$$E[V_w|Hs = hs] = b + \alpha\, hs \tag{7}$$

where the expected value of V_w, given that $Hs = hs$, is a linear function of *hs*; b and α are constants to be determined by linear regression analysis. However, guideline expressions that relate wind velocities and wave heights, as well as fitted functions found in the literature [26], commonly have the following mathematical form:

$$V_w = bH_s^{\alpha} \tag{8}$$

which can be linearized by taking the natural logarithm, leading to:

$$\ln V_w = \beta + \alpha \ln H_s \tag{9}$$

where $\beta = \ln b$; the notation in terms of the expected value is skipped for simplicity. Equations (7) and (9) are used in the linear regression analysis. For using Equation (9), the wind velocities and significant wave heights are first transformed into logarithmic space [33].

Figure 3a,b shows the linear regression analysis by using the nonlinear model (i.e., Equation (9)) and the linear model (i.e., Equation (7)), respectively, for October (around hurricane season); the residuals versus the fitted values of *ln* V_w (Figure 3c) and V_w (Figure 3d) are also shown.

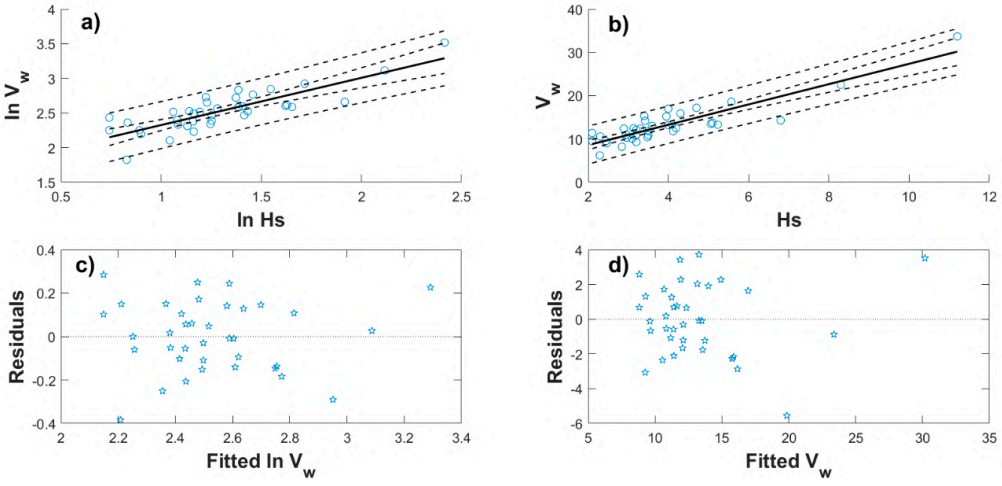

Figure 3. Regression and residual analysis by using (**a**) nonlinear (Equation (9)) and (**b**) linear (Equation (7)) models for October. Residuals using (**c**) Equation (9) and (**d**) Equation (7).

As mentioned before, the regression is first performed by using only the historical observed data, shown by circles in Figure 3a,b. It can be observed that the regression line (solid line) in both cases (i.e., Equations (9) and (7)) predicts increasing V_w for increasing Hs. This is consistent with what is reported in the literature. The 95% confidence intervals, which are measures of uncertainty for mean and future values of V_w [33,34], are also shown in Figure 3a,b (inner and outer dashed lines for mean and future values, respectively). Analysis of residuals versus predicted values indicates that the nonlinear model leads to a better scattering of the data along the horizontal axis (i.e., the model is uncorrelated) and better symmetry in the vertical axis (i.e., the zero mean assumption), indicating that the nonlinear model is better for the values observed in October. Both models roughly exhibit a normal distribution behavior in the residuals, as can be observed in Figure 4a for the model in logarithmic space and 4b for the linear model, where the normal probability papers are plotted using the cumulative probability given by $i/(n + 1)$, where n is the number of samples (i.e., the number of residuals) and i corresponds to the number of a datapoint (a residual) in ascending order.

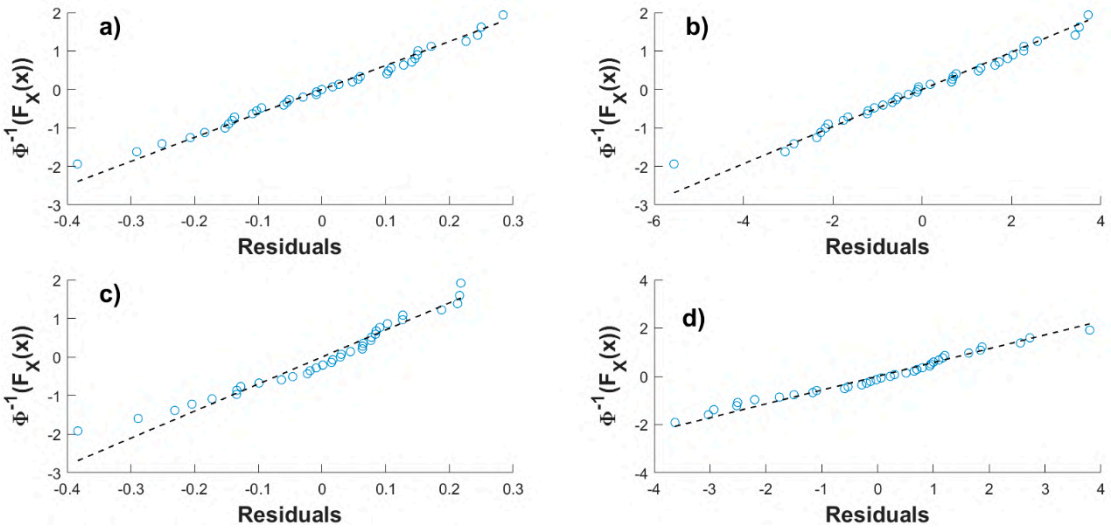

Figure 4. Normal probability papers for residuals. October: (**a**) nonlinear model and (**b**) linear model. February: (**c**) nonlinear model and (**d**) linear model.

Figure 5 is analogous to Figure 3, except that February instead of October is considered (i.e., around cold front season). Opposite to what occurs in the regression analysis for October, the analysis for February is better represented using the linear model (Figure 5b), rather than by using the linearized model in the natural logarithmic space (Figure 5a); this can be inspected in the residuals and normal probability papers in Figure 5c,d and Figure 4c,d, for Equations (9) and (7), respectively. It is found in this study that correlation of significant weight height and wind velocity can be better represented (in terms of classic linear regression) by linear (Equation (7)) or power (Equation (9)) expressions, depending on the month of the year (e.g., hurricane season, cold front season or others). This is not clearly stated in other studies.

Nevertheless, it can be observed that both the linear or the nonlinear regression analysis lead to a fairly normal behavior of the residuals, and to a relatively uniform distribution of the variance around the mean, which could be associated with a homoscedastic behavior [33], although this varies depending on the month and type of regression considered (i.e., on using Equation (7) or Equation (9)). The error variance, σ_e^2 is an indication of the uncertainty in the regression, and its squared root is known as the root mean squared error (RMSE). Overall, the residual analyses for all months indicate that the usual assumptions in the regression approach are met [34], and that Equation (7) and Equation (9) can be suitable

alternatives. Although Equation (8) is frequently encountered in codified design and the literature [26] as indicated above, functional forms like those of Equation (7) are also found, as in the standard of the North Atlantic Treaty Organization, Standardized Wave and Wind Environments and Shipboard Reporting of Sea Conditions (NATO-STANAG 4194, see [26]), which can be expressed as:

$$V_w = b + \alpha Hs \tag{10}$$

where the nomenclature used in the present study applies (for the NATO-STANAG 4194, $b = 0$ and $\alpha = 3.2$). Equations with the functional form of Equations (8) and (10) are used for open sea and coastal waters; those employed for coastal waters are also linked to the fetch as an important variable [26]. In the present study, the fetch is not considered since the buoy used is located in open sea.

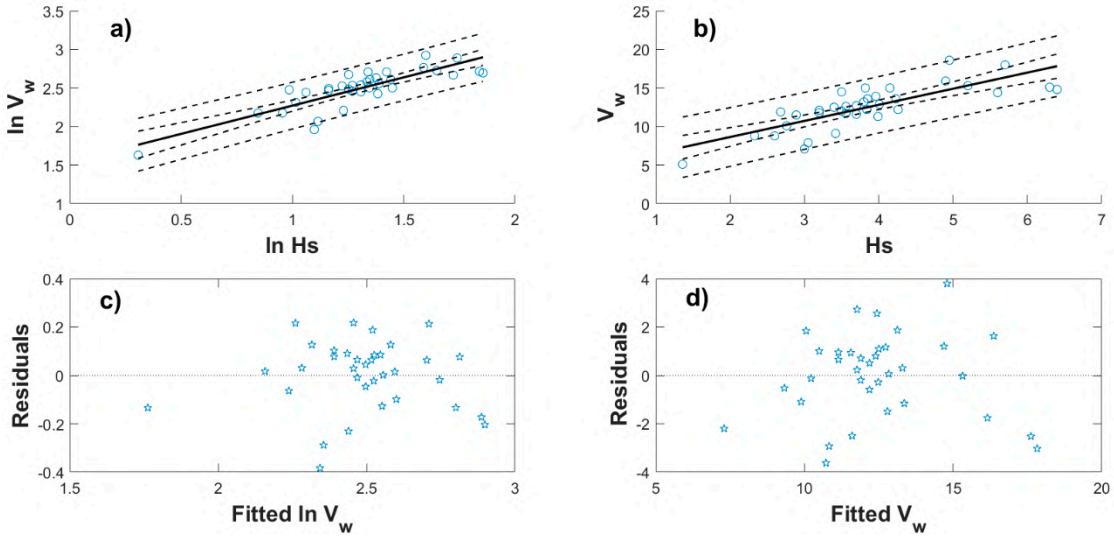

Figure 5. Regression and residual analysis by using (**a**) nonlinear (Equation (9)) and (**b**) linear (Equation (7)) models for February. Residuals using (**c**) Equation (9) and (**d**) Equation (7).

As shown in Figures 3 and 5, the data are approximately contained within the confidence intervals for future values in all cases. It is noticed that the confidence intervals for future values can be simplified by using Equation (11a,b), for the lower and upper interval, respectively.

$$V_{wlow} = b + \alpha Hs - \delta\sigma_e \tag{11a}$$

$$V_{wupp} = b + \alpha Hs + \delta\sigma_e \tag{11b}$$

where $\sigma_e = \sqrt{\sigma_e^2}$ is the so-called RMSE which—advantageously—is part of the information that can be obtained when a regression analysis is performed; δ is a constant value to be discussed. If Equation (8) is to be considered to derive simplified expressions for the confidence intervals, expressions like Equation (11) can be written by including $\pm\delta$ times the RMSE in Equation (9), except that the RMSE corresponds to the regression in logarithmic space. If the equation in the original space is to be used to compute the expected value (i.e., Equation (8)), it can be shown with some algebraic manipulations that the 95% confidence intervals for future values can be approximated by using Equation (12a,b):

$$V_{wlow} = bH_s^{\alpha}\left(\frac{1}{e^{\delta\sigma_e}}\right) \tag{12a}$$

$$V_{wupp} = bH_s^{\alpha}\left(e^{\delta\sigma_e}\right) \tag{12b}$$

The value of δ is adequate to represent the 95% confidence intervals (denoted simply as confidence intervals from now on) for future values by adopting constant values approximately between 1.9 and 2.3, depending on the season considered and for both sets of equations (i.e., Equations (11) or (12)).

Exact confidence intervals (dashed lines) and approximated confidence intervals (Equations (11) or (12); dotted lines) are shown in Figure 6a–d for the four cases depicted in Figure 3a,b and Figure 5a,b, respectively; the original instead of the logarithmic scale is used for the cases corresponding to Equations (8) and (12). A value of δ equal to 2.3 is used for October (Figure 6a,b), while δ = 2.2 is employed for February (Figure 6c,d). It can be observed that Equations (11) and (12) are reasonable alternatives to represent the uncertainty in a simplified (practical) way. Even though simple, as far as the authors know, Equations (11) and (12) are not reported in the literature for extreme values accounting for seasonality; therefore, they are an important contribution of this study that include the uncertainty in correlated metocean variables for design purposes.

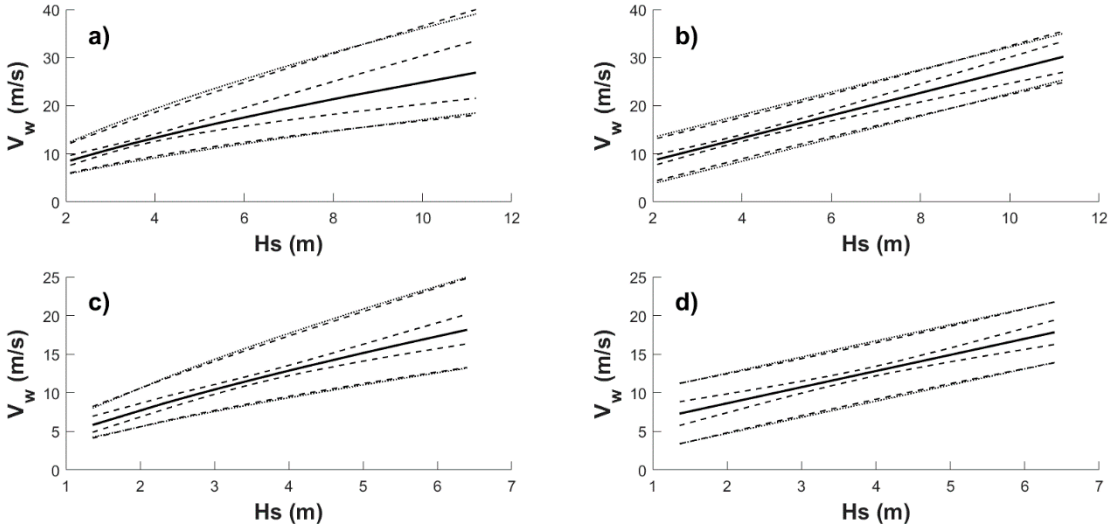

Figure 6. Comparison of exact and approximated (Equations (11) and (12)) 95% confidence intervals, considering October (upper row; (**a**) and (**b**) for non-linear and linear cases, respectively) and February (lower row; (**c**) and (**d**) for non-linear and linear cases, respectively).

The proposed approach to estimate concurrent metocean variables (*Hs* and V_w in this case), is based on using the time-dependent GEV model for *Hs* obtained in the previous section, to compute a *Hs* value associated with a selected return period in years, $T_{\text{-}yr}$ (the subscript is used to denote the selected return period, e.g., $T_{\text{-}30}$ corresponds to a 30-yr return period); the *Hs* for a given $T_{\text{-}yr}$ can then be used as input for Equations (8) and (10)–(12), to determine the corresponding expected companion V_w for the same $T_{\text{-}yr}$, including an uncertainty measure (i.e., the confidence intervals).

To investigate whether the previous proposal is consistent with both time-dependent GEV models in the previous section, estimated values of *Hs* and V_w associated with $T_{\text{-}20}$, $T_{\text{-}30}$, $T_{\text{-}50}$, $T_{\text{-}75}$ and $T_{\text{-}100}$ are included in the scattergrams and regression analyses as can be observed in Figure 7, where the $T_{\text{-}yr}$ values for October are indicated by black filled circles with embedded perpendicular lines (lines to be explained below). Selection of these return periods is somewhat arbitrary but based on the usage of such return periods for design.

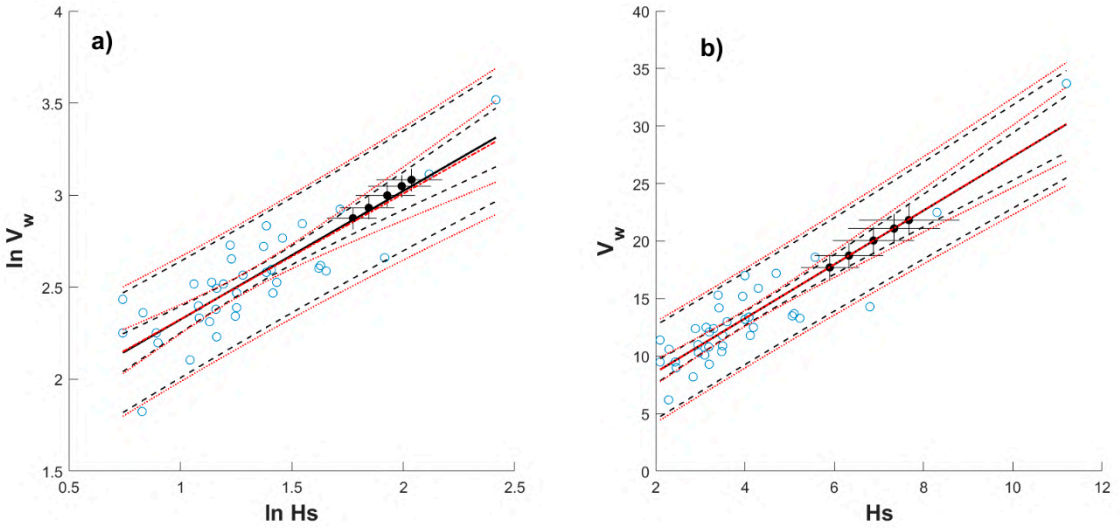

Figure 7. Regression lines and confidence intervals including (solid and dashed lines, respectively) and excluding (dashed–dotted and dotted lines, respectively) $T_{\text{-}yr}$ values for October; (**a**) and (**b**) for logarithmic space and linear space, respectively. Filled circles are given by $T_{\text{-}yr}$ values with embedded perpendicular lines indicating confidence intervals from GEV models.

Figure 7a,b correspond to the logarithmic and linear cases as before, with the regression line depicted with a solid line and confidence intervals with dashed lines (it is emphasized once more that they are derived by including the set of $T_{\text{-}yr}$ values from the GEV models in the regression). In fact, the regression lines and confidence intervals previously obtained (i.e., without including the black filled circles in the regression) are also plotted in Figure 7a,b using dashed–dotted and dotted lines, respectively. It can be observed that the regression lines are almost coincidental, that the estimated $T_{\text{-}yr}$ values are very near or over the regression line (especially for Figure 7b), and that the inclusion of $T_{\text{-}yr}$ values in the regression slightly decreases the uncertainty in terms of confidence intervals (i.e., the previously computed intervals are wider), which applies to both, Figure 7a,b.

Additionally, the amplitude between the lower and upper limits of the 95% confidence intervals from the GEV models for Hs and V_w are depicted with the perpendicular embedded lines in the $T_{\text{-}yr}$ values (i.e., embedded lines in the black filled circles) in Figure 7; vertical and horizontal embedded lines correspond to the confidence intervals for V_w and Hs, respectively. The confidence intervals from the GEV models (the embedded lines in Figure 7) are obtained by using return period values (Equation (6)) and their variance, linked to the variance–covariance matrix and obtained through the delta method [29]. It can be observed in Figure 7a,b that confidence intervals from the GEV models surpass the limits of the confidence intervals for mean values (inner dashed and dotted lines) but are contained within the boundaries of those corresponding to future values (outer dashed and dotted lines) from the regression analysis; it can also be observed that intervals for Hs are wider than for V_w. If it were of interest to delimit in a simplified way the confidence intervals from the GEV models for a given $T_{\text{-}yr}$, Equations (11) and (12) could be an option by providing a suitable δ value. Neither this comparison between the uncertainty of the GEV models and the uncertainty from the linear regression, nor the idea of using Equations (11) and (12) to relate both uncertainties, are found in the literature. Therefore, this can be also considered as a contribution of the present study.

Figure 8 shows the residuals and normal probability papers by including the $T_{\text{-}yr}$ values in the regression, where the residuals of $T_{\text{-}yr}$ values lie very close to or on the zero-mean line, and the probability

papers preserve roughly similar trends than without considering the $T_{\text{-}yr}$ values and follow an approximately normal distribution.

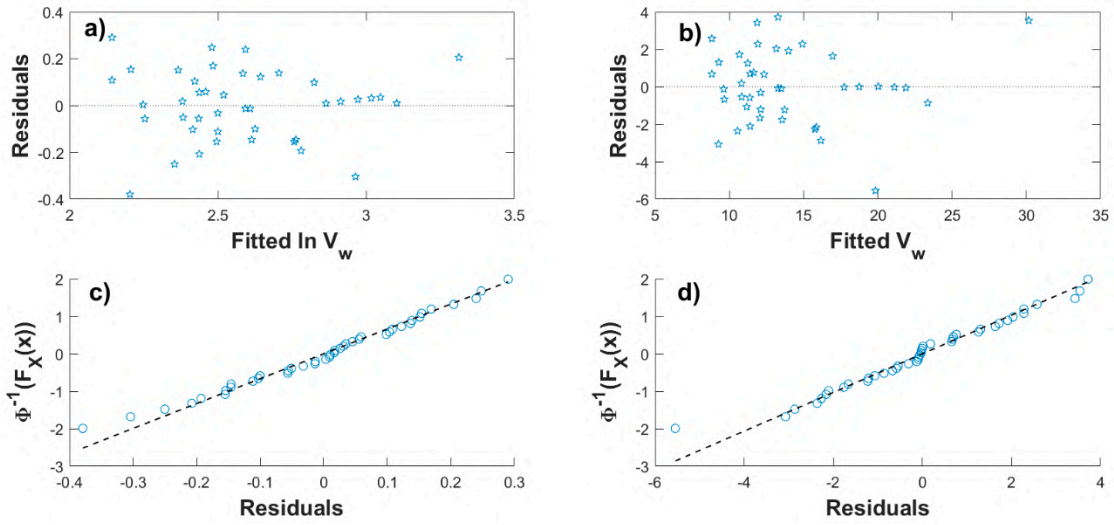

Figure 8. Residuals and normal probability papers including $T_{\text{-}yr}$ values in the regression: (**a**,**c**) for the logarithmic case and (**b**,**d**) for the linear case.

Figure 9a,b is analogous to Figure 6a,b and they are comparable, as can be observed in these figures, with slightly less wider confidence intervals in Figure 9; as in Figure 6 for October, $\delta = 2.3$ is also used in Figure 9. For illustration purposes, the expression of Pierson–Moskowitz (PM), the one from the International Towing Tank Conference (ITTC) recommendations and a fitted equation for West Shetland at a North Atlantic location, are shown in Figure 9a, and the equations recommended by the NATO-STANAG 4194 and the 2013 Interim Guidelines proposed in MEPC 232 (65) are shown in Figure 9b; all these equations are retrieved from [26], where details and proper citation can be found. Some of these equations are given as a function of V_w instead of Hs [26]; in such cases, equations are solved for V_w as a function of Hs. The PM, ITTC and West Shetland expressions have the functional form of Equation (8) with values of b equal to 6.376, 4.636 and 5.31, respectively, and values of α equal to 0.5, 0.709 and 0.603, respectively. Likewise, for the NATO-STANAG and 2013 Interim Guidelines, the corresponding functional form is given by Equation (10) with parameters b equal to 0 and 6.9 and α equal to 3.2 and 2.2, respectively. For the previous expressions Hs is given in m and V_w in m/s. Note that the NATO-STANAG and 2013 Interim Guidelines equations are developed for coastal waters but included in Figure 9b for comparison. Figure 9 shows that the ITTC and the 2013 Interim Guidelines equations are similar in shape to those developed in this study, but under- or overestimating the predicted values for October the former and the latter, respectively. The other equations lead to not so dissimilar results as those reported here, and they are roughly in between the confidence intervals for future values.

To inspect how the proposed approach varies when considering seasonality, and how results compare with respect to the equations reported in [26] for other seasons, results like those shown in Figure 7 are also shown in Figures 10 and 11, but for the months of February and August, when the highest predicted $T_{\text{-}yr}$ values are obtained at cold front and hurricane seasons, respectively; in addition, results like those in Figure 9 are plotted in Figures 12 and 13. Unlike Figure 9, $\delta = 2.0$ is used in Figures 12 and 13, since it leads to a better approximation of the exact confidence intervals. As mentioned before, δ can be varied to better represent the exact confidence intervals; nevertheless, the range of values is not large and δ can be roughly set between 1.9 and 2.3.

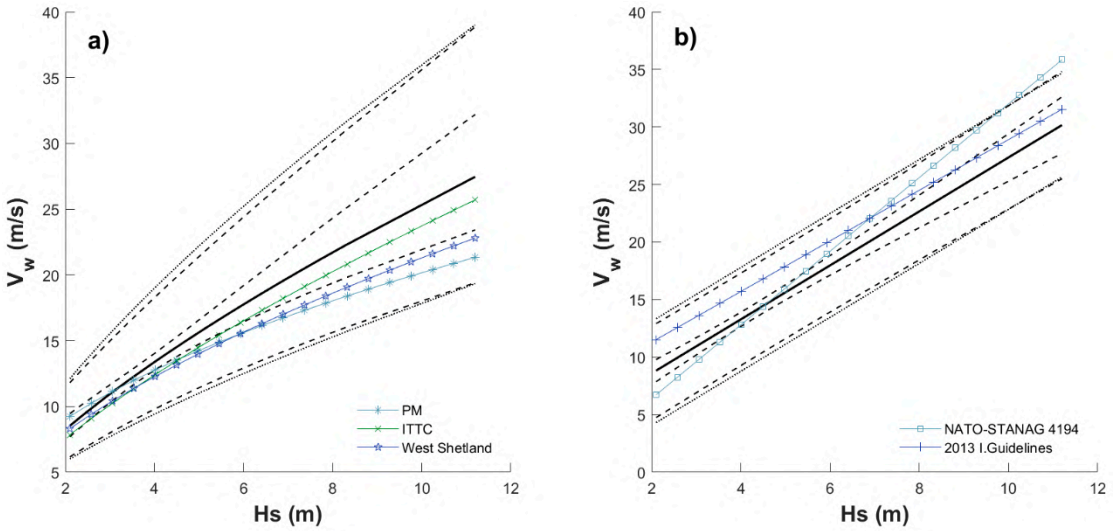

Figure 9. Exact and approximated 95% confidence intervals for October considering the $T_{\text{-}yr}$ values: regression (**a**) in logarithmic space and (**b**) in linear space. Legends indicate expressions referred in [28].

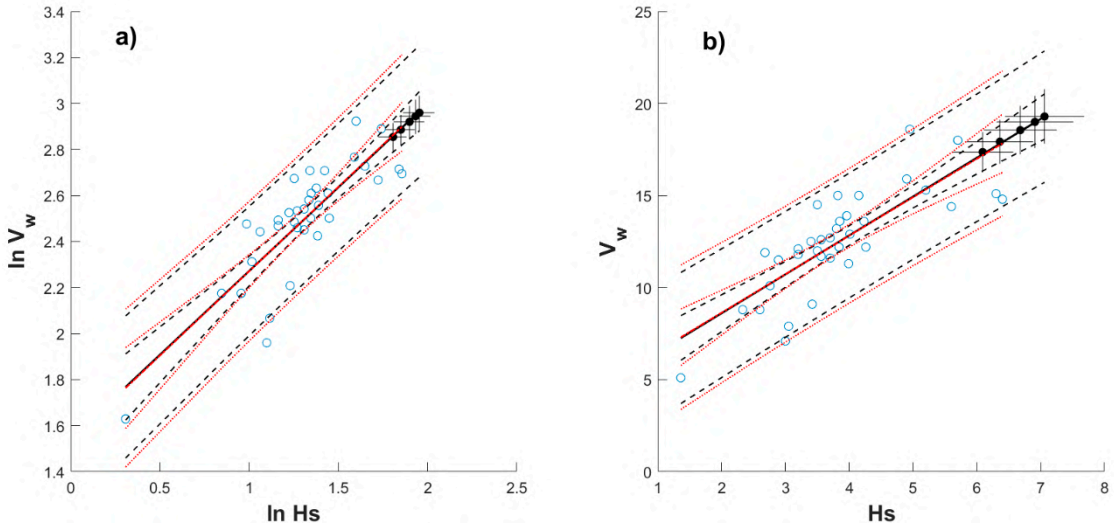

Figure 10. Regression lines and confidence intervals including (solid and dashed lines, respectively) and excluding (dashed–dotted and dotted lines, respectively) $T_{\text{-}yr}$ values for February; (**a**) and (**b**) for logarithmic space and linear space, respectively. Filled circles represent $T_{\text{-}yr}$ values with embedded perpendicular lines indicating confidence intervals from GEV models.

It can be observed from Figures 7, 10 and 11 that expected V_w values as function of *Hs* depend on the season and month considered, that the uncertainty also varies for each case and that the regression is relatively irrespective of the selected scheme (linear or logarithmic space) for October and February, but it does vary when August is considered. Figure 11 for August corresponds to the largest estimated $T_{\text{-}yr}$ values for *Hs* (hurricane season) and, as shown in Figure 11, the regression line predicts better estimates when the regression is performed in the logarithmic space; in fact, when the $T_{\text{-}yr}$ values are included in the regression (solid line), there is not significant deviation from the regression with the observed data only (dashed–dotted line); conversely, an important change in the slope of the regression line is observed for

Figure 11b, implying better estimates of correlated values for given T_{-yr} if the regression is carried out in the logarithmic space.

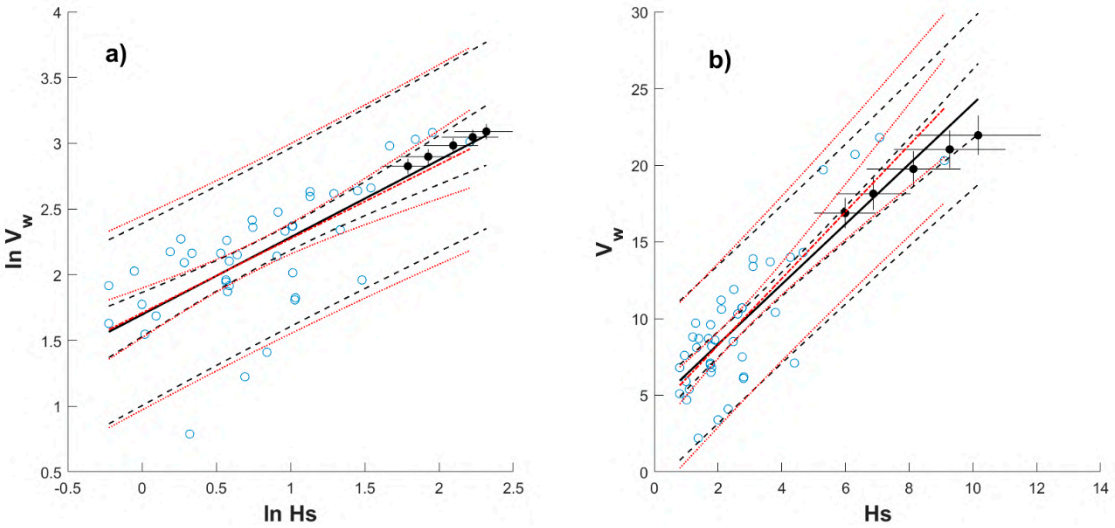

Figure 11. Regression lines and confidence intervals including (solid and dashed lines, respectively) and excluding (dashed–dotted and dotted lines, respectively) T_{-yr} values for August; (**a**) and (**b**) for logarithmic space and linear space, respectively. Filled circles represent T_{-yr} values with embedded perpendicular lines indicating confidence intervals from GEV models.

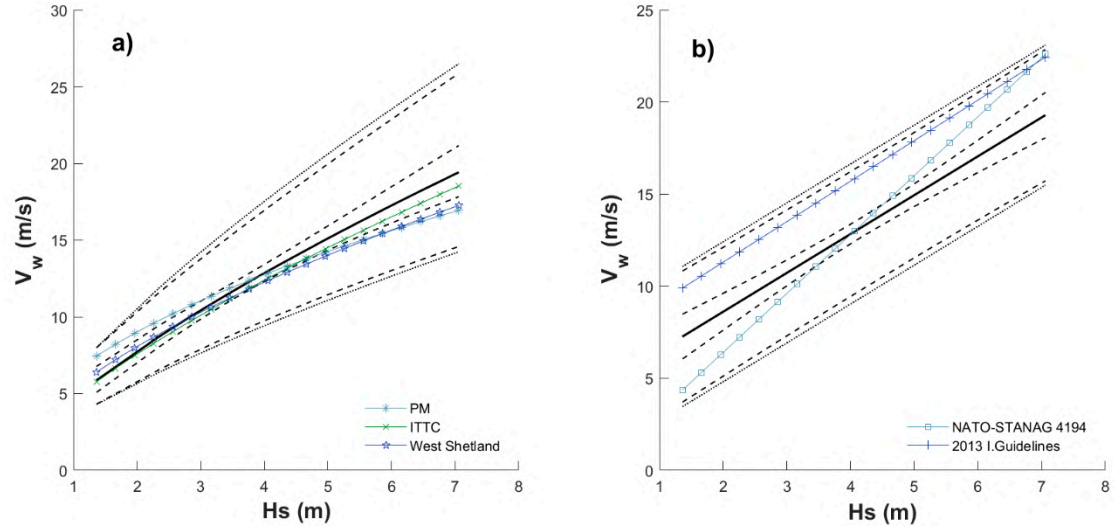

Figure 12. Exact and approximated 95% confidence intervals for February considering the T_{-yr} values: regression (**a**) in logarithmic space and (**b**) in in linear space. Legends indicate expressions referred in [28].

Figures 9, 12 and 13 show that a single equation cannot capture the seasonality of correlated metocean variables, because it can overestimate or underestimate the correlated values when comparing against the equations compiled in [26], at least for the case of V_w and *Hs* and buoy 42001, but it is possibly the case for other metocean variables and buoys, in the Gulf of Mexico or anywhere else. Therefore, suitable sets of region-specific and site-specific equations should be developed to take into account seasonal effects.

Nonetheless, it is interesting to note that the equation developed in [26] for West Shetland is practically coincident with the regression line in Figure 13a at hurricane season.

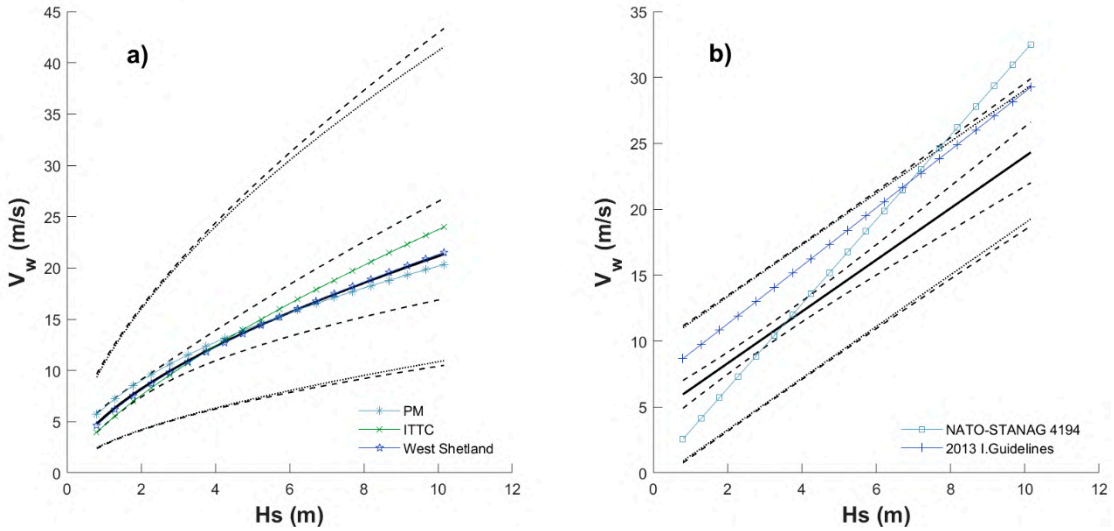

Figure 13. Exact and approximated 95% confidence intervals for August considering the T_{-yr} values: regression (**a**) in logarithmic space and (**b**) in in linear space. Legends indicate expressions referred in [28].

For values associated with T_{-yr} levels in Figure 11a (or in other figures), the uncertainty from the GEV models for each T_{-yr} (i.e., the embedded perpendicular lines in the black filled circles) are a sort of envelope roughly covered by the confidence intervals for mean values in Figure 11a. Furthermore, such an envelope can be covered by using Equation (12) and a smaller value of δ (e.g., $\delta = 1$) than that used for the confidence intervals of future values. Therefore, Equations (8) and (10) can be considered as possible design aids—simple expressions for design—like those contained in guidelines [26], but also accounting for the uncertainty in a simplified way (Equations (11) and (12)), either based on simplified confidence intervals for future values or confidence intervals within which the GEV uncertainty is confined. Since sets of such equations can be obtained for any desired season, the proposal here represents a simpler alternative than the more complex models reported in the introduction; consequently, they could be more attractive for designers since they are consistent with expressions recommended in guidelines.

Results for other months (not shown before) are reported in Figures A1–A9 in Appendix B. By observing Figures 7, 10 and 11 and Figures A1–A9, it can be concluded that the regression in the logarithmic or linear space could be both alternatives, with better results depending on the month considered. An exception is shown by Figure A8 for November, where neither a good fit is obtained for the logarithmic case (Figure A8a) nor for the linear one (Figure A8b) (also see Table 1). This is attributed to atypical simultaneous occurrence of larger *Hs* and smaller V_w values, as can be observed in Figure A8, but also to a large dispersion of the data along the whole range of *Hs* values, leading to a regression line somewhat horizontal (and roughly around 12 m/s), implying no correlation of *Hs* and V_w for November. It would be interesting to investigate in the future why this behavior is found specifically for November at buoy 42,001 in the Gulf of Mexico. For all the residual analyses shown in Figures 7, 10 and 11, and Figures A1–A9 for the observed data, mean values of these residuals are listed in Table A3 of Appendix C. In general, it can be observed in Table A3 that the zero mean assumption is met.

Table 1. Fitted parameters of regression analysis for buoy 42,001 in this study considering seasonality.

Month	For Equations (8) and (12)				For Equations (10) and (11)			
	[1] b	α	σ_e	ε_V(%)	b	α	σ_e	ε_V(%)
January	6.3130	0.5050	0.1323	12.6	6.0266	1.6565	1.8380	9.4
February	4.6311	0.7332	0.1448	0.48	4.4597	2.0891	1.7735	0.73
March	6.2270	0.5223	0.1692	6.92	6.5585	1.5731	2.0592	5.87
April	4.7280	0.7117	0.1757	0.16	3.914	2.1898	1.7927	0.44
May	4.6922	0.6616	0.4018	9.5	5.0670	1.5891	2.7234	13.1
June	6.3611	0.4104	0.3205	16.1	5.2639	1.7290	2.5623	4.2
July	6.0159	0.5132	0.4005	5.7	4.3002	2.3281	2.9474	18.5
August	5.5229	0.5648	0.3529	8.7	3.8972	2.1768	2.6075	9.3
September	4.6209	0.7596	0.2295	5.4	2.7402	2.6259	2.607	11.2
October	5.1243	0.6823	0.1626	4.7	3.8933	2.3476	2.0973	0.03
November	10.3253	0.1050	0.1742	34.0	10.5871	0.3736	1.9726	31.7
December	4.6688	0.6860	0.1899	10.1	3.3722	2.2109	2.2703	5.5

[1] $b = exp(\beta)$, where β is the intercept obtained from the regression in the logarithmic space.

Results of the regression are listed for each month in Table 1 for buoy 42,001. Table 1 includes the regression parameters using only the observed data and the two approaches described above, i.e., the direct linear regression and the regression in the logarithmic space. It also includes σ_e and relative errors of the predicted correlated V_w in relation to those obtained from the GEV model for a selected return period (50 years) using:

$$\varepsilon_V = \left| \frac{V_{bench} - V_{est}}{V_{bench}} \right| \times 100 \quad (13)$$

where the relative error is given in percentage, V_{bench} is the computed $T_{\text{-}50}$ value of V_w using the GEV model and V_{est} is obtained as proposed in this study, i.e., by using Hs for $T_{\text{-}50}$ obtained from the GEV model as input value of Equations (8) and (10) (with regression parameters estimated from observed data only). Selection of $T_{\text{-}50}$ is somewhat arbitrary and used to compare deviations of V_w estimated with the GEV model with respect to this study's proposal, but any other $T_{\text{-}yr}$ could be considered. For a more detailed inspection of these deviations, Figures 7, 10 and 11 and those in the Appendix B can be used. Errors in Table 1 are an additional aid to compare which regression scheme leads to better results for any given month.

The proposal in this study can be summarized in the following steps:

(1) Select an Hs value associated with a $T_{\text{-}yr}$ and month of interest (e.g., see Table A1 in Appendix A) as input for Equations (8) or (10).
(2) Select the season (month) for which the correlated values are desired, and the corresponding parameters (Table 1) to be also plugged into Equation (8) or (10), and compute V_w.
(3) Use Hs in step (1) and V_w in step (2) as simultaneous demands associated with the selected $T_{\text{-}yr}$ and month acting over a maritime system to be designed.
(4) If uncertainty is to be used by the designer, the corresponding σ_e together with Equations (11) or (12) can be used to establish upper (or lower) limits by using a δ value (e.g., $\delta = 2$ could be used to approximate the 95% confidence intervals for future values).

5. Discussion

For the proposal briefly outlined in the four steps of the previous section, it is noted that for step (1) the $T_{\text{-}yr}$ values of Hs are related to the GEV model, but any projected return level of the significant wave height available to the designer could be useful, at least as an approximation. Also, since for any given

month selected, two options are available in step (2), namely, Equation (8) or Equation (10), the decision for the more suitable option can be based on the ε_V reported in Table 1, as well as on Figures 7, 10 and 11 and Figures A1–A9. Justification for considering *Hs* and V_w for $T_{\text{-}yr}$ in step (3) as simultaneously occurring metocean variables is based not only on the correlation of recorded (observed) data, but also in checking that the correlation of projected *Hs* and V_w for $T_{\text{-}yr}$, obtained from the time-dependent GEV models, are consistent with the trend of the observed data. Finally, the uncertainty obtained as per Equations (11) or (12) in step (4) approximately delimits all data points if $\delta = 2$ is used (confidence intervals for future values); if the uncertainty from the GEV models is to be employed as reference (perhaps considering the perpendicular embedded lines as an envelope), lower δ values could be used, for instance $\delta = 1.5$, which would be a conservative value to delimit the uncertainty given by the GEV models. Use of Equations (11) or (12) using δ values could be seen as factored demands like the ones used in codified design.

The proposed method allows the possibility of using other metocean variables, data from other buoys and hindcast data. It could use other probabilistic models. More than two variables could be considered if multilinear regression analysis is implemented. If additional recorded data becomes available for any month, the matrix approach in [35] can be implemented to update the parameters in Table 1.

Since the maximum *Hs* and companion V_w may not yield the maximum demand in a given system—like the points in an environmental contour associated with a $T_{\text{-}yr}$ may not lead to the maximum demand in the system [20]—other pairs of simultaneously recorded data could be considered; one obvious combination is using maximum monthly V_w and companion *Hs*, but also other data pairs could be used, for instance the second largest monthly *Hs* and companion V_w, the second largest V_w and companion *Hs*, the third largest monthly *Hs* and companion V_w and so on. Each of the previous combinations would lead to pairs of $T_{\text{-}yr}$ values to which a system could be subjected to for estimating load effects, and the maximum demand could be used for design (in fact, different pairs of $T_{\text{-}yr}$ values could be more critical to different elements of the system). It could be investigated whether these pairs of $T_{\text{-}yr}$ values correspond to points of environmental contours proposed by other authors. Nonetheless, the idea is consistent with the approach of using multiple points from the contours to evaluate a system [20].

6. Conclusions

In this study, a simplified methodology to compute maximum significant wave heights and companion wind velocities associated with given return periods, accounting for seasonality, is presented. Simultaneous data from a buoy in the Gulf of Mexico are used. The approach is developed from projected return levels of significant wave heights based on a time-dependent GEV model and classical regression of the two metocean variables. A time-dependent GEV model for the companion wind velocities is also developed, to assess the adequacy of the method to predict the wind velocity as a function of significant wave height for a given return period.

It is found that the time window selected to estimate return period values of metocean variables can have an important impact in the predicted return levels for some seasons.

It is concluded that correlation of significant weight height and companion wind velocity can be adequately represented by linear or power equations, which could be easily implemented for design purposes, with different parameters to account for seasonality, but with the same functional form. Results are not very dissimilar with predictions from simplified equations in the literature or guidelines; however, it is found that a single equation with given parameters cannot capture the seasonality effects.

It is also found that the uncertainty in the predicted companion wind velocities as a function of significant wave height can be determined in a simplified way by using the root mean squared error from the regression analysis, expressed as a set of proposed equations to determine approximately (but closely)

the 95% confidence intervals of future values. These same equations can be used to represent the envelope of the uncertainty estimated from the GEV models for different return periods.

It is considered that the proposed approach is a simple but adequate method to determine concurrent metocean hazards associated with given return periods, which could be imposed on a system to estimate the demand for design purposes, while also providing measures of uncertainty. The proposed expressions do not differ substantially to those provided in guidelines; thus, they could be amenable to designers, while also incorporating the seasonality effects in a simpler way as compared to other methods available in the literature. To the authors' knowledge, some of the findings in the present study—like the simplified proposal to include the uncertainty in the correlated metocean variables—are not reported elsewhere.

Author Contributions: Conceptualization, F.C.-V., A.-D.G.-S. and C.M.; Formal analysis, F.C.-V., A.-D.G.-S. and C.M.; Funding acquisition, A.-D.G.-S. and C.M.; Investigation, F.C.-V., A.-D.G.-S. and C.M.; Methodology, F.C.-V., A.-D.G.-S and C.M.; Project administration, C.M.; Supervision, A.-D.G.-S. and C.M. All authors have read and agreed to the published version of the manuscript.

Funding: The financial support from the Erasmus Mundus Coastal and Marine Engineering and Management (CoMEM) programme and support from Laboratori d'Enginyeria Marítima, Universitat Politècnica de Catalunya and from Universidad de Guanajuato (CIIC 2020 Research Projects) is gratefully acknowledged.

Acknowledgments: We thank two anonymous reviewers for their comments, suggestions and constructive criticism. We also thank guess Editor Guido Ventura and the editorial team of *Applied Sciences* for their help in the editorial process.

Conflicts of Interest: The authors declare no conflict of interest.

Appendix A

Table A1. Selected return period values for *Hs* in each month.

	***Hs* (m)**				
Month\Tr (yr)	20	30	50	75	100
January	6.08	6.34	6.62	6.83	6.97
February	6.09	6.36	6.68	6.91	7.06
March	5.65	5.94	6.29	6.55	6.73
April	4.78	5.08	5.46	5.76	5.97
May	3.92	4.25	4.71	5.09	5.38
June	4.03	4.53	5.25	5.88	6.36
July	5.03	5.81	6.92	7.93	8.73
August	5.99	6.87	8.13	9.27	10.16
September	6.17	6.84	7.77	8.57	9.18
October	5.90	6.33	6.88	7.34	7.67
November	5.76	6.05	6.41	6.69	6.88
December	5.89	6.14	6.43	6.64	6.78

Table A2. Selected return period values for V_w in each month.

	V_w (m/s)				
Month\Tr (yr)	20	30	50	75	100
January	17.39	18.03	18.76	19.29	19.64
February	17.36	17.92	18.55	19.00	19.29
March	16.41	16.92	17.48	17.88	18.14
April	14.77	15.25	15.80	16.20	16.46
May	13.23	13.79	14.45	14.93	15.26
June	13.30	14.06	14.97	15.66	16.14
July	14.88	15.92	17.22	18.23	18.95
August	16.88	18.14	19.75	21.03	21.95
September	17.98	19.22	20.81	22.09	23.01
October	17.71	18.74	20.05	21.09	21.83
November	17.15	17.99	19.01	19.81	20.37
December	17.08	17.79	18.62	19.25	19.68

Appendix B

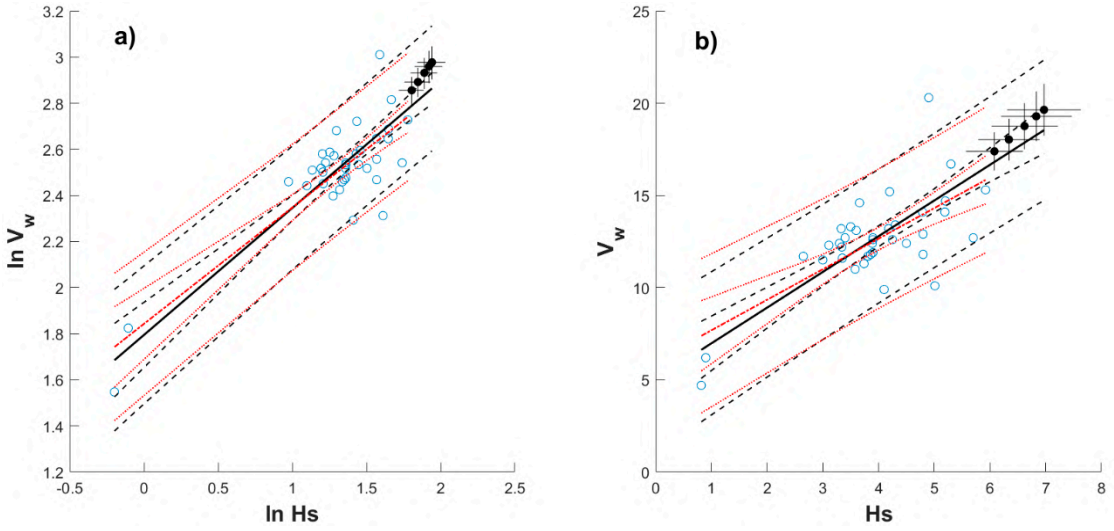

Figure A1. Regression lines and confidence intervals including (solid and dashed lines, respectively) and excluding (dashed–dotted and dotted lines, respectively) $T_{\text{-}yr}$ values for January; (**a**) and (**b**) for logarithmic space and linear space, respectively. Filled circles represent $T_{\text{-}yr}$ values with embedded perpendicular lines indicating confidence intervals from GEV models.

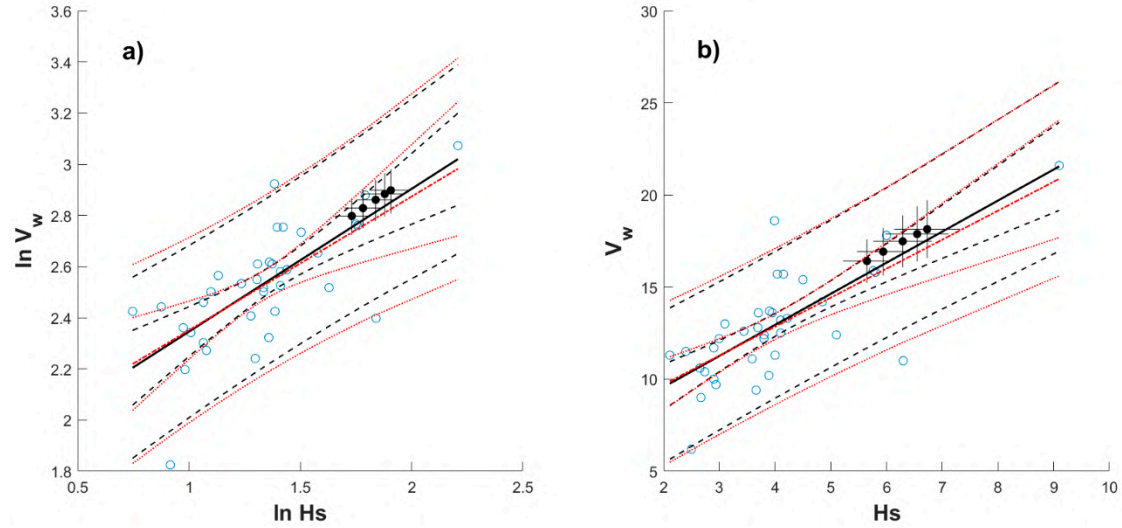

Figure A2. Regression lines and confidence intervals including (solid and dashed lines, respectively) and excluding (dashed–dotted and dotted lines, respectively) $T_{\text{-}yr}$ values for March; (**a**) and (**b**) for logarithmic space and linear space, respectively. Filled circles represent $T_{\text{-}yr}$ values with embedded perpendicular lines indicating confidence intervals from GEV models.

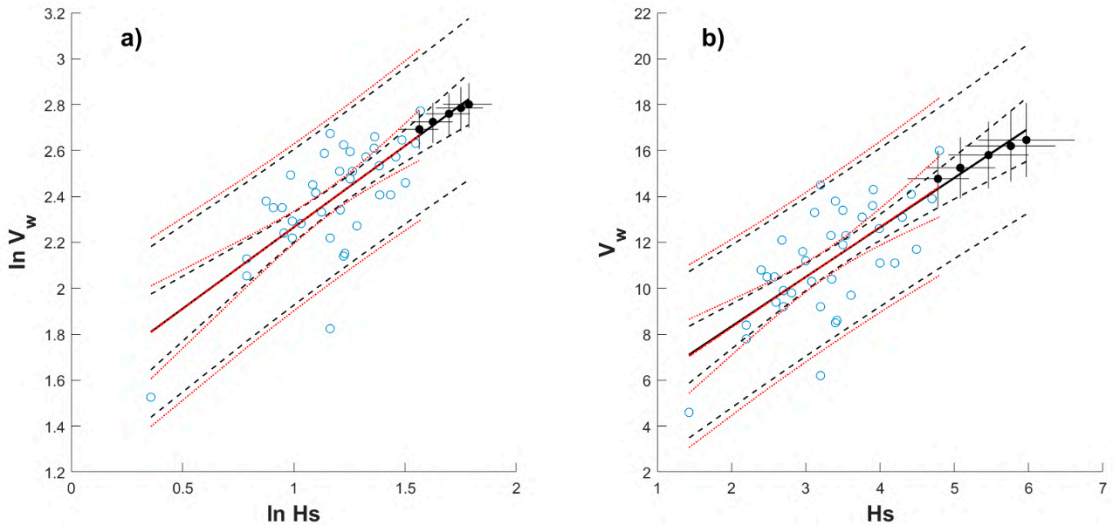

Figure A3. Regression lines and confidence intervals including (solid and dashed lines, respectively) and excluding (dashed–dotted and dotted lines, respectively) $T_{\text{-}yr}$ values for April; (**a**) and (**b**) for logarithmic space and linear space, respectively. Filled circles represent $T_{\text{-}yr}$ values with embedded perpendicular lines indicating confidence intervals from GEV models.

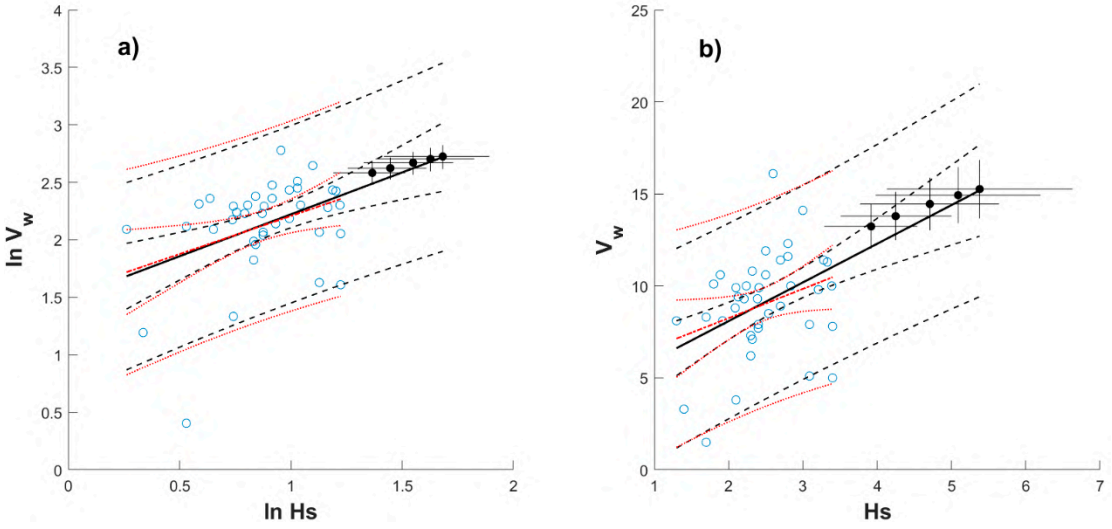

Figure A4. Regression lines and confidence intervals including (solid and dashed lines, respectively) and excluding (dashed–dotted and dotted lines, respectively) $T_{\text{-}yr}$ values for May; (**a**) and (**b**) for logarithmic space and linear space, respectively. Filled circles represent $T_{\text{-}yr}$ values with embedded perpendicular lines indicating confidence intervals from GEV models.

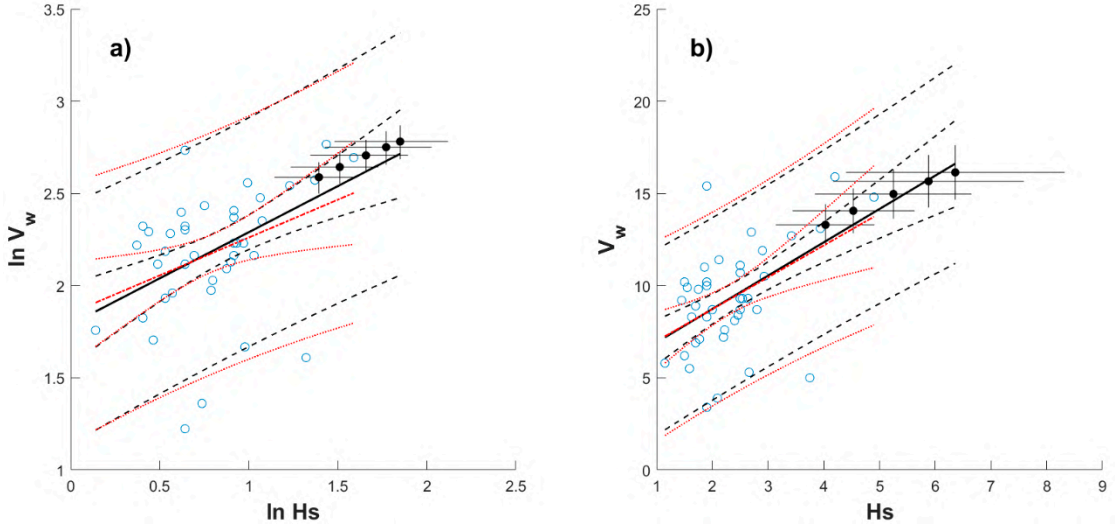

Figure A5. Regression lines and confidence intervals including (solid and dashed lines, respectively) and excluding (dashed–dotted and dotted lines, respectively) $T_{\text{-}yr}$ values for June; (**a**) and (**b**) for logarithmic space and linear space, respectively. Filled circles represent $T_{\text{-}yr}$ values with embedded perpendicular lines indicating confidence intervals from GEV models.

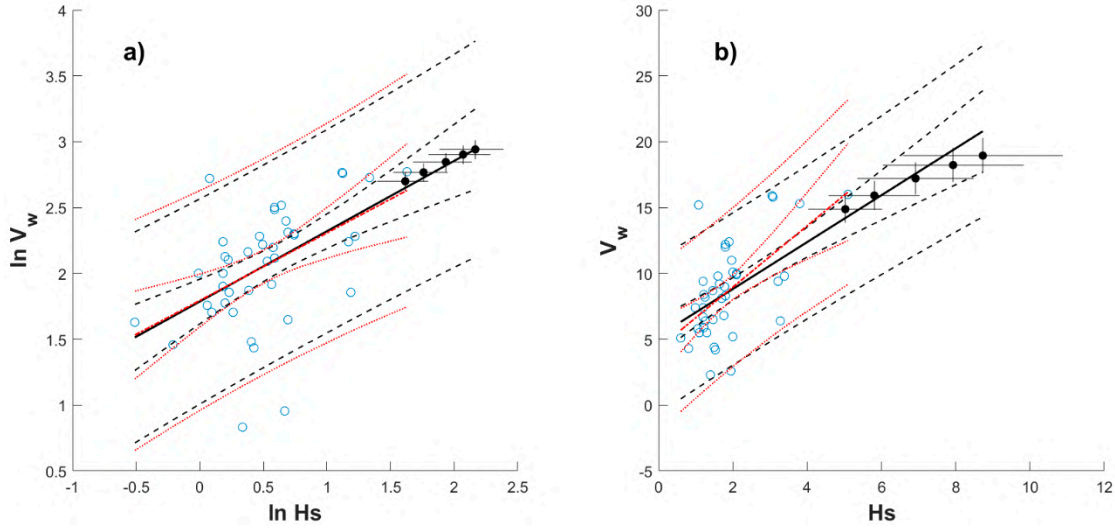

Figure A6. Regression lines and confidence intervals including (solid and dashed lines, respectively) and excluding (dashed–dotted and dotted lines, respectively) $T_{\text{-}yr}$ values for July; (**a**) and (**b**) for logarithmic space and linear space, respectively. Filled circles represent $T_{\text{-}yr}$ values with embedded perpendicular lines indicating confidence intervals from GEV models.

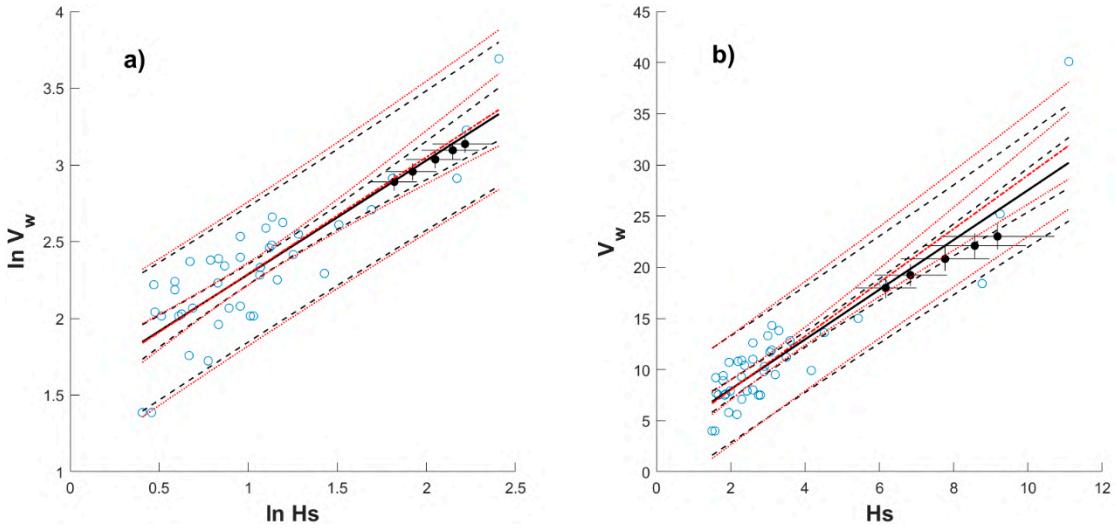

Figure A7. Regression lines and confidence intervals including (solid and dashed lines, respectively) and excluding (dashed–dotted and dotted lines, respectively) $T_{\text{-}yr}$ values for September; (**a**) and (**b**) for logarithmic space and linear space, respectively. Filled circles represent $T_{\text{-}yr}$ values with embedded perpendicular lines indicating confidence intervals from GEV models.

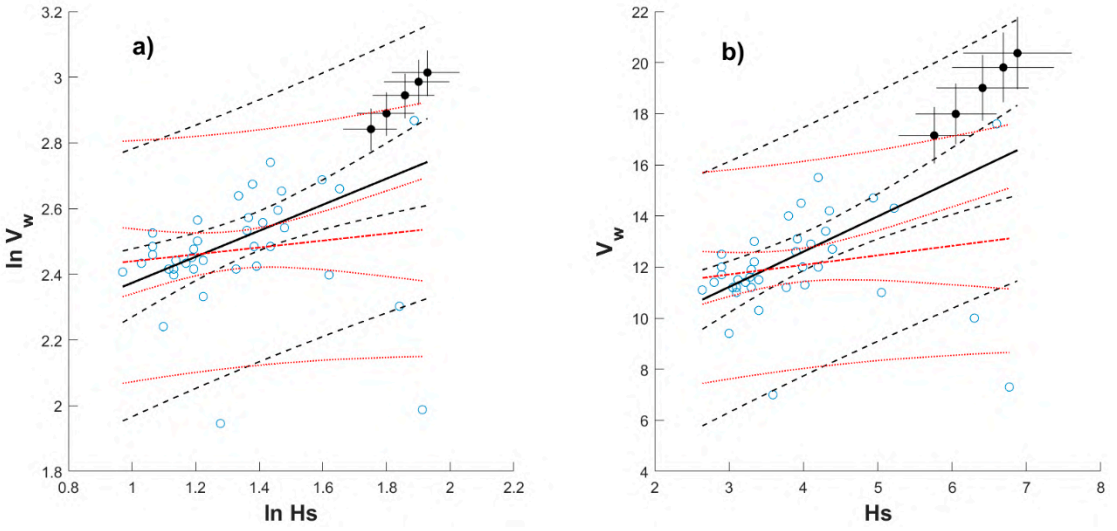

Figure A8. Regression lines and confidence intervals including (solid and dashed lines, respectively) and excluding (dashed–dotted and dotted lines, respectively) $T_{\text{-}yr}$ values for November; (**a**) and (**b**) for logarithmic space and linear space, respectively. Filled circles represent $T_{\text{-}yr}$ values with embedded perpendicular lines indicating confidence intervals from GEV models.

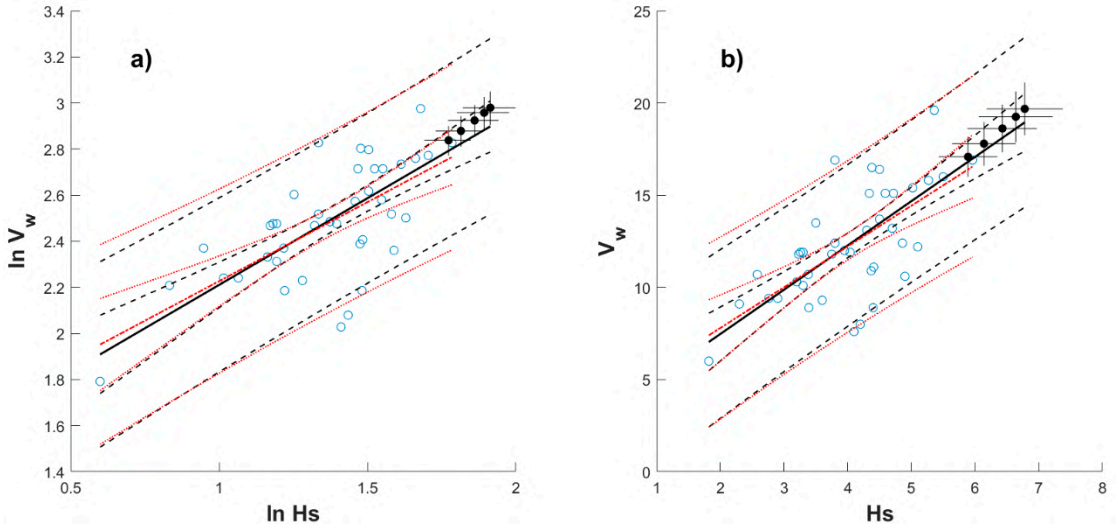

Figure A9. Regression lines and confidence intervals including (solid and dashed lines, respectively) and excluding (dashed–dotted and dotted lines, respectively) T_{-yr} values for December; (**a**) and (**b**) for logarithmic space and linear space, respectively. Filled circles represent T_{-yr} values with embedded perpendicular lines indicating confidence intervals from GEV models.

Appendix C

Table A3. Mean values of residuals for each month and regression scheme.

Month	Log. Space	Lin. Space
January	7.8×10^{-17}	-4.5×10^{-16}
February	3.4×10^{-16}	1.9×10^{-15}
March	-5.1×10^{-16}	1.4×10^{-15}
April	1.8×10^{-17}	1.4×10^{-15}
May	-3.3×10^{-16}	9.1×10^{-17}
June	4.8×10^{-17}	-1.3×10^{-15}
July	1.4×10^{-16}	8.9×10^{-16}
August	4.3×10^{-16}	-3.2×10^{-15}
September	-4.4×10^{-16}	9.5×10^{-16}
October	0.0	8.9×10^{-16}
November	9.9×10^{-17}	-1.4×10^{-15}
December	-5.6×10^{-17}	-2.4×10^{-16}

References

1. Castillo, E.; Hadi, A.S.; Balakrishnan, N.; Sarabia, J.M. *Extreme Value and Related Models with Applications in Engineering and Science*; Wiley: Hoboken, NJ, USA, 2004; Volume 4, pp. 1–362.
2. Hong, H.P. Estimate of extreme wind and wave loading and safety level of offshore structures. In Proceedings of the Risk Analysis: Proceedings of a Symposium, Ann Arbor, MI, USA, 11–12 August 1994; University of Michigan: Ann Arbor, MI, USA, 1994; Volume 4, pp. 107–117.
3. Nessim, M.A.; Hong, H.P.; Swail, V.R.; Henderson, C.A. Design criteria for offshore structures under combined wind and wave loading. *J. Offshore Mech. Arct. Eng.* **1995**, *117*, 1–11. [CrossRef]
4. Shao, Z.; Liang, B.; Li, H.; Lee, D. Study of sampling methods for assessment of extreme significant wave heights in the South China Sea. *Ocean Eng.* **2018**, *168*, 173. [CrossRef]

5. Shao, Z.; Liang, B.; Li, H.; Wu, G.; Wu, Z. Blended wind fields for wave modeling of tropical cyclones in the the South China Sea and East China Sea. *Appl. Ocean Res.* **2018**, *71*, 20. [CrossRef]
6. Ludeno, G.; Serafino, F. Estimation of the Significant Wave Height from Marine Radar Images without External Reference. *J. Mar. Sci. Eng.* **2019**, *7*, 432. [CrossRef]
7. Chen, S.-T.; Wang, Y.-W. Improving Coastal Ocean Wave Height Forecasting during Typhoons by using Local Meteorological and Neighboring Wave Data in Support Vector Regression Models. *J. Mar. Sci. Eng.* **2020**, *8*, 149. [CrossRef]
8. Gao, H.; Shao, Z.; Wu, G.; Li, P. Study of Directional Declustering for Estimating Extreme Wave Heights in the Yellow Sea. *J. Mar. Sci. Eng.* **2020**, *8*, 236. [CrossRef]
9. Katalinić, M.; Parunov, J. Uncertainties of Estimating Extreme Significant Wave Height for Engineering Applications Depending on the Approach and Fitting Technique—Adriatic Sea Case Study. *J. Mar. Sci. Eng.* **2020**, *8*, 259. [CrossRef]
10. Cavaleri, L.; Barbariol, F.; Benetazzo, A. Wind–Wave Modeling: Where We Are, Where to Go. *J. Mar. Sci. Eng.* **2020**, *8*, 260. [CrossRef]
11. Weisse, R.; Gaslikova, L.; Geyer, B.; Groll, N.; Meyer, E. Coastdat—Model data for science and industry. *Kuste Westholsteinische Verl. Boyens Co.* **2014**, *81*, 5–18.
12. Weisse, R.; Groll, N. A multi-decadal wind-wave hindcast for the North Sea 1949–2014: CoastDat2. *Earth Syst. Sci. Data* **2017**, *9*, 955.
13. Monish, N.T.; Rehana, S. Suitability of distributions for standard precipitation and evapotranspiration index over meteorologically homogeneous zones of India. *J. Earth Syst. Sci.* **2020**, *129*, 25. [CrossRef]
14. Schardong, A.; Simonovic, S.P.; Gaur, A.; Sandink, D. Web-Based Tool for the Development of Intensity Duration Frequency Curves under Changing Climate at Gauged and Ungauged Locations. *Water* **2020**, *12*, 1243. [CrossRef]
15. Prakash, A.; Panchang, V.; Ding, Y.; Ntaimo, L. Sign Constrained Bayesian Inference for Nonstationary Models of Extreme Events. *J. Waterw. Port Coast. Ocean Eng. ASCE* **2020**, *146*, 04020029. [CrossRef]
16. Kim, H.-J.; Suh, S.-W. Improved Hypothetical Typhoon Generation Technique for Storm Surge Frequency Analyses on the Southwest Korean Coast. *J. Coast. Res.* **2018**, *85*, 516. [CrossRef]
17. Weinan, H.; Shanshan, T.; Qiang, B.; Sheng, D. Bivariate Distribution Modelling for Wave Height and Period in Jiaozhou Bay. In Proceedings of the ASME 2018 37th International Conference on Ocean, Offshore and Arctic Engineering 2018, Volume 11B: Honoring Symposium for Professor Carlos Guedes Soares on Marine Technology and Ocean Engineering, Madrid, Spain, 17–22 June 2018. V11BT12A054. [CrossRef]
18. Sartini, L.; Besio, G.; Cassola, F. Spatio-temporal modelling of extreme wave heights in the Mediterranean Sea. *Ocean Model.* **2017**, *117*, 52. [CrossRef]
19. Muraleedharan, G.; Lucas, C.; Guedes Soares, C. Regression quantile models for estimating trends in extreme significant wave heights. *Ocean Eng.* **2016**, *118*, 204. [CrossRef]
20. Ross, E.; Astrup, O.C.; Bitner-Gregersen, E.; Bunn, N.; Feld, G.; Gouldby, B.; Liu, Y.; Randell, D.; Vanem, E.; Jonathan, P. On environmental contours for marine and coastal design. *Ocean Eng.* **2020**, *195*, 1. [CrossRef]
21. Vanem, E. A simple approach to account for seasonality in the description of extreme ocean environments. *Mar. Syst. Ocean Technol.* **2018**, *13*, 63. [CrossRef]
22. Randell, D.; Feld, G.; Ewans, K.; Jonathan, P. Distributions of return values for the ocean wave characteristics in the South China Sea using directional-seasonal extreme value analysis. *Environmetrics* **2015**, *26*, 442. [CrossRef]
23. Randell, D.; Turnbull, K.; Ewans, K.; Jonathan, P. Bayesian inference for nonstationary marginal extremes. *Environmetrics* **2016**, *27*, 439. [CrossRef]
24. Ross, E.; Randell, D.; Ewans, K.; Feld, G.; Jonathan, P. Efficient estimation of return value distributions from non-stationary marginal extreme value models using Bayesian inference. *Ocean Eng.* **2017**, *142*, 315. [CrossRef]
25. Anokhin, V.; Randell, D.; Ross, E.; Jonathan, P. Spatial and seasonal variability of metocean design criteria in the southern south China Sea from covariate extreme value analysis. In Proceedings of the ASME 2019 38th International Conference on Ocean, Offshore and Artic Engineering, OMAE, Glasgow, Scotland, UK, 9–14 June 2019; Volume 1.

26. Bitner-Gregersen, E.M. Comparison of wind and wave climate in open sea and coastal waters. *Ocean Eng.* **2018**, *170*, 199. [CrossRef]
27. National Data Buoy Center (NDBC). Available online: www.ndbc.noaa.gov (accessed on 30 June 2020).
28. Calderón-Vega, F.; Vázquez-Hernández, A.O.; García-Soto, A.D. Analysis of extreme waves with seasonal variation in the Gulf of Mexico using a time-dependent GEV model. *Ocean Eng.* **2013**, *73*, 68–82. [CrossRef]
29. Coles, S.G. *An Introduction to Statistical Modelling of Extreme Values*, 1st ed.; Springer: London, UK, 2001; Volume 4, pp. 1–208.
30. Calderón Vega, F. Caracterización del Régimen Extremal del Oleaje en el Golfo de México Considerando la Variación Estacional. Master's Thesis, Universidad de Cantabria, Santander, Spain, 2009. (In Spanish)
31. Bitner-Gregersen, E.M.; Gramstad, O. Potential Changes in the Joint Probabilistic Description of the North Atlantic Wave Climate. In Proceedings of the ASME 2018 37th International Conference on Ocean, Offshore and Arctic Engineering, Volume 11B: Honoring Symposium for Professor Carlos Guedes Soares on Marine Technology and Ocean Engineering, Madrid, Spain, 17–22 June 2018. V11BT12A056. [CrossRef]
32. Hong, H.P.; Zimmerman, T.J.; Bach, L. Probabilistic basis of resistance factors for use in oriented strand board. In Proceedings of the 1st Structural Specialty Conference, Canadian Society of Civil Engineering, Edmonton, AB, Canada, 29 May–1 June 1996; pp. 1223–1235.
33. Jordaan, I. *Decisions under Uncertainty: Probabilistic Analysis for Engineering Decisions*, 1st ed.; Cambridge University Press: Cambridge, UK, 2005; pp. 1–672.
34. Kottegoda, N.T.; Rosso, R. *Applied Statistics for Civil and Environmental Engineers*, 2nd ed.; Blackwell Publishing-Wiley: Oxford, UK, 2008; pp. 1–718.
35. Faber, M.H. *Statistics and Probability Theory: In Pursuit of Engineering Decision Support*, 2nd ed.; Springer: Dordrecht, The Netherlands; Heidelberg, Germany; London, UK; New York, NY, USA, 2012; pp. 1–190.

Paper B

Revisiting Two Simulation-Based Reliability Approaches for Coastal and Structural Engineering Applications.

Adrián-David García-Soto, Felícitas Calderón-Vega, César Mösso, Jesús-Gerardo Valdés-Vázquez and Alejandro Hernández-Martínez

Applied Sciences. Appl. Sci. 2020, 10, 8176; doi:10.3390/app10228176.

applied sciences

MDPI

Article

Revisiting Two Simulation-Based Reliability Approaches for Coastal and Structural Engineering Applications

Adrián-David García-Soto [1,*], Felícitas Calderón-Vega [1,2], César Mösso [2,3], Jesús-Gerardo Valdés-Vázquez [1] and Alejandro Hernández-Martínez [1]

[1] Department of Civil Engineering, Universidad de Guanajuato, Juárez 77, Zona Centro, Guanajuato 36000, Gto., Mexico; felicitas.calderon@upc.edu (F.C.-V.); valdes@ugto.mx (J.-G.V.-V.); alejandro.hernandez@ugto.mx (A.H.-M.)

[2] Laboratori d'Enginyeria Marítima, Universitat Politècnica de Catalunya, Jordi Girona 1-3, Mòdul D1, Campus Nord, 08034 Barcelona, Spain; cesar.mosso@upc.edu

[3] Centre Internacional d'Investigació dels Recursos Costaners, Jordi Girona 1-3, Mòdul D1, Campus Nord, 08034 Barcelona, Spain

* Correspondence: adgarcia@ugto.mx; Tel.: +52-473-1020-100 (ext. 2235)

Received: 17 October 2020; Accepted: 17 November 2020; Published: 18 November 2020

Featured Application: Normality polynomials can be used to compute reliabilities for coastal and structural engineering applications, including the assessment of uncertainty in the estimated reliability index. Additionally, multi-linear regression can be applied to the simulated results to determine design points and sensitivity factors. These applications can be potentially extended to different engineering (or other) fields and to system reliability (e.g., for reinforced concrete frame buildings).

Abstract: The normality polynomial and multi-linear regression approaches are revisited for estimating the reliability index, its precision, and other reliability-related values for coastal and structural engineering applications. In previous studies, neither the error in the reliability estimation is mathematically defined nor the adequacy of varying the tolerance is investigated. This is addressed in the present study. First, sets of given numbers of Monte Carlo simulations are obtained for three limit state functions and probabilities of failure are computed. Then, the normality polynomial approach is applied to each set and mean errors in estimating the reliability index are obtained, together with its associated uncertainty; this is defined mathematically. The data is also used to derive design points and sensitivity factors by multi-linear regression analysis for given tolerances. Results indicate that power laws define the mean error of the reliability index and its standard deviation as a function of the number of simulations for the normality polynomial approach. Results also indicate that the multi-linear regression approach accurately predicts reliability-related values if enough simulations are performed for a given tolerance. It is concluded that the revisited approaches are a valuable option to compute reliability-associated values with reduced simulations, by accepting a quantitative precision level.

Keywords: reliability index error; power law; normality polynomial; multi-linear regression; sensitivity factors; coastal engineering; structural engineering

1. Introduction

Simulations are often used to estimate the probability of failure of structural elements and systems because they are a very versatile option which is not restricted by complex and implicit limit state functions (LSF), the use of sophisticated methods (e.g., finite element method), and/or highly non-linear structural behavior. However, millions of crude Monte Carlo simulations (MCS) could be required to adequately estimate structural probabilities of failure, which may not be feasible; also, the results could differ from a set of simulations to another. To cope with this issue, modified versions of the crude simulation approach, surrogate modeling, subset simulation, and other techniques have emerged and been used in the last decades not only for structural engineering but also in other fields. To mention only a few studies which employ some of these techniques, optimization using surrogate modeling, reliability analysis of deteriorating structural systems and the reliability assessment of a structure affected by chloride attack are reported in the studies by [1–3], respectively. Importance sampling has also been used to estimate the system reliability of deteriorating pipelines [4]. Other kind of approaches are also reported in the literature to compute reliabilities [5]. The different reliability methods can be applied not only to different fields in structural and geotechnical engineering, as for the case of sudden column removal in reinforced concrete buildings and rockfall protection structures [6–8], but also to many other research and engineering fields, for instance to artic oil and gas facilities [9] and to coastal engineering applications [10]. This last case is used in the present study to show the applicability of two revisited methods to obtain the reliability of coastal structures.

Other simulation-based reliability methods have not been given so much attention. In this study a couple of these alternatives are revisited to inspect their feasibility and adequacy to estimate reliability indices. One of them employs polynomial transformations of a nonnormal variable to a normal one by fitting simulated data with fractile constraints and can be referred to as normality polynomial approach [11]. The second approach was developed to derive the design point and sensitivity factors (in the FORM, first order reliability method, perspective) from simulated data [12] and it is referred to as the multi-linear regression approach in this study. A similar approach to the normality polynomial method was previously developed by Hong and Lind [13] and named normal polynomial approach (note that the names are slightly different); unlike the normality polynomial approach, the normal polynomial approach has been paid much more attention (judging by number of citations), even very recently (e.g., [14]). Both methods are based on the fact [15,16] that a fractile of a random variable can be expressed as polynomial of a fractile of a standard normal variable (normal polynomial), and that a fractile of a standard normal variable can be expressed as a polynomial of a fractile of a random variable (normality polynomial). Although the normal polynomial approach [13] is not considered in the present study (we prefer to focus in the less explored alternative), the findings here could be extended to do so.

To inspect the adequacy of the normality polynomial approach and the multi-linear regression approach (the methods revisited in the present study), three LSFs are considered. One is based on a very simple classical case; other one is based on a structural application from a previous study and the last one is related to the reliability of a coastal structure. Extensive simulations are performed to estimate the error level by using the normality polynomial approach and its associated uncertainty; neither of these was thoroughly carried out in previous studies, nor the application to coastal engineering. The design point and sensitivity factors (also the reliability index) obtained from simulated data are compared with those obtained from FORM; they are derived from a multi-linear regression of the simulated data. It is worth to mention that these methods, and others developed in the 1990s, used to state that a large number of simulations were not feasible; nevertheless, the computer power has increased substantially in the last decades, and the limitations of those days may not be as restrictive as before and thus the applicability could be currently extended. Furthermore, the commercial software available nowadays for engineering applications normally includes amenable built-in functions for linear and multi-linear regression analysis which simplifies the programming.

The main objective of this study is to define the error statistics in the reliability index by using normality polynomials and to reassess the feasibility and adequacy of this method and the multi-linear regression approach for estimating the reliability of structural and coastal engineering systems including the determination of sensitivity factors.

This study is of significance to the coastal and structural engineering fields because the number of simulations required to compute reliabilities can be reduced by accepting defined error levels when using normality polynomials, which was not established in previous studies. This is possible because the error in the estimation of the reliability index is mathematically defined as a function of the number of simulations for the cases investigated. Additionally, other contribution is the use of multi-linear regression applied to simulated results as a mean to determine sensitivity factors, design points and the probability of failure; not only a slightly modified (improved) version of the multi-linear regression approach but also the number of simulations and tolerances required to achieve adequate results are provided for guidance.

2. Methods Revisited

2.1. Normality Polynomial

In this section the normality polynomial proposed in [11] is described. The mathematical form is given by

$$z_p = \sum_{j=0}^{r} a_j \left(y_p\right)^j \tag{1}$$

where z_p denotes p-fractile of a standard normal variable Z with probability density function (PDF), $\Phi(z)$, and cumulative distribution function (CDF), $\Phi(z)$; y_p denotes p-fractile of a random variable Y with PDF, $f_Y(y)$, and CDF, $F_Y(y)$; a_j, j = 1, 2, …, r, are the coefficients of a rth-order polynomial determined by fractile fitting. The fractile fitting is based on considering the following fractile constraints from a set of independent random observations of Y (i.e., y_1, y_2, … y_i, … y_n) arranged in ascending order

$$(y_i, F(y_i)) = \left(y_i, \frac{i}{n+1}\right), \qquad i = 1, 2, \ldots, n \tag{2}$$

These fractile constraints can be mapped into a normal space by using

$$z_i = \Phi^{-1}\left(F(y_i)\right), \qquad i = 1, 2, \ldots, n \tag{3}$$

where $\Phi^{-1}(\bullet)$ denotes the inverse of the standardized normal distribution function. The rth-order polynomial (Equation (1)) with $r + 1 < n$ is used to model the distribution of the transformed random variable Y. By considering the constraints in Equation (2), the coefficients a_j in Equation (1) can be determined using the least square method by minimizing the error ε_{fit} given by

$$\varepsilon_{fit} = \sum_{j=1}^{m} \left(z_j - \sum_{i=0}^{r} a_i \left(y_j\right)^i \right)^2 \tag{4}$$

where m is the number of constraints. The probability P ($Y \le y_0$) is given by the CDF, i.e., $F(y_0)$, and can be computed with

$$F(y_0) = \Phi(z_p) \tag{5}$$

where z_p is obtained by substituting y_0 instead of y_p in Equation (1). If Y is the resulting random variable of the LSF, the probability of failure, p_f, is

$$p_f = F(0) = \Phi(a_0) \tag{6}$$

and the reliability index is [17]

$$\beta = -\Phi^{-1}\left(p_f\right) \tag{7}$$

From Equation (7), it can be inferred that the reliability index can be readily obtained once the coefficients a_j are determined (i.e., $\beta = -a_0$). This is so, because a_0 has a similar meaning to the so-called generalized reliability index [11]. It is noted that the roots of the polynomial are not required [11] (unlike in the method in [13]). In the applications shown later, a third-order normality polynomial is used [11].

It is pointed out that although the mathematical background of the normality polynomials is not thoroughly described here, it is based on sound grounds [11], like the advance theory of statistics [15,16] and the fact that fractile constraints hold by a combinatorial argument [18,19].

Before going to the applications, the second revisited approach in this study is described in the following section.

2.2. Design Point and Sensitivity Factors from Simulations

The obtaining of the design point and sensitivity factors (from the FORM standpoint) based on a previous study [12] is described herein. The basic idea is that simulated data close to the limit state surface (within a prescribed tolerance, e) can be retrieved, as well as their associated sampled values for each or the random variables given by the LSF (input values combinations considered as a point in the hyperspace), and a multi-linear regression is performed to approximate the linearized limit state surface at the design point. Before the multi-linear regression is performed to fit the hyperplane, the considered points are mapped into a standard normal space. Such hyperplane is an approximation of the LSF, g, and is used to assess the design point and sensitivity factors. The mathematical formulation is given below.

A set of n independent random variables is denoted by $\boldsymbol{X} = (x_1, x_2, \ldots, x_n)$. $\boldsymbol{X}^j$ *defines* the j-th randomly generated value of $\boldsymbol{X}$. For a given number of crude Monte Carlo simulations, n_{sim}, X_{js} which satisfy the criterion below (slightly changed from the original formulation in [12]) are selected

$$|0 - \mathrm{g}(\boldsymbol{X}^k)| < e_l \tag{8}$$

where $\boldsymbol{X}^k$ in the LSF is included to emphasize that it is a function of a set of random variables. Hong and Nessim [12] used $e = 0.05$ (i.e., 5%) in their study (instead of e_l in Equation (8) and defined below). However, it was noticed that this value could be inadequate depending on the units and magnitude of the considered random variables. Therefore, the distance between zero and the smallest simulated value of g in absolute terms (l_{low}) is used to set the tolerance as the fraction given by l_{low} multiplied by e (i.e., $e_l = e \times l_{low}$ is used instead of e in Equation (8)). The selected values of $\boldsymbol{X}^k$ based on the described criterion are then mapped into a standard normal space [17] using

$$\boldsymbol{Z} = [z_1, z_2, \ldots, z_n] = \left[\Phi^{-1}\left(F_1(x_1)\right), \Phi^{-1}\left(F_2(x_2)\right), \ldots, \Phi^{-1}\left(F_n(x_n)\right)\right] \tag{9}$$

where $\boldsymbol{Z}$ is the image of $\boldsymbol{X}$ in standard normal space, Φ is the normal standard CDF and F_i, $I = 1, 2, \ldots, n$, are the CDFs of the random variables x_i. In the standard normal space, a linear function is fitted to the set of selected points using multi-linear regression. Such linear function is given by

$$\sum_{i=1}^{n} b_i z_i + c = 0 \tag{10}$$

where b_i and c are constants to be determined in the multi-linear regression analysis. The resulting linear regression equation is to be used in the same sense as the FORM [17] to estimate the design point and sensitivity factors. The latter are denoted by α_i, $i = 1, 2, \ldots, n$, and given by the gradient vector of Equation (10) as indicated below

$$\alpha_i = {-b_i}\Big/{\sqrt{\sum_{i=1}^{n} b_i^2}} \tag{11}$$

Note that the reliability index can also be estimated as the smallest distance between the linear surface and the origin as

$$\beta = {c}\Big/{\sqrt{\sum_{i=1}^{n} b_i^2}} \tag{12}$$

As regards the design point (in the normal space) it is given by

$$z_{id} = \alpha_i \beta \tag{13}$$

The design point in the original space can now be determined with the inverse transformation of z_{id}, as

$$x_{id} = F_i^{-1}\left(\Phi(z_{id})\right) \tag{14}$$

The subscript i in Equations (11)–(14) is associated to the random variable x_i. The inverse transformation in Equation (14) is dependent on the PDF of x_{id} and, in the case of the Longuet-Higgins distribution [20] used for the coastal engineering example, the inverse transformations of z_{id} requires of a numerical approach to be determined.

The formulation in this section, and the one in the previous section, are to be applied to three case studies in the following section to evaluate their adequacy for structural and coastal engineering, and to assess their deviation with respect to the exact reliability index.

3. Applications and Results

3.1. A Classical Limit State Funtion

The two approaches described in the previous section are applied here to the simplest classical LSF

$$g = R - L \tag{15}$$

where R and L can be considered, in a broad sense, as random variables for the capacity and demand of a system element. For the sake of simplicity and illustration purposes, units are skipped and both random variables are assumed independent and characterized with lognormal distributions, with mean values and standard deviations m_R = 10, m_L = 5.6, σ_R = 1, and σ_L = 0.75 for the capacity and demand, respectively. These values are arbitrary, except by the fact that they lead to a reliability index equal to practically 3.5, which is a common reference for code calibration and that can be computed with the following expression [21,22]

$$\beta_{RE} = \frac{\left(ln\, m_R - \frac{1}{2}\ln(1+v_R^2)\right) - \left(ln\, m_L - \frac{1}{2}\ln(1+v_L^2)\right)}{\sqrt{\ln(1+v_R^2) + \ln(1+v_L^2)}} \approx \frac{\ln m_R - \ln m_L}{\sqrt{v_R^2 + v_L^2}} \tag{16}$$

where v_R and v_L are the coefficients of variation of R and L, respectively. This reliability index is shown in Figure 1a (dashed line), as a reference to inspect how close are the βs obtained by crude Monte Carlo simulations as a function of the number of simulations (shown in logarithmic scale in the horizontal axis from 2×10^1 to 2×10^7) to the exact value. The reliability index for Equation (15) using Monte Carlo simulations (dashed-dotted line in Figure 1a) is obtained by plugging into Equation (7) the following probability of failure

$$p_f = {}^{n_{fail}}/_{n_{sim}} \tag{17}$$

which is simply the ratio of number of failures, n_{fail}, to the total number of simulations. The latter (i.e., n_{sim}) is also the number of fractile constraints when the reliability index is computed with the normality polynomial approach, also depicted in Figure 1a (solid line).

Additional runs are shown in Figure 1b–d, which indicate that the results are different and dependent on the generated random numbers of each run, but they stabilize if enough simulations are performed or enough fractile constraints are used. Other observations from Figure 1 include that β cannot always be computed with the Monte Carlo simulations (MCS) (not a single failure is obtained), while the opposite occurs when using normality polynomials, although significant deviations are observed for a limited number of simulations, that the fitted normality polynomials tends to deviate less from the exact reliability index for fewer n_{sim}, and that such error in the precision may not be large for a relative small n_{sim}, (e.g., 1×10^3).

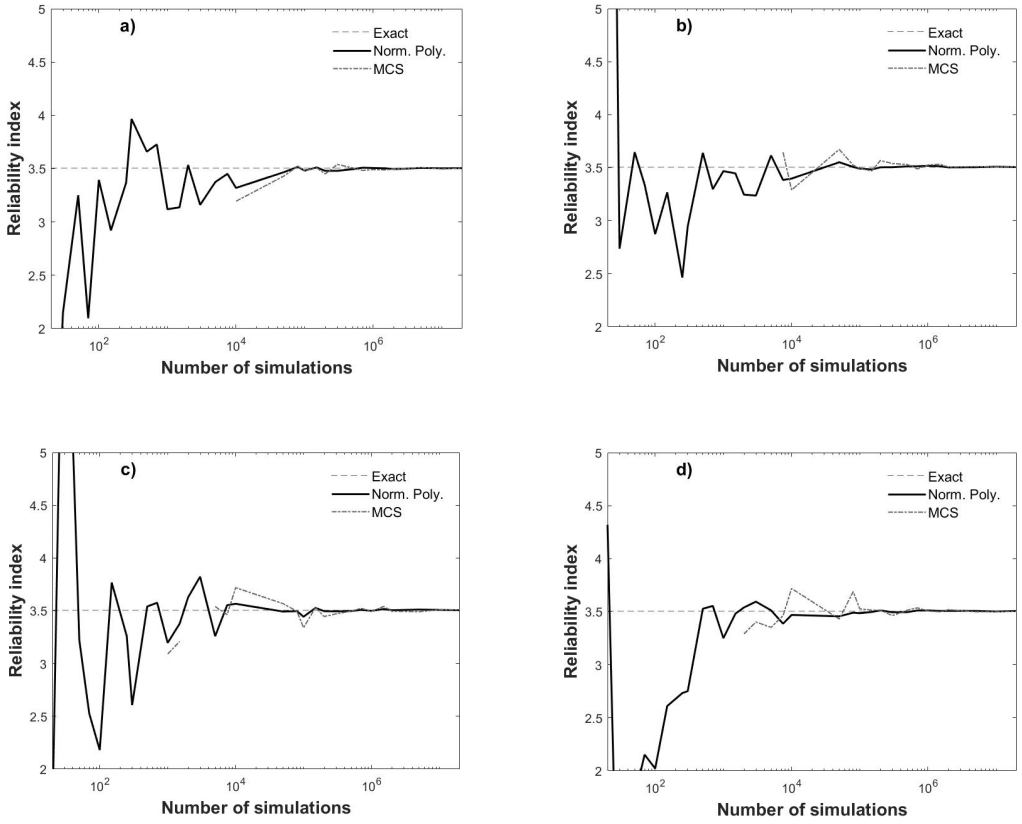

Figure 1. Reliability index as a function of the number of simulations. (**a**), (**b**), (**c**) and (**d**) are different runs for the MCS.

To quantitatively inspect these deviations, β_{RE} is to be used as benchmark to assess the exactness of the used methods (i.e., normality polynomials and MCS) in terms of the relative percentual error given by

$$\varepsilon = \left| \frac{\beta_{bench} - \beta_{oth}}{\beta_{bench}} \right| \times 100 \tag{18}$$

where β_{bench} denotes the reliability index considered as benchmark and β_{oth} is the reliability index computed with any other method. A total of 1000 runs are performed for each n_{sim}, and ε is computed for each of the runs. Then, the mean values of the error and their uncertainties (the unbiased standard deviation) are computed and plotted for the whole range of n_{sim} in Figure 2 (solid lines and dashed lines for normality polynomial and MCS mean errors, respectively), where the mean errors ± one standard deviation are also depicted in grey lines.

Figure 2 shows that is not always possible to compute the statistics for the MCS; this happens when not a single failure is reported in one or more of the 1000 runs for a given n_{sim} (at least 5×10^4 are necessary). This is not a problem when using the fitted polynomials. Additionally, the MCS approach always tend to larger mean errors and standard deviations for a decreasing number of simulations. This makes the normality polynomial approach more adequate for estimating the reliability indices; however, for few simulations the errors are too large. Nevertheless, the designer could decide which precision level (quantitatively) is willing to accept using information like the one in Figure 2 as an aid (and reduce the number of required simulations as a function of such an accepted error).

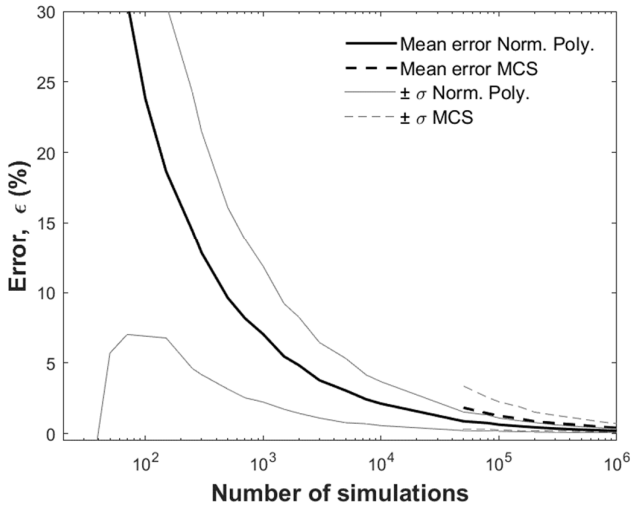

Figure 2. Deviations from the exact reliability index as percentage error.

If desired, the curves in Figure 2 could be casted as a mathematical expression. For instance, the following power equations fit very well the mean (μ_ε) and standard deviation (σ_ε) of the error in Figure 2 (by fitting from 2.5×10^2 simulations and over)

$$\mu_\varepsilon = 257.2 \times n_{sim}^{-0.5244} \tag{19}$$

$$\sigma_\varepsilon = 157.3 \times n_{sim}^{-0.5068} \tag{20}$$

If the power in Equations (19) and (20) is assumed as −0.5 in both expressions, the coefficient of variation of the error is $v_\varepsilon \approx 150/250 \approx 0.6$, i.e., it is constant and roughly independent of the number of simulations; the actual v_ε obtained from the 1000 runs does exhibit such a roughly constant behavior for this case, except that it is ≈0.7 (difference related to the actual different powers in Equations (19) and (20)). Power equations like Equations (19) and (20) can be linearized by taking logarithms on both sides. Therefore, if the involved variables are transformed into the logarithmic space, a linear fitting can be performed. In this study, we simply used a built-in function in the commercial software for the fitting.

Coefficients for the fitted normality polynomial in Figure 1a are shown in Table 1 (upper set of values) for selected values of n_{sim}. The computing of these coefficients is based on minimizing the error in Equation (4) and was implemented in the coded program by using a built-in function of the programming language employed (MATLAB). As mentioned before, the coefficients a_0 can be linked to the generalized reliability index. Coefficients for results in Figure 1b–d (or those associated to Figure 2) were computed but not shown for brevity.

As regards the reliability index, design point and sensitivity factors derived from the simulations (i.e., those obtained with Equations (11), (12), and (14)), they are compared with those obtained by applying the FORM to Equation (15). They are summarized in Table 2 for selected values of n_{sim}.

Results listed in Table 2 indicate that when the points obtained by applying the criterion in Equation (8) were enough to successfully perform a multi-linear regression (also with a built-in function, as in the case of the normality polynomial fitting), β did not deviate from the exact value, but marginally, just like the reliability index obtained with FORM. However, a relatively large n_{sim} was required, usually at least 1×10^5 simulations (by inspecting all the $1000 \times n_{sim}$ cases used to derived Figure 2); this depends on each run (implicitly the generated random numbers in each simulation), and sometimes less than 1×10^5 simulations are required. For the considered runs, 2×10^5 simulations seem to guarantee the obtaining of the values reported in Table 2. In any case, when the muti-linear regression is successfully performed, the results are quite adequate and invariant for increasing number of simulations; this is also the case for the coefficients of the regression (i.e., they remain independent of n_{sim}), which are $c = 0.5837$, $b_1 = 0.0998$, and $b_2 = -0.1333$.

Table 1. Coefficients of the fitted normality polynomials.

Classic LSF, Equation (15)					
n_{sim}	a_0	a_1	a_2	a_3	a_4
1 × 10³	−3.1193	3.9078	3.6571	−1.9371	----
1 × 10⁴	−3.3195	4.9672	1.8106	−0.9905	----
1 × 10⁵	−3.4813	5.8709	0.2415	−0.1324	----
Structural LSF, Equation (21) $r_{V/D}$ **= 0.4**					
n_{sim}	a_0	a_1	a_2	a_3	a_4
1 × 10³	−3.0950	6.3170×10^{-07}	3.8257×10^{-14}	-3.2619×10^{-21}	----
1 × 10⁴	−3.2923	7.3372×10^{-07}	2.1457×10^{-14}	-2.3097×10^{-21}	----
1 × 10⁵	−3.3341	7.8972×10^{-07}	5.2658×10^{-15}	-1.0534×10^{-21}	----
Structural LSF, Equation (21) $r_{V/D}$ **= 0.4 4th-order**					
n_{sim}	a_0	a_1	a_2	a_3	a_4
1 × 10³	−2.8726	1.7464×10^{-07}	2.7997×10^{-13}	-5.0461×10^{-20}	3.1134×10^{-27}
1 × 10⁴	−3.2802	6.7401×10^{-07}	6.0193×10^{-14}	-1.0616×10^{-20}	5.7321×10^{-28}
1 × 10⁵	−3.2799	7.1276×10^{-07}	3.6215×10^{-14}	-5.7785×10^{-21}	2.4322×10^{-28}

Table 2. Design point, β and α_i by using multi-linear regression and first order reliability method (FORM).

		Design Point		**Sensitivity Factors**	
n_{sim}	β	x_R	x_L	α_R	α_L
1 × 10⁴	----	----	----	----	----
5 × 10⁴	----	----	----	----	----
1 × 10⁵	3.5055	8.0699	8.0699	−0.5990	0.8007
2 × 10⁵	3.5055	8.0699	8.0699	−0.5990	0.8007
1 × 10⁶	3.5055	8.0699	8.0699	−0.5990	0.8007
FORM	3.5055	8.0670	8.0670	−0.5990	0.8007

If the tolerance e_l in Equation (8) is increased, the minimum number of required simulations can be decreased. For instance, if $e = 0.25$ were used (instead of the actual used $e = 0.05$), 5×10^4 simulations would be enough for a successful multi-linear regression. Moreover, the design point, sensitivity factors and reliability index would be the same as those reported in Table 2. The opposite would occur if $e = 0.005$ were used (instead of the actual used $e = 0.05$), i.e., a much larger number of simulations would be required to determine the reliability parameters from the regression.

Therefore, this approach based on multi-linear regression can be quite an adequate alternative by itself to compute β, conditioned on the feasibility of performing enough simulations, the number of which can be decreased by using a large e; with the additional advantage that the design point and sensitivity factors can also be determined.

In the following section a more realistic LSF for a structural application is used to further investigate the revisited methods.

3.2. Reliability of Reinforced Concrete Beam under Flexure Moment

In this section the approaches described before are applied to a reinforced concrete beam (RCB) subjected to flexure moment. The example is the same investigated in a previous study [23] but focused only in one design code [24] and three ratios of the mean live to the mean dead load effect for the beam. The rectangular beam section information, LSF, and statistics are succinctly reproduced below. The LSF is

$$g_{ACI} = BA_s f_y d\left(1 - 0.59\frac{A_s f_y}{f_c' bd}\right) - D - V \quad (21)$$

where B is the modeling error, f'_c is the concrete compressive strength, A_s is the reinforcement steel area, f_y is the yielding stress of the reinforcement steel, b is the section width, h is the effective depth, and D and V are the dead load and live load effect, respectively (flexure moment). The information

of all the independent variables in Equation (21) is summarized in Table 3. A_s is assumed deterministic and equal to 3000 mm^2. The PDFs of the random variables in Table 3 are based on previous literature, which in turn reflects results from experimental projects, field information, observed phenomena, and even the engineers experience to characterized these variables properly, since such PDFs have a direct impact in the computed reliabilities, code calibration tasks, and ultimately in the safety of real structures. More details can be found in [23] and the references therein.

Table 3. Random variables for the limit state functions (LSF) of the reinforced concrete beam (RCB) considered.

Random Variable	Mean	coeff. of var.	PDF
B	1.01	0.06	Normal
f'_c (MPa)	31.6	0.145	Normal
f_y (MPa)	474	0.05	Lognormal
b (mm)	303	0.04	Normal
d (mm)	990	0.04	Normal
D (kN·m)	*	0.05	Normal
V (kN·m)	*	0.18	Gumbel

* denotes that these values are not determined until a $r_{V/D}$ value is selected and used together with Equation (22).

Mean values of D and V are not defined in Table 3, but they are derived by considering given mean live load effect (m_V) to mean dead load effect (m_D) ratios ($r_{V/D}$ = 0.4, 1.0 and 2.0 are used in this study) and the assumption that the RCB just meets the code requirement; thus, the following expression is used to determine the mean values.

$$1.2m_D + 1.6m_V = \phi A_s m_{f_y}\left(m_d - 0.59\frac{A_s m_{f_y}}{m_{f'_c} m_b}\right) \quad (22)$$

where m denotes the mean values of the variables in the corresponding subscripts, and Φ = 0.9.

Using the previous information, the normality polynomial approach is applied to Equation (21) and the results are shown in Figures 3 and 4. These figures are analogous to Figures 1 and 2, except that the reference reliability indices (dashed lines) correspond to the values computed using FORM, that three cases of the ratio $r_{V/D} = m_V/m_D$ are depicted (the largest βs correspond to $r_{V/D}$ = 0.4 and the smallest to $r_{V/D}$ = 2.0, as shown in Figure 3a) and that the error in Figure 4 is shown for $r_{V/D}$ = 0.4 (Figure 4a) and for $r_{V/D}$ = 2.0 (Figure 4b), which is computed by considering in Equation (18) β_{bench} as the average of the 1000 runs for $n_{sim} = 2 \times 10^7$ (assumed as the exact value). MCS results are depicted with dashed-doted lines. To perform the MCS, m_D and m_V are defined using Equation (22) and $r_{V/D}$ as mentioned before. Once they are determined, MCS can then be performed to obtain samples of D and V (and all other random variables in Table 3) and the probability of failure as per Equation (17) can be computed. As an example of the simulated bending moments, histograms of D and V are shown in Appendix A (Figure A1) for 1×10^6 MCS and $r_{V/D}$ = 1.0; it can be observed that the values are comparable in average (because $r_{V/D}$ = 1.0 is considered), and that histograms for D and V clearly resemble normal and Gumbel distributions, respectively, which is expected given that these variables were sampled from such PDFs.

From Figures 3 and 4 similar conclusions to those drawn from Figures 1 and 2 can be extracted. Some additional observations worth to mention are that $n_{sim} = 1 \times 10^4$ seems a reasonable number of simulations for the normality polynomial approach, if a compromise between n_{sim} and error (in terms of mean and standard deviation) is envisaged, that the fitted polynomials lead to better results than the FORM for increasing n_{sim} and that larger errors are obtained for smaller $r_{V/D}$; this latter aspect could be attributed to a better approximation of the failure surface for larger $r_{V/D}$, since the first order approximation to the failure surface by the other method shown in Figure 3 (i.e., the FORM), also deviates more from the exact value for decreasing $r_{V/D}$.

By observing Figure 4, it is pointed out once more that error and its uncertainty is less for normality polynomial when decreasing n_{sim} than for MCS for this case too and, as previously mentioned, is not always possible to estimate the error for MCS for decreasing number of simulations.

The error for β obtained with the normality polynomial approach exhibits an asymptotic behavior towards approximately μ_ε = 1% for large n_{sim}. As before, power laws fit adequately the error and its uncertainty and are defined as

$$\mu_\varepsilon = \delta \times n_{sim}^{-\gamma} + 1 \tag{23}$$

$$\sigma_\varepsilon = \kappa \times n_{sim}^{-\tau} \tag{24}$$

where δ = 656, 1103, and 1349, γ = 0.7401, 0.8493, and 0.9062, κ = 129.8, 201, and 179.1, τ = 0.4937, 0.5609, and 0.5703 for $r_{V/D}$ = 0.4, 1.0, and 2.0, respectively. In Equation (23) the constant unity is included to shift the curve upwards to reproduce the asymptotic behavior mentioned; nonetheless, it could be skipped, and the equations will still fairly adequately describe the mean error. The fitting for μ_ε was performed for the whole range of n_{sim}, while for σ_ε, n_{sim} from 250 and over was employed. Note that although the range for the fitting could be established based on practical grounds and fitting improvement, in any case the errors and their uncertainties follow a power law; this is the case for the three case studies carried out in this study.

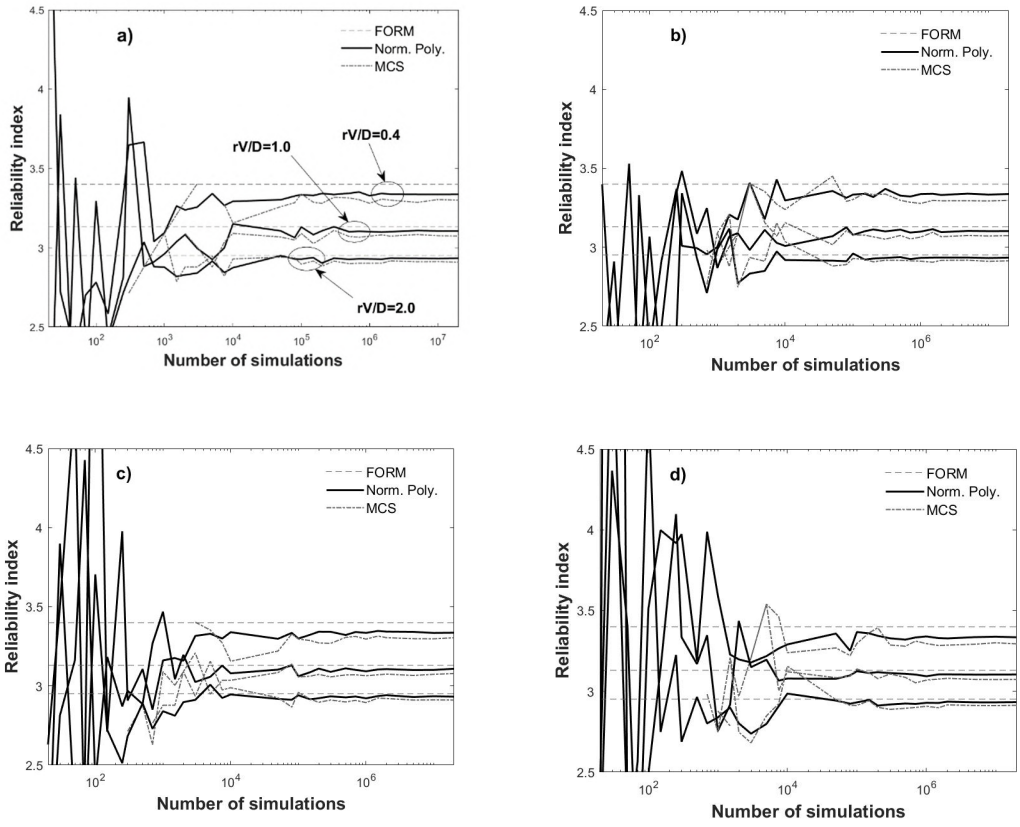

Figure 3. Reliability index as a function of the number of simulations for RCB. (**a**), (**b**), (**c**) and (**d**) are different runs for the MCS.

It is noteworthy that the normality polynomial approach leads to comparable μ_ε and σ_ε for Figures 2 and 4, considering that the LSF for the RCB is a more complex (non-linear) function, and that it has much more random variables and several PDFs.

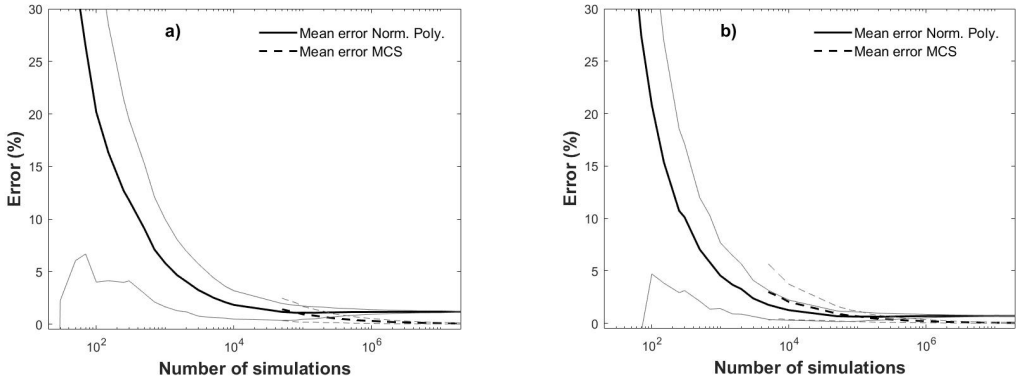

Figure 4. Deviations from the exact reliability index as percentage error for RCB; (**a**) $r_{V/D} = 0.4$ and (**b**) $r_{V/D} = 2.0$.

The fitted coefficients of the polynomials for Figure 3 (corresponding to $r_{V/D} = 0.4$) and selected n_{sim} are listed in Table 1 (middle set of values). If normality polynomials of order higher than 3 are used, no further accuracy is gained (or even higher inaccuracies could be obtained; [11]). This is confirmed by carrying out a single case for $r_{V/D} = 0.4$ using a 4th-order polynomial, since the results are comparable to those of the 3rd-order polynomial case (Table 1, lower set of values). Note that the order of the coefficients of the normality polynomials for the RCB problem can be very small (compared to the classical LSF problem and to a coastal engineering application shown later); this could be due to the units employed, and should not be understood as if the order of the polynomial could be decreased, whereas obtaining comparable precision, because the use of at least third-order normality polynomials was illustrated and found adequate in [11].

To end this section, the results of using the multi-linear regression approach for the LSF defined in Equation (21) are listed in Table 4 for $r_{V/D} = 1.0$. The subscripts in Table 4 (and the units of the design point) are associated to the random variables in Table 3. The reported values correspond to the last of the 1000 runs used to develop Figure 4. As an example of the coefficients obtained by multi-linear regression, the ones from the last of the 1000 runs (for deriving Figure 4) corresponding to $r_{V/D} = 1.0$ and 1×10^6 simulations resulted in $c = 3.3635 \times 10^6$, $b_1 = 4.0861 \times 10^5$, $b_2 = 2.7767 \times 10^5$, $b_3 = 1.1215 \times 10^5$, $b_4 = -1.1888 \times 10^5$, $b_5 = -9.1330 \times 10^5$, $b_6 = 3.1471 \times 10^4$, and $b_7 = 2.8878 \times 10^5$.

The previous information indicates that a similar conclusion to that of the previous example (i.e., for the case of Equation (15)) can be drawn, i.e., at least a sufficiently large number of simulations is required for a successful multi-linear regression. However, unlike in the previous example, the design point and sensitivity factors are not invariant by varying n_{sim}. The differences are not so significant though; therefore, once a minimum number of simulations is ensured (around 8×10^4 simulations) a very precise β is obtained; it is also observed that the required number of simulations for adequately carrying out the multi-linear regressions decreases with increasing $r_{V/D}$ (this could be attributed to the same reason argued before about the larger errors obtained for smaller $r_{V/D}$). If the tolerance e is increased, the number of simulations can be reduced, but not as significantly as for the classical LSF case (i.e., Equation (15)). For instance, an increment to $e = 0.35$ reduces n_{sim} to around 5×10^4; this also changes the values of the design point and sensitivity factors, but not substantially. From Table 4, it is also observed that the values are in very good agreement with the FORM results, with even higher precision from the regression approach for the reliability index. Therefore, it is concluded that the multi-linear regression by itself can be a very attractive alternative to compute β, if a minimum n_{sim} (similar to those mentioned above) is feasible; it is emphasized once more that an additional advantage is that the design point and sensitivity factors are also determined.

Table 4. Design point, β and α_i by using multi-linear regression and FORM for the RCB.

		Design Point/(Sensitivity Factors)						
n_{sim}	β	$x_B/(\alpha_B)$	$x_{fy}/(\alpha_{fy})$	$x_{fc}/(\alpha_{fc})$	$x_D/(\alpha_D)$	$x_V/(\alpha_V)$	$x_b/(\alpha_b)$	$x_d/(\alpha_d)$
1 × 10⁴	----	----	----	----	----	----	----	----
5 × 10⁴	----	----	----	----	----	----	----	----
1 × 10⁵	3.0798	0.9429 (−0.3521)	455.528 (−0.245)	29.802 (−0.1248)	420.037 (0.1170)	534.156 (0.8520)	301.950 (−0.0276)	959.454 (−0.2453)
2 × 10⁵	3.0747	0.9354 (−0.3732)	453.722 (−0.2575)	30.099 (−0.0992)	420.169 (0.1134)	539.456 (0.8395)	302.109 (−0.0223)	956.271 (−0.2580)
1 × 10⁶	3.0842	0.9350 (−0.3747)	453.914 (−0.2546)	30.042 (−0.1028)	419.88 (0.1090)	539.275 (0.8375)	301.844 (−0.0289)	955.342 (−0.2648)
FORM	3.130	0.9424 (−0.3562)	455.332 (−0.2489)	30.393 (−0.0841)	419.026 (0.1019)	702.302 (0.8543)	302.151 (−0.0224)	958.785 (−0.2518)

One final application of the revisited described methods is performed for a coastal structure in the following section.

3.3. Overtopping Reliability of a Breakwater

In this section, we consider for the coastal engineering application the example reported in [10], where certain conditions are assumed and where the reader is referred to for further details and used references. It is a breakwater with deterministic slope, $tan\ \tau$ = 1/1.5, and freeboard, F_b = 10 m. When the water runs up the breakwater, overtopping could occur (i.e., the water surpasses the freeboard), which is considered as a failure. This is defined by the LSF given by

$$g_{bkw} = F_c - A_u H\left(1 - e^{B_u 1.25T\frac{tan\,\tau}{\sqrt{H}}}\right) \tag{25}$$

where A_u and B_u are coefficients characterized as independent normally distributed random variables, with mean values equal to 1.05 and −0.67, respectively, and coefficients of variation both equal to 0.2 [10]; H denotes de wave height and T represents wave period. H and T are random variables probabilistically characterized by the joint Longuet-Higgins distribution [20] with parameter ν = 0.25. The joint PDF of the Longuet-Higgins distribution is given by

$$f_{H_n,T_n}(H_n, T_n) = L(\nu)\frac{2}{\pi^{1/2}\nu}\left(\frac{H_n^2}{T_n^2}\right)e^{-H_n^2}\left[1 + \left(1 - \frac{1}{T_n}\right)^2/\nu^2\right] \tag{26}$$

where $H_n = H/H_s$ and $T_n = T/T_z$ are normalized wave heights and periods by considering H_s = 5 m and T_z = 10 s, which are the significant wave height and the zero up-crossing mean period, respectively, which define the sea state [10]; $L(\nu)$ is a normalization factor implying only positive values of T_n and defined by

$$L(\nu) = \left(\frac{1}{2}\left[1 + (1 + \nu^2)^{-1/2}\right]\right)^{-1} \tag{27}$$

First, the FORM is applied to Equation (25). Salient points of performing the FORM to this overtopping LSF are briefly described in the following. First, it is noted that since H_n and T_n are not independent, the Rosenblatt transformation is performed for the joint distribution to map the equivalent distribution parameters into the normal space by using [17]

$$\begin{cases} z_1 = \Phi^{-1}\left(F_{H_n}(H_n)\right) \\ z_2 = \Phi^{-1}\left(F_{T_n|H_n}(T_n|H_n)\right) \end{cases} \tag{28}$$

where $\Phi^{-1}(\bullet)$ denotes the inverse of the CDF of a standard normal variable, $F_{H_n}(H_n)$ and $F_{T_n|H_n}(T_n|H_n)$ are the marginal distribution of H_n and the conditional distribution of T_n given H_n for Equation(26), respectively, and defined by

$$F_{H_n}(H_n) = H_n L(\nu) e^{-H_n^2}[1 + erf(R_n / \nu)] \tag{29}$$

$$F_{T_n|H_n}(T_n|H_n) = 2(\pi^2 \nu[1 + erf(H_n / \nu)])^{-1} \left(\frac{H_n}{T_n^2}\right) e^{-H_n^2\left(1-1/T_n\right)^2/\nu^2} \tag{30}$$

where the error function is given by

$$erf(H_n / \nu) = \frac{2}{\sqrt{\pi}} \int_0^{H_n/\nu} e^{-t^2}\, dt \tag{31}$$

In Equation (29) the equivalent version reported in [25], rather than the original version in [10], is considered. This is so, simply because the error function used in [25] is more readily available in current software. Then, to derive the conditional probability distribution, we divided Equation (26) by Equation (29) yielding Equation (30) given above. Since the CDFs of Equation (29) and Equation (30) are also required to obtain the equivalent parameters mapped in the standardized normal space, other point to highlight is that they were obtained numerically at the design point, unlike for the normal distributed random variables, where simple analytical expressions can be used (which is also possible for other common PDFs).

Additionally, it is noted that as part of the procedure to obtain the reliability index in each iteration of the FORM, usually a vector obtained by multiplying each partial derivative of the LSF (i.e., Equation (25)), evaluated at the design point, by the equivalent second moment in the normal space (for the corresponding random variable) is enough. However, this approach is not possible for the joint random variables in this example. Therefore, the Jacobian (and its inverse) is required [17]; once the inverse of the Jacobian is computed, it is multiplied by the vector of partial derivatives evaluated at the design point mentioned above, and the reliability index can then be obtained in each iteration in the regular way for the FORM (i.e., as when the variables are independent). This approach is followed in the present study. Note that for a set of jointly distributed random variables x_i (z_i in the normalized space), the inverse of the Jacobian is a lower-triangular matrix determined (often numerically) as [17]

$$J_{ij}^{-1} = \frac{\partial z_i}{\partial x_i} = \begin{cases} 0, & i < j \\ \dfrac{f_i(x_i|x_1, \ldots, x_{i-1})}{\phi(z_i)}, & i = j \\ \dfrac{\dfrac{\partial F_i}{\partial x_i}(x_i|x_1, \ldots, x_{i-1})}{\phi(z_i)}, & i > j \end{cases} \tag{32}$$

where $\Phi(z_i)$ is the PDF of a standard normal random variable, with the argument z_i obtained in an analogous way to Equation (28); f_i and F_i refers to the PDF and CDF for the variable with subscript i, respectively. It was noticed that for the present example, disregarding the elements outside the Jacobian diagonal does not impact very significantly the computed reliability indices.

A few final important aspects regarding the FORM worth to mention, include that the order of the variables in defining Equation (28) does matter, although similar results may be expected [17]. For instance, in [10] the marginal distribution of T_n and the conditional distribution of H_n given T_n are used to define Equation (28) (i.e., the order of the variables is inverted as compared with this study), which results in a reliability index, β, equal to 2.01 for the problem in question, whereas β = 2.10 is obtained in this study with the FORM formulation described earlier, and adopted in the following; β = 2.10 is also closer to the exact value to be discussed later. Another slight difference between [10] and this study when applying the FORM, is that in the present work, when assuming initial design points, one is determined by setting g_{bkw} = 0, to ensure that the design point is on the failure boundary (e.g., [26]).

To inspect the variation of β for different F_c values, the FORM is performed by varying the freeboard between 9 m and 12 m and the resulting reliability index is shown in Figure 5a with a black dashed line. As expected, it can be observed that β increases for increasing freeboard; if the slope of the breakwater is increased to $tan\ \tau$ = 1/2◎and the FORM is carried out for the same range of F_c, it

further increases reliability levels, as shown by the dashed grey line in Figure 5a. These results are used as reference and for comparison purposes, with respect to the results from the normality polynomial and multi-linear regression approaches revisited in this study.

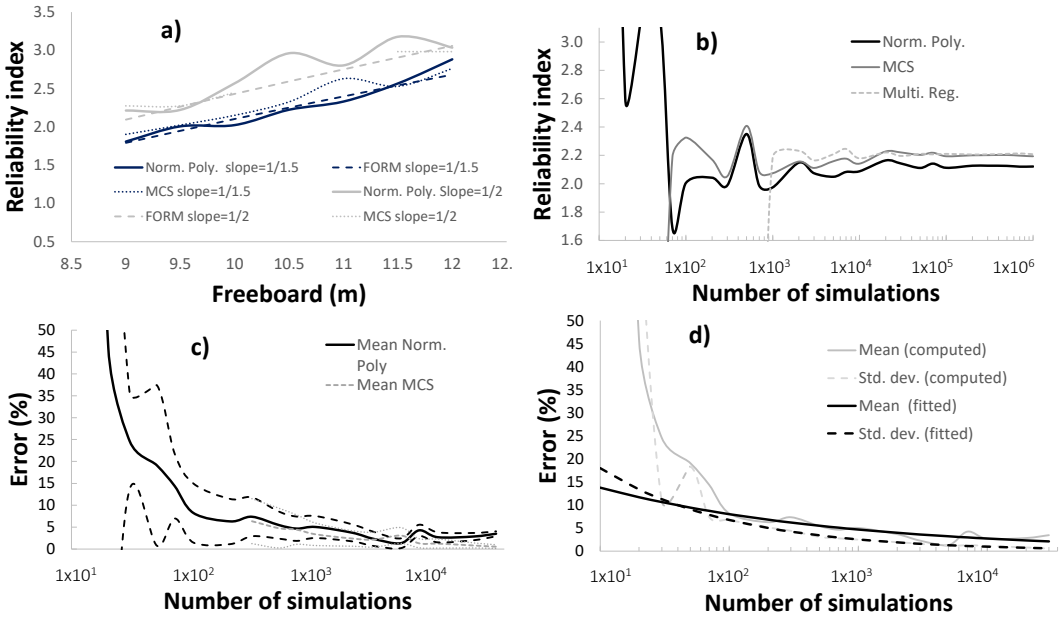

Figure 5. Reliability of breakwater and error estimation in the reliability index. (**a**) Reliability index as a function of F_c; (**b**) Reliability index as a function of n_{sim}; (**c**) Computed error for the reliability index; (**d**) Fitted mean and standard deviation for the error in the reliability index estimation.

The simulations for this coastal engineering application, used as the basis of the revisited methods, are much more computationally intensive than for the classical and structural examples, because of the dependency between the wave height and period and inclusion of the Longuet-Higgins distribution, which imposes numerical computing for the probability levels (e.g., values from CDFs) and a different method for the sampling. This latter aspect, i.e., the generation of jointly distributed random numbers when a set of x_i variables are dependent, is based on expressing the joint PDF as [22]

$$f_X(x) = f_{X1}(x_1) f_{X2}(x_2|x_1) \dots f_{Xn}(x_n|x_1, \dots, x_{n-1}) \tag{33}$$

with the corresponding CDF given by

$$F_X(x) = F_{X1}(x_1) F_{X2}(x_2|x_1) \dots F_{Xn}(x_n|x_1, \dots, x_{n-1}) \tag{34}$$

Using the previous concepts, and considering a set of values $\boldsymbol{U}$ generated from n independent standard uniformly distributed random variables, the set of dependent random variables can be determined as

$$\begin{cases} x_1 = F_{x_1}^{-1}(u_1) \\ \quad x_2 = F_{x_2}^{-1}(u_2|x_1) \\ \qquad \cdot \\ \qquad \cdot \\ \qquad \cdot \\ \quad x_n = F_{x_n}^{-1}(u_n|x_1, \dots, x_{n-1}) \end{cases} \tag{35}$$

where $F^{-1}(\bullet)$ denotes the inverse of the CDF. The obtaining of this inverse of the CDF can be relatively straightforward for some common probability distributions, where an analytical expression can be used for Equation (35). This is not the case for the Longuet-Higgins distribution. In this case, the

jointly distributed random wave height and period must be determined numerically. Figure 6 shows samples of jointly generated random values of wave height and period in the normalized space (for $n_{sim} = 1 \times 10^3$, 5×10^3; 1×10^4 and 5×10^4). A few contours of the theoretical Longuet-Higgins distribution (i.e., Equation (26)) are also shown in Figure 6; it can be observed that they are in good agreement. The values in the non-normalized space can be obtained simply by recognizing that $H_n = H/H_s$ and $T_n = T/T_z$.

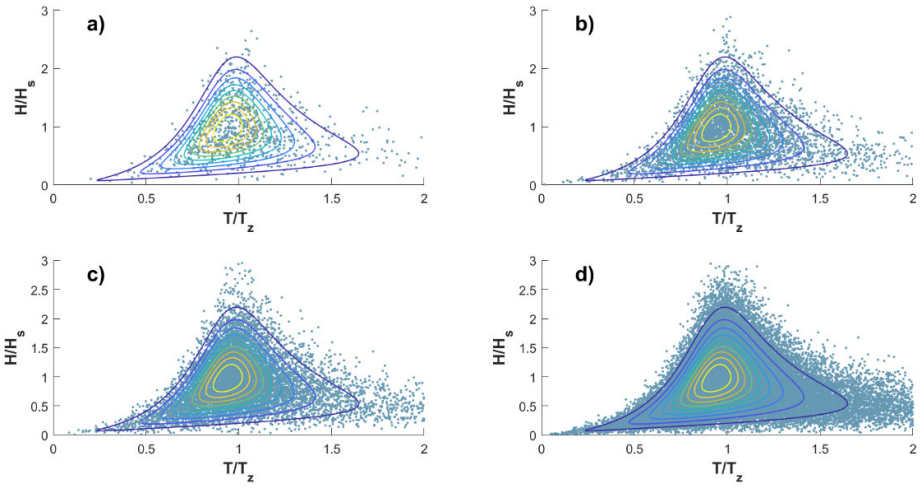

Figure 6. Randomly generated joint values of H_n and T_n for (**a**) 1×10^3, (**b**) 5×10^3, (**c**) 1×10^4, and (**d**) 5×10^4 simulations.

As mentioned before, the sampling procedure is significantly more time-consuming than for the LSFs in previous sections. Therefore, MCS are sampled only up to 1×10^6 simulations for all the variables of the LSF represented by Equation (25), and the reliability index is determined by employing Equation (17) and Equation (7), only for the case reported in [10] (i.e., $F_c = 10$ m and $tan\ \tau = 1/1.5$). Nonetheless, results depicted in Figure 5b indicate that the reliability index stabilizes, from approximately $n_{sim} = 1 \times 10^5$ and over, to a reliability index practically equal to 2.2 (gray solid line). Therefore, $\beta = 2.2$ is adopted as the exact value of the reliability index for the breakwater under overtopping. This value is to be used to assess the error by estimating the reliability index with the normality polynomial approach, and to compare versus the results obtained with the multi-linear regression approach. In fact, the results from these two approaches are also shown in Figure 5b (black solid line for the normality polynomial; grey dashed line for the multi-linear regression approach), where it is observed that the normality polynomial approach converges to a stable value (approximately $\beta = 2.12$) from about 2×10^3 simulations on, leading in average to a slightly smaller reliability index (i.e., in the conservative side) but closer to the exact value than by using the FORM. The multi-linear regression approach (like the MCS and unlike the normality polynomial) requires a minimum number of simulations to be carried out, being this number 1×10^3 for Figure 5b, but sometimes more simulations are required; nevertheless, when a sufficient large number of simulations is performed (e.g., about 3×10^4 or more in Figure 5b), the results of the multi-linear regression leads to practically the exact β, and the design point and sensitivity factors can also be determined.

For brevity, the coefficients of the polynomials and multi-linear regression, design points and sensitivity factors are not extensively listed in this section, but as an example values are given for a single case of 2×10^4 simulations, which led to coefficients for the normality polynomial of $a_0 = -2.164$, $a_1 = 0.3175$, $a_2 = -0.0110$ and $a_3 = 0.0028$, and for the multi-linear regression of $c = 1.4760$, $b_1 = -0.3382$, $b_2 = 0.1235$, $b_3 = -0.5550$ and $b_4 = -0.0633$, as well as sensitivity factors equal to $\alpha_{Au} = 0.5089$, $\alpha_{Bu} = -0.1859$, $\alpha_H = 0.8351$, and $\alpha_T = 0.0953$ and design points equal to $x_{Au} = 1.2874$, $x_{Bu} = -0.7263$, $x_H = 9.3045$ m, and $x_T = 10.2051$ s, which compares very well with the corresponding sensitivity factors computed with

the FORM, that are equal to 0.4959, −0.1712, 0.8466, and 0.0900, respectively, and also very well to the design points from FORM equal to 1.2689, −0.7182, 9.0796 m, and 10.1933 s, respectively. These values of sensitivity factors and design points are also very similar with those reported in [10].

It is noted that Figure 5b corresponds to only one set of simulations for every n_{sim}, which may vary for different sets of generated random numbers (as shown in Figures 1 and 3), implying an uncertainty in the deviation from the exact value for different number of simulations. This uncertainty is assessed as for the classical and structural LFSs in previous sections, i.e., by computing the errors in the reliability index as per Equation (18) and fitting them to power laws with the mathematical functional form represented in Equations (19) and (20) (or Equations (23) and (24)), but with different values of the parameters. To do so, and unlike the case of the classical LSF and the reinforced concrete beam under flexure moment, not 1000 but only 100 sets of simulations are computed for each n_{sim}, due to the more extensive required time and computational resources referred to earlier (A comparison in terms of computing time (CPU time), a description and a discussion are given in Appendix B and Figure A2 of the appendix). This leads to the mean errors shown in Figure 5c with a black solid line for the normality polynomial case (including mean values ± one standard deviation indicated in black dashed lines), and with a grey dashed line for the MCS case (including mean values ± one standard deviation indicated in grey dotted lines).

Even though errors reported in Figure 5c exhibit not as a smooth behavior as those observed in Figures 2 and 4 (obtained in an analogous way but for 1000 sets of n_{sim}), the qualitative trend is fairly similar, especially for mean values and not so small n_{sim}. Indeed, power laws can be adequately fitted to μ_ε and σ_ε, as shown in Figure 5d by fitting the computed errors from 1×10^2 simulations and over; the mathematical functional form is analogous to that of Equations (23) and (24), except that the constant 1 in Equation (23) is omitted. The obtained fitted parameters are $\delta = 23.62$, $\gamma = 0.2342$, $\kappa = 47.94$ and $\tau = 0.4254$. As observed in Figure 5d the fitting is very adequate for σ_ε and adequate for μ_ε, albeit only 100 sets of n_{sim} were employed for the statistics.

From Figure 5c,d similar conclusions to those found before can be drawn, namely, that for decreasing n_{sim} the MCS tends to deviate more from the exact value than the normality polynomials (in terms of ε), that for decreasing number of simulations the error for the MCS can be unknown and that power laws are adequate to mathematically defined μ_ε and σ_ε for the normality polynomial approach. Therefore, a designer could for instance use the normality polynomial method to compute the reliability index for a reduced number of simulations, whereas accepting an error in the estimation. However, such an error could be estimated if expressions of μ_ε and σ_ε (like the power laws determined in this study) are known.

As an example, in Figure 5a $n_{sim} = 7 \times 10^2$ is used for the normality polynomial approach (black solid line) and, as it is shown, this leads to reasonably adequate results (using a fairly small number of simulations) when compared with the FORM and the MCS (also included in Figure 5a with a black dotted line). Moreover, the fitted equations shown in Figure 5d can be used to quantitatively compute the associated error and its standard deviation with respect to the exact reliability index, that is $\mu_\varepsilon = 5.09\%$ and $\sigma_\varepsilon = 2.95\%$. This is strictly applicable only to $F_c = 10$ m; however, comparable errors may be expected for a range of freeboard values by inspecting Figure 5a. Naturally, the contents of this paper could be extended to investigate how the error changes by varying one or more parameters of the LFSs. In such a case, one would expect that functional forms like those reported in this study can be used to assess ε, but possibly with higher mean errors (and/or standard deviations) for higher reliability levels, because usually more simulations are required for lower probabilities of failure. This could be inferred from Figure 5a, where a last set of calculations is shown by increasing the breakwater slope to 1/2 (dashed and dotted grey lines for the normality polynomial and MCS techniques, respectively), where higher variations of the normality polynomial in relation to the FORM are observed; this higher reliability levels also have the effect of decreasing the ability of the MCS to capture the probability of failure, as also observed in Figure 5a for a wide range of F_c. Additionally, although not shown in Figure 5a, it was observed that the minimum number of simulations required to adequately performed the multi-linear regression increases for higher reliability levels (e.g., larger breakwater slopes).

Overall, results in this section indicate that the revisited simulation-based methods can be also effective for coastal engineering applications.

4. Discussion

Results in the previous section suggest that the two revisited approaches based on simulations, namely, the normality polynomial and the multi-linear regression approaches, are effective in reducing the number of required simulations while adequately computing the reliability index, design point and sensitivity factors. It could be argued that still a relatively large number of simulations are required. However, the computing power is becoming higher every year, and these methods proposed at the end of the 1990s could become a feasible alternative for some complex models two or three decades later.

The power law (Equations (19), (20), (23), and (24)), which describes the precision in computing β for the normality polynomial approach, was found very adequate for the three LSFs considered. Albeit it cannot be concluded that the underlaying error is based on the power law for every possible LSF, since one of LSFs studied here was a simple classical case using only one type of PDF, and the other LSFs were more complex (non-linear functions), with much more random variables and included several PDFs, as well as dependency between variables and the joint Longuet-Higgins distribution, it is reasonable to believe that the error for other LSFs for a wide range of coastal and structural engineering applications could follow the power law. A designer could opt to reduce the number of simulations while accepting an error level (including its uncertainty) by using the power laws as an aid.

The multi-linear regression approach was originally developed to derive the design point and sensitivity factors not obtained when performing MCS; however, it is considered that it can be an alternative by itself to compute β in an accurate way, conditioned on performing enough simulations for a successful regression; the number of simulations can be reduced by increasing the tolerance e. Values reported in this study can be used as a guide.

It is acknowledged that some differences with respect to the present study could be found when other LSFs and applications are used. However, the values reported in this study could be used for guidance, and it is believed that the power law may hold in many coastal and structural engineering applications, since the normality polynomials are based in strong mathematical foundations, as referenced before; nevertheless, future research to further inspect the findings in this study is recommended by using mathematical LSFs considered as benchmark in the literature, but also more ultimate and serviceability LSFs for other coastal and structural engineering applications. It is also believed that the revisited methods and the findings in this study can be exported to other engineering fields if practical applications can be posed as a capacity–demand problem and when extensive simulations are required, including system reliability (for instance for reinforced concrete frame buildings, among many other possibilities). Future research could also include a systematic study for the multi-linear regression approach by varying the tolerance, for given number of simulations, so that the number of MCS can be limited to a minimum while guaranteeing the obtaining of adequate reliability-related values.

If more LSFs are investigated in future studies, perhaps it could be possible to infer general bounds for a wider applicability of the findings in the present study.

5. Conclusions

Two reliability methods based on simulations are revisited. One method fits normality polynomials to the simulated data with fractile constraints, and the other approximates the linearized limit state surface at the design point using multi-linear regression; for the latter, a slight modification is proposed. Three limit state functions, a very simple one, other for a structural engineering application and another for a coastal engineering application, are employed.

The most relevant findings of this study are that for the normality polynomial approach, a power law was found to adequately represent the mean and standard deviation of the error in the estimated reliability index as a function of the number of simulations. It could be used as an aid for decision

makers to select a precision level (quantitatively) associated to a selected reliability index, thus reducing the number of required simulations by expressively accepting an error level. Additionally, it is found that the multi-linear regression approach is an excellent option to obtained accurate reliability levels, although a sufficiently large number of simulations is required (not prohibitive though). It also has the advantage that the design point and sensitivity factors are determined.

Other findings in this study are:

1. When the normality polynomial approach is used, the reliability index is dependent on the generated random numbers of each run, but it becomes stable for a large number of simulations.
2. The reliability index cannot always be determined with the Monte Carlo simulations, while the opposite occurs when normality polynomials are used, although significant deviations from the exact value are observed for small numbers of simulations. In general, for an intermediate number of simulations (e.g., 1×10^3), the fitted normality polynomials lead to a better estimate of the reliability index than the Monte Carlo simulations.
3. When the mean relative error and its standard deviation are computed for the reliability index (compared to the exact value), for decreasing number of simulations the Monte Carlo simulation approach tend to larger mean errors and standard deviations than the normality polynomial approach.
4. 3rd-order normality polynomials were mostly used; when 4th order ones are used, the fitting leads to comparable results.
5. When the multi-linear regression approach is considered, a minimum number of simulations is required for successfully performing the regression (in the order of 10^4 to 10^5simulations), but once this is ensured, a very precise reliability index is obtained (more precise than by using the first order reliability method (FORM)), and the design point and sensitivity factors are also determined and in good agreement with those determined with the FORM.
6. If the tolerance for the multi-linear regression approach is increased (i.e., if a wider range in the nearest of the failure surface is stipulated to gather the vectors of simulated data), the number of simulations can be reduced.

Author Contributions: Conceptualization, A.-D.G.-S., F.C.-V., C.M., J.-G.V.-V. and A.H.-M.; Formal analysis, A.-D.G.-S., F.C.-V., C.M., J.-G.V.-V. and A.H.-M.; Funding acquisition, C.M., A.-D.G.-S.; Investigation, A.-D.G.-S., F.C.-V., C.M., J.-G.V.-V. and A.H.-M.; Methodology, A.-D.G.-S., F.C.-V., C.M., J.-G.V.-V. and A.H.-M.; Project administration, C.M.; Supervision, A.-D.G.-S. and C.M. All authors have read and agreed to the published version of the manuscript.

Funding: The financial support from the Erasmus Mundus Coastal and Marine Engineering and Management (CoMEM) programme for one of the authors of this study and from Universidad de Guanajuato (División de Ingenierías and Campus Guanajuato) is gratefully acknowledged.

Acknowledgments: We thank Laboratori d'Enginyeria Marítima, Universitat Politècnica de Catalunya. We are also very thankful to Sonja Marie Ekrann Hammer and Ø. Arntsen for their assistance, to one of the authors of this study, through the Erasmus Mundus CoMEM programme procedure. We thank three anonymous reviewers for their comments, suggestions and constructive criticism which help to improve this article. Finally, we also thank guest Editor Valerio De Biagi and the editorial team of *Applied Sciences* for their help in the editorial process.

Conflicts of Interest: The authors declare no conflict of interest.

Appendix A

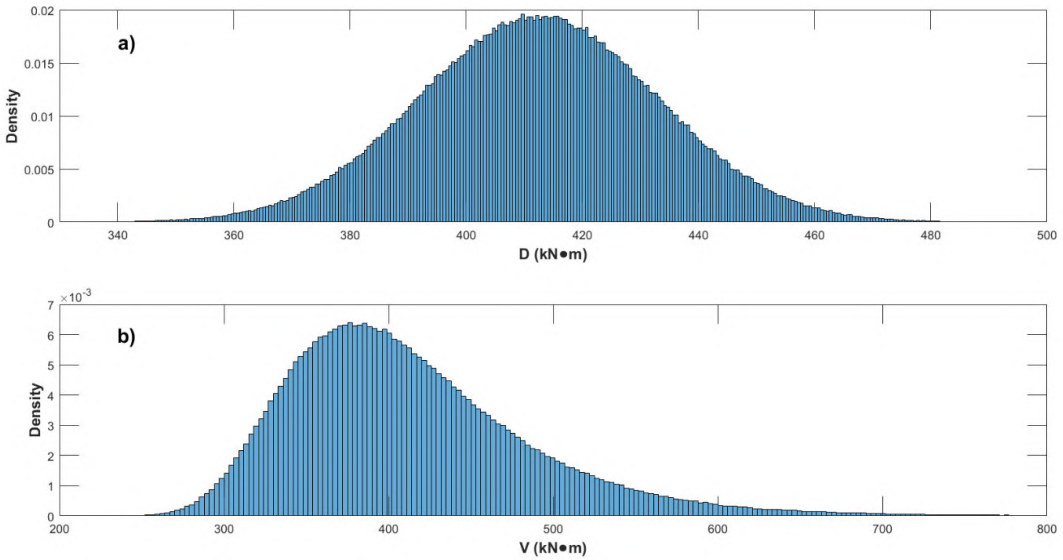

Figure A1. Histograms for 1×10^6 Monte Carlo simulations (MCS) of bending moment due to (**a**) dead load (D) and (**b**) live load (V).

Appendix B

Figure A2 shows the computing (CPU) time required for the classical and structural engineering LSFs (Figure A2a) and for the coastal engineering LSF (Figure A2b). The CPU times include computing of MCS and probabilities of failure, fitting of the normality polynomials and obtaining of the reliability parameters by multi-linear regression. The employed processor is an Intel(R) Core(TM) i7-9750H CPU @ 2.60 GHz with RAM of 16.0 GB and operating system of 64 bits.

It is highlighted that CPU times are for 1000 sets of n_{sim} and for 100 sets of n_{sim} (as indicated in the horizontal axes of the figure) for the classical and RCB LFSs and overtopping LSF, respectively. It can be observed in Figure A2 that the CPU times are significantly larger for the coastal engineering application, as shown by the different ranges used in the vertical and horizontal axes and by the fact that only 100 sets of n_{sim} are used for this case (compared to 1000 sets for the others, as mentioned before). This significant larger computing time is imposed by the joint distribution of wave heights and periods and the Longuet-Higgins distribution used to represent them, which must be solved numerically and for which a different sampling technique is required, as indicated in the main body of this article.

Figure A2 could assist the readers to establish feasible simulation schemes. It was noticed that efficient computing time is obtained if 10,000 simulations at a time are considered for the overtopping LSF. See for instance that for $n_{sim} = 100$ in Figure A2b (which translates into $100 \times 100 = 10{,}000$ MCS), a reasonable CPU time is required; in fact, it is shown in Figure A2b that over this threshold the CPU time starts to increase to a much faster rate. Therefore, once the random numbers are simulated (this is not a problem in terms of CPU times for millions of random numbers), a programming scheme dividing the computing in 10,000 MCS can be used to improve the efficiency (e.g., subdividing the tasks within the same program, running several windows simultaneously and/or using several computers).

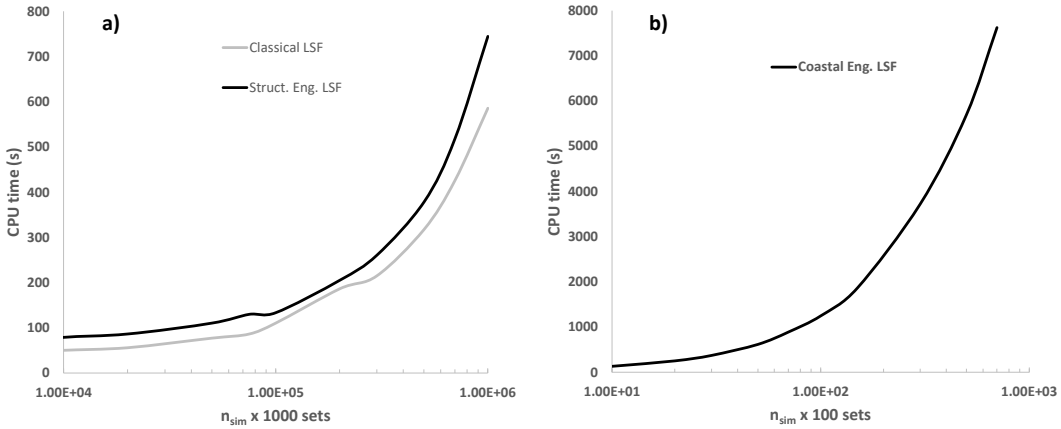

Figure A2. Computing (CPU) time for the different LSFs; (**a**) classical and RCB LSFs and (**b**) overtopping LSF.

References

1. Maliki, M.; Sudret, B. Surrogate-assisted reliability-based design optimization: A survey and a unified modular framework. *Struct. Multidiscip. Optim.* **2109**, *60*, 2157.
2. Straub, D.; Schneider, N.; Bismut, E.; Kim, H. Reliability analysis of deteriorating structural systems. *Struct. Saf.* **2020**, *82*, 101877.
3. Leira, B.; Thöns, S.; Faber, M.H. Reliability assessment of a bridge structure subjected to chloride attack. *Struct. Eng. Int.* **2018**, *28*, 318–324.
4. Gong, C.; Zhou, W. Importance sampling-based system reliability analysis of corroding pipelines considering multiple failure modes. *Reliab. Eng. Syst. Safe*. **2018**, *169*, 199.
5. Huang, P.; Huang, H.-Z.; Huang, T. A Novel Algorithm for Structural Reliability Analysis Based on Finite Step Length and Armijo Line Search. *Appl. Sci.* **2019**, *9*, 2546.
6. Biagi, V.D.; Kiakojouri, F.; Chiaia, B.; Sheidaii, M.R. A Simplified Method for Assessing the Response of RC Frame Structures to Sudden Column Removal. *Appl. Sci.* **2020**, *10*, 3081.
7. Marchelli, M.; Biagi, V.D.; Peila, D. Reliability-Based Design of Protection Net Fences: Influence of Rockfall Uncertainties through a Statistical Analysis. *Geosciences* **2020**, *10*, 280.
8. Biagi, V.D.; Marchelli, M.; Peila, D. Reliability Analysis and Partial Safety Factors Approach for Rockfall Protection Structures. *Eng. Struct.* **2020**, *213*, 110553.
9. Naseri, M.; Barabady, J. An Expert-Based Model for Reliability Analysis of Arctic Oil and Gas Processing Facilities. *ASME J. Offshore Mech. Arct. Eng*. **2016**, *138*, 051602.
10. Losada, M.A. ROM 0.0, Puertos del Estado Level II and III Verification Methods. In *General Procedure and Requirements in the Design of Harbor and Maritime Structures*, *Part I*, 1st ed; Puertos del Estado: Madrid, Spain, 2002; Volume 1, pp. 160–185.
11. Hong, H.P. Application of polynomial transformation to normality in structural reliability analysis. *Can. J. Civ. Eng*. **1998**, *25*, 241.
12. Hong, H.P.; Nessim, M. The development of a design point and sensitivity factors from simulation results. In Proceedings of the sixth international conference on applications of statistics and probability in civil engineering, CERRA-ICASP 6, Mexico City, Mexico, 17–21 June 1991; pp. 313–319.
13. Hong, H.P.; Lind, N. Approximate reliability analysis using normal polynomial and simulation results. *Struct. Saf.* **1996**, *18*, 329.
14. Lima-Castillo, I.F.; Gómez-Martínez, R.; Pozos-Estrada, A. Methodology to Develop Fragility Curves of Glass Façades under Wind-Induced Pressure. *Int. J. Civ. Eng.* **2019**, *17*, 347.
15. Hall, P. Inverting an Edgeworth expansion. *Ann. Stat.* **1983**, *11*, 569.
16. Kendall, M.; Stuart, A.; Ord, J.K. *Kendall's Advance Theory of Statistics*; Oxford University Press: New York, NY, USA, 1987; Volume I.
17. Madsen, H.O.; Krenk, S.; Lind, N.C. *Methods of Structural Safety*; Prentice-Hall, Inc.: Englewood Cliffs, NJ, USA, 1986.

18. Lind, N.C. Information Theory and maximum product spacings estimation. *J. R. Stat. Soc. B* **1994**, *56*, 341–343.
19. Lind, N.C. Statistical method for concrete quality control. In Proceeding of the 2nd International Colloquia on Concrete in Developing Countries, Bombay, India, 3-8 January 1998; Volume 1, pp 21–26.
20. Longuet-Higgins, M.S. On the Joint Distribution of Wave Periods and Amplitudes in a Random Wave Field. *Proc. R. Soc. Lond.* **1983**, *389*, 241.
21. Rosenblueth, E.; Esteva, L. Reliability basis for some Mexican codes. *Am. Concr. Inst. Spec. Publ.* **1972**, *31*, 1–42.
22. Hong, H.P. *Risk Analysis and Decision Making in Engineering*; Course Notes; Western University: London, ON, Canada, 2008; 194p.
23. García-Soto, A.D.; Hernández-Martínez, A.; Valdés-Vazquez, J.G. Reliability analysis of reinforced concrete beams subjected to bending using different methods and design codes. *Struct. Eng. Int*. **2017** *27*, 300–307.
24. American Concrete Institute (ACI). *Building Code Requirements for Structural Concrete*; ACI 318-14; American Concrete Institute (ACI): Farmington Hills, MI, USA, 2014.
25. Zhang, H.D.; Soares, C.G. Modified Joint Distribution of Wave Heights and Periods. *China Ocean Eng.* **2016**, *30*, 359.
26. Nowak, A.S.; Collins, K.R. *Reliability of Structures*, 1st ed.; Mc Graw-Hill: Boston, MA, USA, 2000; pp. 120–129.

Book Chapter 1

Emerging Issues in Science and Technology Vol. 1. Chapter 11, Influence of an Atypical Value in the Extreme Wave Analysis Using Non-Stationary GEV Models.

F. Calderón-Vega, C. Mösso and A. D. García-Soto

Print ISBN: 978-93-89562-66-8, eBook ISBN: 978-93-89562-67-5. DOI: 10.9734/bpi/eist/v1

Chapter 11
Print ISBN: 978-93-89562-66-8, eBook ISBN: 978-93-89562-67-5

Influence of an Atypical Value in the Extreme Wave Analysis Using Non-Stationary GEV Models

F. Calderón-Vega[1,2*], C. Mosso[2,3] and A. D. García-Soto[1]

DOI: 10.9734/bpi/eist/v1

ABSTRACT

In the present study an extreme value analysis of maximum significant waves recorded at a buoy located in the Pacific Ocean was carried out by including/excluding an atypical extreme wave height. The analysis was carried out using a non-stationary Generalized Extreme Value (GEV) model, which incorporates the monthly seasonality of maximum observed values in time increments; the maximum significant wave behavior was parameterized using harmonic functions for the distribution measures. A single buoy was considered for the scope of this paper. In the study differences in the seasonality effect were found due to the exclusion of the atypical value, which is especially significant because it occurred in a season with supposedly low wave heights values.

Keywords: GEV model; atypical value; non-stationary; seasonality; projections.

1. INTRODUCTION

In the recent literature, [1] the Gumbel probability density function (PDF) is used to estimate the extreme maximum annual significant wave height. In [2] non-stationary GEV models are employed. In [3] design values for significant wave height accounting for direction and seasonality are proposed. In [4] the behavior of tropical cyclone is compared for two Chinese seas. In [5] peak over threshold (POT) methods are used for estimating significant wave heights for given reference periods.

Several studies historically developed and extended the Extreme value theory [6,7,8,9,10,11,12,13, 14,15,16,17,18,19,20,21,22,23]. More recently these extreme value concepts have been applied to designing maritime structures [24]. The seasonality of extreme waves in the Gulf of Mexico has been investigated [25]. Seasonality effects can have an impact on the meteo-oceanographic variables [26,27].

The main objective of this study is to compare the effect of excluding an atypically large wave height value on the seasonality of such meteo-oceanographic variable. A single buoy site in the Pacific Ocean is used for this aim.

2. SINGLE BUOY CONSIDERED

Buoy number 51004 in the Pacific Ocean is considered, which is operated by the National Data Buoy Center (NDBC, www.ndbc.noaa.gov).

Fig. 1 shows the buoy location which is located to the south of the Hawaii islands. It has recorded wave heights from 1984 to 2017, except 2010. The significant wave height (Hs) is used within this study. This buoy recorded an atypically large Hs in July, 1986, when the largest values usually do not occur.

[1]Department of Civil Engineering, Universidad de Guanajuato, Juárez 77, Zona Centro, P.C. 36000 Guanajuato, Gto. Mexico.
[2]Laboratori d'Enginyeria Marítima, Universitat Politècnica de Catalunya, Jordi Girona 1-3, Mòdul D1, Campus Nord, 08034, Barcelona, Spain.
[3]Centre Internacional d'Investigació dels Recursos Costaners, Jordi Girona 1-3, Mòdul D1, Campus Nord, 08034, Barcelona, Spain.
**Corresponding author: E-mail: f.calderon@ugto.mx, felicitas.calderon@upc.edu;*

Fig. 1. Buoy number 51004

3. COMPUTED VALUES

3.1 Simple Statistics

Simple statistics were computed in a previous study [28] and are reproduced herein. In Fig. 2a (upper part) a main wave incidence to the NEE is observed. The atypical recorded Hs referred earlier is equal to 10.60 m; see Fig. 2b (lower part). The most frequently observed significant wave height is roughly 2 m.

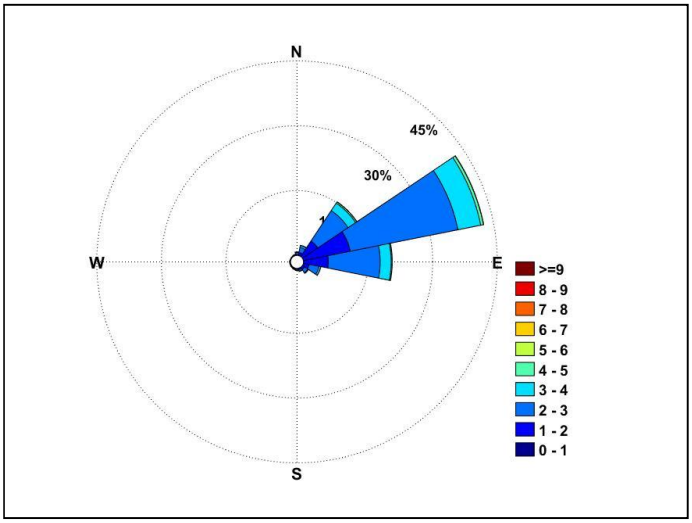

(a)

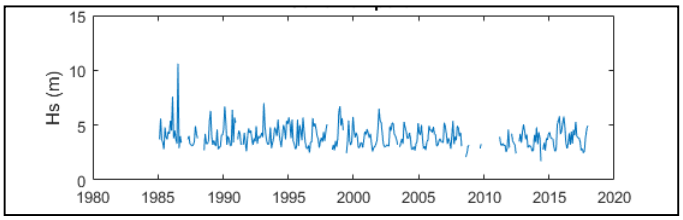

(b)

Fig. 2. Basic Statistics of the buoy under study (after [28]) (a) Wave rose and, (b) time series data

3.2 Analysis of Extreme Values

3.2.1 Generalized extreme value distribution

The governing equations can be found in [29]. It is stated that the only non-degenerate family of distributions obtained from EVT are the well-known Weibull, Gumbel and Fréchet families for maxima, given by

Maximal Weibull or Reversed Weibull:

$$H(x) = \begin{cases} exp\left[-\left(\frac{\lambda - x}{\delta}\right)^{\beta}\right], if\ x \le \lambda,\ \beta > 0 \\ 1, \quad Otherwise \end{cases} \tag{1}$$

Gumbel or Maximal Gumbel:

$$H(x) = \exp\left[-exp\left(\frac{x-\lambda}{\delta}\right)\right], \qquad -\infty < x < \infty \tag{2}$$

Fréchet or Maximal Fréchet:

$$H(x) = \begin{cases} 0, & if\ x < \lambda, \\ exp\left[-\left(\frac{\delta}{x-\lambda}\right)^{\beta}\right], & if\ x \le \lambda,\ \beta > 0 \end{cases} \tag{3}$$

where β, δ and λ are distributions parameters.

The used GEV distribution e.g., [22,30], reduces to a single mathematical expression, the three well-known families of extreme distributions, as follows

$$G(x) = \exp\left\{-\left[1 + \xi\left(\frac{x-\mu}{\psi}\right)\right]_{+}^{-1/\xi}\right\} \rightarrow \xi \neq 0$$

$$G(x) = \exp\left\{-\exp\left[-\left(\frac{x-\mu}{\psi}\right)\right]\right\} \rightarrow \xi = 0 \tag{4}$$

The PDF is defined by

$$g(x) = \frac{1}{\psi}\left[1 + \xi\left(\frac{x-\mu}{\psi}\right)\right]_{+}^{-\left(1+1/\xi\right)} exp\left\{-\left[1 + \xi\left(\frac{x-\mu}{\psi}\right)\right]_{+}^{-1/\xi}\right\} if\ \xi \neq 0$$

$$g(x) = \frac{1}{\psi} exp\left(-\frac{x-\mu}{\psi}\right) exp\left[-exp\left(-\frac{x-\mu}{\psi}\right)\right] if\ \xi = 0 \tag{5}$$

where $-\infty < \mu < \infty$ is the location parameter, $\psi > 0$ is the scale parameter and ξ the shape parameter.

The location parameter represents the mean values of the random variable, *x*, and defines the value with a non-exceedance probability *exp(-1)*. The scale parameter denotes the sample dispersion. The shape parameter defines the distribution family as a function of the tail behavior; when ξ exists, *G(x)* includes two distribution families.

3.2.2 Non-stationary GEV model

GEV model is used for block maxima of a time interval for modelling Hs. The monthly maximum values are employed. Note that throughout this study; the methodology in [25] is used.

The seasonality is defined as the cyclic changes during the year which is related to climatic patrons and usually repeats itself for many years and behaves in a sinusoidal way. However, sometimes atypical values do occur, as shown in Fig. 3 where it can be observed that a very large value happened in July, 1986.

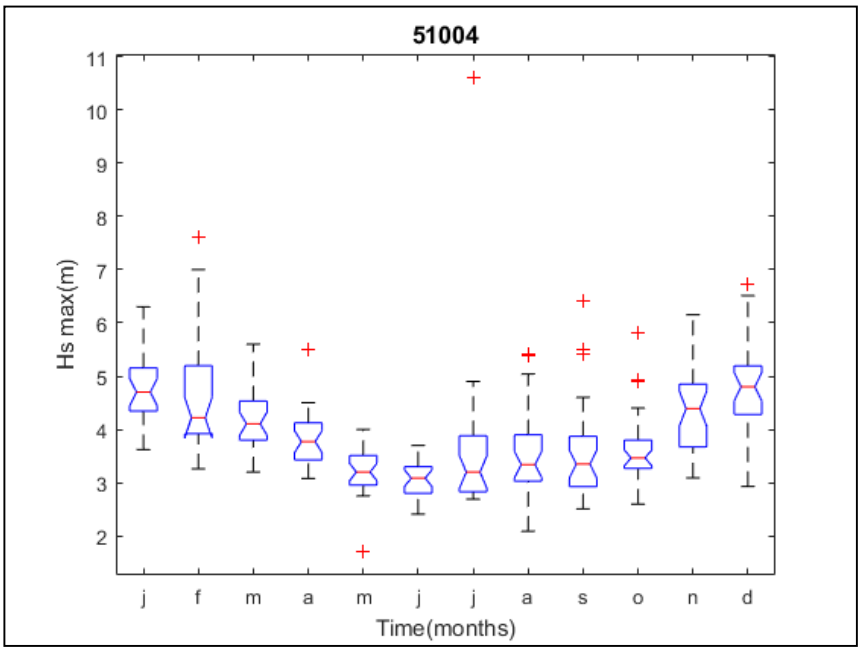

Fig. 3. Seasonality of monthly maxima and atypical value

For the assessment of time-dependency the successive monthly maxima are considered as independent random variables; homogeneity hypothesis is not necessary [28]. The maximum monthly value Z_t of the observed Hs in month *t* is supposed to follow a GEV distribution, with location $\mu(t)>0$, scale $\psi(t)>0$ and shape $\xi(t)$ parameters being time-dependent.

The cumulative distribution function (CDF) of Z_i is

$$F_t(z) = \begin{cases} \left\{ exp\left\{ -\left[1 + \xi(t)\left(\frac{z-\mu(t)}{\psi(t)}\right)\right]_+^{\frac{-1}{\xi(t)}} \right\} \right. \\ \left. exp\left\{ -exp\left[-\left(\frac{z-\mu(t)}{\psi(t)}\right)\right]\right\} \end{cases} \quad (6)$$

The non-stationarity of the models is introduced by means of

$$\theta = \begin{cases} \mu(t) = \beta_0 + \beta_1\, cos(2\pi t) + \beta_2 sen(2\pi t) + \beta_3\, cos(4\pi t) + \beta_4 sen(4\pi t) \\ \psi(t) = \alpha_0 + \alpha_1\, cos(2\pi t) + \alpha_2 sen(2\pi t) + \alpha_3\, cos(4\pi t) + \alpha_4 sen(4\pi t) \\ \xi(t) = \gamma_0 + \gamma_1\, cos(2\pi t) + \gamma_2 sen(2\pi t) + \gamma_3\, cos(4\pi t) + \gamma_4 sen(4\pi t) \end{cases} \quad (7)$$

where $\psi(t>0)$, β_0, α_0 and γ_0 are mean values; β_i, α_i y γ_i (for *i=1,2*) are the harmonic amplitudes; β_i, α_i y γ_i (for *i=3,4*) are the subharmonic amplitudes and *t* is in years.

In Fig. 4 the results from the variability analysis within a year of the maximum-likelihood estimators for the location, μ, scale, ψ, and shape, ξ, parameters along the year are depicted by including the atypical value. The line is obtained by regression fitting with two harmonics.

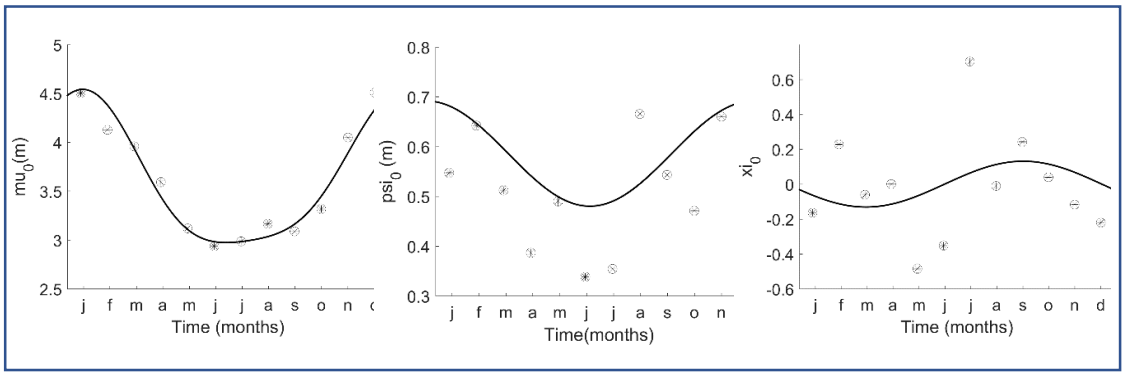

Fig. 4. Estimators for distribution parameters including atypical value

3.2.3 Non-stationary model fitting

The maximum likelihood (MML) approach is employed to estimate the probability distribution parameters. Such approach is based in the search for point estimators *(θ)* for the parameters of a *X* function, so that the probability of observing the sample data *{x₁,…xₙ}* is maximum. The likelihood function *L(x;θ)* is the joint density function associated to all initial extreme values, from a previously selected distribution and, in general terms, is given by

$$L(x;\theta) = f(x_1,\dots x_n;\theta) = \prod_{i=1}^{n} f(x_i;\theta) \tag{8}$$

The location $\mu(t)>0$, scale $\psi(t)>0$ and shape $\xi(t)$ parameters are expressed in terms of harmonic functions, whose amplitudes are regression parameters to be mathematically estimated [29].

For our case it is denoted with

$$l(\theta \mid t_i x_i) = -\sum_{i=1}^{m}\left\{\log\psi(t_i + \left(1+ {}^{1}\!/_{\xi(t_i)}\right)\log\left[1+\xi(t_i)\left(\frac{x_i-\mu(t_i)}{\psi(t_i)}\right)\right]_{+} + \left[1+\xi(t_i)\left(\frac{x_i-\mu(t_i)}{\psi(t_i)}\right)\right]_{+}^{-{}^{1}\!/_{\xi(t_i)}}\right\} \tag{9}$$

Finding of the best model is based on a previous study [25,28], and leads to the values associated to a return period by using

$$X_q(t,\theta) = X_q(\mu(t),\psi(t),\xi(t)) = \begin{cases} \mu(t) - \dfrac{\psi(t)}{\xi(t)}\left\{1-\left[-\log(1-q)\right]^{-\xi(t)}\right\} & if \quad \xi(t)\neq 0 \\ \mu(t) - \psi(t)\log\left[-\log(1-q)\right] & if \quad \xi(t)=0 \end{cases} \tag{10}$$

where q is the exceedance probability defined from $G_t(x)=1-q$ and the estimated quantile, and $X_q(t,\theta)$ is the time-dependent value associated to the return period $R=1/q$.

4. EXCLUSION OF ATYPICAL VALUE AND DISCUSSION

4.1 Stationary Model

For reference only, considered the stationary case, in which the location, scale and shape parameters do not change with time. Table 1 lists the computed values of the distribution parameters, as well as

the maximum recorded significant wave height, Hs_{max}, and the projected value for Hs associated to a return period of 30 years, by including or excluding the atypically large Hs.

Table 1. Parameters for the stationary model, Hs_{max} and Hs and Tr=30 years (including and excluding atypical value)

Hs_{max} (m)	10.60	Hs_{max} (m)	7.60
Hs (m) for Tr= 30 yr	5.60	Hs (m) for Tr= 30 yr	4.99
μ	360.34	μ	359.59
ψ	58.59	ψ	57.40
ξ	$1x10^{-4}$	ξ	$1x10^{-4}$

From the values reported in Table 1, it can be inferred that the stationary model is dominated by a Frechet type (heavy tail) distribution behavior, and that the exclusion of the atypical Hs leads to significant differences in the average value and corresponding projections to return periods of Hs. The impact on the model parameters is not captured by the stationary model. Similar conclusions can be drawn by observing Fig. 5.

4.2 Non Stationary Model

The emphasis on the tail behavior is useful for engineering purposes, and the use of the GEV model is preferred as an adequate and objective criterion for the extremes [31], and the non-stationary GEV is useful to capture the seasonality effect. Using the non-stationary GEV model, the best fitted parameters for the distribution are obtained and shown in Fig. 6, where the red line shows the time-dependent quantile associated to a 30-year return period; the black line depicts the location parameter, the green line corresponds to the scale parameter and the yellow line corresponds to the shape parameter. The monthly maxima for Hs are shown by the black dots. Note that the inclusion (Fig. 6, left) or exclusion (Fig. 6, right) of the atypical Hs does not change the general qualitative trend of the values associated to a 30-year return period; however, it does have an important impact at a quantitative level, as can be observed in Fig. 6. Fitting to the empirical probabilities seem to improve by excluding the atypical value as shown in Fig. 7.

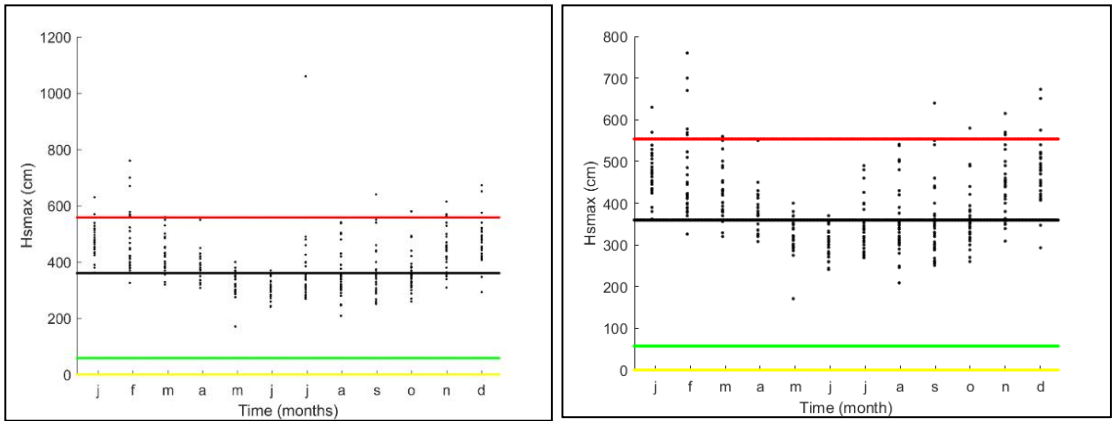

Fig. 5. Quantile values for Tr=30 years, monthly maximums and location, scale and shape parameters by including/excluding atypical Hs

Further comparisons in Fig. 8 (analogous to Fig. 6, but for 100-yr return period) and in Fig. 9 (confidence intervals for the month-to-month non-stationary GEV model), further support the findings previously discussed.

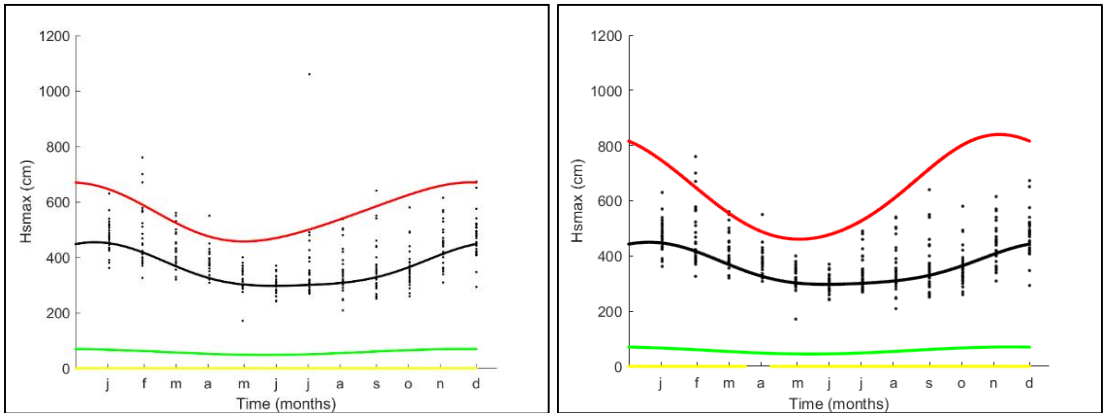

Fig. 6. Fitting for the monthly maximum for the non-stationary GEV model (by including/excluding atypical Hs)

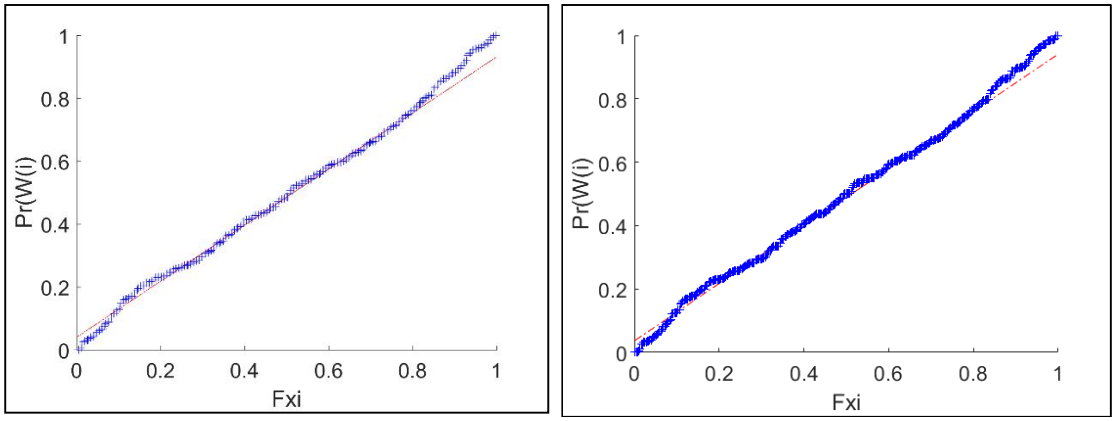

(a) **(b)**

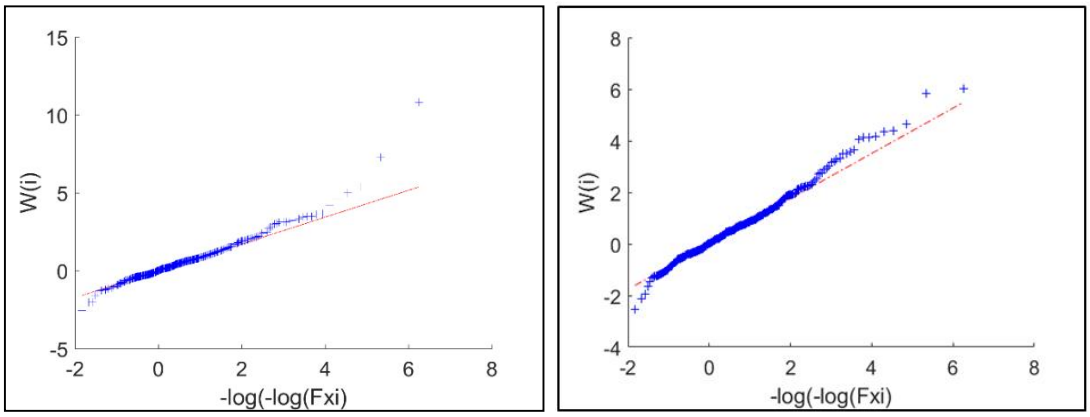

(c) **(d)**

Fig. 7. Diagnostic plots for the non-stationary GEV model; (a and (c includes atypical value; b) and d) excludes atypical value

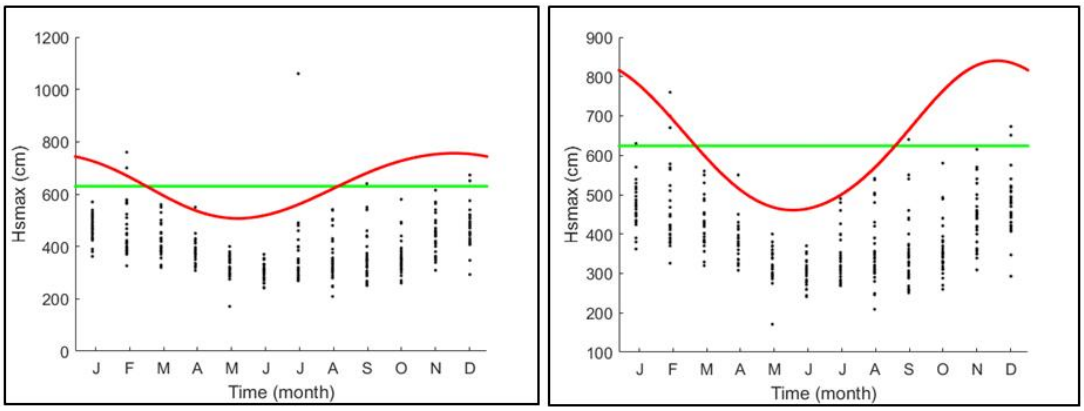

Fig. 8. Quantiles comparison for 100-year return period and measured Hs

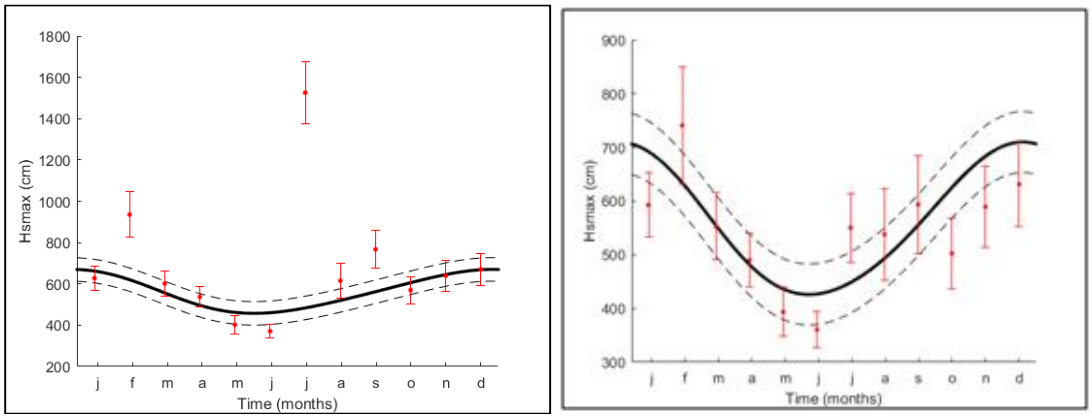

Fig. 9. 30-year return period quantile and 95% confidence interval for the non-stationary GEV model and the month-to-month stationary GEV

5. CONCLUSIONS

In this study the impact of including or excluding an atypical significant wave height on a non-stationary GEV model is investigated using a single buoy located near the Hawaiian Islands in the Pacific Ocean.

For reference only, parameters using a stationary model were also included, and it was found that the stationary model is dominated by a Frechet type (heavy tail) distribution behavior, and that the exclusion of the atypical Hs leads to important differences in the average value and corresponding projections to return periods of Hs; nevertheless, the effect on the other model parameters is not captured by the stationary model.

By using the non-stationary GEV model the main finding of this study was found, namely, that the inclusion or exclusion of the atypical significant wave height may not change the general qualitative trend of the values associated to given return periods, but it does have a markedly important impact at a quantitative level. Also, fitting to the empirical probabilities seem to improve by excluding the atypical value.

ACKNOWLEDGEMENTS

The financial support from the Erasmus Mundus Coastal and Marine Engineering and Management (CoMEM) programme and from Universidad de Guanajuato is gratefully acknowledged. We are thankful for the comments, suggestions and constructive criticism from two anonymous reviewers, as well as to Ms. Ruma Bag and the Editorial team for their invitation and help in the editorial process.

COMPETING INTERESTS

Authors have declared that no competing interests exist.

REFERENCES

1. Shao Z, Liang B, Li H, Lee D. Study of sampling methods for assessment of extreme significant wave heights in the South China Sea. Ocean Eng. 2018;168:173-184.
   DOI: 10.1016/j.oceaneng.2018.09.015
2. Vanem E. Non-stationary extreme value models to account for trends and shifts in the extreme wave climate due to climate change. Appl Ocean Res. 2015;52:201-211.
   DOI: 10.1016/j.apor.2015.06.010
3. Feld G, Randell D, Wu Y, Ewans K, Jonathan P. Estimation of storm peak and intrastorm directional-seasonal design conditions in the North Sea. Journal of Offshore Mechanics and Arctic Engineering. 2015;137(2):021102.
   DOI: 10.1115/1.4029639.
4. Shao Z, Liang B, Li H, Wu G, Wu Z. Blended wind fields for wave modeling of tropical cyclones in the South China Sea and East China Sea. Appl Ocean Res. 2018;71:20-33. DOI: 10.1016/j.apor.2017.11.012.
5. Kapelonis Zacharias G, Gavriliadis Panagiotis N, Athanassoulis Gerassimos A. Extreme value análisis of dynamical wave climate projections in the Mediterranean Sea. Procedia Computer Science. YSC 4th International Young Scientists Conference on Computacional Science. 2015; 66:210-219.
6. Chaplin RG. Abrasion resistant concrete floors. Advances in Concrete Slab Technology. Ed. R.K. Dhir and J.G.L. Munday. 1980;164-72.
7. Chaplin RG. The influence of cement replacement materials. Fine Agregate and curing on the abrasion resistance of industrial concrete floor slabs. Cement and Concrete Association, Slough, UK. 1986;32.
8. Bortkiewicz L Von. Variationsbreite und mittlerer Fehler, Sitzungsber. Berli. Math. Ges. 1922; 21:3-11.
9. Dodd EL. The greatest and the least variate under general laws of error. Tans. Amer. Math Soc. 1923;25:525-39.
10. Tippett LHC. On the extreme individuals and the range of samples taken from a normal population. Biometrika. 1925;17:364-387.
    Available:https://doi.org/10.1093/biomet/17.3-4.364
11. Fréchet M. Sur la loi de probabilité de l'écart máximum. Ann. Soc. Polon. Math. Cracovie. 1957;6:93-116.
12. Fisher RA, Tippett LHC. Limiting forms of the frequency distribution of the largest or smallest members of a sample. Proceedings of the Cambridge Philosophical Society. 1928;24:180-190.
13. De Finetti B, Obry S. L'optimum nella misura del riscatto, Atti del II Congresso Nazionale di Scienza delle Assicurazioni. Bardi, Trieste, Rome. 1932;2:99–123.
14. Gumbel EJ. Statistical theory of extreme values and some practical applications. Applied Mathematics 1954 Series. 33 (1st Ed.) U.S. Department of Commerce, National Bureau of Standards.
15. Gumbel EJ. Les valeurs extrêmes des distributions statistiques. Annales de l'Institut Henri Poincaré. 1935;5:115-158.
16. Mises R. Von. (1936) La distribution de la plus grande de n valeurs. Amer. Math. Soc Reproduced in Selected Papers of Richard von Mises, II. 1954;271-294.
17. Rice J. Mathematical statistics and data analysis. 2nd Ed. Duxbury; 1994.
18. Gnedenko B. Sur la distribution limite du terme maximum d'une série aléatoire. Springer-Verlag. 1943;195-225.
19. Gumbel EJ. Statistics of extremes. Columbia University Press; 1958.
20. Galambos J. The asymptotic theory of extreme order statistics. Robert E. Krieger. Malabar, Florida. 2nd Ed.; 1987.
21. Leadbetter MR, Lindgrem G, Rootzén H. Extremes and related properties of random sequences and series. Springer. Verlag, New York; 1983.

22. Coles SG. An introduction to statistical modelling of extreme values. 1st Ed.; Springer-Verlag: London, UK. 2001;1-208.
23. Katz RW. Stochastic modeling of hurricane damage. J. of App. Meteor. 2002;41:754-762.
24. Johathan P, Ewans K. Statistical modelling of extreme ocean environments for marine design: A review. Ocean Eng. 2013;91-109.
DOI: 10.1016/j.oceaneng.2013.01.004
25. Calderón-Vega F, Vázquez-Hernández AO, García-Soto AD. Analysis of extreme waves with seasonal variation in the Gulf of Mexico using a time-dependent GEV model. Ocean Eng. 2013; 73:68-82.
DOI: 10.1016/j.oceaneng. 2013.08.007.
26. Sanchez-Arcilla A, Sierra JP, Gracia V, Garcia M, Jimenez JA, Mösso C, Valdemoro H. Coastal sustainability for uncertain futures: A Spanish Mediterranean case from the RISES-AM project. A: Intenational Association for Hydraulic Research Congress. E-proceedings of the 36th IAHR World Congres. L'Haia. 2015;1-8.
27. Sanchez-Arcilla A, Sierra JP, Mösso C, Gracia V, Garcia M. Progress on climate change detection and projections over Spain since the findings of the IPCC AR5. International Symposium CLIMATE-ES. 2015;146.
28. Calderón-Vega F, Mösso C, García-Soto AD, Delgadillo-Ruiz E. Single site extreme wave analysis in the pacific ocean comparing stationary and non-stationary GEV models. Current Journal of Applied Science and Technology. 2019;32(6):1-12.
Available:https://doi.org/10.9734/cjast/2019/v32i630038.
29. Menéndez M, Méndez FJ, Izaguirre C, Luceño A, Losada IJ. The influence of seasonality on estimating return values of significant wave height. Ocean Eng. 2009;56:211-219.
DOI: 10.1016/j.coastaleng.2008.07.004.
30. Castillo E, Hadi AS, Balakrishnan N, Sarabia JM. Extreme value and related models with applications in engineering and science. Wiley-Interscience. New Jersey; 2005.
31. Panchang V, Kwon Jeong Ch., Demirbilek Z. Analyses of extreme wave heights in the Gulf of Mexico for offshore engineering applications. J Offshore Mech Arct. 2013;135(3):1-15.

Biography of author(s)

F. Calderón-Vega
Department of Civil Engineering, Universidad de Guanajuato, Juárez 77, Zona Centro, P.C. 36000 Guanajuato, Gto. Mexico and Laboratori d'Enginyeria Marítima, Universitat Politècnica de Catalunya, Jordi Girona 1-3, Mòdul D1, Campus Nord, 08034, Barcelona, Spain.

She is a Ph.D Candidate at the Polytechnic University of Catalunya, Barcelona Tech. She is a Researcher at the University of Guanajuato in Guanajuato, Mexico. Her research interests include maritime engineering and structures, hydraulics, extreme value theory applied to meteo-oceanographic variables and others. She has published several technical papers in international journals.

C. Mosso
Laboratori d'Enginyeria Marítima, Universitat Politècnica de Catalunya, Jordi Girona 1-3, Mòdul D1, Campus Nord, 08034, Barcelona, Spain and Centre Internacional d'Investigació dels Recursos Costaners, Jordi Girona 1-3, Mòdul D1, Campus Nord, 08034, Barcelona, Spain.

He is a Researcher at the Department of Civil and Environmental Engineering (hydraulics, maritime and environmental Section) at the Universitat Politècnica de Catalunya (UPC) BarcelonaTech, as well as in the Laboratori d'Enginyeria Marítima (LIM/UPC). His research interests include coastal engineering, climate change, maritime hydrodynamics among others. He has published several technical papers in international journals.

A. D. García-Soto
Department of Civil Engineering, Universidad de Guanajuato, Juárez 77, Zona Centro, P.C. 36000 Guanajuato, Gto. Mexico.

He is a Researcher at the University of Guanajuato in Guanajuato, Mexico. He holds a Ph.D. degree from the University of Western Ontario and a master's degree from UNAM, Mexico. His research interests include structural reliability, live loads on bridges, seismic hazard and others. He has published several technical papers in international journals.

Book Chapter 2

New Ideas Concerning Science and Technology. Describing the Summary of Single Site Extreme Wave Analysis in the Pacific Ocean Comparing Stationary and Non-Stationary GEV Models.

F. Calderón-Vega, C. Mösso, A. D. García-Soto and E. Delgadillo-Ruiz

https://doi.org/10.9734/bpi/nicst/v4/2310E

Chapter 11
Print ISBN: 978-81-949988-9-1, eBook ISBN: 978-81-949988-0-8

Describing the Summary of Single Site Extreme Wave Analysis in the Pacific Ocean Comparing Stationary and Non-Stationary GEV Models

F. Calderón-Vega[1,2*], C. Mösso[2,3], A. D. García-Soto[1] and E. Delgadillo-Ruiz[1]

DOI: 10.9734/bpi/nicst/v4/2310E

ABSTRACT

An extreme value analysis of maximum significant waves recorded at a buoy located in the Pacific Ocean is summarized from a previous study in this book chapter. The analysis was carried out from two perspectives, by considering a Generalized Extreme Value (GEV) model with stationary distribution (i.e., the time variations are not accounted for), and by considering a non-stationary GEV model, which incorporates the monthly seasonality of maximum observed values in time increments; the maximum significant wave behavior was parameterized using harmonic functions for the distribution measures. Both approaches were compared for a single buoy. In the study a seasonality effect was found, which was also present at the Gulf of Mexico in previous studies, and which cannot be captured by a stationary model. Future studies for more buoys and wider regions are desirable, to characterized extreme wave activity, aimed at improving the design and management of coasts and ports by including seasonality.

Keywords: GEV model; stationary; non-stationary; seasonality; projections.

1. INTRODUCTION

In a recent study, [1] used the Gumbel probability density function (PDF) together with maximum annual values to assess the extreme maximum annual significant wave height for projection purposes. [2] and [3] described the weather variability in the geophysical variables of events.

More recently [4] referred to the Bayesian inference for modelling extreme values of characteristic marine environments and for designing maritime structures. Calderón-Vega et al. [5] investigated the seasonality of extreme waves in the Gulf of Mexico; it was found that, for the Gulf of Mexico, there is indeed seasonality effects on the extreme values; moreover, two clear peaks were found which are associated to hurricanes and cold fronts in distinctives seasons of the year. The study was carried out for several buoy sites in the Gulf of Mexico, but it was not performed for buoys in the Pacific. The use of stationary models is very common when carrying out analyses of extremes, however, as already mentioned and found in a previous study [5], seasonality may play a role in the probabilistic characterization of meteo-oceanographic variables, and it may also have an impact on design, management and reliability-oriented tasks; furthermore, since meteo-oceanographic variables are directly linked to climate change detection, vulnerability, future projection and sustainability of coasts and coastal infrastructure [6,7], an impact due to seasonality effects would be expected on all these issues for extreme waves. The significant wave height of the sea surface is an important parameter of the “digital ocean”, and plays an important role in ocean environmental prediction and safety [8].

[1]Department of Civil Engineering, Universidad de Guanajuato, Juárez 77, Zona Centro, P.C. 36000 Guanajuato, Gto. Mexico.
[2]Laboratori d’Enginyeria Marítima, Universitat Politècnica de Catalunya, Jordi Girona 1-3, Mòdul D1, Campus Nord, 08034, Barcelona, Spain.
[3]Centre Internacional d'Investigació dels Recursos Costaners, Jordi Girona 1-3, Mòdul D1, Campus Nord, 08034, Barcelona, Spain.
**Corresponding author: E-mail: f.calderon@ugto.mx, felicitas.calderon@upc.edu;*

The main objective of this study is to select a single buoy site to compare stationary versus non-stationary GEV models for significant wave height projections and to inspect possible seasonality effects in the Pacific Coast for this meteo-oceanographic variable.

2. DATA USED

Significant wave data recorded at 51004 buoy located at the Pacific Ocean are analyzed; the buoy is operated by the National Data Buoy Center (NDBC, www.ndbc.noaa.gov).

Fig. 1 shows the buoy location and general information. The 51004 buoy geographical coordinate are 17.602N 152.395W, and is located to the south of the Hawaii islands. It comprises a time window from 1984 to 2017 including all years, except 2010. The significant wave height (Hs) is obtained as the mean of the highest third for wave heights during a given sample time period, which is 20 minutes for the used NDBC data. The NDBC Hs is preliminarily processed for uniformizing the data series, so that they can be employed in the probabilistic model.

3. RESULTS AND DISCUSSION

3.1 Preliminary Analysis

A preliminary analysis of the data is carried out to broadly inspect the behavior of the variable under study at the selected site. In Fig. 2a (upper part) a main wave incidence to the NEE is observed. The maximum recorded Hs is equal to 10.60 m; see Fig. 2b (lower part). The most frequently observed significant wave height fluctuates around 2 m.

Fig. 1. NOAA 51004 buoy

3.2 Extreme Value Model

3.2.1 GEV model

The governing equations for the extreme value theory (EVT) can be found in [9] and they are used to establish feasible limit distributions for maxima. The only non-degenerate family of distributions obtained from EVT are the well-known Weibull, Gumbel and Fréchet families for maxima, and they are given below [9].

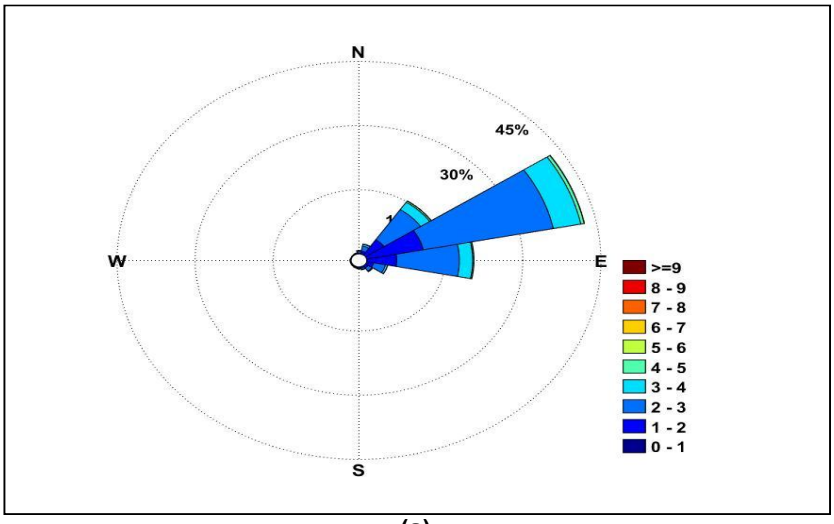

(a)

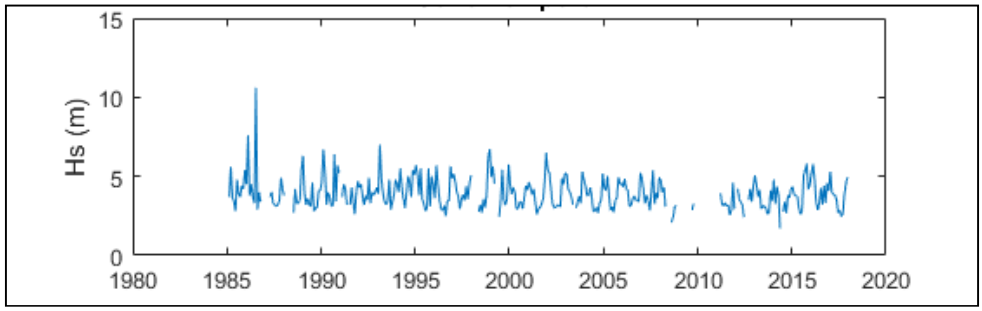

(b)

Fig. 2. Basic statistics of the buoy under study (a) wave rose and, (b) time series data

Maximal Weibull or Reversed Weibull

$$H(x) = \begin{cases} exp\left[-\left(\frac{\lambda - x}{\delta}\right)^{\beta}\right], if\ x \le \lambda,\ \beta > 0 \\ 1, \quad Otherwise \end{cases} \tag{1}$$

Gumbel or Maximal Gumbel

$$H(x) = \exp\left[-exp\left(\frac{x-\lambda}{\delta}\right)\right], \qquad -\infty < x < \infty \tag{2}$$

Fréchet or Maximal Fréchet

$$H(x) = \begin{cases} 0, & if\ x < \lambda, \\ exp\left[-\left(\frac{\delta}{x-\lambda}\right)^{\beta}\right], & if\ x \le \lambda,\ \beta > 0 \end{cases} \tag{3}$$

where β, δ and λ are distributions parameters.

The used model is the Generalized Extreme Value (GEV) distribution e.g., [2,9], which encompasses, in a single mathematical expression, the three well-known families of extreme distributions, i.e., the Gumbel, Weibull and Frechet Distributions given above, and is given by:

$$G(x)=\exp\left\{-\left[1+\xi\left(\frac{x-\mu}{\psi}\right)\right]_{+}^{-1/\xi}\right\}\rightarrow\xi\neq 0$$

$$G(x)=\exp\left\{-\exp\left[-\left(\frac{x-\mu}{\psi}\right)\right]\right\}\rightarrow\xi=0 \quad (4)$$

The PDF is defined by means of

$$g(x)=\frac{1}{\psi}\left[1+\xi\left(\frac{x-\mu}{\psi}\right)\right]_{+}^{-\left(1+1/\xi\right)}exp\left\{-\left[1+\xi\left(\frac{x-\mu}{\psi}\right)\right]_{+}^{-1/\xi}\right\}if\ \xi\neq 0$$

$$g(x)=\frac{1}{\psi}exp\left(-\frac{x-\mu}{\psi}\right)exp\left[-exp\left(-\frac{x-\mu}{\psi}\right)\right]if\ \xi=0 \quad (5)$$

where $-\infty<\mu<\infty$ is the location parameter, $\psi>0$ is the scale parameter and ξ the shape parameter.

To develop the model, the lack of data should be accounted for, since this issue affects the parameters estimation stability for the extreme value distribution. Therefore, since it is known that data for some years may be absent (e.g., due to buoys maintenance), a minimum of data per time unit is considered to define the maximum values, by adopting the criterion of rejecting maximum monthly events with data blank spaces of up to 40% e.g. [5].

3.2.2 Non-stationary GEV model

For modelling Hs the GEV is used for block maxima of a time interval. In this study, the monthly maximum values are used for the extreme value samples. Note that throughout this study, the methodology used and referenced by [5] is followed.

The seasonality is defined as the cyclic changes during the year. Usually, this cycle is linked to established climatic patrons; consequently, it repeats itself for many years and behaves in a sinusoidal way, as shown in Fig. 3. In Fig. 3 the marine weather variation is exhibited; in the winter the wave heights are larger than in the spring.

For the assessment of time-dependency an extension of traditional stationary models in extreme value theory is used. In this case the successive monthly maxima are considered as independent random variables, disregarding the need of the homogeneity hypothesis for the consecutive months, because they do not have identical distributions. It is assumed that the maximum monthly value Z_t of the observed Hs in month t follows a GEV distribution, where the location $\mu(t)>0$, scale $\psi(t)>0$ and shape $\xi(t)$ parameters are time-dependent.

The cumulative distribution function (CDF) of Z_i is given by

$$F_t(z)=\begin{cases}\left\{exp\left\{-\left[1+\xi(t)\left(\frac{z-\mu(t)}{\psi(t)}\right)\right]_{+}^{\frac{-1}{\xi(t)}}\right\}\\ exp\left\{-exp\left[-\left(\frac{z-\mu(t)}{\psi(t)}\right)\right]\right\}\end{cases} \quad (6)$$

The non-stationarity of the models is introduced in the GEV parameters as:

$$\theta = \begin{cases} \mu(t) = \beta_0 + \beta_1 \cos(2\pi t) + \beta_2 sen(2\pi t) \\ \quad +\beta_3 \cos(4\pi t) + \beta_4 sen(4\pi t) \\ \psi(t) = \alpha_0 + \alpha_1 \cos(2\pi t) + \alpha_2 sen(2\pi t) \\ \quad +\alpha_3 \cos(4\pi t) + \alpha_4 sen(4\pi t) \\ \xi(t) = \gamma_0 + \gamma_1 \cos(2\pi t) + \gamma_2 sen(2\pi t) \\ \quad +\gamma_3 \cos(4\pi t) + \gamma_4 sen(4\pi t) \end{cases} \quad (7)$$

Where, $\psi(t>0)$, β_0, α_0 y γ_0 are mean values, β_i, α_i and γ_i (for *i=1,2*) are the harmonic amplitudes; β_i, α_i and γ_i (for *i=3,4*) are the subharmonic amplitudes and *t* is in years.

In Fig. 4 the results from the variability analysis within a year of the maximum-likelihood estimators for the location, *μ*, scale, *ψ*, and shape, *ξ*, parameters along the year are depicted. The circles represent the values computed with the stationary GEV model, month to month, and the line is the resulting function from the regression fitting with two harmonics.

The location parameter exhibits maximum values in winter season, which indicates, in general terms, larger wave heights in November, December, January and February.

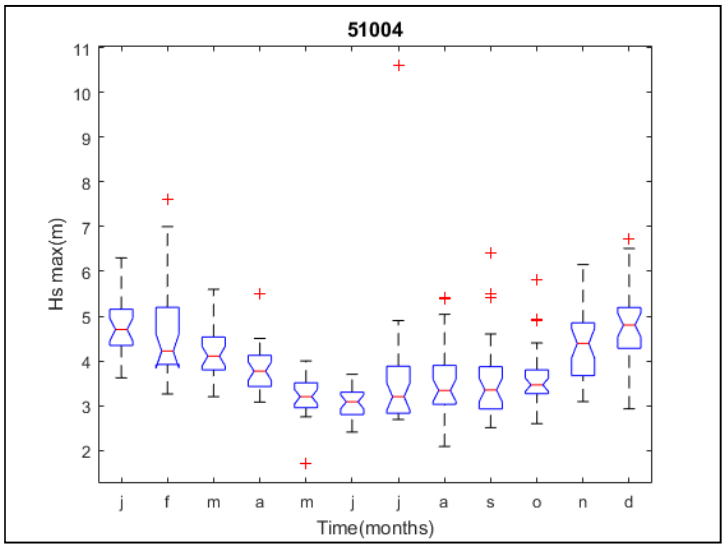

Fig. 3. Seasonality of monthly maxima

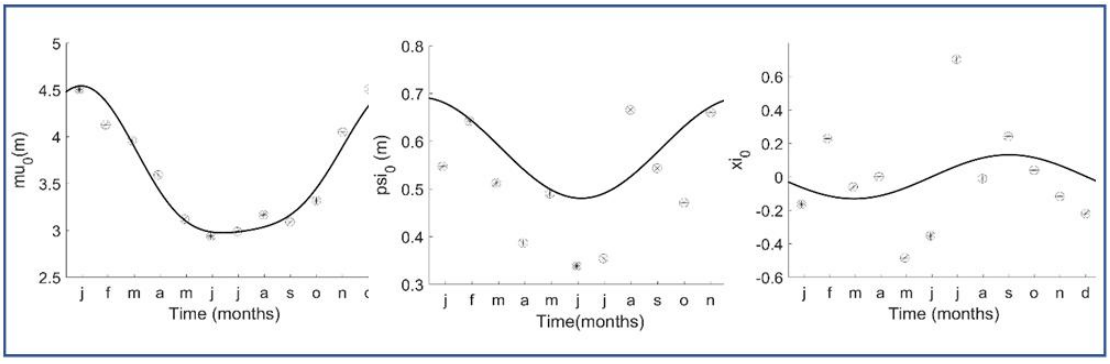

Fig. 4. Estimators for distribution parameters month to month by regression fitting

3.2.3 Non-stationary model fitting

To estimate the regression coefficients and the probability distribution parameters, the method of maximum likelihood (MML) is employed.

This method is based in the search for point estimators *(θ)* for the parameters of a *X* function, so that the probability of observing the sample data *{x_1,…x_n}* is maximum. The likelihood function *L(x;θ)* is the joint density function associated to all initial extreme values, from a previously selected distribution and, in general terms, is given by

$$L(x;\theta) = f(x_1,\dots x_n;\theta) = \prod_{i=1}^{n} f(x_i;\theta) \tag{8}$$

The location *$\mu(t)>0$*, scale *$\psi(t)>0$* and shape *$\xi(t)$* parameters are expressed in terms of harmonic functions, whose amplitudes are regression parameters to be mathematically estimated [10].
For our study the specific maximum likelihood function is given by

$$l(\theta \mid t_i, x_i) = -\sum_{i=1}^{m}\left\{\log\psi(t_i) + \left(1+1/\xi(t_i)\right)\log\left[1+\xi(t_i)\left(\frac{x_i-\mu(t_i)}{\psi(t_i)}\right)\right]_+ + \left[1+\xi(t_i)\left(\frac{x_i-\mu(t_i)}{\psi(t_i)}\right)\right]_+^{-1/\xi(t_i)}\right\} \tag{9}$$

3.2.4 Automatic selection, confidence intervals and return period values

To find the best model, a selective search methodology named Stepwise is carried out [5]. Standard errors and confidence intervals are used to deal with the uncertainty. Finally, with regard to the values associated to a return period of interest, the following equations are adopted

$$X_q(t,\theta) = X_q(\mu(t),\psi(t),\xi(t)) = \begin{cases} \mu(t) - \dfrac{\psi(t)}{\xi(t)}\left\{1-\left[-\log(1-q)\right]^{-\xi(t)}\right\} & if \quad \xi(t)\neq 0 \\ \mu(t) - \psi(t)\log\left[-\log(1-q)\right] & if \quad \xi(t)=0 \end{cases} \tag{10}$$

where *q* is the exceedance probability.

3.3 Discussion

3.3.1 Stationary model

For the stationary model the location, scale and shape parameters, which are invariant in time, are obtained. Table 1 lists the computed values of these parameters, the maximum recorded significant wave height, and the projected value for Hs associated to a return period of 30 years.

Table 1. Parameters for the stationary model, Hs_{max} and Hs and Tr=30 years

Hs_{max} (m)	**10.60**
Hs (m) for Tr= 30 yr	5.60
μ	360.34
ψ	58.59
ξ	$1x10^{-4}$

From Table 1, it can be inferred that the stationary model is dominated by a Frechet type distribution. Note that in Table 1, Hs_{max} = 10.60 m is an atypical value recorded on 23 July, 1986 during hurricane Estelle. It can be clearly observed in Fig. 5.

In Fig. 5 instantaneous quantiles for 30 years for the location and scale parameters are shown, the depiction corresponds to the stationary GEV over the monthly extreme values distributed month to month along the year; dots indicate the monthly maximum Hs; the red line the time-dependent quantile for a 30-year return period; the black, green and yellow lines location, scale and shape parameters, respectively.

QQ and probability Plots are shown in Fig. 6; for buoy 51004 the probability paper implies an adequate fit for the data.

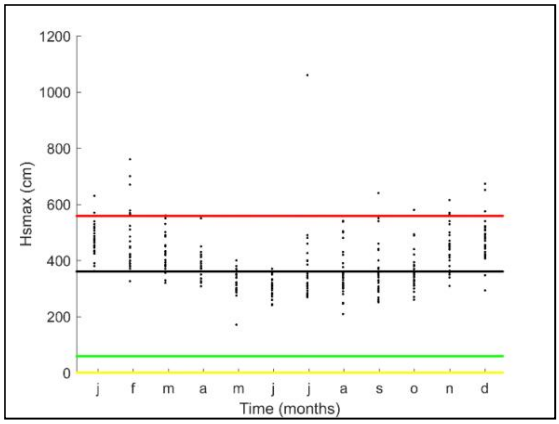

Fig. 5. Estimated quantile values for Tr=30 years, monthly maximums and location, scale and shape parameters

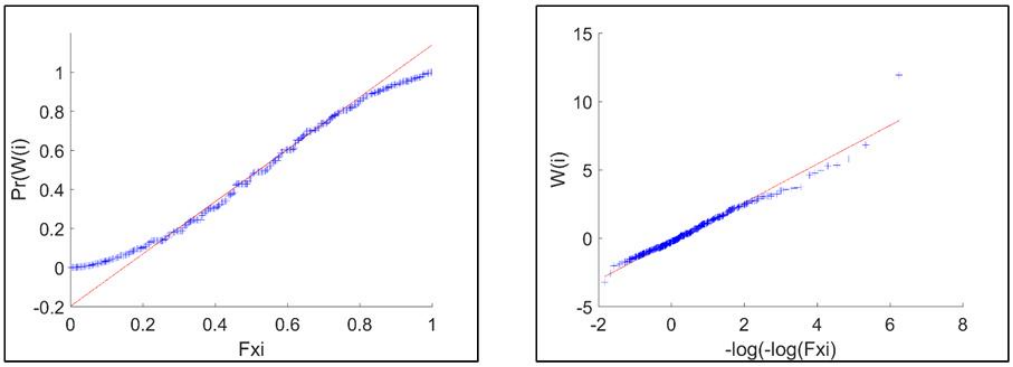

(a) **(b)**

Fig. 6. (a) Probability and (b) quantile plots for the stationary GEV model

3.3.2 Non stationary model

For the non-stationary model, it was found that values for the annual and semiannual cycles for the location and scale parameters are present, as well as the annual cycle for the shape parameter. The zero positive gamma value indicates that data exhibit a heavy-tailed Frechet type distribution, which is expected, if it is considered that the buoy maximum value is related to a hurricane activity, which is quite large as compared to the regular maximum recoded waves. Using the computed numerical values in the non-stationary GEV distribution equations, the best fitted parameters for the distribution are obtained. In Fig. 7 the red line shows the time-dependent quantile associated to a 30-year return period; the black line depicts the location parameter, the green line corresponds to the scale parameter and the yellow line corresponds to the shape parameter. The monthly maxima for Hs are shown by the black dots. An adequate fit for the studied case can be observed in Fig. 7. Note that the maximum Hs associated to hurricane Estelle (mentioned previously), does not significantly deviate the trend of the values associated to a 30-year return period. Nevertheless, it may lead to a smoother curve as compared with the trend for buoys in the Gulf of Mexico, where two peaks associated to cold fronts and hurricanes are shown; Fig. 7 also seems to show that kind of behavior, but the peaks may be somehow attenuated due to the atypical maximum Hs in July. Nevertheless, a seasonality effect does exist also in the Pacific Coast; it could be preliminarily concluded that seasonal trends are existent in both, the Gulf of Mexico and the Pacific Ocean.

In Fig. 8; the probability associated to the Gumbel distribution from the W(t) statistic is shown.

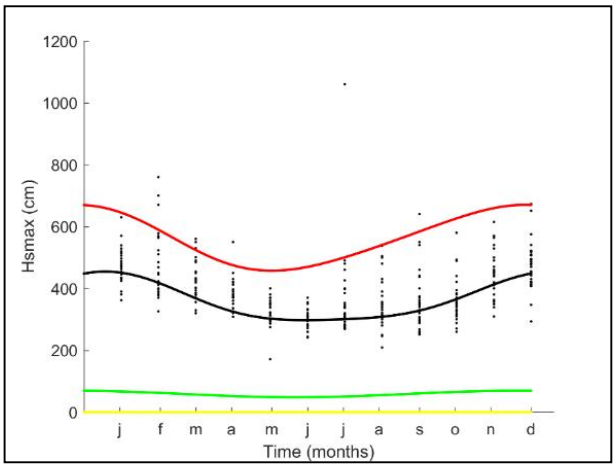

Fig. 7. Fitting for the monthly maximum for the non-stationary GEV model

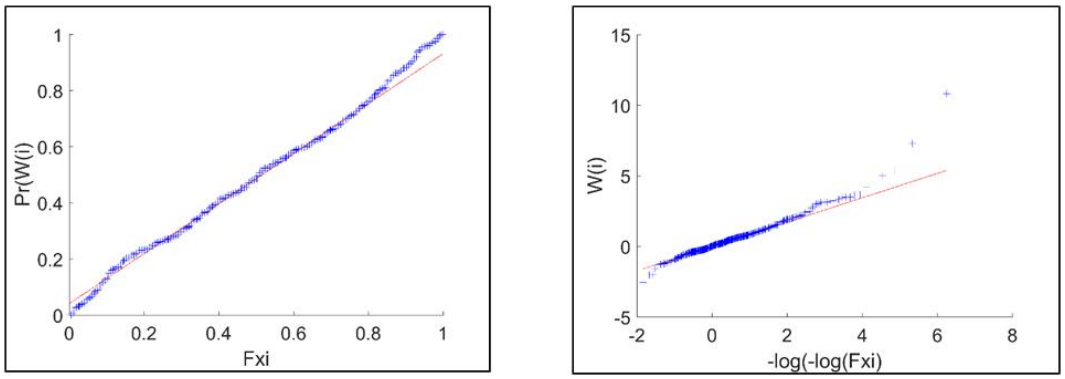

(a) (b)

Fig. 8. Diagnostic plots (a and b) for the non-stationary GEV model

3.3.3 Comparison of stationary versus non-stationary GEV models

In this section a comparison of the two employed models for the extreme value analysis is carried out. The basic stationary GEV model and the non-stationary GEV model.

In Fig. 9 the most adequate fitting of the non-stationary GEV model to the data can be clearly observed, since the curve follows the seasonal trends; conversely, it can be seen that the stationary GEV model is unable to capture the seasonality of the significant wave heights. Fig. 10 shows also the best fitted results month-to-month, but for a 100-year return period. Fig. 11 shows 95% confidence intervals, where it can be observed that the bounds are more reduced for the non-stationary model and better correlated to the month-to month data.

Results in Figs. 10 and 11 show the advantage of using the non-stationary GEV model, since the computed seasonal trend tend to capture the maximum values and fits better the data series. This is important, because extreme wave heights are applied to different engineering fields, for instance to offshore engineering applications [11].

A final Figure in this study, Fig. 12, shows that the best behavior (in terms of representing the selected meteo-oceanographic variable) for the used empirical data is obtained with the non-stationary GEV distribution, at least for the selected buoy, as observed by the goodness-of-fit for both models in Fig. 12 (left side column for the stationary model and right side column for the non-stationary model, respectively).

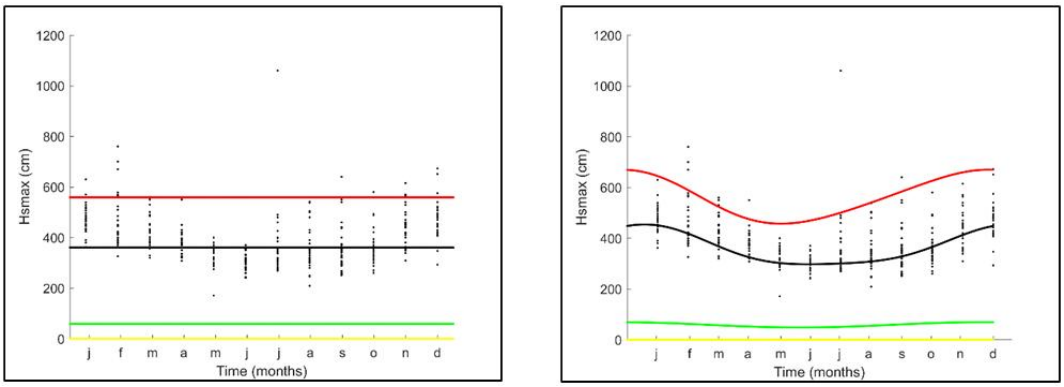

Fig. 9. Quantiles associated to 30-year return period for (a) the stationary and (b) non-stationary GEV models

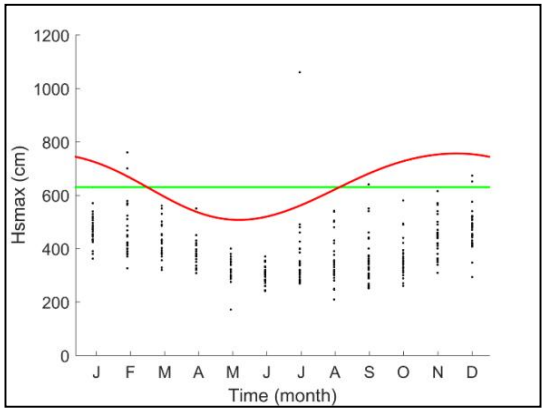

Fig. 10. Quantiles comparison for 100-year return period and measured Hs

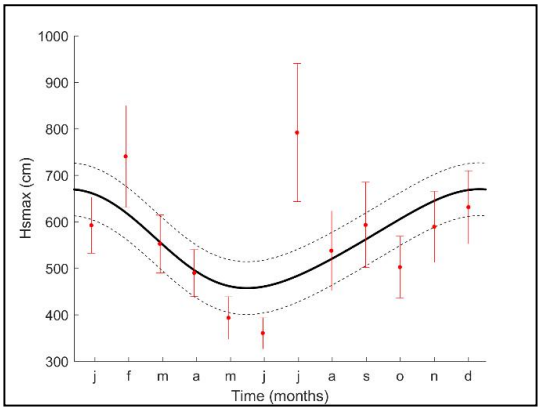

Fig. 11. 30-year return period quantile and 95% confidence interval for the non-stationary GEV model and the month-to-month stationary GEV

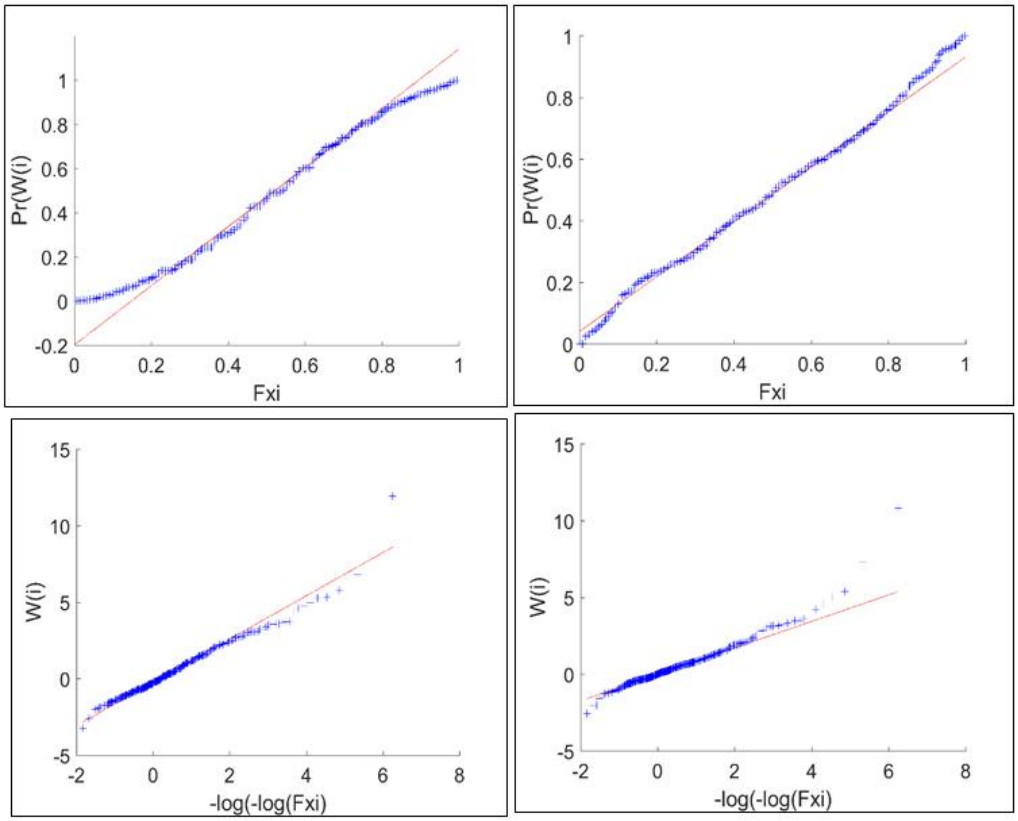

Fig. 12. Goodness-of-fit plots for stationary (a) and non-stationary (b) models

4. CONCLUSION

In this study a methodology for fitting empirical meteo-oceanographic data to extreme value models for projections purposes is published as a summary of a book chapter, based on a previous study. The selected meteo-oceanographic variable is significant wave height. The GEV model is used from two perspectives: stationarity and non-stationarity. A comparison is carried out between the two approaches for a single site. For the non-stationary GEV model the seasonality is model by means of sinusoidal curves for a single buoy in the Pacific Ocean.

From the comparison of the stationary and non-stationary GEV models, it is concluded that the later leads to a better representation of the significant wave height, and also leads to larger projected return period values than the former for winter season.

It is also concluded that, at least for the selected buoy and its recorded data, a seasonality trend is found, as it was the case for the Gulf of Mexico [5], although some differences are found in the trends. Future studies for more buoys and wider regions are desirable, to characterized extreme wave activity, aimed at improving the design and management of coasts and ports by including seasonality.

ACKNOWLEDGEMENTS

The financial support from the Erasmus Mundus Coastal and Marine Engineering and Management (CoMEM) programme and from Universidad de Guanajuato is gratefully acknowledged. We are thankful for the comments, suggestions and constructive criticism from two anonymous reviewers.

We are also very thankful to Ms. Ruma Bag and the Editorial team for their invitation and help in the editorial process.

COMPETING INTERESTS

Authors have declared that no competing interests exist.

REFERENCES

1. Shao Z, Liang B, Li H, Lee D. Study of sampling methods for assessment of extreme significant wave heights in the South China Sea. Ocean Eng. 2018;168:173-184. DOI: 10.1016/j.oceaneng.2018.09.015.
2. Coles SG. An introduction to statistical modelling of extreme values. 1st ed.; Springer-Verlag: London, UK. 2001;1-208.
3. Katz RW. Stochastic modeling of hurricane damage. J. of App. Meteor. 2002;41:754-762.
4. Johathan P, Ewans K. Statistical modelling of extreme ocean environments for marine design: A review. Ocean Eng. 2013;91-109 DOI: 10.1016/j.oceaneng.2013.01.004
5. Calderón-Vega F, Vázquez-Hernández AO, García-Soto AD. Analysis of extreme waves with seasonal variation in the Gulf of Mexico using a time-dependent GEV model. Ocean Eng. 2013;73:68-82. DOI: 10.1016/j.oceaneng. 2013.08.007
6. Sanchez-Arcilla A, Sierra JP, Gracia V, Garcia M, Jimenez JA, Mösso C, Valdemoro H. Coastal sustainability for uncertain futures: A spanish mediterranean case from the RISES-AM project. A: Intenational Association for Hydraulic Research Congress. E-proceedings of the 36th IAHR World Congres. L'Haia. 2015;1-8.
7. Sanchez-arcilla A, Sierra JP, Mösso C, Gracia V, Garcia M. Progress on climate change detection and projections over Spain since the findings of the IPCC AR5. International Symposium CLIMATE-ES. 2015;146.
8. Peng Q, Jin S. Significant wave height estimation from space-borne cyclone-GNSS reflectometry. Remote Sensing. 2019;11(5):584.
9. Castillo E, Hadi AS, Balakrishnan N, Sarabia JM. Extreme value and related models with applications in engineering and science. Wiley-Interscience. New Jersey; 2005.
10. Menéndez M, Méndez FJ, Izaguirre C, Luceño A, Losada IJ. The influence of seasonality on estimating return values of significant wave height. Ocean Eng. 2009;56:211-219. DOI: 10.1016/j.coastaleng.2008.07.004.
11. Panchang V, Kwon Jeong Ch, Demirbilek Z. Analyses of extreme wave heights in the Gulf of Mexico for offshore engineering applications. J Offshore Mech Arct. 2013;135(3):1-15.

Biography of author(s)

F. Calderón-Vega
Department of Civil Engineering, Universidad de Guanajuato, Juárez 77, Zona Centro, P.C. 36000 Guanajuato, Gto. Mexico and Laboratori d'Enginyeria Marítima, Universitat Politècnica de Catalunya, Jordi Girona 1-3, Mòdul D1, Campus Nord, 08034, Barcelona, Spain.

She is a Ph.D. Candidate at the Polytechnic University of Catalunya, BarcelonaTech. She is a Researcher at the University of Guanajuato in Guanajuato, Mexico. Her research interests include maritime engineering and structures, hydraulics, extreme value theory applied to meteo-oceanographic variables and others. She has published several technical papers in international journals.

C. Mösso
Laboratori d'Enginyeria Marítima, Universitat Politècnica de Catalunya, Jordi Girona 1-3, Mòdul D1, Campus Nord, 08034, Barcelona, Spain and Centre Internacional d'Investigació dels Recursos Costaners, Jordi Girona 1-3, Mòdul D1, Campus Nord, 08034, Barcelona, Spain.

He is a Researcher at the Department of Civil and Environmental Engineering (hydraulics, maritime and environmental Section) at the Universitat Politècnica de Catalunya (UPC) BarcelonaTech, as well as in the Laboratori d'Enginyeria Marítima (LIM/UPC). His research interests include coastal engineering, climate change, maritime hydrodynamics among others. He has published several technical papers in international journals.

A. D. García-Soto
Department of Civil Engineering, Universidad de Guanajuato, Juárez 77, Zona Centro, P.C. 36000 Guanajuato, Gto. Mexico.

He is a Researcher at the University of Guanajuato in Guanajuato, Mexico. He holds a Ph.D. degree from the University of Western Ontario and a master's degree from UNAM, Mexico. His research interests include structural reliability, live loads on bridges, seismic hazard and others. He has published several technical papers in international journals.

E. Delgadillo-Ruiz
Department of Civil Engineering, Universidad de Guanajuato, Juárez 77, Zona Centro, P.C. 36000 Guanajuato, Gto. Mexico.

He is currently a research professor at the University of Guanajuato Mexico. He has a Ph.D. in engineering with a terminal line in physical process modelling. His lines of research include the modelling of the components of the surface and underground water balance, as well as the study of the effects of global climate change. In addition, he belongs to the water resources and environmental engineering research group of the civil and environmental engineering department of the University of Guanajuato.

DISCLAIMER
This chapter is an extended version of the article published by the same author(s) in the following journal.
Current Journal of Applied Science and Technology, 32(6): 1-12, 2019.

Reviewers' Information
(1)Dr. Olumide Adesina, Olabisi Onabanjo University, Nigeria.
(2)Zlatin Zlatev, Trakia University, Bulgaria.

APENDIX

Paper C

Single Site Extreme Wave Analysis in the Pacific Ocean Comparing Stationary and Non-stationary GEV Models. Current Journal of Applied Science and Technology.

Calderón-Vega, C. Mösso, A. D. García-Soto and E. Delgadillo-Ruiz

Current Journal of Applied Science and Technology. 32(6): 1-12, 2019; Article no.CJAST.47420

Current Journal of Applied Science and Technology

32(6): 1-12, 2019; Article no.CJAST.47420
ISSN: 2457-1024
(Past name: British Journal of Applied Science & Technology, Past ISSN: 2231-0843, NLM ID: 101664541)

Single Site Extreme Wave Analysis in the Pacific Ocean Comparing Stationary and Non-stationary GEV Models

F. Calderón-Vega[1,2*], C. Mösso[2,3], A. D. García-Soto[1] and E. Delgadillo-Ruiz[1]

[1]Department of Civil Engineering, Universidad de Guanajuato, Juárez 77, Zona Centro, P.C. 36000 Guanajuato, Gto, Mexico.
[2]Laboratori d'Enginyeria Marítima, Universitat Politècnica de Catalunya, Jordi Girona 1-3, Mòdul D1, Campus Nord, 08034, Barcelona, Spain.
[3]Centre Internacional d'Investigació dels Recursos Costaners, Jordi Girona 1-3, Mòdul D1, Campus Nord, 08034, Barcelona, Spain.

Authors' contributions

This work was carried out in collaboration between all authors. All authors designed the study, performed the statistical analysis, wrote the protocol, wrote the first draft of the manuscript, managed the analyses of the study and managed the literature searches. All authors read and approved the final manuscript.

Article Information

DOI: 10.9734/CJAST/2019/v32i630038
Editor(s):
(1) Dr. Vyacheslav O Vakhnenko, Professor, Division of Geodynamics of Explosion, Subbotin Institute of Geophysics, National Academy of Sciences of Ukrainian, Ukraine.
(2) Dr. João Miguel Dias, Assistant Professor, Habilitation in Department of Physics, CESAM, University of Aveiro, Portugal.
Reviewers:
(1) Dr. Olumide Adesina, Olabisi Onabanjo University, Nigeria.
(2) Zlatin Zlatev, Trakia University, Bulgaria.
Complete Peer review History: http://www.sdiarticle3.com/review-history/47420

Original Research Article

Received 25 October 2018
Accepted 09 February 2019
Published 23 February 2019

ABSTRACT

The adequate knowledge of the weather behavior is very important for the design and management of socioeconomical, environmental and sustainability human interests in the coasts and oceans. In the present study an extreme value analysis of maximum significant waves recorded at a buoy located in the Pacific Ocean was carried out. The analysis was carried out from two perspectives, by considering a Generalized Extreme Value (GEV) model with stationary distribution (i.e., the time variations are not accounted for), and by considering a non-stationary GEV model, which incorporates the monthly seasonality of maximum observed values in time increments; the

**Corresponding author: E-mail: f.calderon@ugto.mx, felicitas.calderon@upc.edu*

maximum significant wave behavior was parameterized using harmonic functions for the distribution measures. Both approaches were compared for a single buoy. In the study a seasonality effect was found, which was also present at the Gulf of Mexico in previous studies, and which cannot be captured by a stationary model.

Keywords: GEV model; stationary; non-stationary; seasonality; projections.

1. INTRODUCTION

The use of the extreme value theory has been widely extended in recent years to meteo-oceanographic variables. In a recent study, [1] used the Gumbel probability density function (PDF) together with maximum annual values to assess the extreme maximum annual significant wave height for projection purposes. [2] used non-stationary GEV models for investigating period trends in extreme waves. [3] developed design values for significant wave height accounting for direction and seasonality by means of a non-stationary model. [4] compared the behavior of tropical cyclone data (extreme values), obtained through simulations, versus those recorded at buoys located in the Meridional Chinese Sea and the Oriental Chinese Sea, and proposed an approach combining the set of data. [5] used peak over threshold (POT) methods and block maxima for the assessment of return values for significant wave heights.

The Extreme value theory encompass methods and techniques to quantify and model the stochastic behavior, in terms of magnitude as well as in terms of frequency, of extreme events. [6,7] already mentioned the size effect on the materials strength, and in 1922 [8] introduced the concept of extreme values, while [9] studied the maximum and minimum distributions for a sample, problem which also [10] approached for normal samples. A keystone in the development of extreme value analysis was given by [11] and [12], who demonstrated that only three limiting parametric distribution families for maximum (and their minimum counterparts) are possible. [13], [14,15,16] and [17], worked on the problem of maximum and minimum distributions for a sample and found the generalized proof for [18] on the extremes type theorem. Gumbel [19] published the book "Statistics of extremes", one of the greatest contributions in the history of extreme value statistics. Later on, [20] and [21] incorporated the dependency and related results for the multivariate case. [22] and [23] described the weather variability in the geophysical variables of events.

More recently [24] referred to the Bayesian inference for modelling extreme values of characteristic marine environments and for designing maritime structures. Calderón-Vega et al. [25] investigated the seasonality of extreme waves in the Gulf of Mexico; it was found that, for the Gulf of Mexico, there is indeed seasonality effects on the extreme values; moreover, two clear peaks were found which are associated to hurricanes and cold fronts in distinctives seasons of the year. The study was carried out for several buoy sites in the Gulf of Mexico, but it was not performed for buoys in the Pacific. The use of stationary models is very common when carrying out analyses of extremes, however, as already mentioned and found in a previous study [25], seasonality may play a role in the probabilistic characterization of meteo-oceanographic variables, and it may also have an impact on design, management and reliability-oriented tasks; furthermore, since meteo-oceanographic variables are directly linked to climate change detection, vulnerability, future projection and sustainability of coasts and coastal infrastructure [26,27], an impact due to seasonality effects would be expected on all these issues for extreme waves. Although not pursued in the present study, the relation between extreme wave heights and sustainability (using stationary versus non-stationary models) could be explored in future projects; the present study can be considered as a first step in that direction.

The main objective of this study is to select a single buoy site to compare stationary versus non-stationary GEV models for significant wave height projections and to inspect possible seasonality effects in the Pacific Coast for this meteo-oceanographic variable.

2. DATA USED

Significant wave data recorded at 51004 buoy located at the Pacific Ocean are analyzed; the buoy is operated by the National Data Buoy Center (NDBC, www.ndbc.noaa.gov).

Fig. 1 shows the buoy location and general information. The 51004 buoy geographical coordinate are 17.602N 152.395W, and is located to the south of the Hawaii islands. It comprises a time window from 1984 to 2017 including all years, except 2010. The significant wave height (Hs) is obtained as the mean of the highest third for wave heights during a given sample time period, which is 20 minutes for the used NDBC data. The NDBC Hs is preliminarily processed for uniformizing the data series, so that they can be employed in the probabilistic model.

3. RESULTS AND DISCUSSION

3.1 Preliminary Analysis

A preliminary analysis of the data is carried out to broadly inspect the behavior of the variable under study at the selected site. In Fig. 2a (upper part) a main wave incidence to the NEE is observed. The maximum recorded Hs is equal to 10.60 m; see Fig. 2b (lower part). The most frequently observed significant wave height fluctuates around 2 m.

Fig. 1. NOAA 51004 buoy

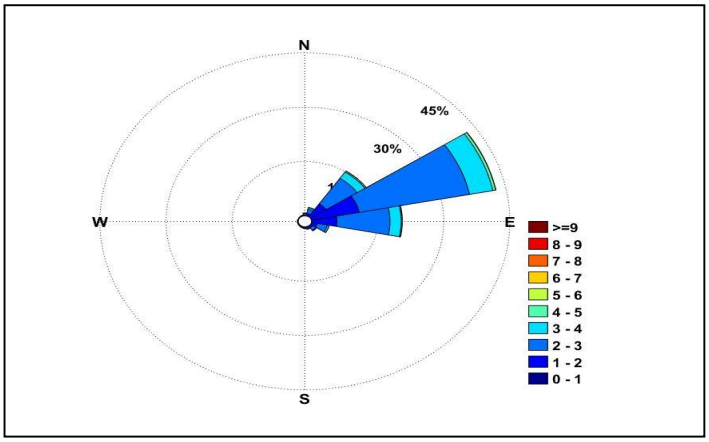

(a)

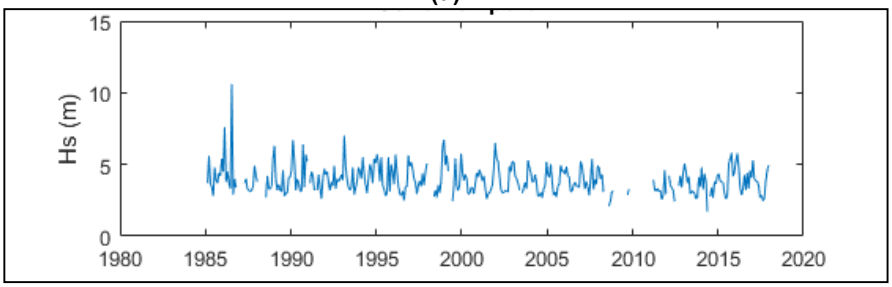

(b)

Fig. 2. Basic statistics of the buoy under study (a) wave rose and, (b) time series data

3.2 Extreme Value Model

3.1.1 GEV model

The governing equations for the extreme value theory (EVT) can be found in [28] and they are used to establish feasible limit distributions for maxima. The only non-degenerate family of distributions obtained from EVT are the well-known Weibull, Gumbel and Fréchet families for maxima, and they are given below [28].

Maximal Weibull or Reversed Weibull

$$H(x) = \begin{cases} exp\left[-\left(\frac{\lambda - x}{\delta}\right)^{\beta}\right], if\ x \le \lambda,\ \beta > 0 \\ 1, \quad Otherwise \end{cases} \quad (1)$$

Gumbel or Maximal Gumbel

$$H(x) = \exp\left[-exp\left(\frac{x-\lambda}{\delta}\right)\right], \qquad -\infty < x < \infty \quad (2)$$

Fréchet or Maximal Fréchet

$$H(x) = \begin{cases} 0, & if\ x < \lambda, \\ exp\left[-\left(\frac{\delta}{x-\lambda}\right)^{\beta}\right], & if\ x \le \lambda,\ \beta > 0 \end{cases} \quad (3)$$

where β, δ and λ are distributions parameters.

The used model is the Generalized Extreme Value (GEV) distribution e.g., [22,28], which encompass, in a single mathematical expression, the three well-known families of extreme distributions, i.e., the Gumbel, Weibull and Frechet Distributions given above, and is given by:

$$G(x) = \exp\left\{-\left[1 + \xi\left(\frac{x-\mu}{\psi}\right)\right]_{+}^{-1/\xi}\right\} \rightarrow \xi \neq 0$$

$$G(x) = \exp\left\{-\exp\left[-\left(\frac{x-\mu}{\psi}\right)\right]\right\} \rightarrow \xi = 0 \quad (4)$$

The PDF is defined by means of

$$g(x) = \frac{1}{\psi}\left[1 + \xi\left(\frac{x-\mu}{\psi}\right)\right]_{+}^{-\left(1+1/\xi\right)} exp\left\{-\left[1 + \right.\right.$$

$$\xi x - \mu\psi + -1\xi if\ \xi \neq 0$$

$$g(x) = \frac{1}{\psi} exp\left(-\frac{x-\mu}{\psi}\right) exp\left[-exp\left(-\frac{x-\mu}{\psi}\right)\right] if\ \xi = 0 \quad (5)$$

where $-\infty < \mu < \infty$ is the location parameter, $\psi > 0$ is the scale parameter and ξ the shape parameter.

The location parameter represents the mean values of the random variable, x, and defines the value with a non-exceedance probability $exp(-1)$. The scale parameter represents the sample dispersion. Finally, the shape parameter defines the distribution family as a function of the tail behavior; when ξ exists, $G(x)$ includes two distribution families.

To develop the model, the lack of data should be accounted for, since this issue affects the parameters estimation stability for the extreme value distribution. Therefore, since it is known that data for some years may be absent (e.g., due to buoys maintenance), a minimum of data per time unit is considered to define the maximum values, by adopting the criterion of rejecting maximum monthly events with data blank spaces of up to 40% e.g. [25].

3.1.2 Non-stationary GEV model

For modelling Hs the GEV is used for block maxima of a time interval. In this study, the monthly maximum values are used for the extreme value samples. Note that throughout this study, the methodology used and referenced by [25] is followed.

The seasonality is defined as the cyclic changes during the year. Usually, this cycle is linked to established climatic patrons; consequently, it repeats itself for many years and behaves in a sinusoidal way, as shown in Fig. 3. In Fig. 3 the marine weather variation is exhibited; in the winter the wave heights are larger than in the spring.

For the assessment of time-dependency an extension of traditional stationary models in extreme value theory is used. In this case the successive monthly maxima are considered as independent random variables, disregarding the need of the homogeneity hypothesis for the consecutive months, because they do not have identical distributions. It is assumed that the maximum monthly value Z_t of the observed Hs in month t follows a GEV distribution, where the location $\mu(t)>0$, scale $\psi(t)>0$ and shape $\xi(t)$ parameters are time-dependent.

The cumulative distribution function (CDF) of Z_i is given by

$$F_t(z) = \begin{cases} \left\{ exp\left\{ -\left[1 + \xi(t)\left(\frac{z-\mu(t)}{\psi(t)}\right)\right]_+^{\frac{-1}{\xi(t)}} \right\} \\ exp\left\{ -exp\left[-\left(\frac{z-\mu(t)}{\psi(t)}\right)\right]\right\} \end{cases} \quad (6)$$

The non-stationarity of the models is introduced in the GEV parameters as:

$$\theta = \begin{cases} \mu(t) = \beta_0 + \beta_1 cos(2\pi t) + \beta_2 sen(2\pi t) \\ \quad +\beta_3 cos(4\pi t) + \beta_4 sen(4\pi t) \\ \psi(t) = \alpha_0 + \alpha_1 cos(2\pi t) + \alpha_2 sen(2\pi t) \\ \quad +\alpha_3 cos(4\pi t) + \alpha_4 sen(4\pi t) \\ \xi(t) = \gamma_0 + \gamma_1 cos(2\pi t) + \gamma_2 sen(2\pi t) \\ \quad +\gamma_3 cos(4\pi t) + \gamma_4 sen(4\pi t) \end{cases} \quad (7)$$

Where, $\psi(t > 0)$, β_0, α_0 y γ_0 are mean values, β_i, α_i y γ_i (for *i=1,2*) are the harmonic amplitudes; β_i, α_i y γ_i (for *i=3,4*) are the subharmonic amplitudes and *t* is in years.

In Fig. 4 the results from the variability analysis within a year of the maximum-likelihood estimators for the location, *μ*, scale, *ψ*, and shape, *ξ*, parameters along the year are depicted. The circles represent the values computed with the stationary GEV model, month to month, and the line is the resulting function from the regression fitting with two harmonics.

The location parameter exhibits maximum values in winter season, which indicates, in general terms, larger wave heights in November, December, January and February.

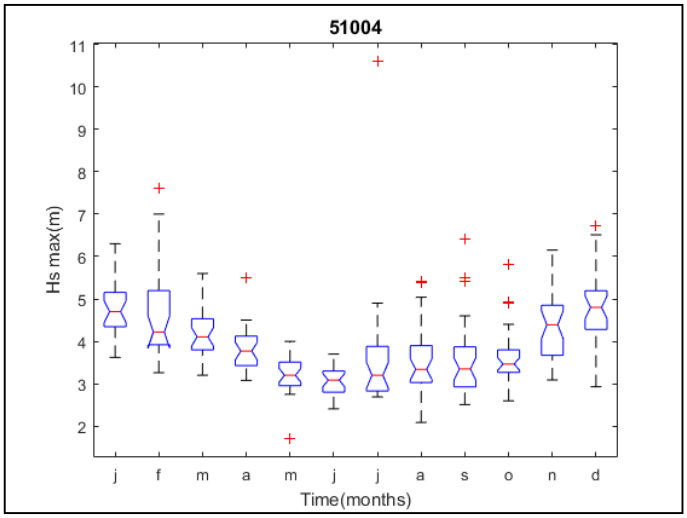

Fig. 3. Seasonality of monthly maxima

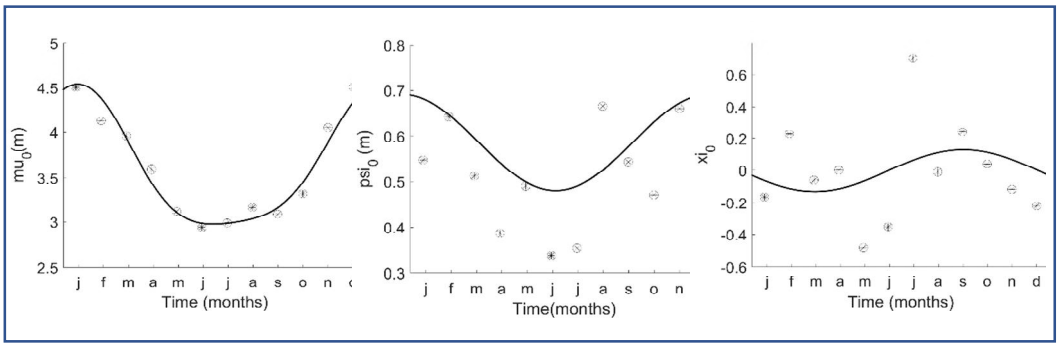

Fig. 4. Estimators for distribution parameters month to month by regression fitting

3.1.3 Non-stationary model fitting

To estimate the regression coefficients and the probability distribution parameters, the method of maximum likelihood (MML) is employed.

This method is based in the search for point estimators *(θ)* for the parameters of a *X* function, so that the probability of observing the sample data *{x₁,…xₙ}* is maximum. The likelihood function *L(x;θ)* is the joint density function associated to all initial extreme values, from a previously selected distribution and, in general terms, is given by

$$L(x;\theta) = f(x_1,\dots x_n;\theta) = \prod_{i=1}^{n} f(x_i;\theta) \qquad (8)$$

The location *μ(t)>0*, scale *ψ(t)>0* and shape *ξ (t)* parameters are expressed in terms of harmonic functions, whose amplitudes are regression parameters to be mathematically estimated [29].

For our study the specific maximum likelihood function is given by

$$l(\theta \mid t, x_i) = -\sum_{i=1}^{m}\left\{\log\psi(t_i) + \left(1 + 1/\xi(t_i)\right)\log\left[1+\xi(t_i)\left(\frac{x_i-\mu(t_i)}{\psi(t_i)}\right)\right]_{+} + \left[1+\xi(t_i)\left(\frac{x_i-\mu(t_i)}{\psi(t_i)}\right)\right]_{+}^{-1/\xi(t_i)}\right\} \qquad (9)$$

3.1.4 Automatic selection, confidence intervals and return period values

To find the best model, a selective search methodology named Stepwise is carried out; the Stepwise is in turn based on combining two approaches denoted “Forward Selection” and “Backward Elimination”. Any probabilistic model should ideally incorporate some measure of uncertainty to evaluate the randomness or error from the selected model; for the present study standard errors and confidence intervals are used to deal with the uncertainty. Finally, with regard to the values associated to a return period of interest, the following equations are adopted,

$$X_q(t,\theta) = X_q(\mu(t),\psi(t),\xi(t)) = \begin{cases} \mu(t) - \dfrac{\psi(t)}{\xi(t)}\left\{1-\left[-\log(1-q)\right]^{-\xi(t)}\right\} & \text{if} \quad \xi(t)\neq 0 \\ \mu(t) - \psi(t)\log\left[-\log(1-q)\right] & \text{if} \quad \xi(t)=0 \end{cases} \qquad (10)$$

where *q* is the exceedance probability defined from $G_t(x)=1-q$ and the estimated quantile, and $X_q(t,\theta)$ is the time-dependent value associated to the return period $R=1/q$.

A more detailed description can be found in the study by [25] and the references cited in that paper.

4. DISCUSSION

4.1 Stationary Model

For the stationary model the location, scale and shape parameters, which are invariant in time, are obtained. Table 1 lists the computed values of the distribution parameters, as well as the maximum recorded significant wave height, Hs_{max}, and the projected value for Hs associated to a return period of 30 years.

Table 1. Parameters for the stationary model, Hs_{max} and Hs and Tr=30 years

Hs_{max} (m)	**10.60**
Hs (m) for Tr= 30 yr	5.60
μ	360.34
ψ	58.59
ξ	$1\text{x}10^{-4}$

From the values reported in Table 1, it can be inferred that the stationary model is dominated by a Frechet type (heavy tail) distribution behavior. Note that in Table 1, Hs_{max} = 10.60 m is an atypical value recorded on 23 July, 1986 during hurricane Estelle (http://www.prh.noaa.gov/cphc/summaries/1986.php); it can be clearly observed in Fig. 5.

In Fig. 5 the instantaneous quantiles for a return period of 30 years for the location and scale parameters are shown, the depiction corresponds to the stationary GEV over the monthly extreme values distributed month to month along the year. In Fig. 5, dots indicate the monthly maximum Hs; the red line represents the time-dependent quantile associated to a 30-year return period; the black, green and yellow lines depict the location, scale and shape parameters, respectively.

In addition to the previous figure, QQ and probability Plots are shown in Fig. 6, where it can be observed that for buoy 51004 the probability paper implies an adequate fit for the data; nonetheless, the QQ plot underestimates the quantiles of the extreme values.

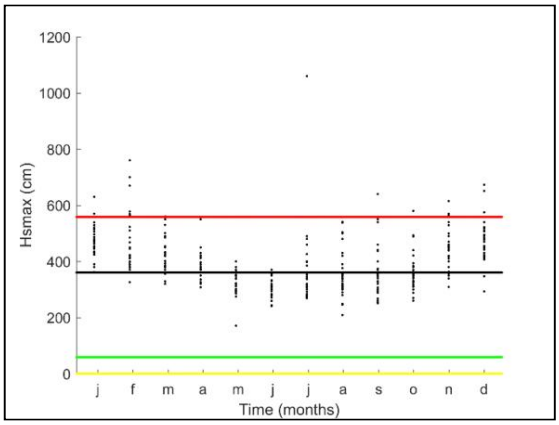

Fig. 5. Estimated quantile values for Tr=30 years, monthly maximums and location, scale and shape parameters

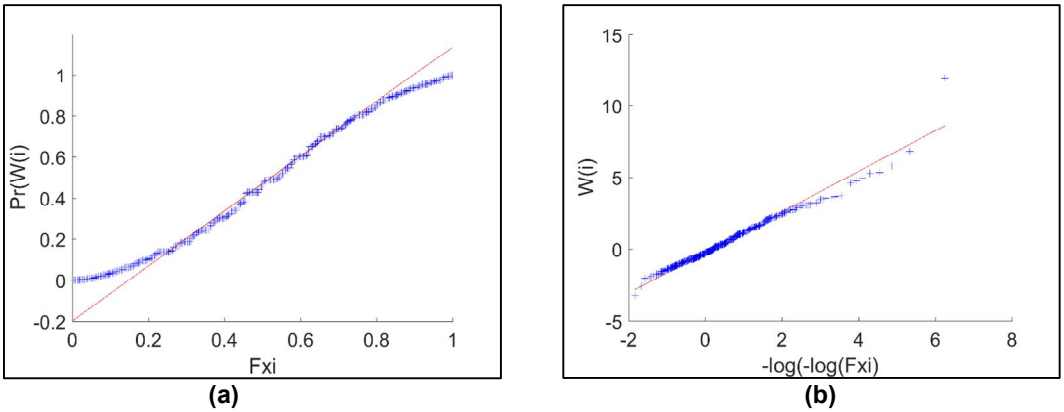

(a) **(b)**

Fig. 6. (a) Probability and (b) quantile plots for the stationary GEV model

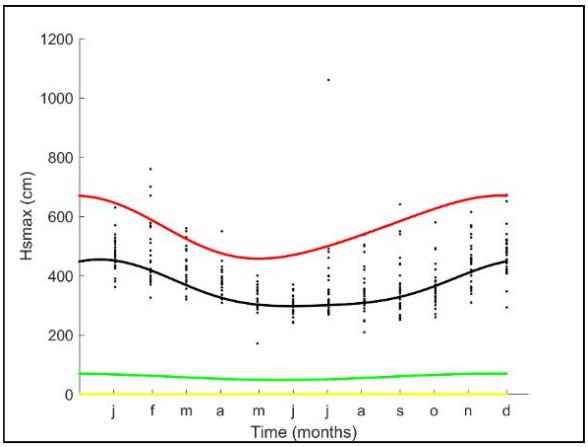

Fig. 7. Fitting for the monthly maximum for the non-stationary GEV model

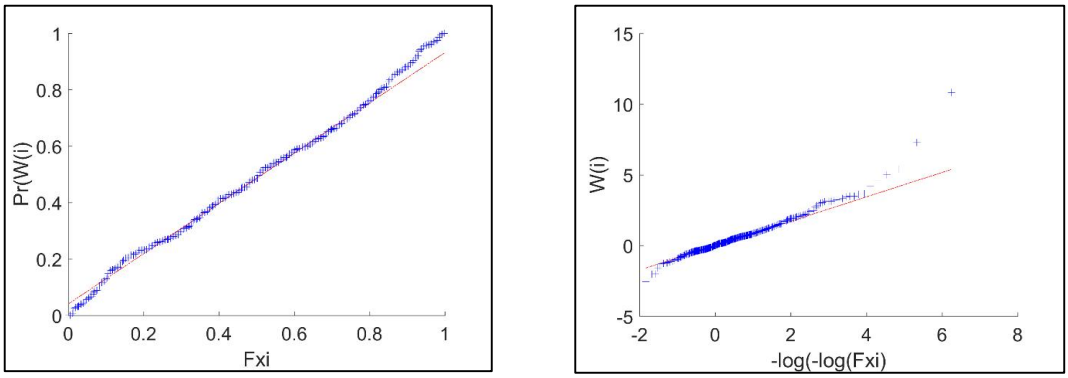

Fig. 8. Diagnostic plots (a and b) for the non-stationary GEV model

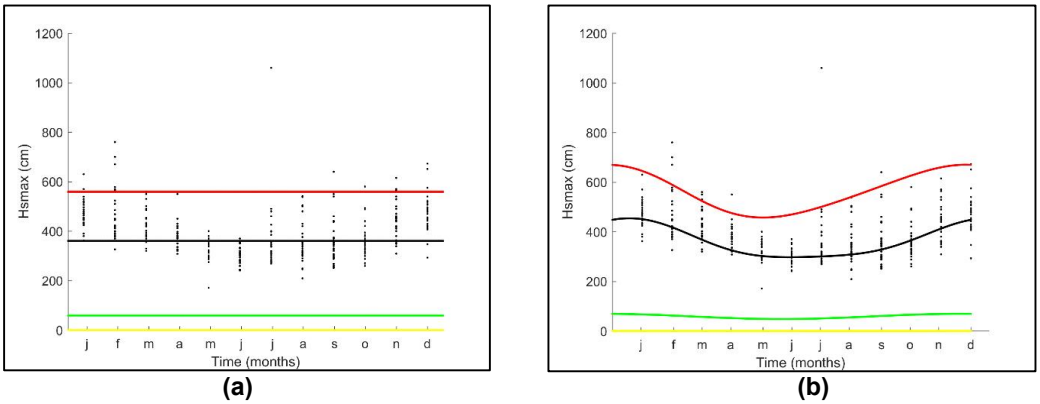

Fig. 9. Quantiles associated to 30-year return period for (a) the stationary and (b) non-stationary GEV models

4.2 Non Stationary Model

For the non-stationary model, it was found that values for the annual and semiannual cycles for the location and scale parameters are present, as well as the annual cycle for the shape parameter. The zero positive gamma value indicates that data exhibit a heavy-tailed Frechet type distribution, which is expected, if it is considered that the buoy maximum value is related to a hurricane activity, which is quite large as compared to the regular maximum recoded waves. Note that an emphasis on the tail behavior is useful for engineering purposes, and the use of the GEV model is preferred as an adequate and objective criterion for the extremes [30]. Using the computed numerical values in the non-stationary GEV distribution equations, the best fitted parameters for the distribution are obtained. In Fig. 7 the red line shows the time-dependent quantile associated to a 30-year return period; the black line depicts the location parameter, the green line corresponds to the scale parameter and the yellow line corresponds to the shape parameter. The monthly maxima for Hs are shown by the black dots. An adequate fit for the studied case can be observed in Fig. 7 Note that the maximum Hs associated to hurricane Estelle (mentioned previously), does not significantly deviate the trend of the values associated to a 30-year return period. Nevertheless, it may lead to a smoother curve as compared with the trend for buoys in the Gulf of Mexico [6], where two peaks associated to cold fronts are hurricanes are shown; Fig. 7 also seems to show that kind of behavior, if the black dots (monthly maxima) are observed for February and September, but those peaks may be somehow attenuated due to the atypical maximum Hs in July. Nevertheless, it is noteworthy that a seasonality effect does exists also in the Pacific Coast and, although the results in the present study are limited to one site only, it could be preliminarily concluded that seasonal trends are existent in both, the Gulf of Mexico and the Pacific Ocean. Consequently,

further studies to compare the trends for more buoys in the Pacific are strongly recommended.

To represent the adequacy of the fitting, the empirical probabilities obtained with the model and with the quantiles are shown in Fig. 8; the probability associated to the Gumbel distribution from the W(t) statistic is shown.

4.3 Comparison of Stationary Versus Non-stationary GEV Models

In this section a comparison of the two employed models for the extreme value analysis is carried out. The basic stationary GEV model and the non-stationary GEV model, which, unlike the former, captures seasonal variation for monthly maxima data series, are contrasted.

In Fig. 9 the most adequate fitting of the non-stationary GEV model to the data can be clearly observed, since the curve follows the seasonal trends; conversely, it can be seen that the stationary GEV model is unable to capture the seasonality of the significant wave heights. Fig. 10 shows also the best fitted results month-to-month, but for a 100-year return period. In Fig. 10 the depicted quantile for a 100-year return period shows that the non-stationary model includes the extreme values and represents more adequately the seasonality of the used data (red line), as compared to the stationary model (green line), except by the extreme value in July (see black dots for monthly Hs).

Fig. 11 shows 95% confidence intervals, where it can be observed that the bounds are more reduced for the non-stationary model and better correlated to the month-to month data.

Results in Figs. 10 and 11 show the advantage of using the non-stationary GEV model, since the computed seasonal trend tend to capture the maximum values and fits better the data series; the expected wave heights for T_R=100 years computed for the non-stationary case are larger than those computed with the stationary one for the winter season, and the opposite occurs for the summer season; this is important, since an impact in design, management, reliability related tasks and sustainability related issues is expected. The reason of the smaller values with the stationary GEV model for some months, is that it does not effectively account for scarce and extreme wave heights associated to hurricanes. In contrast, the non-stationary GEV model can capture these extreme values (also included in the integrated quantile) by means of the sinusoidal trend.

A final Figure in this study, Fig. 12, shows that the best behavior (in terms of representing the selected meteo-oceanographic variable) for the used empirical data is obtained with the non-stationary GEV distribution, at least for selected buoy, as observed by the goodness-of-fit for both models in Fig. 12 (left side column for the stationary model and right side column for the non-stationary model, respectively). It is pointed out once more, that this is due to the fact that the non-stationary model try to capture the majority of extreme values through a sinusoidal computing scheme; also, the existent extreme wave values caused by hurricanes, which significantly alter the seasonal periodic variation, are more adequately incorporated by the non-stationary GEV model in general terms; moreover, the uncertainty induced by hurricane activity, is compensated by the non-stationary GEV model for the monthly data series.

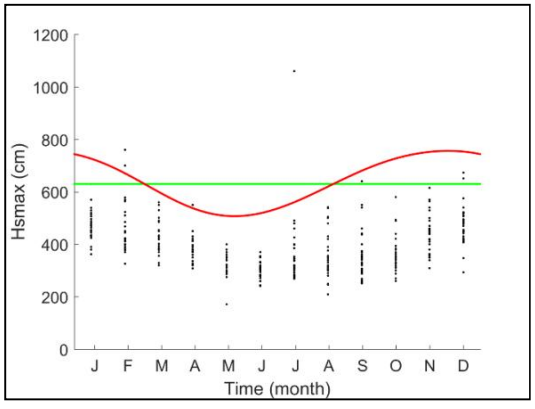

Fig. 10. Quantiles comparison for 100-year return period and measured Hs

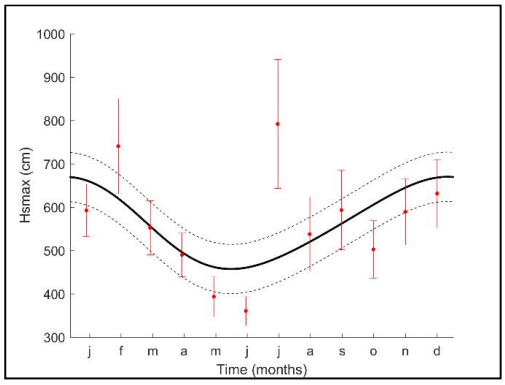

Fig. 11. 30-year return period quantile and 95% confidence interval for the non-stationary GEV model and the month-to-month stationary GEV

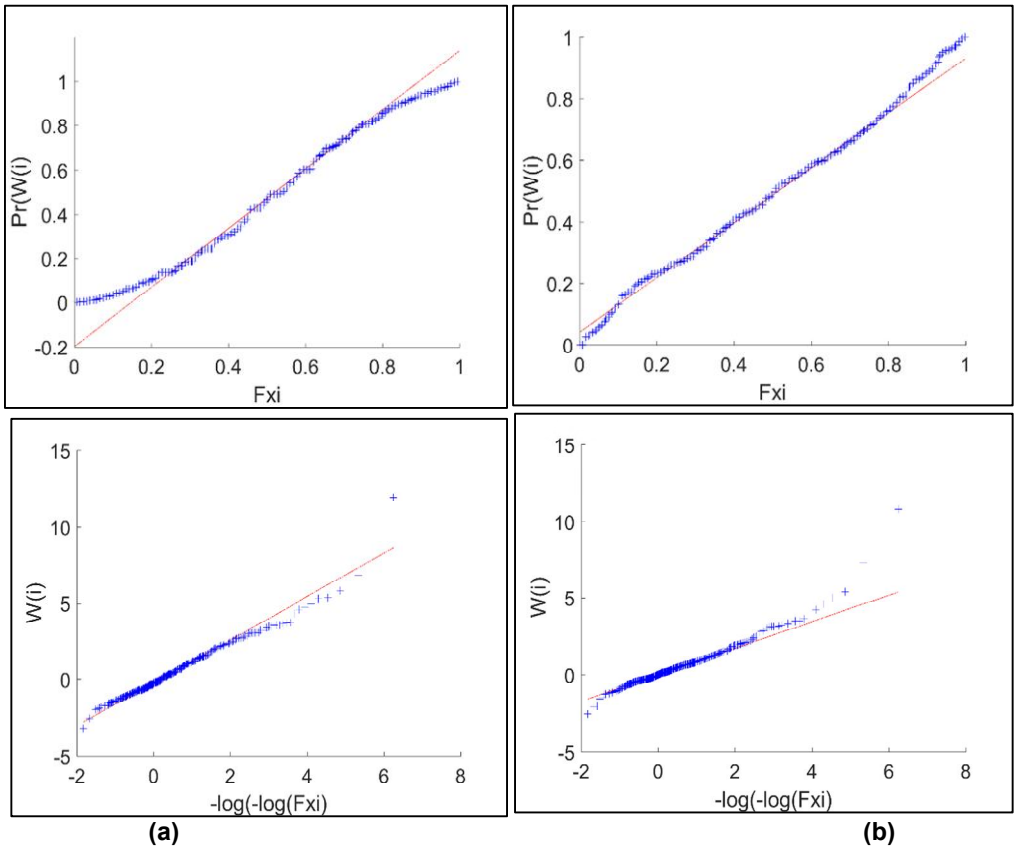

Fig. 12. Goodness-of-fit plots for stationary (a) and non-stationary (b) models

5. CONCLUSION

In this study a methodology for fitting empirical meteo-oceanographic data to extreme value models for projections purposes is presented. The selected meteo-oceanographic variable is significant wave height. The GEV model is used from two perspectives: Stationarity and non-stationarity. A comparison is carried out between the two approaches for a single site. For the non-stationary GEV model the seasonality is model by means of sinusoidal curves for a single buoy in the Pacific Ocean.

The non-stationary GEV model predicts adequately the monthly maximum significant

wave heights and reduce the uncertainty of the estimated quantiles; it also projects in a better way the wave heights associated to given return periods, since the methodology includes not only the point maxima, but also the peripheric values along the year. From the comparison of the stationary and non-stationary GEV models, it is concluded that the later leads to a better representation of the meteo-oceanographic variable, and also leads to larger projected return period values than the former for winter season. This is important, since implications in design of maritime structures, managements tasks, reliability and risk assessments, as well as sustainability related issues, are expected depending on the selected model.

It is also concluded that, at least for the selected buoy and its recorded data, a seasonality trend is found, as it was the case for the Gulf of Mexico [6], although some differences are found in the trends. Future studies for more buoys and wider regions are desirable, to characterized extreme wave activity, aimed at improving the design and management of coasts and ports by including seasonality. It is suggested to investigate the impact of selecting different models (i.e., stationary versus non-stationary models for extreme waves) in the sustainability of coasts and coast infrastructure. Further research for other meteo-oceanographic variables is also recommended.

ACKNOWLEDGMENTS

The financial support from the Erasmus Mundus Coastal and Marine Engineering and Management (CoMEM) programme and from Universidad de Guanajuato is gratefully acknowledged. We are thankful for the comments, suggestions and constructive criticism from two anonymous reviewers.

COMPETING INTERESTS

Authors have declared that no competing interests exist.

REFERENCES

1. Shao Z, Liang B, Li H, Lee D. Study of sampling methods for assessment of extreme significant wave heights in the South China Sea. Ocean Eng. 2018;168: 173-184.
DOI: 10.1016/j.oceaneng.2018.09.015
2. Vanem E. Non-stationary extreme value models to account for trends and shifts in the extreme wave climate due to climate change. Appl Ocean Res. 2015;52:201-211.
DOI: 10.1016/j.apor.2015.06.010
3. Feld G, Randell D, Wu Y, Ewans, K, Jonathan P. Estimation of storm peak and intrastorm directional-seasonal design conditions in the North Sea. Journal of Offshore Mechanics and Arctic Engineering. 2015;137(2):021102.
DOI: 10.1115/1.4029639
4. Shao Z, Liang B, Li H, Wu G, Wu Z. Blended wind fields for wave modeling of tropical cyclones in the South China Sea and East China Sea. Appl Ocean Res. 2018;71:20-33.
DOI: 10.1016/j.apor.2017.11.012
5. Kapelonis Zacharias G, Gavriliadis Panagiotis N, Athanassoulis Gerassimos A. Extreme value análisis of dynamical wave climate projections in the Mediterranean Sea. Procedia Computer Science. YSC 4Th International Young Scientists Conference on Computacional Science. 2015;66:210-219.
6. Chaplin RG. Abrasion resistant concrete floors. Advances in Concrete Slab Technology. Ed. Dhir RK, Munday JGL. 1980;164-72.
7. Chaplin RG. The influence of cement replacement materials. Fine Agregate and curing on the abrasion resistance of industrial concrete floor slabs. Cement and Concrete Association. Slough, UK. 1986; 32.
8. Bortkiewicz L, von Variationsbreite, mittlerer Fehler, Sitzungsber. Berli. Math. Ges. 1922;21:3-11.
9. Dodd EL. The greatest and the least variate under general laws of error. Tans.Amer. Math Soc. 1923;25:525-39.
10. Tippett LHC. On the extreme individuals and the range of samples taken from a normal population, Biometrika. 1925;17: 364-387
Available:https://doi.org/10.1093/biomet/17.3-4.364
11. Fréchet M. Sur la loi de probabilité de l'écart maximum, Ann. Soc. Polon. Math. Cracovie. 1957;6:93-116.
12. Fisher RA, Tippett LHC. Limiting forms of the frequency distribution of the largest or smallest members of a sample. Proceedings of the Cambridge Philosophical Society.1928;24:180-190.
13. De Finetti B, Obry S. L'optimum nella misura del riscatto, Atti del II Congresso

Nazionale di Scienza delle Assicurazioni. Bardi, Trieste, Rome. 1932;2:99–123.
14. Gumbel EJ. Statistical theory of extreme values and some practical applications. Applied Mathematics Series. 33 (1st ed.) U.S. Department of Commerce, National Bureau of Standards; 1954.
15. Gumbel EJ. Les valeurs extrêmes des distributions statistiques. Annales de l'Institut Henri Poincaré. 1935;5:115-158.
16. Mises R. von. La distribution de la plus grande de n valeurs. Amer. Math. Soc Reproduced in Selected Papers of Richard von Mises, II. 1954. 1936;271-294.
17. Rice J. Mathematical statistics and data analysis. 2nd ed. Duxbury; 1994.
18. Gnedenko B. Sur la distribution limite du terme maximum d'une série aléatoire. Springer-Verlag. 1943;195-225.
19. Gumbel EJ. Statistics of extremes. Columbia University Press; 1958.
20. Galambos J. The asymptotic theory of extreme order statistics, Robert E. Krieger. Malabar, Florida. 2nd ed; 1987.
21. Leadbetter MR, Lindgrem G, Rootzén H. Extremes and related properties of random sequences and series. Springer. Verlag, New York; 1983.
22. Coles SG. An introduction to statistical modelling of extreme values. 1st ed.; Springer-Verlag: London, UK. 2001;1-208.
23. Katz RW. Stochastic modeling of hurricane damage. J. of App. Meteor. 2002;41:754-762.
24. Johathan P, Ewans K. Statistical modelling of extreme ocean environments for marine design: A review. Ocean Eng. 2013;91-109.
DOI: 10.1016/j.oceaneng.2013.01.004
25. Calderón-Vega F, Vázquez-Hernández AO, García-Soto AD. Analysis of extreme waves with seasonal variation in the Gulf of Mexico using a time-dependent GEV model. Ocean Eng. 2013;73:68-82.
DOI: 10.1016/j.oceaneng. 2013.08.007
26. Sanchez-Arcilla A, Sierra JP, Gracia V, Garcia M, Jimenez JA, Mösso C, Valdemoro H. Coastal sustainability for uncertain futures: A Spanish Mediterranean case from the RISES-AM project. A: Intenational Association for Hydraulic Research Congress. E-proceedings of the 36th IAHR World Congres. L'Haia. 2015;1-8.
27. Sanchez-arcilla A, Sierra JP, Mösso C, Gracia V, Garcia M. Progress on climate change detection and projections over Spain since the findings of the IPCC AR5. International Symposium Climatees. 2015; 146.
28. Castillo E, Hadi AS, Balakrishnan N, Sarabia JM. Extreme value and related models with applications in engineering and science. Wiley-Interscience. New Jersey; 2005.
29. Menéndez M, Méndez FJ, Izaguirre C, Luceño A, Losada IJ. The influence of seasonality on estimating return values of significant wave height. Ocean Eng. 2009; 56:211-219.
DOI: 10.1016/j.coastaleng.2008.07.004
30. Panchang V, Kwon Jeong Ch, Demirbilek Z. Analyses of extreme wave heights in the Gulf of Mexico for offshore engineering applications. J Offshore Mech Arct. 2013; 135(3):1-15.

Peer-review history:
The peer review history for this paper can be accessed here:
http://www.sdiarticle3.com/review-history/47420

Paper D

Analysis of extreme waves with seasonal variation in the Gulf of Mexico using a time-dependent GEV model

F.Calderón-Vega, A.O.Vázquez-Hernández, A.D.García-Soto

Ocean Engineering. Ocean Engineering 73 (2013) 68–82

Ocean Engineering 73 (2013) 68–82

Contents lists available at ScienceDirect

Ocean Engineering

journal homepage: www.elsevier.com/locate/oceaneng

Analysis of extreme waves with seasonal variation in the gulf of Mexico using a time-dependent GEV model

F. Calderón-Vega [a], A.O. Vázquez-Hernández [b,*], A.D. García-Soto [c]

[a] Universidad de Cantabria, Avda. de los Castros s/n, 39005 Santander, Spain
[b] Instituto Mexicano del Petróleo, Deep Waters Explotation Department, Eje Central Lázaro Cárdenas Norte 152, Gustavo A. Madero, 07730 Mexico City, Mexico
[c] Department of Applied Mechanics, Institute of Engineering, National Autonomous University of Mexico, Mexico City, Mexico

ARTICLE INFO

Article history:
Received 24 November 2012
Accepted 24 August 2013

Keywords:
Extreme wave statistics
Extreme value distribution
Significant wave height
Seasonality
GEV distribution

ABSTRACT

This paper considers a time-dependent GEV model to assess the extreme value of significant wave. The model incorporates the monthly seasonality of maximum values in a block of time of recorded events. The extreme value distribution parameters are fitted considering the seasonal behavior of the significant wave height using harmonic functions representing annual and semiannual cycles. The model is applied to the records in 10 buoys in the Gulf of Mexico. The obtained results are compared with some of the available results in the literature.

1. Introduction

Correct characterization of the maritime climate is crucial for the design and operation of coastal and marine infrastructure. Seasonal variation of extreme values of waves influences the risk of flooding. It also affects the design, construction, installation and operation activities of structures such as breakwaters, ports, and oil rigs. Often the design and operation of the structures requires the estimation of the extreme wave height for specified return periods. The selection and assignment of an appropriate probability distribution based on available statistical data is of paramount importance for the estimation of the return period values of the wave height.

According to the asymptotic theory, the maximum values of random sequences could be adequately modeled by the generalized extreme value (GEV) distribution, which is a reformulation of the limiting distributions originally developed by Fisher and Tippet, and later systematized by Gumbel (Chakrabarti, 2001). It is important to note that, depending on the employed statistical method, the available records and the sample selection can significantly influence the assessment of the extreme values (Prpiĉ-Orsîc et al., 2007; Martucci et al., 2010).

Several statistical models have been proposed to adequately represent the ocean behavior considering site conditions (Isaacson and Mackenzie, 1981; Muir and ElShaarawi, 1986; Prevosto et al., 2000; Stansell, 2005; Tayfun and Fedele, 2007; Jensen et al., 2011; Mazas and Hamm, 2011; Muraleedharan et al., 2012; Solari and Losada, 2012; Soares and Carvalho, 2012). However, only a few studies have focused on the seasonal variation. For example, Mietus (1998) carried out an analysis of the seasonal variation on the surface level wind speed in the Baltic Sea. Jönsson et al. (2002) showed that there is a large seasonal variation in maximum monthly wave heights in the Baltic Sea. Méndez et al. (2008) presented a statistical model to characterize the long-term extreme value distribution of significant wave height, conditioned to the duration of the storm and accounting for seasonality; they basically used a time-dependent version of the peak over threshold (POT) approach to build a model that considers the annual and semiannual cycles parameterized in terms of harmonic functions. Mackay et al. (2010) showed that estimates of extreme wave conditions from stationary models have a lower bias and variance than those from discrete seasonal models. They also showed that the estimations from discrete seasonal models tend to be highly biased. Räämet and Soomere (2010) estimated the seasonal variation in wave climate in the Baltic Sea using a high-resolution version of a wave model.

There are some studies for extreme wave heights in the Gulf of Mexico; most of them do not consider the seasonal variation. Although Jonathan and Ewans (2011) modeled the seasonality of extreme waves in the Gulf of Mexico using a non-homogeneous

* Corresponding author. Tel.: +52 55 9175 8228; fax: +52 55 9175 8258.
E-mail addresses: ovazquez@imp.mx, ovazquezmx@yahoo.com (A.O. Vázquez-Hernández).

0029-8018/$ - see front matter © 2013 Elsevier Ltd. All rights reserved.
http://dx.doi.org/10.1016/j.oceaneng.2013.08.007

Poisson model, it was carried out only for two unspecified locations and considering only peak significant wave heights for storm events. They used information from GOMOS hindcast data (2005) instead of NOAA buoys. They employed the generalized Pareto distribution including shape and scale parameters only, and concluded that seasonal variation may be dependent on the location in the Gulf of Mexico. Therefore, it would be desirable to carry out a study considering the seasonal variations of extreme wave heights during the year at several sites in the Gulf of Mexico, and to incorporate the seasonal variability in the probabilistic model. This can be important for the design of maritime structures, coast management, and estimation of wave loading and reliability of offshore structures (e.g. Hong, 1994).

The main objective of this study is to characterize the seasonal behavior of extreme wave heights in the Gulf of Mexico. It uses the model presented by Méndez et al. (2008) but with additional terms that take into account the seasonality of the shape parameter of the GEV (i.e., time-dependent GEV model), through harmonic functions that represents the annual and semiannual cycles (e.g. Menéndez et al., 2009). The seasonality is the main covariate in this work, although it is acknowledged that other covariates such as the directionality (e.g. Jonathan and Ewans, 2007) could be important but are out of the scope of this study. The estimated extremes are compared with those presented by Panchang and Li (2006).

2. Extreme time-dependent GEV distribution

The GEV distribution for maximum values in a block of time is used for modeling the significant wave height (Leadbetter et al., 1983). The GEV distribution that in the extreme cases, becomes the well-known Gumbel, Weibull and Frechet distributions, can be expressed as (Coles, 2001)

$$G(x)=\exp\left\{-\left[1+\xi\left(\frac{x-\mu}{\psi}\right)\right]_+^{-1/\xi}\right\}\rightarrow\xi\neq 0$$
$$G(x)=\exp\left\{-\exp\left[-\left(\frac{x-\mu}{\psi}\right)\right]\right\}\rightarrow\xi=0 \quad (1)$$

The density function is defined by:

$$g(x)=\frac{1}{\psi}\left[1+\xi\left(\frac{x-\mu}{\psi}\right)\right]_+^{-(1+1/\xi)}\exp\left\{-\left[1+\xi\left(\frac{x-\mu}{\psi}\right)\right]_+^{(-1/\xi)}\right\}\rightarrow\xi\neq 0$$
$$g(x)=\frac{1}{\psi}\exp\left(-\frac{x-\mu}{\psi}\right)\exp\left\{-\exp\left[-\left(\frac{x-\mu}{\psi}\right)\right]\right\}\rightarrow\xi=0 \quad (2)$$

where $[a]_+$ implies max $(a, 0)$, $-\infty<\mu<\infty$ is the location parameter, $\psi>0$ is the scale parameter and ξ is the shape parameter, which defines the type of distribution; $\xi\neq 0$, corresponds to two distribution families: Fréchet for $\xi>0$ and Weibull $\xi<0$; when $\xi\rightarrow 0$ the GEV tends to the Gumbel distribution.

The behavior of Weibull, Frechet and Gumbel distributions in the tail of the distribution function differs. The tails are bounded, heavy and light, for the Weibull, Frechet and Gumbel distributions, respectively. In the Gumbel distribution the tail decays exponentially, whereas in the Fréchet distribution the tail decays as a function of a power. Only one of the three extreme value distributions is often selected for practical applications.

In this study, a time-dependent GEV distribution model, which takes into account the seasonality using independent monthly maximum values, x_i, observed at times t_i, is employed. The consideration of independent monthly maximum series is adequate because: first, the seasonality for quasi-homogeneous time distributed data could be modeled (Mendez et al., 2007), and second, because the monthly maxima provides additional information about the upper tail of the distribution (Katz et al., 2002). The model is applied to the records of wave heights from several buoys located in the Gulf of Mexico and described in Table 1.

Table 1
Information of the buoys used in the study.

Station (Buoy)	Recorded years	No. of recorded years	No. of monthly maximum values	Maximum recorded SWH (m)	Distance to shore (Km)	Water depth (m)
42,001	1975–2011	36	393	11.2	334	3246
42,002	1973–2011	33	391	9.7	346	3566
42,003	1976–2011	35	374	11.04	307	3233
42,007	1981–2009	29	183	9.09	35	14
42,019	1990–2011	22	228	6.30	92	82
42,020	1990–2011	22	233	8.20	68	88
42,035	1993–2011	19	223	6.03	25	16
42,036	1994–2011	18	194	8.60	127	54
42,039	1995–2011	17	143	12.05	114	307
42,040	1995–2011	17	142	16.91	79	274

The lack of data in the series must be taken into account to apply the model, because this affects the stability of the parameter estimation for the extreme value distribution. Since there are seasons without recorded data in the series, a minimum number of data points per unit time (or a time interval in which the maximum value is extracted) is considered. For this, the criterion proposed in Mendez et al. (2007) is adopted. This criterion states that the record for a month is rejected if up to 40% of data of the month is missing.

2.1. Regression model

The seasonal variation in this study is defined as the cyclical changes within one year. Authors such as Morton et al. (1997), and Carter and Challenor (1981), modeled the intra-annual variability by analyzing the seasonal behavior of extreme wave heights using extreme value distribution. Räämet and Soomere (2010) developed a model that adequately reproduced the seasonal patterns of wave intensity and the probability distribution functions for different wave heights. Normally, the seasonal variation is linked to established weather patterns, so it is usually recurrent over the years and has a sinusoidal behavior. The seasonal variability for geophysic variables is manifested in different ways. However, a predominant factor is presented in all cases: the annual cycle, generally defined by the winter–summer variability. In Fig. 1, this cycle is observed in the monthly maxima wave heights for the shown buoys in the Gulf of Mexico. It is also observed that the annual cycle clearly defines the variable behavior along the time. The semiannual cycle is not only referred to the winter–summer variability, but also to a systematic climate pattern during the year, such as the hurricanes.

After observing the boxplots in Fig. 1, it is considered that the seasonal variability can be modeled as a superposition of sinusoidal waves by using harmonic functions and include them in the model. To justify the inclusion of the seasonality in the model, the one-year variability of the location, scale and shape parameters of the fitted time-independent GEV for every month has been analyzed.

The time dependency is introduced in the model parameters in the GEV model by employing harmonic functions defined by

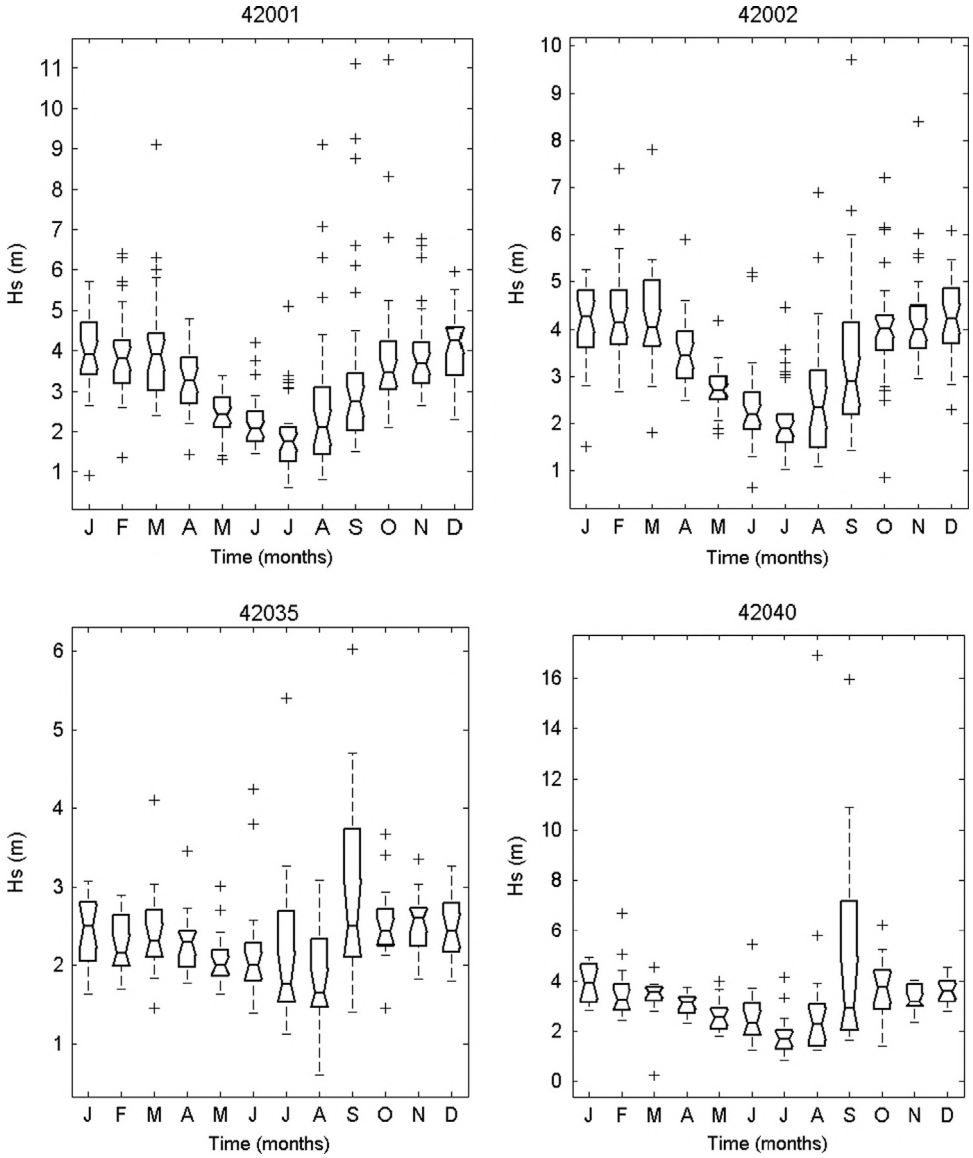

Fig. 1. Boxplots for monthly maxima significant wave height in 42,001, 42,002, 42,035, and 42,040 buoys. Trapezoidal boxes have lines at the lower, median and upper quartile values. The whiskers extend to the 1.5 interquartile range, and crosses show unusual values.

(Méndez et al., 2008; Menéndez et al., 2007; Menéndez et al., 2009),

$$\theta = \begin{cases} \mu(t) = \beta_0 + \beta_1 \cos(2\pi t) + \beta_2 \sin(2\pi t) + \beta_3 \cos(4\pi t) + \beta_4 \sin(4\pi t) \\ \psi(t) = \alpha_0 + \alpha_1 \cos(2\pi t) + \alpha_2 \sin(2\pi t) + \alpha_3 \cos(4\pi t) + \alpha_4 \sin(4\pi t) \\ \xi(t) = \gamma_0 + \gamma_1 \cos(2\pi t) + \gamma_2 \sin(2\pi t) + \gamma_3 \cos(4\pi t) + \gamma_4 \sin(4\pi t) \end{cases} \tag{3}$$

where $\psi(t>0)$. θ includes the three parameters: location, scale and shape ($\mu(t)$, $\psi(t)$ and $\xi(t)$), respectively. To simplify the notation, in the following it is considered that θ represents the vector of all the model parameters involved in Eq. (3) that are to be estimated, $\theta = (\beta_0, \beta_1, \beta_2, \beta_3, \beta_4, \alpha_0, \alpha_1, \alpha_2, \alpha_3, \alpha_4, \gamma_0, \gamma_1, \gamma_2, \gamma_3, \gamma_4)$. Note that β_0, α_0 and γ_0 represent the mean of ($\mu(t)$, $\psi(t)$ and $\xi(t)$); β_i, α_i and γ_i (for $i=1,2$) are the amplitudes of the harmonics; β_i, α_i and γ_i (for $i=3,4$) are the amplitudes of the subharmonics, and t is given in years.

2.2. Fitting to the data

Different procedures to estimate the model regression coefficients, or to estimate the probability distribution parameters are available. In this study the maximum likelihood method has been employed for the analysis. In general, this technique results in adequate fitting, and in less biased and more efficient estimators, especially for long return periods and for small data samples (Lettenmaier and Burges, 1982). The maximum likelihood method consists in estimating the point parameter estimators of a likelihood function so that the likelihood of observing the samples $\{x_1,\ldots x_n\}$ is maximum. More specifically, the likelihood function can be expressed as (Benjamin and Cornell, 1970)

$$L(\theta; x_1, x_2, \ldots, x_n) = f(x_1, \ldots x_n; \theta) = \prod_{i=1}^{n} f(x_i; \theta) \tag{4}$$

where $L(\theta; x_1, x_2, \ldots, x_n)$ is the likelihood function and $f(x_1, \ldots x_n; \theta)$ represents the joint probability density function conditioned on the model parameters θ. The last equality holds if the sample is independent and identically distributed with density function $f(x; \theta)$. To simplify the computing, Eq. (4) can be re-written as,

$$l(\theta; x_1, x_2, \ldots, x_n) = \sum_{i=1}^{n} \log\left[f(x_1, \ldots x_n; \theta)\right] \tag{5}$$

where the log-likelihood function $l(\theta; x_1, x_2, \ldots, x_n) \equiv \log L(\theta; x_1, x_2, \ldots, x_n)$.

The maximum likelihood estimators, $\hat{\theta}$, that maximizes $l(\hat{\theta}; x_1, x_2, ..., x_n)$ is obtained by solving

$$\sum_{i=1}^{n} \frac{\partial}{\partial \theta_j} \log\ [f(x_1, ...x_n; \theta)] = 0 \text{ for } j = 1, ..., p \tag{6}$$

where p denotes the total number of parameters to be estimated.

For the GEV model shown in Eq. (2), the log-likelihood function is

$$l(\theta|t_i, x_i) = -\sum_{i=1}^{n} \left\{ \log\ \psi(t_i) + (1+1/\xi(t_i)) \log\ \left[1+\xi(t_i)\left(\frac{x_i-\mu(t_i)}{\psi(t_i)}\right)\right]_+ + \left[1+\xi(t_i)\left(\frac{x_i-\mu(t_i)}{\psi(t_i)}\right)\right]_+^{(-1/\xi(t_i))} \right\} \tag{7}$$

where $x_1,...,x_n$ are defined as the n observations of maxima for a block of time. The obtained distribution parameters $\hat{\mu}$, $\hat{\psi}$and $\hat{\xi}$, for the considered wave height data are shown in Fig. 2.

It can be observed from the figure that the location parameter presents minimum values in summer and maximum values in winter. This means that higher wave heights occur in November, December, January and February. The scale parameter shows a harmonic behavior in all buoys, which generally has a lower value in summer. The shape parameter is also seasonally modulated; when it is not zero and adopts positive or negative values, it indicates that the sample behaves as a Frechet or Weibull distribution, respectively.

2.3. Uncertainty

An estimate of the uncertainty associated with the point estimate of the distribution model parameters are given below. This estimation is carried out using Hessian matrix of $-l(x;\theta)$ evaluated at $\hat{\theta}$, known as information matrix, I_0,

$$I_0 = \begin{bmatrix} -\frac{\partial^2 l(\hat{\theta})}{\partial \theta_1{}^2} & \cdots & \cdots & -\frac{\partial^2 l(\hat{\theta})}{\partial \theta_1 \partial \theta_p} \\ \vdots & \ddots & -\frac{\partial^2 l(\hat{\theta})}{\partial \theta_i \partial \theta_j} & \vdots \\ \vdots & -\frac{\partial^2 l(\hat{\theta})}{\partial \theta_j \partial \theta_i} & \ddots & \vdots \\ -\frac{\partial^2 l(\hat{\theta})}{\partial \theta_p \partial \theta_1} & \cdots & \cdots & -\frac{\partial^2 l(\hat{\theta})}{\partial \theta_p{}^2} \end{bmatrix} = \tag{8}$$

where p is the number of estimated parameters defining the distribution function. The I_0 matrix is asymptotically equivalent to the Fisher information matrix (the same matrix but with the real parameter values instead of the point estimators), showing that the $\hat{\theta}$ distribution is normal. The I_0 matrix represents the surface curvature of the approximated log-likelihood function, and the square roots of the diagonal elements of its inverse, $J = I_0^{-1}$, represents the standard deviations of $\hat{\theta}_1 ..., \hat{\theta}_p$, which will be denoted as (Coles, 2001),

$$se(\theta_i) = \sqrt{J_{i,j}} \tag{9}$$

From the normality property of the maximum likelihood estimators, the confidence interval at level $(1-\alpha)$ for each estimator is

$$ci(\theta_i) = \theta_i \pm z_{\alpha/2} se(\theta_i) \tag{10}$$

where $z_{\alpha/2}$ is the quantil $(1-\alpha/2)$ of the standard normal distribution function (1.96 for a confidence level of 0.05). Although Bootstrap approaches have been employed by some authors to quantify uncertainties (e.g. Chavez-Demoulin and Davison, 2005), we rather prefer to quantify them by using the above described theory (Coles, 2001).

2.4. Model selection

Once the parametric equations defining the different processes are determined, the next step is to find an optimal model representing the non-stationary behavior of the studied extreme values. To achieve this, the parsimony principle must be satisfied. This means that the simplest possible model which results in a good fitting is pursued, and that a set covering all possible parametric combinations must be found. However, this search implies the fitting of many candidate models.

In this study the largest parameterization with two sinusoidal harmonics is considered. There are a wide variety of models to choose with several degrees of freedom. Following the genetic algorithms nomenclature (Goldberg, 1989), a binary codification to represent the model, according to the involved factors, is adopted. Every model is coded with a binary chromosome $c=[g_1g_2 g_3g_4g_5g_6g_7]$ where g_i are the binary genes representing the given factors. Each gene, g_i, has two possible values: $g_i=1$ when the ith factor is turned on, and $g_i=0$ when it is turned off (Menéndez et al., 2009). The gene $g_1(\beta_1, \beta_2)$ represents the annual cycle for the location parameter; $g_2(\beta_3, \beta_4)$ represents the semiannual cycle for the location parameter; $g_3(\alpha_1, \alpha_2)$represents the annual cycle for the scale parameter; $g_4(\alpha_3, \alpha_4)$ represents the semiannual cycle for the scale parameter; g_5 is a gene representing a constant shape parameter ($\gamma_0 \neq 0$); $g_6(\gamma_1, \gamma_2)$ represents the annual cycle for the shape parameter; and $g_7(\gamma_3, \gamma_4)$ represents the semiannual cycle for the shape parameter. To find the best model a search selective methodology denominated as Stepwise, a mixed of the Forward Selection and Backward Elimination, is carried out. In this methodology, every time that a gene is activated in the Forward Selection, the Backward Elimination is employed to check if the gene must be eliminated. This procedure allows the elimination of an initially considered factor, which later on is not considered representative of the data variation. For more detailed information on the binary codification and the search selective methodology, the reader is referred to Menéndez et al. (2009).

To select the preferred model the Akaike Information Criterion (AIC) (Akaike, 1973) given below is adopted,

$$\text{AIC}_i = -2l(\hat{\theta}^i|t_i, x_j) + 2p_i \tag{11}$$

where p_i is the number of parameters and $l(\hat{\theta}^i|t_i, x_j)$is the maximum of the log-likelihood resulting from the model i for the sample $\{t_i, x_j\}$; this equation holds for a particular model i with a binary chromosome c^i and a corresponding vector parameter θ^i (Menéndez et al., 2009). Note that the criterion that considers the number of free parameters and the maximum likelihood dictate that the model with the lowest AIC is the preferred.

2.5. Model verification

To prove that the adopted model adequately represents the analyzed extreme events, verification is carried out by establishing diagnostic techniques. In this study the diagnostic is focused on descriptive methods based on quantil–quantil plots (QQ) and the probability plots. If a non-stationary behavior occurs, the lack of homogeneity in the hypothetically considered distributions for each observation, leads to modifications before the QQ and probability plots are employed. These modifications are based on a standardization of the data, aimed to simplify their diagnostic behavior. The standardization varies depending on the parametric equation describing the distribution function for each model of extremes.

A very convenient standardization for the extreme events, considering that there is special interest in the distribution tail, consists in transforming the statistical model distribution into a

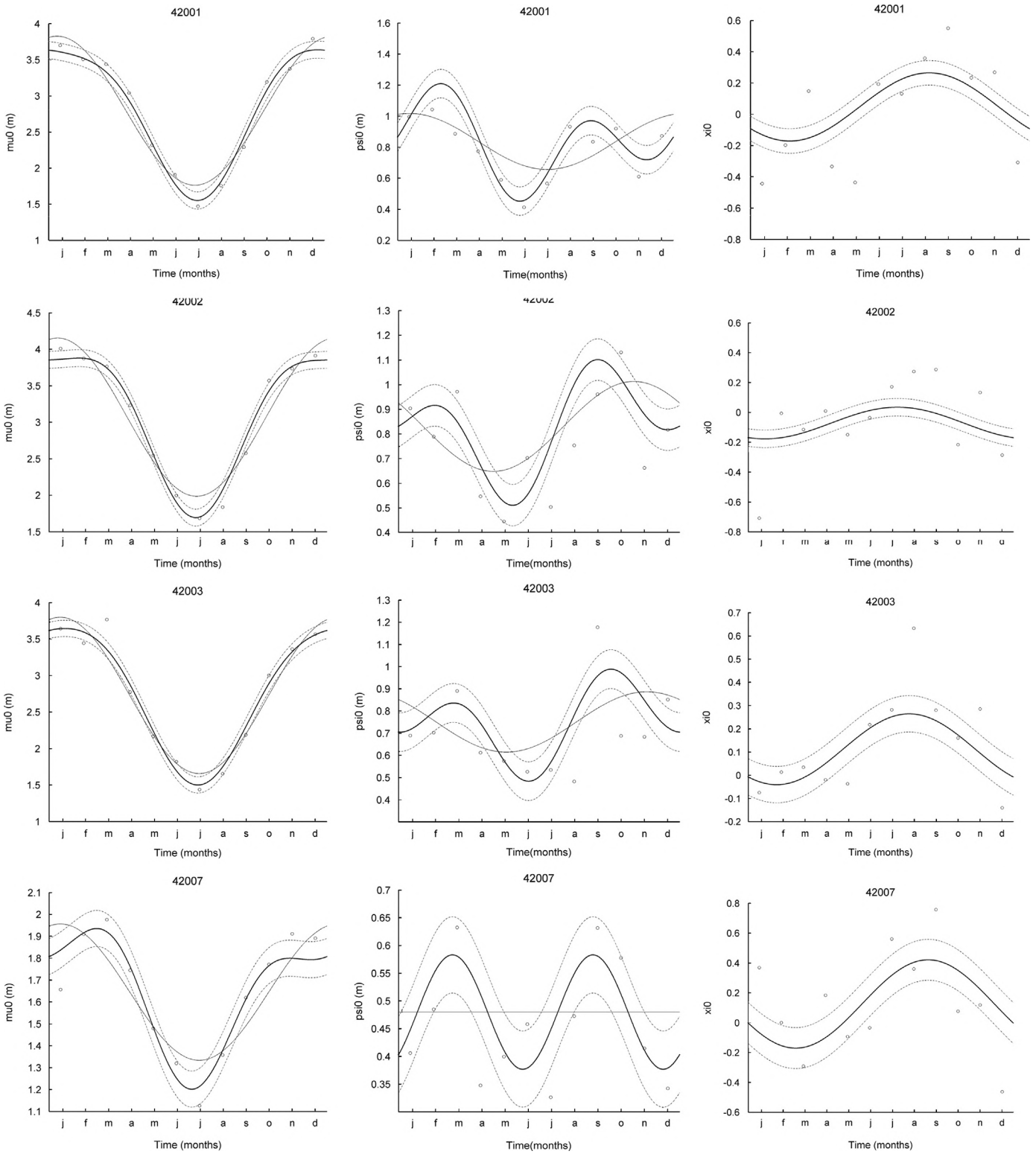

Fig. 2. Values of the estimators for the GEV distribution parameters for each month and the resulting functions from the regression fitting with one (gray line) and two (solid line) harmonics. 95% confidence bands (dashed lines) are shown only for two harmonics.

Gumbel distribution. This allows representing a linearized process, so that it is easier to qualitatively describe how good the fitting is. The resulting statistics from this change of variable is denoted as W corresponding to the following equation:

$$W(t)=\frac{1}{\hat{\xi}(t)}\log\left[1+\hat{\xi}(t)\left(\frac{x-\hat{\mu}(t)}{\hat{\psi}(t)}\right)\right] \tag{12}$$

where each of the maximum n observations $\{x_1,\ldots,x_n\}$ are denoted in a block time and occur at the times $\{t_1,\ldots,t_n\}$.

If the studied variable is adequately modeled, the resulting statistics represent a random standardize Gumbel variable. The representation of the $W(t)$ statistics as a function of time, allows to asses the stationarity in the variable behavior. The probability associated to the Gumbel distribution based on

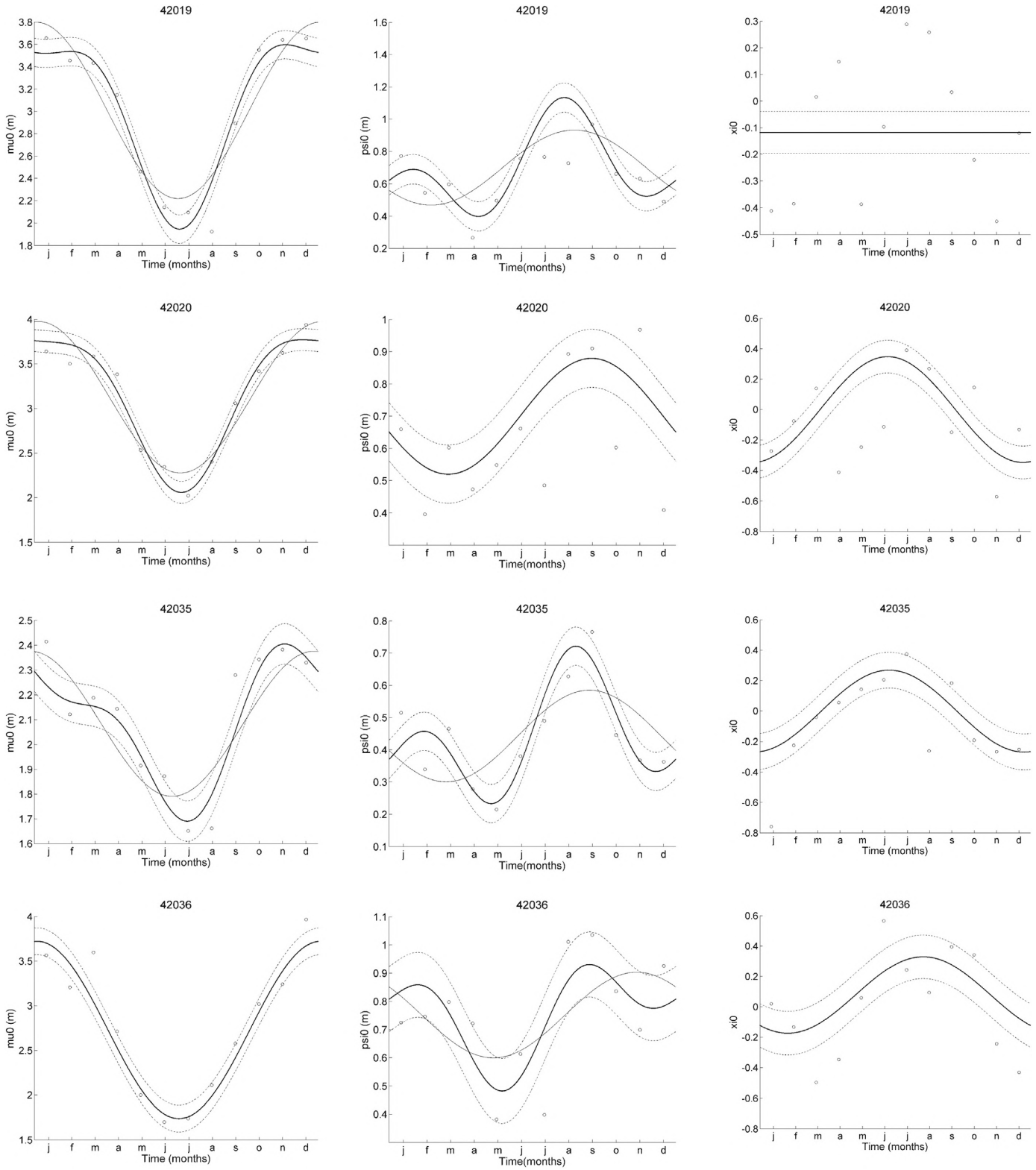

Fig. 2. (*continued*)

the $W(t)$ statistic is obtained with the equation

$$\Pr\{W \le x\} = \exp(-e^{-x}) \tag{13}$$

In the probability plots, the probability values associated to the extreme values samples, $\{\tilde{F}(x_{(i)})\}$, and the estimated probabilities by using the statistic $W(\mathrm{t})$, are compared.

The QQ plots are obtained by sorting the sample values and plotting them; the quantiles obtained with the supposed theoretical distribution of the model of extremes are also plotted. With the considered scaling, the resulting model quantiles will be $W_{(i)}=W(x_{(i)}, t_{(i)})$, while the corresponding logarithmic transformation must be applied to the direct sample values, in order to scale

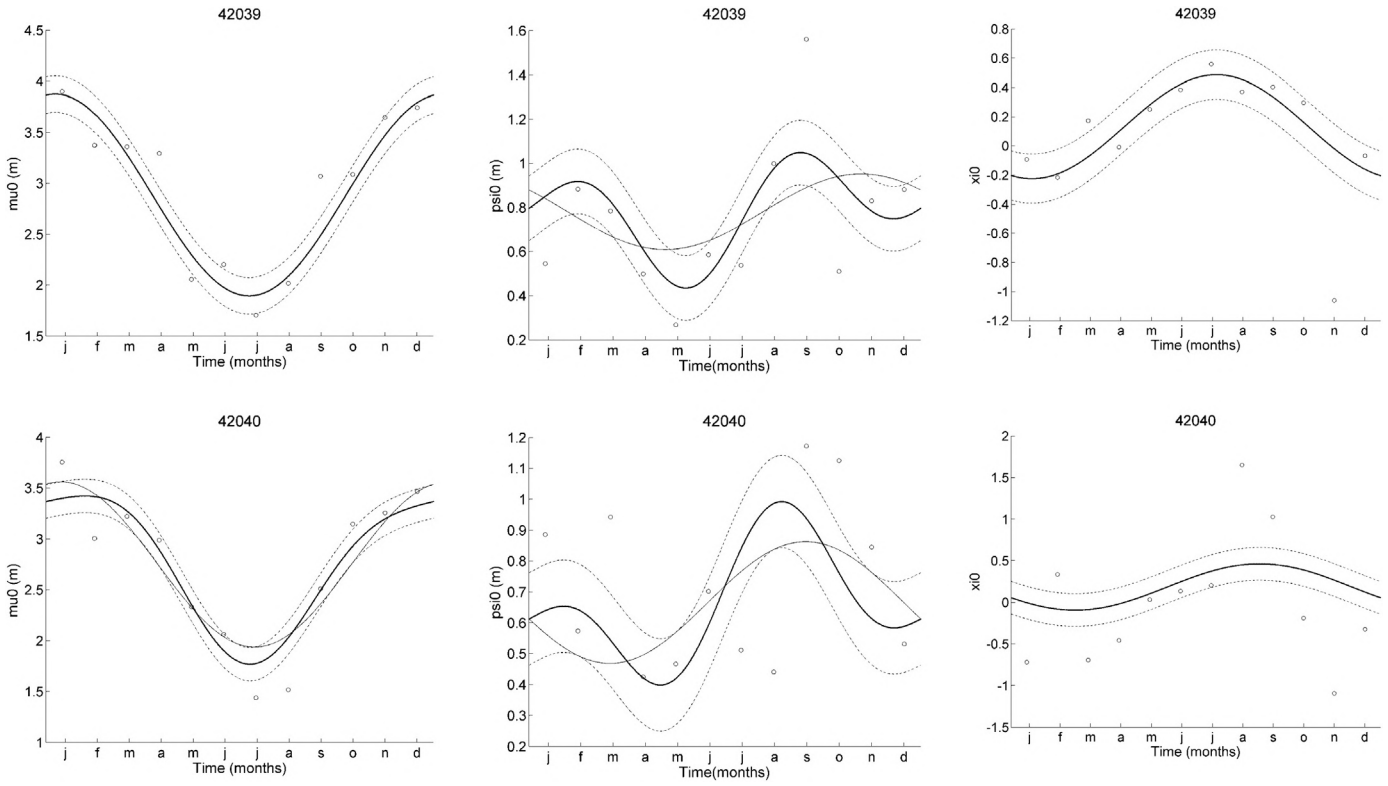

Fig. 2. (*continued*)

them to Gumbel by using the following equation:

$$\{-\log(-\log(\tilde{F}(x_{(i)}))), W_{(i)}\} \tag{14}$$

2.6. Values associated to quantiles

The values associated with given return periods are deduced from the x variable equation in the time-dependent GEV distribution function, $G_t(x)$, resulting in (Menéndez et al., 2009)

$$X_q(t,\theta) = X_q(\mu(t),\psi(t),\xi(t)) = \begin{cases} \mu(t)-\frac{\psi(t)}{\xi(t)}\left\{1-[-\log(1-q)]^{-\xi(t)}\right\} & \text{if} \quad \xi(t)\neq 0 \\ \mu(t)-\psi(t)\log\,[-\log(1-q)] & \text{if} \quad \xi(t)=0 \end{cases} \tag{15}$$

where q is the exceedance probability defined from $G_t(x)=1-q$, and the estimated quantil $X_q(t,\theta)$, is the time dependent variable value associated to the return period $R=1/q$.

3. Analysis of extreme waves in the Gulf of Mexico

In this section, recorded data at 10 locations detailed in Table 1 and shown in Fig. 3 are employed. The significant wave height (SWH) data obtained from the NOAA (National Oceanic and Atmospheric Administration) buoys operated by the National Data Buoy Center (NDBC, www.ndbc.noaa.gov) are analyzed. SWH is computed as the mean of the highest third of wave height during the sampling period for a given time.

Considering the existent records for each buoy, it is possible to carry out the models fitting by obtaining the chromosomes representing the annual and semiannual cycle values for the location parameters, the annual and semiannual cycle for the scale parameter, the constant value γ_0 (defining the distribution type: GEV or Gumbel), and the annual cycle for the shape parameter. The estimated mean values, and the amplitudes of the harmonics and subharmonics of the parameters obtained with the Stepwise method for each buoy are summarized in Table 2. The estimated standard errors associated with each parameter are also shown in Table 2.

It can be observed from the table that, for buoys 42,001, 42,003 and 42,040 the location and scale parameters show annual and semiannual cycles, while the shape parameter shows an annual cycle; the positive γ_0 value indicates that for these buoys the Frechet distribution was the more adequate.

Note that significant wave heights for 42,003, 42,007, 42,039 and 42,040 buoys were registered in the wake of Hurricane Ivan on September 2004. The values of waves caused by hurricanes could affect the type of distribution obtained with the time-dependent GEV model. For the mentioned buoys the distribution type is Frechet.

The negative γ_0 value for buoys 42,002 and 42,019 in Table 2 indicates that the data is better characterized by Weibull ditributions. These buoys also show annual and semiannual cycles for the location and scale parameters; and an annual cycle in the shape parameter is observed only for buoy 42,002.

Annual cycles for the location, scale and shape parameters, and semiannual cycles for the scale parameter can be observed for buoys 42,036 and 42,039 (defined by Frechet distributions) in Table 2. On the other hand, annual and semiannual cycles for the location parameter, a semiannual cycle for the scale parameter and an annual cycle for the shape parameter can be observed for 42,007 buoy. Finally, γ_0 equal to zero, implying Gumbel distributions, is observed for 42,020 and 42,035 buoys.

For the recorded wave heights at almost all the buoys there are annual and semiannual cycles for the location parameter; this suggests two seasons of extreme events during the year.

Considering the values obtained with the time-dependent GEV distribution equations, the parameters which best fit the distribution model were determined and illustrated in Fig. 4. The bold line represents the 30-year return period value (i.e., $(1-1/30)$-quantile),

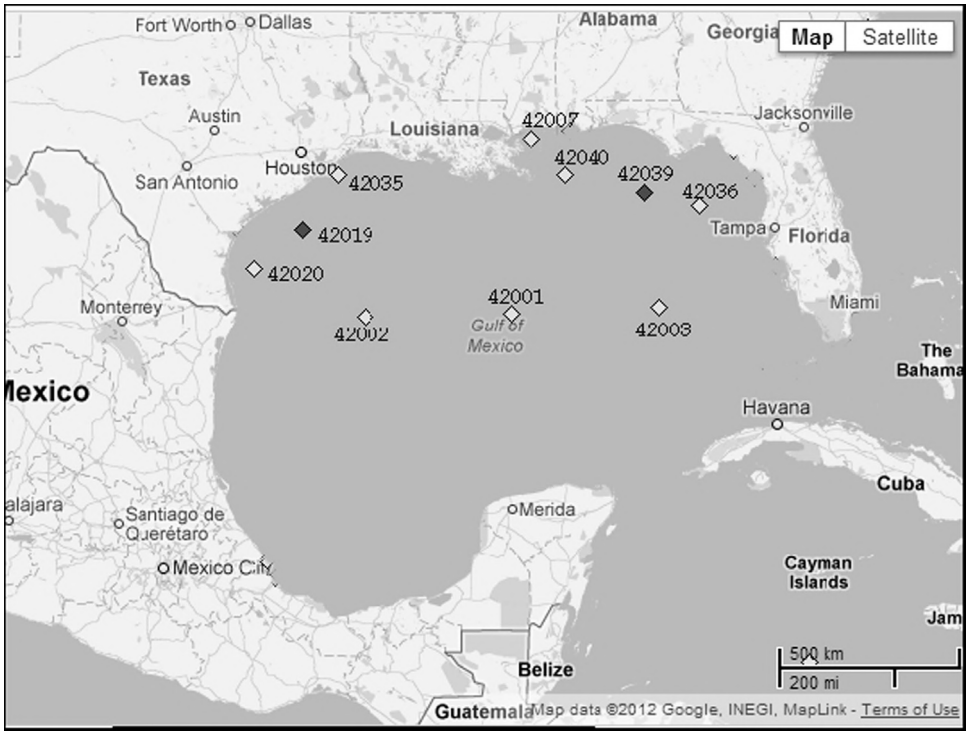

Fig. 3. NOAA Buoys considered in the analysis.

Table 2
Numerical values of the maximum likelihood estimates for the location, scale and shape parameters (with standard errors in brakets); final chromosome, maximum of the log-likelihood function (l) number of involved parameters (p) and Akaike Information Criterion statistic (AIC) for the studied buoys.

Buoy Number		42,001	42,002	42,003	42,007	42,019	42,020	42,035	42,036	42,039	42,040
Cycle	Chromosome	[1,1,1,1,1,1,0]	[1,1,1,1,1,1,0]	[1,1,1,1,1,1,0]	[1,1,0,1,1,1,0]	[1,1,1,1,1,0,0]	[1,1,1,0,0,1,0]	[1,1,1,1,0,1,0]	[1,0,1,1,1,1,0]	[1,0,1,1,1,1,0]	[1,1,1,1,1,1,0]
	β_0	2.795	3.070	2.728	1.645	3.009	3.125	2.083	2.730	2.884	2.749
		(4.84)	(4.62)	(4.40)	(3.51)	(5.37)	(4.88)	(3.26)	(6.03)	(7.19)	(6.76)
Annual	β_1	1.012	1.062	1.036	0.301	0.789	0.844	0.291	0.990	0.979	0.788
		(6.00)	(6.02)	(5.64)	(3.93)	(7.02)	(6.96)	(4.45)	(8.11)	(9.57)	(8.99)
	β_2	0.196	0.210	0.268	0.078	0.033	0.077	−0.026	0.058	0.0149	0.192
		(7.03)	(6.85)	(6.66)	(4.69)	(6.52)	(7.03)	(4.73)	(8.93)	(10.77)	(9.41)
Semi annual	β_3	−0.173	−0.278	−0.147	−0.138	−0.269	−0.210	−0.080	–	–	−0.171
		(5.91)	(6.00)	(5.80)	(4.36)	(6.72)	(6.55)	(4.19)			(8.09)
	β_4	−0.127	−0.094	−0.054	0.002	−0.053	−0.060	−0.096	–	–	−0.026
		(6.30)	(6.04)	(5.90)	(4.55)	(6.62)	(5.93)	(4.16)			(8.63)
	α_0	0.837	0.830	0.751	0.480	0.701	0.699	0.442	0.751	0.780	0.665
		(3.55)	(3.19)	(3.31)	(2.87)	(3.94)	(3.66)	(2.45)	(4.72)	(6.00)	(5.90)
Annual	α_1	0.174	0.095	0.100	–	−0.140	−0.048	−0.044	0.099	0.099	−0.052
		(4.16)	(4.26)	(4.16)		(5.01)	(4.95)	(3.12)	(6.16)	(7.67)	(8.14)
	α_2	0.047	−0.155	−0.099	–	−0.184	−0.173	−0.134	−0.114	−0.139	−0.189
		(5.64)	(4.95)	(5.22)		(4.67)	(5.20)	(3.38)	(6.84)	(8.74)	(8.50)
Semi annual	α_3	−0.145	−0.093	−0.146	−0.076	0.061	–	−0.027	−0.042	−0.083	−0.001
		(4.99)	(4.04)	(4.41)	(3.65)	(4.58)		(3.08)	(5.78)	(8.45)	(7.72)
	α_4	0.195	0.128	0.037	0.068	0.200	–	0.141	0.113	0.166	0.149
		(5.09)	(5.05)	(5.19)	(4.01)	(5.06)		(3.14)	(5.90)	(6.56)	(7.90)
	γ_0	0.047	−0.071	0.11	0.12	−0.12	0.00	0.00	0.08	0.13	0.18
		(0.03)	(0.02)	(0.03)	(0.06)	(0.04)			(0.05)	(0.07)	(0.07)
Annual	γ_1	−0.13	−0.097	−0.11	−0.12	–	–0.34	−0.26	−0.20	−0.33	−0.13
		(0.05)	(0.04)	(0.05)	(0.08)		(0.06)	(0.07)	(0.07)	(0.09)	(0.12)
	γ_2	−0.16	−0.041	−0.09	−0.26	–	0.06	0.03	−0.15	−0.12	−0.24
		(0.04)	(0.03)	(0.04)	(0,08)		(0.05)	(0.05)	(0.10)	(0.10)	(0.12)
Semi annual	γ_3	–	–	–	–	–	–	–	–	–	–
	γ_4	–	–	–	–	–	–	–	–	–	–
	l	−2351.50	−2313.51	−2220.92	−1339.54	−1302.62	−1349.43	−2220.92	−1152.21	−1029.40	−1385.42
	p	13	13	13	11	11	10	12	11	11	13
	AIC	4729.01	4653.03	2627.24	2701.09	2627.24	2718.87	2390.75	2326.42	1737.17	1684.68
Location parameter $\mu(t)$: β_0–β_4 (m)				Scale parameter $\psi(t)$: α_0–α_4 (m)				Shape parameter $\xi(t)$: γ_0–γ_4			

and the dashed lines represent the 95% confidence intervals, the lower dotted line represents the location parameter, and the lower solid line represents the scale parameter. The maximum monthly values of significant wave height are represented with dots.

In Fig. 4, a bimodal behavior for many of the buoys in the 30-year return period value (bold line) can be observed. The peaks happen approximately between February and April, and between August and October. This behavior may be related to two seasonal patterns, the latter associated to hurricanes and the former associated to cold fronts. The assessment of this behavior can be relevant because, although the larger wave heights are associated to the hurricanes, the values associated to the cold fronts can be important during the construction phase of maritime and offshore structures, for planning issues, etc. Results for other return periods not shown here for brevity present similar trends.

Fig. 4 also shows a good fitting of all the parameters for the considered cases. To further illustrate the adequacy of the fit, comparison of the empirical distributions and fitted distributions is presented in Fig. 5 for data from each of the considered buoys.

It is observed that in 42,007 buoy, the model lightly overestimated the maximum values. In the case of 42,001, 42,002 and 42,003 buoys, the model underestimated the quantile. For the monthly maximum series of 42,019, 42,020, 42,035, 42,036, 42,039 and 42,040 buoys, a very good fitting of the model is shown.

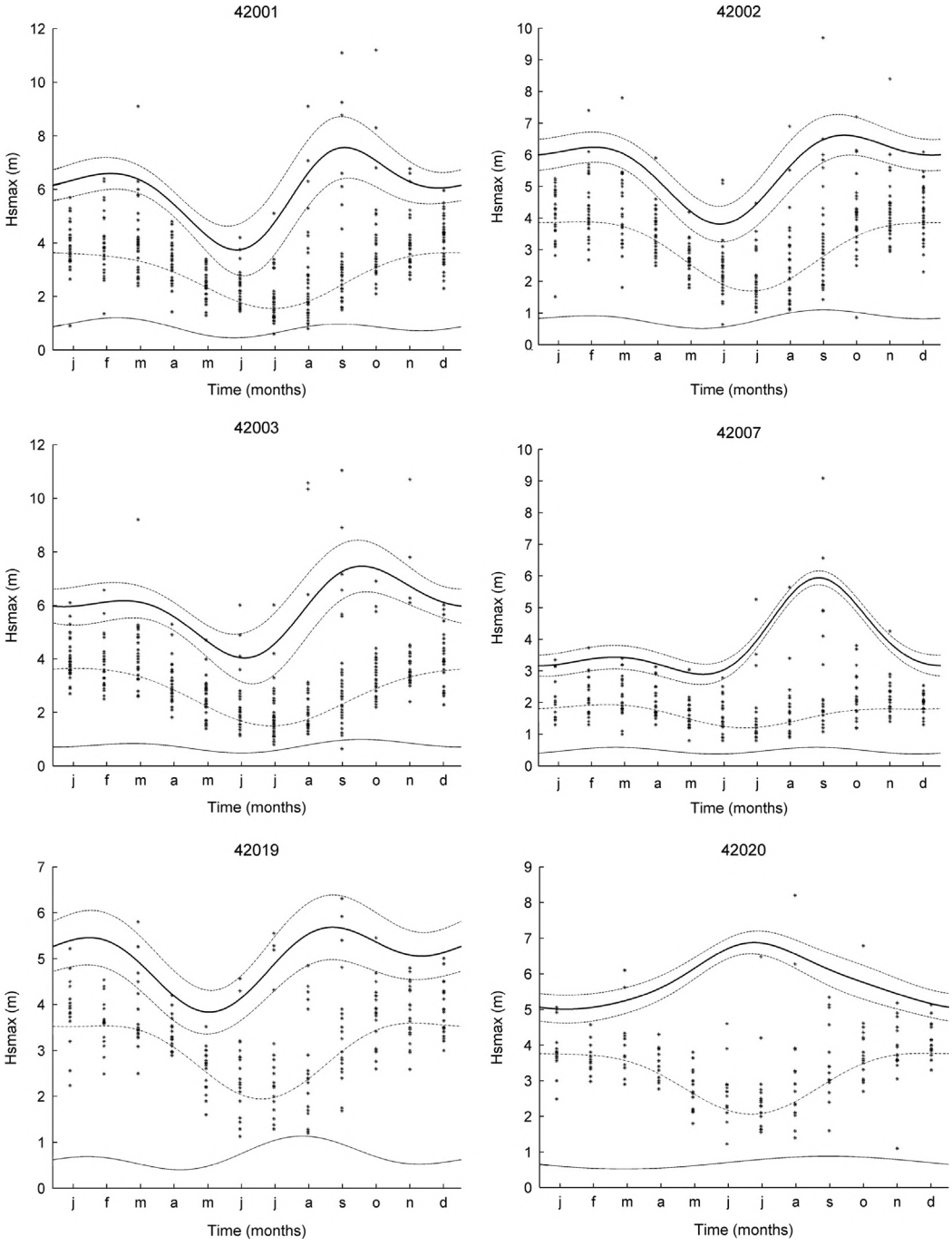

Fig. 4. Fittings for the monthly maximum values for 30-year return period quantiles (bold lines) within a year and 95% confidence intervals (dashed lines) including location and scale parameters (lower dotted and lower solid lines respectively).

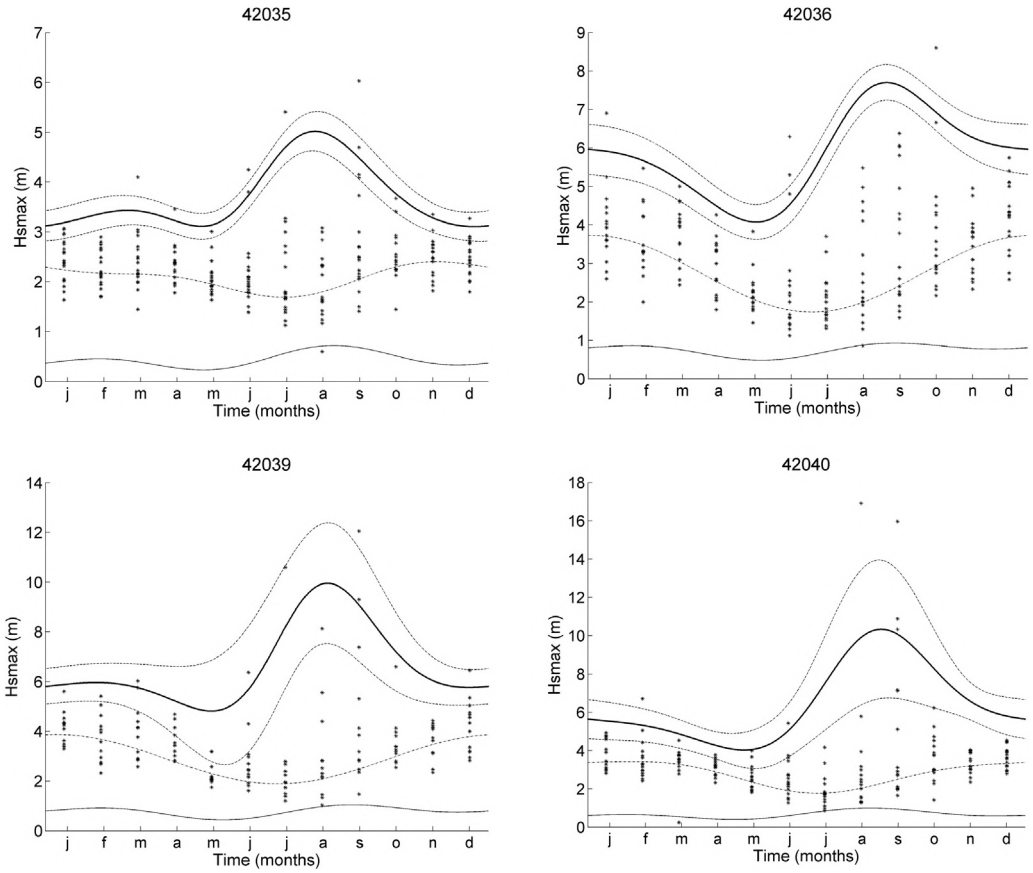

Fig. 4. (*continued*)

4. Comparison with the study results from Panchang and Li (2006)

In this section some of the results from the statistical study by Panchang and Li (2006) for 11 buoys in the Gulf of Mexico (with information recorded by NDBC) are reproduced and compared with those obtained in this study (for 10 buoys only). Panchang and Li (2006) employed annual maximum and monthly maximum significant wave height (SWH) values and carried out an analysis of extremes by employing Weibull and Gumbel distributions. They reported that the wave heights associated to a return period of N years (SWH_N) using the Weibull distribution are slightly lower than those estimated using the Gumbel distribution. In general, they found that the SWH_N values were on the order of the maximum recorded SWH, as long as the data sets were not very short and for the return periods considered in their study (50–500 years).

Particular attention is focused on large waves caused by Hurricane Ivan; for example, it was found that at the locations for buoys 42,003, 42,007, 42,039 and 42,040 during this hurricane, the SWH_S were the largest ever recorded. They noted that the differences in the maxima, in special at buoys 42,007 and 42,040, with those prior to Hurricane Ivan were considerable. They also reported SWH_S up to 17.9 m in the vicinity of buoy 42,040 measured by the Naval Research Laboratory. This measurement is the largest SWH ever recorded in U.S. waters.

Before describing the comparison with the work by Panchang and Li (2006), it is important to notice that in addition to Panchang and Li (2006) Jonathan and Ewans (2011) investigated the extreme waves in the Gulf of Mexico modeling the seasonality based on the hindcast data from GOMOS (2005) rather than records from the NOAA buoys. They employed a Generalized Pareto distribution to describe storm peak significant wave heights. The modeling was performed for two unknown locations in the Gulf of Mexico, covering two areas of about 80 × 180 km each. This makes difficult to carry out a quantitative comparison between the referred study and the present one. Therefore, in the following, a quantitative comparison is carried out, but only for the study by Panchang and Li (2006).

In Table 3 values of maximum monthly recorded SWH and SWH_{100} for Gumbel and Weibull distributions reported by Panchang and Li (2006) are reproduced. Table 3 also shows the results from the time-dependent GEV-model for maximum significant wave heights associated to a return period of 100 years including their corresponding distribution types and 95% confidence interval values. This information is shown for the 10 buoys considered in this study, but in this case, information recorded up to 2004 was employed, so that the data is consistent with that used by Panchang and Li (2006). Note that for buoys 42,007 and 42,040 the analysis was performed including or excluding the SWH associated to Hurricane Ivan, as it was done by Panchang and Li (2006). Actually, for reasons which will be explained later, one more analysis was carried out for buoy 42,040 excluding not only the SWH associated to Hurricane Ivan, but also the SWH associated to Hurricane Mitch. Note also that the SWH_{100} for the time-dependent GEV model in Table 3 are the maximum within the year months.

When comparing SWH_{100} from both studies, it can be observed that the values are similar. However, for the time-dependent GEV model the month when the expected value occurs can be determined, as indicated in brackets beside the SWH_{100} values in Table 3. In fact, the values for any month within the year

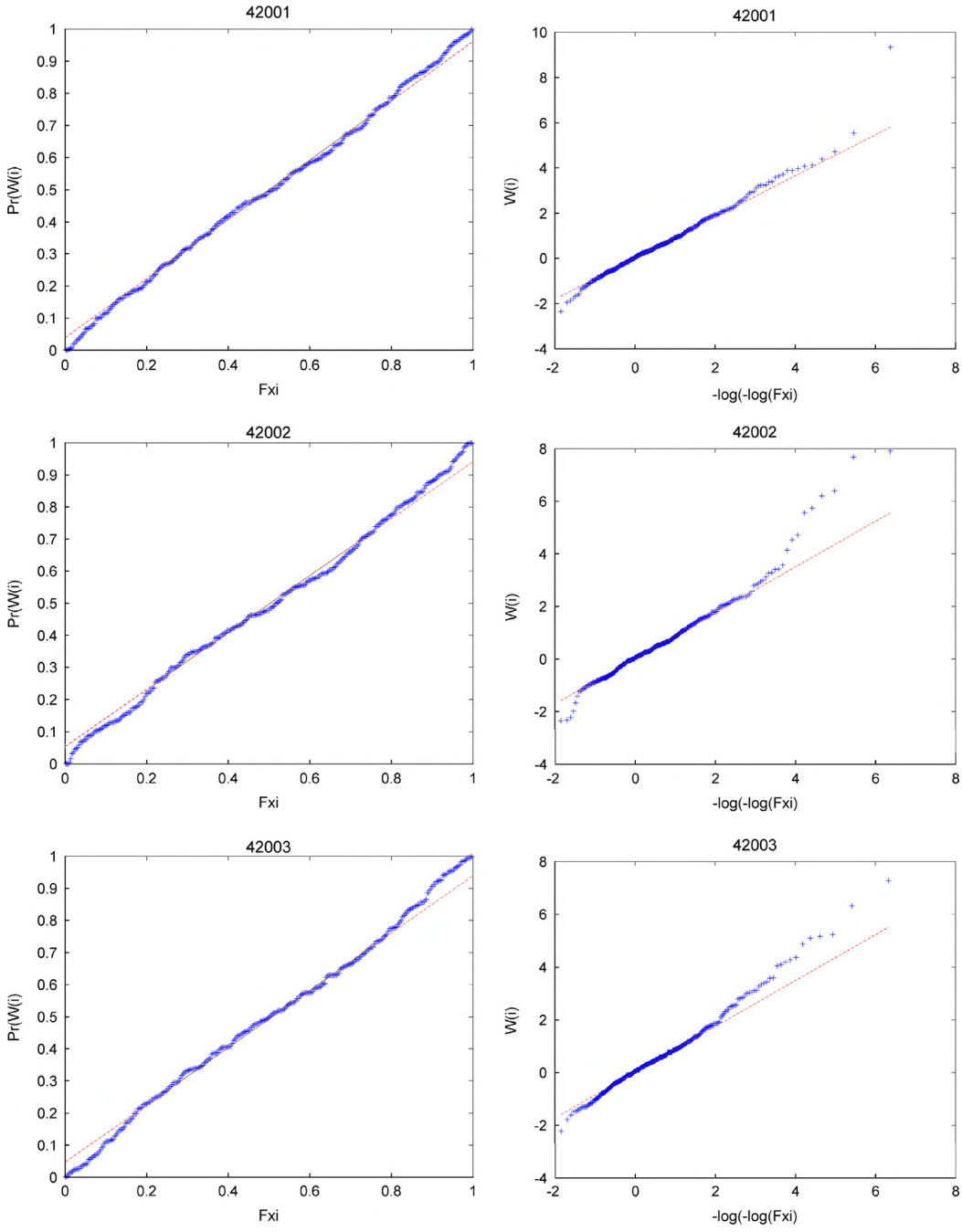

Fig. 5. Probability and QQ plots (left and right) for each buoy.

(not shown here for brevity) can be obtained. Moreover, the time-dependent GEV model directly determines the extreme distribution type which best characterizes the data.

Panchang and Li (2006) computed the SWH_N with or without the SWH associated to Hurricane Ivan for buoys 42,007 and 42,040. This was also considered in this study for comparison purposes. This led to obtaining two different distribution types for buoy 42,007 by using the time-dependent GEV model, possibly because the maximum SWH with and without considering the Hurricane Ivan vary significantly (9.09 m and 4.91 m, respectively). By excluding and including SWHs associated to the hurricane, Gumbel and Frechet distribution types are obtained, respectively. Results for the Frechet distribution are not included by Panchang and Li (2006).

For the case of buoy 42,040 a Frechet distribution type was found in both cases (with and without SWHs associated to Hurricane Ivan). However, it was noted that the difference in maximum SWH value was not as remarkable as for the case of buoy 42,007 (15.96 m and 10.88 m, respectively). This could be explained because the maximum SWH after excluding Hurricane Ivan, is still associated to another hurricane, in this case, the Hurricane Mitch. A last row was included in Table 3 excluding both, SWHs associated to Hurricanes Ivan and Mitch for buoy 42,040. The new analysis, for a maximum SWH equal to 7.12 m, resulted in a Gumbel distribution. It is believed that this change in the distribution type (from Frechet to Gumbel), depending on whether a typical maximum SWHs are included in the analysis or not, could be associated to the occurrence of infrequent events like

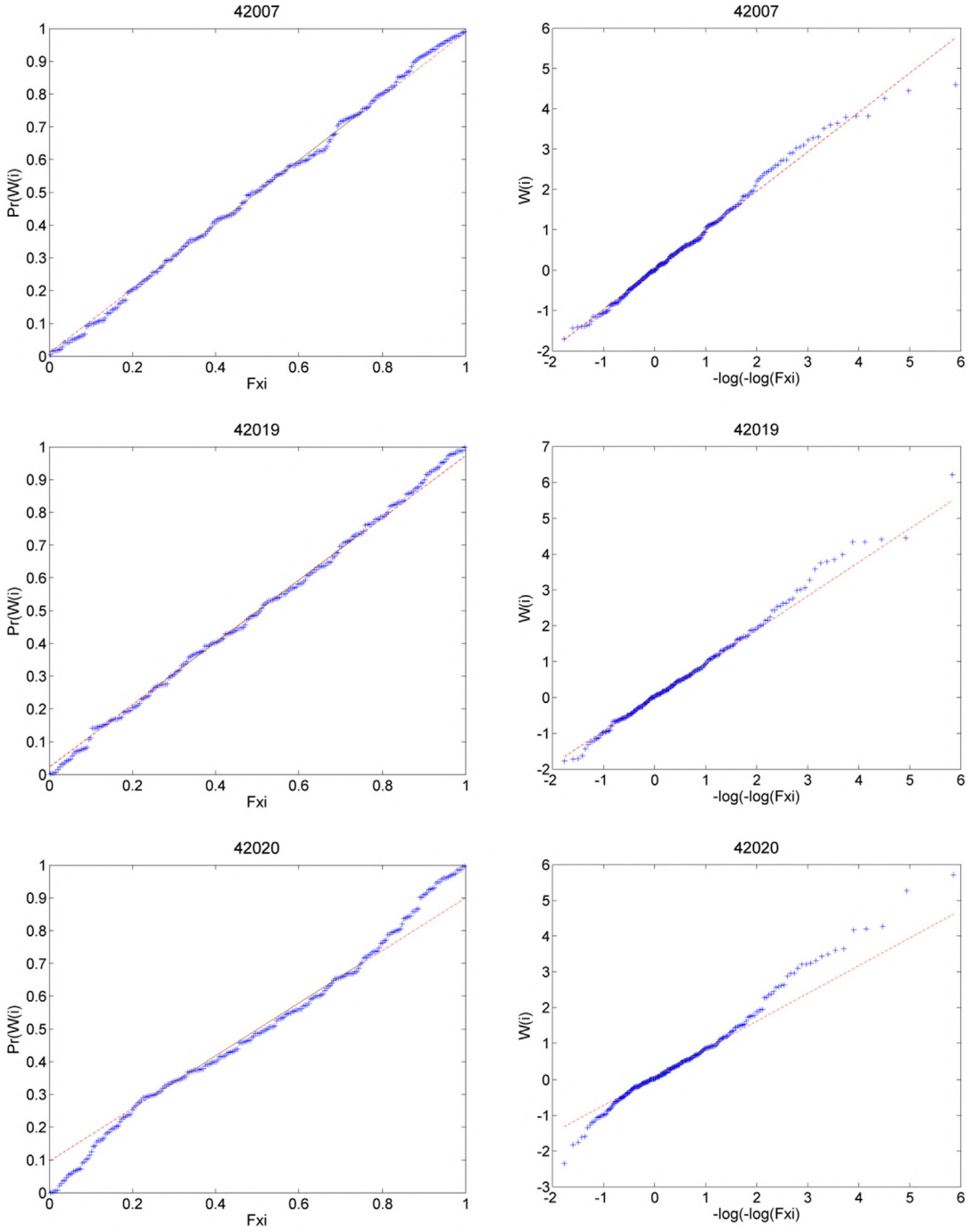

Fig. 5. (*continued*)

Hurricanes at the site of interest. This point, however, deserves further research for more cases and more detailed analyses before a sound conclusion could be drawn.

Note that the results presented in the comparison are from data recorded up to 2004. In Section 3, by using data recorded up to 2011, in some cases different distribution types were found for the same buoys. Also, unlike the case of Table 3 (using buoys data up to 2011), Weibull distributions where found (42,002 and 42,019 buoys). This means that the fitting could be sensible to the time period considered in the analysis.

Panchang and Li (2006) considered 42,001, 42,002 and 42,003 buoys to assess the recurrence interval for the maximum SWH reported in U.S. waters until now (17.9 m). Note that Panchang and Li (2006) computed the recurrence intervals using annual maxima. In this work the return periods by using monthly maximum values, and the equations and distribution parameters given by Panchang and Li (2006), were obtained. Then, the return periods were compared with those computed with the time-dependent GEV model, and are shown in Table 4.

Fretchet distributions using the GEV model for buoys 42,001, 42,002 and 42,003 were obtained (see Table 3). As it was previously mentioned, the employed data is the same considered by Panchang and Li (2006) (from 1973 to 2004). For the Panchang and Li model, Table 4 shows recurrence intervals of 75,000, 49,000 and 63,000 years, for buoys 42,001, 42,002 and 42,003, respectively; whereas, for the time- dependent GEV model recurrence intervals of 630, 95,000 and 15,000 years, for buoys 42,001, 42,002 and 42,003, respectively, are shown. It is considered that these

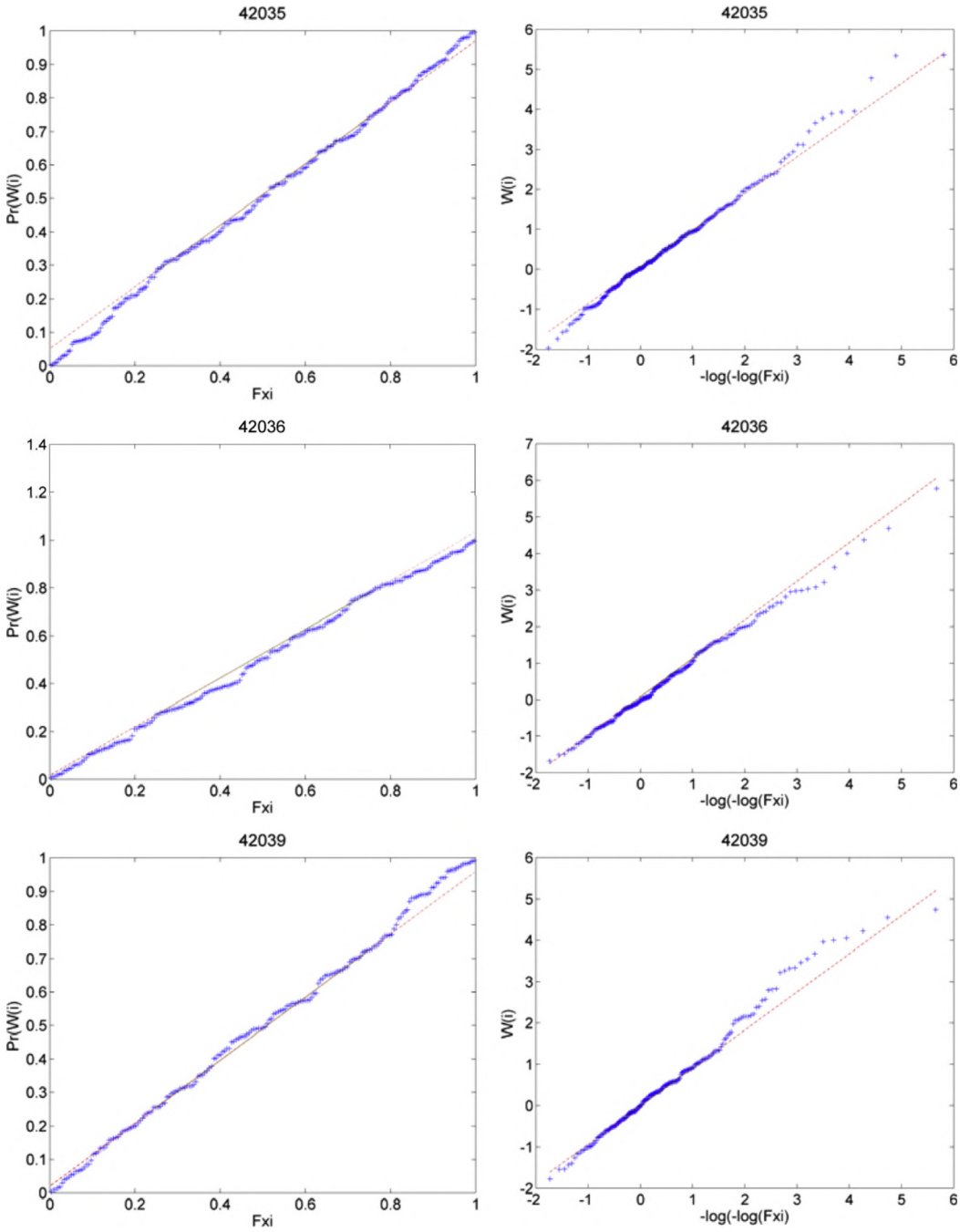

Fig. 5. (*continued*)

dissimilar results are due to the different probability distribution (Gumbel vs Frechet) and the employed model (stationary vs non-stationary). It is noticeable that for buoy 42,001 the maximum SWH considering data up to 2004 was 11.2 m, however, the next year a maximum SWH equal to 11.1 m was recorded; so, the return period of 630 years obtained with the time-dependent GEV model, seems to be more reasonable than the 75,000 years return period obtained with the stationary model. In fact, the recurrence interval considering data up to 2011, by employing the non-stationary model, is even shorter and equal to 350 years.

As a last comparison, to emphasize the differences between the stationary and the time-dependent GEV models, Figs. 6 and 7 are presented. Fig. 6 shows SWHs results from Panchang and Li (2006) for different return periods by using maximum monthly values and the Gumbel distribution; 95% confidence intervals are also shown. Fig. 7 also shows SWHs for different return periods. These results were also computed for the buoys data up to 2004. In contrast to Fig. 6, Fig. 7 shows an evident non-stationary behavior which is not possible to predict with the stationary model; a 95% of confidence interval is included for a return period of 1000 years.

5. Conclusions

A time-dependent GEV model is used to analyze the maximum significant wave height values with seasonal and monthly variability. In the model, the seasonality of time-dependence is introduced by using the harmonic functions to represent the annual and semiannual cycles of the extreme waves. More specifically, it is considered that the scale, location and shape parameters in the

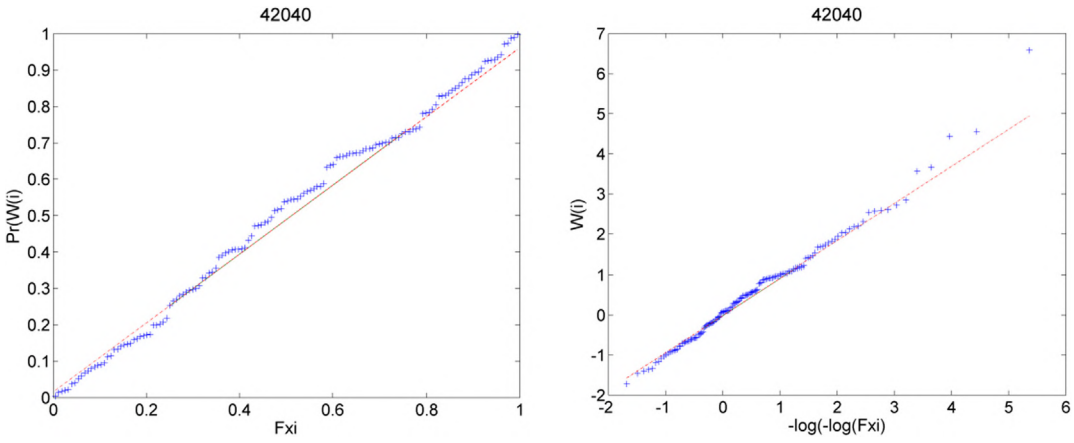

Fig. 5. (*continued*)

Table 3
Comparison of quantiles for a 100 year return period for the analyzed models, vs maximum recorded values.

Buoy	Maximum recorded SWH(m)	Panchang and Li (2006)		Time-dependent (GEV)			
		SWH_{100} (m) using Gumbel	SWH_{100} (m) using Weibull	SWH_{100} (m)	Distribution type	95% Confidence intervals	
						Lower	Upper
42,001	11.20	10.56	9.30	10.47 (September)	Fretchet	8.46	12.49
42,002	9.70	10.89	8.54	7.96 (September)	Fretchet	7.01	8.93
42,003	11.04	10.59	9.24	8.41 (September)	Fretchet	7.33	9.49
42,007 (Without Hurricane Ivan)	4.91	5.28	4.78	5.88	Gumbel	5.49	6.26
42,007 (With Hurricane Ivan)	9.09	5.47	5.66	6.57 (September)	Frechet	6.41	7.13
42,019	6.80	9.28	6.15	6.03 (August)	Gumbel	5.63	7.33
42,020	8.20	9.10	7.17	8.85 (July)	Gumbel	7.01	10.79
42,035	5.40	5.90	4.59	6.83 (August)	Gumbel	6.40	7.28
42,036	8.60	10.27	8.37	10.71 (August)	Gumbel		
42,039	12.05	10.59	10.65	10.91 (August)	Gumbel	9.83	12.05
42,040 (Without Hurricane Ivan)	10.88	9.27	8.51	10.27	Frechet	9.79	10.76
42040 (With Hurricane Ivan)	15.96	9.84	10.88	13.38 (August)	Frechet	12.75	14.05
42,040 (Without Hurricanes Ivan and Mitch)	7.12	–	–	6.57	Gumbel	6.09	7.37

Table 4
Comparison of the time-dependent GEV analysis vs. the Gumbel Analysis in Panchang and Li (2006).

Buoy	Years to $SWH_{max}=17.9$ m)	
	Gumbel (Panchang)	Time-dependent GEV
42,001	≈ 75,000	≈ 630
42,002	≈ 49,000	≈ 95,000
42,003	≈ 63,000	≈ 15,000

GEV model vary from month to month. To select the preferred model and to reduce the number of free parameters to be estimated, the Akaike Information Criterion is employed.

The characteristics of the wave seasonality variation for each site are obtained by applying the mentioned model in 10 buoys in the Gulf of Mexico, showing that the wave heights varies with the season, resulting in the largest wave height for the fall-winter season. The seasonality effect is examined by using the monthly maximum wave height values, and expected wave height values for different return periods. It is expected that the obtained results can be employed for a better understanding of the ocean wave height for each season, and to anticipate the wave heights which could be used for structural design and coast risk management.

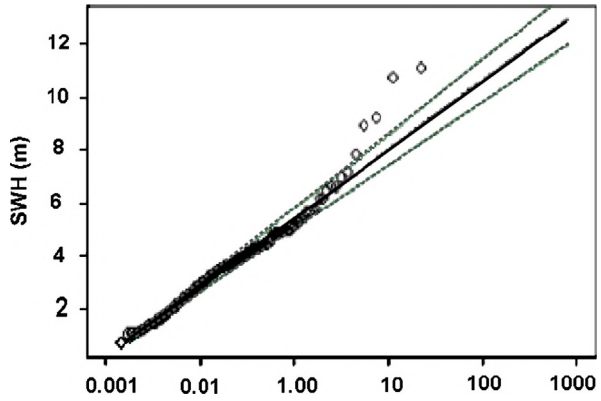

Fig. 6. Return period (years) and 95% confidence intervals for 42,003 buoy for monthly maximum using Gumbel (Panchang and Li, 2006).

It was found that the recorded wave height at the examined locations have annual and semiannual cycles, suggesting two seasons of extreme events during the year. The observed bimodal behavior (the peaks at two different year seasons) in the significant wave height associated to a 30-year return period, could be

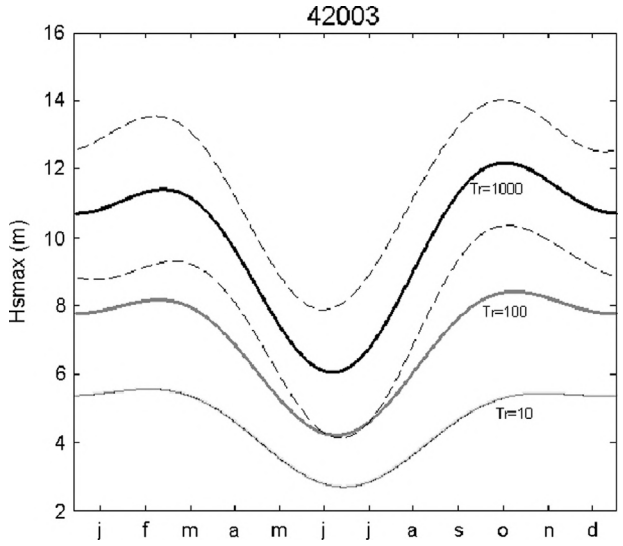

Fig. 7. Return periods for monthly maximum for Tr = 10, 100 and 1000 years and 95% confidence bands (dashed lines, for Tr = 1000 years only) for 42,003 buoy (Time-dependent GEV model).

possibly related to hurricanes and cold fronts. The assessment of this behavior can be relevant for the construction phase of maritime and offshore structures, and for planning activities.

When comparing the time-dependent GEV model and the stationary model (Panchang and Li, 2006), it was observed that the values are similar. However, for the time-dependent GEV model the significant wave heights associated to a given return period can be obtained for any month, whereas this is not possible for a stationary model. The time-dependent GEV model directly determines the extreme distribution type which best characterizes the data.

The time-dependent GEV model appears to give more realistic recurrence intervals for the maxima observed in the measured data sets.

Acknowledgments

The financial support from the Consejo Nacional de Ciencia y Tecnología, from Mexico, (CONACYT) is gratefully acknowledged. The authors are thankful to the National Buoy Data Center of National Oceanic and Atmospheric Administration (NOAA) for the use of buoy data. The authors thank Melisa Menéndez, who supervised the thesis (basis of part of this work) of one of the authors at the Universidad de Cantabria. The authors are also grateful to Professor H.P. Hong from The University of Western Ontario and two anonymous reviewers for their constructive comments, suggestions and criticisms, which greatly improved the content of this study.

References

Akaike, H., 1973. Information theory and an extension of the maximum likelihood principle. In: Petrov, B.N., Csaki, F. (Eds.), Proceedings of the Second International Symposium on Information Theory. Akademia Kiado, Budapest, pp. 267–281.

Benjamin, J.R., Cornell, C.A., 1970. Probability, Satistics, and Decision for Civil Engineers. McGraw-Hill, Inc., New York.

Carter, D.J.T., Challenor, P.G., 1981. Estimating return values of environmental parameters. Quarterly Journal of the Royal Meteorological Society 107, 259–266.

Chakrabarti, S.K., 2001. Hydrodynamics of Offshore Structures. Computational Mechanics Publication. WIT Press, Southampton.

Chavez-Demoulin, V., Davison, A.C., 2005. Generalized additive modeling of sample extremes. Journal of the Royal Statistical Society: Series C (Applied Statistics), 54.

Coles, S.G., 2001. An Introduction to Statistical Modeling of Extreme Values. Springer, London p. 208.

Goldberg, D.E., 1989. Genetic Algorithms in Search, Optimization, and Machine Learning. Addison-Wesley, Reading, Mass p. 372.

GOMOS, 2005. Oceanweather, inc.

Hong, H.P., 1994. Estimate of extreme wind and wave loading and safety level of offshore structures. In: Proceedings of a Symposium, Risk Analysis, University of Michigan, Ann Arbor, Michigan, USA.

Isaacson, M., Mackenzie, N.G., 1981. Long-term distributions of ocean waves: a review. Journal of Waterway, Port, Coastal and Ocean Division, American Society of Civil Engineers 107, 93–109.

Jensen, J.J., Olsen, A.S., Mansour, A.E., 2011. Extreme wave and wind response predictions. Ocean Engineering 38, 2244–2253.

Jonathan, P., Ewans, K.C., 2007. The effect of directionality on extreme wave design criteria. Ocean Engineering 34, 1977–1994.

Jonathan, P., Ewans, K.C., 2011. Modeling the seasonality of extreme waves in the Gulf of Mexico. Journal of Offshore Mechanics and Arctic Engineering 133 (2).

Jönsson, A., Broman, B., Rahm, L., 2002. Variations in the Baltic Sea wave fields. Ocean Engineering 30, 107–126.

Katz, R.W., Parlange, M.B., Naveau, P., 2002. Statistics of extreme in hydrology. Advances in Water Resources 25, 1287–1304.

Leadbetter, M.R., Lindgrem, G., Rootzén, H., 1983. Extremes and Related Properties of Random Sequences and Series, Springer.

Lettenmaier, D.P., Burges, S.J., 1982. Gumbel's extreme value 1 distribution, a new look. Journal of Hydraulics Division – ASCE 108, 502–504.

Mackay, E.B.L., Challenor, P.G., Bahaj, A.S., 2010. On the use of discrete seasonal and directional models for the estimation of extreme wave conditions. Ocean Engineering 37 (5–6), 425–442.

Martucci, G., Carniel, S., Chiggiato, J., Sclavo, M., Lionello, P., Galati, M.B., 2010. Statistical trend analysis and extreme distribution of significant wave height from 1958 to 1999 — an application to the Italian Seas. Ocean Science 6, 525–538.

Mazas, F., Hamm, L., 2011. Multi-distribution approach to POT methods for determining extreme wave heights. Coastal Engineering 58 (5), 385–394.

Mendez, F.J., Menéndez, M., Luceño, Losada, I.J., 2007. Analyzing monthly extreme sea levels with a time-dependent GEV model. Journal of Atmospheric and Oceanic Tecnology 24, 894–911.

Méndez, F.J., Menéndez, M., Luceño, A., Medina, R., Graham, N.E., 2008. Seasonality and duration in extreme value distributions of significant wave height. Ocean Engineering 35 (1), 131–138.

Menéndez, M., Graham, N.E., Méndez, F., Losada, I., 2007. Long-term trends in extreme significant wave height in the Northeast Pacific Ocean — an application of extreme value theory. EGU General Assembly.

Menéndez, M., Méndez, F.J., Izaguirre, C., Luceño, A., Losada, I.J., 2009. The influence of seasonality on estimating return values of significant wave height. Costal Engineering 56, 211–219.

Mietus, M., 1998. The climate of the Baltic Sea basinMarine Meteorology and Related Oceanographic ActivitiesWorld Meteorological Organisation, Geneva p. 64. (Report No. 41).

Morton, I.D., Bowers, J., Mould, G., 1997. Estimating return period wave heights and wind speeds using a seasonal point process model. Coastal Engineering 31, 305–326.

Muir, J.R., ElShaarawi, A.H., 1986. On the calculation of extreme wave heights, a review. Ocean Engineering 13, 93–118.

Muraleedharan, G., Lucas, C., Soares, C.G., et al., 2012. Modeling significant wave height distributions with quantile functions for estimation of extreme wave heights. Ocean Engineering 54, 119–131.

Panchang, V.G., Li, D., 2006. Large Waves in the Gulf of Mexico Caused by Hurricane Ivan. American Meteorological Society 87, 481–489.

Prevosto, M., Krogstad, H.E., Robin, A., 2000. Probability distributions for maximum wave and crest heights. Coastal Engineering 40, 329–360.

Prpić-Orsîc, J., Dejhalla, R., Turk, A., 2007. Design sea state assessment using genetic algoritm approach. Ocean Engineering 34, 148–156.

Räämet, A., Soomere, T., 2010. The wave climate and its seasonal variability in the Northeastern Baltic Sea. Estonian Journal of Earth Sciences.

Soares, C.G, Carvalho, A.N., 2012. Probability distributions of wave heights and periods in combined sea-states measured off the Spanish coast. Ocean Engineering 52, 13–21.

Solari, S., Losada, M.A., 2012. Unified distribution models for met-ocean variables: Application to series of significant wave height. Coastal Engineering 68, 67–77.

Stansell, P., 2005. Distributions of extreme wave, crest and trough heights measured in the North Sea. Ocean Engineering 32, 1015–1036.

Tayfun, M.A., Fedele, F., 2007. Wave-height distributions and nonlinear effects. Ocean Engineering 34 (11–12), 1631–1649.